

**Development of Synthetic α -Helix Mimetics
as Potent Anticancer Agents**

Kérya Long

Submitted in accordance with the requirements for the degree of
Doctor of Philosophy

University of Leeds
School of Chemistry

April 2013

Intellectual Property and Publication Statements

The candidate confirms that the work submitted is her own, except where work which has formed part of jointly-authored publications has been included. The contribution of the candidate and the other authors to this work has been explicitly indicated below. The candidate confirms that appropriate credit has been given within the thesis where reference has been made to the work of others.

The paragraph on 'Foldamers adopting a helical conformation' in Chapter 1 was adapted from a review article published in February 2013: 'Inhibition of alpha-helix mediated protein-protein interactions using designed molecules', V. Azzarito, K. Long, N. S. Murphy and A. J. Wilson, Nat. Chem. 2013, 5, 161–173. The contributions of the authors were as follows: KL (the candidate) wrote the corresponding section of the review and produced the related figures, AJW edited the manuscript into its present form (see attached copy); other authors have equally contributed to the review (on different sections).

The work described in Chapter 2 formed the basis for a research article published online in October 2012: 'Microwave assisted solid phase synthesis of highly functionalized N-alkylated oligobenzamide alpha-helix mimetics', K. Long, T. A. Edwards and A. J. Wilson, Bioorg. Med. Chem., 2013, 21, 4034–4040. The contributions of the authors were as follows: KL (the candidate), AJW and TAE designed the research, KL performed the research, wrote a draft manuscript and prepared all of the figures, AJW and TAE then edited the manuscript into its present form (see attached copy). The draft originally prepared by KL was then rewritten as Chapter 2 of this thesis.

This copy has been supplied on the understanding that it is copyright material and that no quotation from the thesis may be published without proper acknowledgement.

Acknowledgements

First and foremost, I would like to thank my main supervisor, Prof. A. J. Wilson, for giving me this life changing opportunity to join his group and work on such an interesting project; for his guidance, support and enthusiasm for science. I would also like to thank my co-supervisor Dr. T. A. Edwards for his help and support as I was taking my first steps in the 'biological' world, as well as throughout my PhD. Thanks to Yorkshire Cancer Research for funding, and to all the collaborators that have contributed to this project: Dr. S. Warriner for always providing me with useful answers, Dr. C. J. Empson for his help with the robot, Dr. D. Tomlinson and Dr. H. Martin for the cell assays, and all the SoC technical staff. Thanks to all the people in the department for making it a lively place by stopping in the corridor for a chat, or just a smile and Nic, thanks for joining our girly group, you are almost a wilsonian! I was also lucky to have been given the opportunity to work for two months at the IECB, and I would like to thank Dr. G. Guichard, Dr. C. Casassus and all members of the Guichard group for making it such a good time.

Past and present members of the Wilson group deserve my most sincere acknowledgements, for filling these three years with laughters, and becoming some of my closest friends. Adam, Mazza and Maria, thank you for helping me settling in as I was a young PhD; Panchami and Alice for sharing your post-doc-wisdom with me; George, for being so thorough playing the bass! Dave: for being the male target for all my verbal abuse as well as being our GBF (!); Kelly: for being one of the nicest people on Earth; George: for all your hilarious stories; Hannah: for your biological help; Anna: for being the best Post-Doc in the second half of my PhD; Sílvia: for bringing your Spanish touch to the lab; Phil and Vale, thank you for providing me with a nice and warm place to write up; finally Tash and Vale, I just cannot thank you enough for everything we shared, all the good (and also bad) memories in Pennington, but also while not living together (I don't think that here is the appropriate place to enumerate them!), also thank you for your support and understanding when I felt down, you really did help me getting through all this.

Guys, I will not forget you!

Merci à toute ma famille et mes amis en France, pour avoir été ma bouffée d'oxygène durant ces trois ans, pour avoir cru en moi, m'avoir encouragé dans les moments difficiles, et surtout, pour ne m'avoir (presque) jamais parlé de chimie. Pom et Lilou, merci d'être toujours là pour moi, malgré la distance et tout le reste, je sais qu'on sera toujours là les unes pour les autres. Une pensée également à Rémi, Claire, Gim, Tipouce, Loïc, Piwei et tous ceux qui ont trouvé du travail dans le milieu scientifique, preuve que c'est possible !

Ming Peou, merci pour cette escapade à Dublin, elle est arrivée à un moment critique dans la rédaction. Maman, merci pour m'avoir constamment préparé de bons petits plats à chaque fois que je suis rentrée à la maison; Bicket, merci d'avoir fait en sorte qu'on ait toujours quelque chose à regarder ! Papa, tu étais loin mais je sais que tu pensais à moi, merci. Antoine, mon chka, ça y est, c'est la fin! Merci d'avoir traversé les mêmes épreuves que moi et d'être venu m'apporter ton soutien infailible ces derniers mois, sans toi je n'aurais pas tenu.

Abstract

Protein-protein interactions (PPIs) mediate a number of essential cellular processes and their implication in numerous diseased states - including HIV and cancer - makes them desirable targets for therapeutic intervention. It is however still unclear how to target them, considering their relative lack of defining features. A large proportion of PPIs however involve binding of an α -helix into a hydrophobic cleft on the other protein's surface and a few key residues located along one helical face have been identified as a recurring and critical pattern for binding. Mimicking the helical core and replicating the spatial arrangement of these residues has therefore become a desirable strategy to abolish such interactions. Building on previous studies from the group, the work described in this thesis aimed to use an *N*-alkylated oligoamide scaffold to target α -helix mediated PPIs. In particular, the study focused on the assembly and screening of a library of oligobenzamides against two key oncogenic targets (p53/*hDM2* and Noxa B/*Mcl-1*), with a view to setting the basis for a generic approach towards the selective inhibition of α -helix mediated PPIs. The model interactions for this study and their biological context are described in Chapter 1, as well as the different approaches that have emerged to achieve α -helix mimicry. An automated microwave assisted solid phase methodology has been developed which makes use of the Fmoc protection strategy and is reported in Chapter 2. The robustness of this methodology was demonstrated through the assembly of a library of 75 compounds. This library is described in Chapter 3, along with its biophysical assessment and preliminary cell assays. Chapter 4 describes the design and synthesis of oligoureas and their potential as helix mimetics was assessed against the p53/*hDM2* PPI.

Table of Contents

Acknowledgements	iii
Abstract	v
Table of Contents	vi
List of Tables	ix
List of Figures	x
List of Abbreviations	xiii
Chapter 1: Protein-Protein interactions as Therapeutic Targets	1
1.1 Targets and insight into their biological context	4
1.1.1 The p53/ <i>hDM2</i> interaction	4
1.1.1.1 Generalities and structure of p53	4
1.1.1.2 Structures and functions of <i>hDM2</i> and <i>hDMX</i>	7
1.1.2 The Bcl-2 family of interactions	10
1.1.2.1 Generalities and structure of the Bcl-2 family	10
1.1.2.2 Pro-apoptotic members of the Bcl-2 family	12
1.1.2.3 Pro-survival members of the Bcl-2 family	13
1.2 Inhibition of α -helix mediated PPIs	14
1.2.1 Small molecule inhibitors	15
1.2.1.1 Small molecule inhibitors discovered by HTS	15
1.2.1.2 Structure-based designed small molecule inhibitors	18
1.2.2 Peptide inhibitors	20
1.2.2.1 Constrained peptides	21
1.2.2.2 Foldamers adopting a helical conformation	25
1.2.3 Proteomimetics	31
1.3 Project aims	38
Chapter 2: Microwave assisted solid phase synthesis of highly functionalized <i>N</i>-alkylated oligobenzamide α-helix mimetics	39
2.1 Monomer synthesis	42
2.2 Solid Phase Peptide Synthesis	43
2.3 Conclusions	51

Chapter 3: Testing the hypothesis – Assembly and Screening of a library of proteomimetics	53
3.1 Targeting the p53/hDM2 interaction.....	54
3.1.1 The library.....	54
3.1.2 Biophysical evaluation of the library of oligobenzamides	56
3.1.2.1 The fluorescence anisotropy assay	57
3.1.2.2 Initial screening: manual single point assay	60
3.1.2.3 Automated single point screening of the library	68
3.2 Targeting the Bcl-2 family of interactions	69
3.2.1 Testing against the Mcl-1/Noxa B interaction	71
3.2.1.1 Single point assay against the Mcl-1/Noxa B PPI	72
3.2.1.2 Competition assays against the Mcl-1/Noxa B PPI	74
3.3 Selectivity of the scaffold	75
3.4 Proteolytic studies	79
3.5 Cell assays	80
3.6 Discussion	83
3.7 Summary and conclusions	85
Chapter 4: Solid phase synthesis and biological evaluation of oligoureas as α-helix mimetics	87
4.1 Oligoureas as helix mimetics	88
4.1.1 Design and preliminary modelling studies.....	90
4.2 Synthesis	92
4.2.1. Building block synthesis	92
4.2.2 Solid phase synthesis of oligoureas	94
4.3 Biophysical evaluation	98
4.3.1 Competition assay on the original oligourea	99
4.3.2 Competition assays – an attempt to automation	100
4.3.3 Establishment of Structure-Activity Relationships	102
4.4 Conformational investigation of oligourea 133	109
4.5 Target selectivity	111
4.6 Conclusions and future work	112

Chapter 5: Thesis summary and Future directions	114
Chapter 6: Experimental section	117
6.1 Assembling a library of <i>N</i> -alkylated oligobenzamides (Chapters 2 and 3) ...	119
6.1.1 Monomer building blocks	119
6.1.2 Solid phase synthesis experimental and <i>N</i> -alkylated oligobenzamides characterisation (Chapters 2 and 3)	139
6.2 Biophysical assessment of the proteomimetics (Chapters 3 and 4)	167
6.2.1 Molecular cloning and protein expression	167
6.2.2 Fluorescence anisotropy competition assay	171
6.3 Solid phase synthesis of a library of oligoureas	176
6.3.1 Monomer building blocks	177
6.3.2 Microwave assisted solid phase synthesis	185
References	189
Appendix I	198
Appendix II	199
Appendix III	200
Appendix IV	201
Appendix V	202
Appendix VI	203

List of Tables

Table 1.1 Bcl-2 family members and their binding partners	10
Table 2.1 Screening of activating agents under standard conditions	44
Table 2.2 Optimisation of the coupling time using Cl ₂ PPh ₃	45
Table 2.2 Library of <i>N</i> -alkylated tribenzamides with the side chains sequence..	48
Table 2.4 Indole deprotection versus side chain elimination	50
Table 4.1 The library of oligoureas	97
Table 4.2 Summary of the design of the library of oligoureas and Structure-Activity Relationships established based on FA assay results	108

List of Figures

Figure 1.1 The alpha-helix	3
Figure 1.2 Disruption of an α -helix mediated PPI by a designed inhibitor replicating the spatial presentation of key binding residues	3
Figure 1.3 p53 directly binds DNA to exert its post-transcriptional activity	5
Figure 1.4 The p53/ <i>hDM2</i> and related p53/ <i>hDMX</i> interactions	9
Figure 1.5 Role of the Bcl-2 proteins in the induction of apoptosis	11
Figure 1.6 Crystal structures of pro-survival proteins with BH3 ligands.....	13
Figure 1.7 Structures of the Nutlin compounds (1 , 2 and 3 , active enantiomers) and crystal structure of Nutlin-2 bound to <i>hDM2</i>	16
Figure 1.8 Benzodiazepinediones as inhibitors of the p53/ <i>hDM2</i> interaction	17
Figure 1.9 Structures of two natural product-derived Bcl-2 inhibitors	18
Figure 1.10 Spiro-oxindole inhibitors of the p53/ <i>hDM2</i> interaction	19
Figure 1.11 Abbott inhibitors of the Bcl-x _L /Bak interaction	20
Figure 1.12 Covalent cross-linking strategies for the stabilisation of α -helical conformations	22
Figure 1.13 Crystal structures of stapled peptides inhibitors bound to their target proteins	23
Figure 1.14 β -Hairpin inhibitor 13 of the p53/ <i>hDM2</i> interaction	25
Figure 1.15 α - versus β -peptides: Comparison of the most common helical conformations accessible to natural peptides and foldamers	26
Figure 1.16 α/β -Peptide inhibitors of the Bcl-2 family	28
Figure 1.17 α/β -Foldamers applied to the inhibition of the gp41 fusion interaction.....	30
Figure 1.18 Terphenyl scaffold developed by the Hamilton group	32
Figure 1.19 Proteomimetic scaffolds designed after the terphenyl scaffold	34
Figure 1.20 Wilson's <i>N</i> -alkylated oligobenzamide scaffold as a helix mimetic	37
Figure 2.1 The <i>N</i> -alkylated oligobenzamide scaffold as a helix mimetic	40
Figure 2.2 <i>N</i> -alkylated oligobenzamides preferentially adopt a <i>cis</i> -conformation in solution	41

Scheme 2.1 Synthetic route to Fmoc protected building blocks	42
Scheme 2.2 Outline of procedure used for solid-phase synthesis of <i>N</i> -alkylated aromatic oligoamide α -helix mimetics	56
Scheme 2.3 Cascade elimination of the indole functionality during acidic cleavage from the resin	49
Figure 2.3 Extending the scope of the present SPS methodology	51
Figure 3.1 Monomer synthesis and set of monomers used in the library assembly using the automated SPS methodology described in Chapter 2	54
Figure 3.2 The library of 60 proteomimetics targeting the p53/ <i>hDM2</i> interaction. The side chains are named using the nomenclature reported in Fig. 3.1	55
Figure 3.3 The fluorescence anisotropy assay	58
Figure 3.4 The equilibrium preventing K_d determination	59
Figure 3.5 Results from a single point assay on the first subset of 15 compounds at 10 μ M, presented as a percentage of Nutlin-3a efficiency	61
Figure 3.6 Dose-response curves for hits identified in the single point screening against p53/ <i>hDM2</i> (compounds 46 , 47 , 53) along with the least potent compound in this series (compound 48)	63
Figure 3.7 Single point screening on the second subset of 15 compounds	64
Figure 3.8 Dose-response curves for hits identified in the single point assay (compounds 56 , 62 , 63 , 66) as well as for the least potent compound 33	65
Figure 3.9. Results from single point screening on the third and fourth set of compounds against p53/ <i>hDM2</i> , at 10 μ M	66
Figure 3.10. Comparing para (68) and meta (69) substitution on the benzyl ring at position R2.....	67
Figure 3.11. Dose-response curves for hits on the fourth subset of compounds (78-101)	67
Figure 3.12 Targeting the Bcl-2 family: model interactions and SPS strategy	70
Figure 3.13 Library of proteomimetics bearing 4 side chains and targeted to the Bcl-2 family of interactions	71
Figure 3.14 Results from the single point screening of the library against Mcl-1/Noxa B	73
Figure 3.15 Compounds tested against Mcl-1 in a dose-response assay	74

Figure 3.16 Assessment of the selectivity of the <i>N</i> -alkylated oligobenzamide scaffold	76
Figure 3.17 Preliminary testing against the p53/ <i>hDMX</i> PPI	78
Figure 3.18 Proteolytic study on compound 99	79
Figure 3.19 Fluorescence microscopy images showing limited evidence of apoptosis	81
Figure 3.20 Dose-response curves on compounds that appeared to be potentially active in cell assays	82
Figure 4.1 Oligourea scaffold as a helix mimetic	89
Figure 4.2 Preliminary modelling studies	91
Figure 4.3 Monomers used for the synthesis of oligoureas	92
Scheme 4.1 Synthetic route to azido-carbamate building blocks	93
Figure 4.4 Oligourea and hybrid scaffolds designed for the mimicry of the p53 helix	95
Figure 4.5 Cartoon representation of the fluorescence anisotropy assay	98
Figure 4.6 Results from the FA competition assay on the first synthesized oligourea.....	99
Figure 4.7 Comparing results from FA assays conducted on the robot to assays carried out manually	101
Figure 4.8 Results from the FA competition assay on oligoureas containing an additional solubilizing Orn residue	102
Figure 4.9 Effect of the macrodipole orientation on binding: the <i>i</i> , <i>i</i> + 3 and <i>i</i> + 5 substitution pattern	103
Figure 4.10 Structures of hybrids oligoureas 129 and 130	104
Figure 4.11 Structures of oligoureas 131 (capped) and 132 (uncapped).....	105
Figure 4.12 Swapping positions of Orn and Ser	106
Figure 4.13 Introducing an additional key residue: the Leu22 mimic	107
Figure 4.14 Investigating the helicity of oligourea 133 and potential binding to <i>hDM2</i>	110
Figure 4.15 Investigating the target selectivity of the library of oligoureas: single point screening against the Mcl-1/ <i>Noxa B</i> PPI	111
Figure 4.16 The next generation of oligourea	113

List of abbreviations

Biology

Bad	Bcl-2-antagonist of cell death (pro-apoptotic)
Bak	Bcl-2 homologous antagonist killer (pro-apoptotic)
Bax	Bcl-2-associated X protein (pro-apoptotic)
Bcl-2	B-cell lymphoma 2 (anti-apoptotic)
Bcl-w	Bcl-2-like protein 2 (anti-apoptotic)
Bcl-x _L	B-cell lymphoma-extra large (anti-apoptotic)
BH domain	Bcl-2 Homology domain
Bid	BH3 interacting domain death agonist (pro-apoptotic)
Bim	Bcl-2 interacting mediator of cell death (pro-apoptotic)
Bmf	Bcl-2 modifying factor (anti-apoptotic)
CDK	Cyclin Dependent Kinase
DNA	DeoxyriboNucleic Acid
GFP	Green fluorescent protein
gp41	Glycoprotein 41
GPCR	G-Protein Coupled Receptor
GST	Glutathione S-transferase
FA assay	Fluorescence Anisotropy assay
FRET	Förster resonance energy transfer
HAUSP	Herpesvirus-Associated Ubiquitin-Specific Protease
HCMV	Human cytomegalovirus, also known as herpesvirus-5
<i>hDM2</i> / MDM2	Human Double Minute 2/Murine Double Minute 2
<i>hDMX</i> / MDMX	Human Double Minute X/Murine Double Minute X
HIV	Human Immunodeficiency virus
HPV E2	Human Papilloma Virus E2
IC ₅₀	Half maximal Inhibitory Concentration
<i>K_d</i>	Dissociation constant
<i>K_i</i>	Inhibition constant
Mcl-1	Myeloid cell leukemia-sequence 1 (anti-apoptotic)
MOMP	Mitochondrial Outer Membrane Permeabilization
Puma	p53 upregulated modulator of apoptosis (pro-apoptotic)

p14arf	alternate reading frame (ARF) product of the CDKN2A locus
SDS-PAGE	Sodium Dodecyl Sulfate- Polyacrylamide Gel Electrophoresis
SUMO	Small Ubiquitin-like Modifier
WT	Wild Type

Chemistry

BDP	Benzodiazepinedione
Boc	<i>tert</i> -Butoxycarbamate
CHCl ₃	Chloroform
Cl ₂ PPh ₃	Dichlorotriphenylphosphorane
DCM/ CH ₂ Cl ₂	Dichloromethane
DIC	<i>N,N'</i> -Diisopropylcarbodiimide
DIPEA	<i>N,N</i> -Diisopropylethylamine
DMF	<i>N,N</i> -Dimethylformamide
DMSO	Dimethylsulfoxide
EDCI	1-(3-Dimethylaminopropyl)-3-ethyl-carbodiimide hydrochloride
Fmoc	Fluorenylmethyloxycarbonyl
FITC	Fluorescein-isothiocyanate
HCTU	2-(6-Chloro-1H-benzotriazole-1-yl)-1,1,3,3-tetramethylammonium hexafluorophosphate
HOBt	Hydroxybenzotriazole
MSNT	1-(Mesitylene-2-sulfonyl)-3-nitro-1,2,4-triazole
NMI	N-methyl imidazole
PyBOP	Benzotriazol-1-yl-oxytripyrrolidinophosphonium hexafluorophosphate
THF	Tetrahydrofuran
TFA	Trifluoroacetic Acid
TFFH	Tetramethylfluoroformamidinium hexafluorophosphate
Trt-	Trityl

Other terms

HTS	High throughput screening
-----	---------------------------

HPLC	High performance liquid chromatography
HRMS	High resolution mass spectrometry
LC-MS	Liquid phase Chromatography-Mass spectrometry
NMR	Nuclear Magnetic Resonance
NOESY	Nuclear Overhauser Effect Spectroscopy
PPI	Protein-protein interaction
RMSD	Root Mean Square Deviation
SAR	Structure-Activity Relationship
SPS/SPPS	Solid phase synthesis/ Solid phase peptide synthesis

Amino acids codes

Amino acid name	Three-letter code	One letter code
Alanine	Ala	A
Arginine	Arg	R
Asparagine	Asn	N
Aspartic acid	Asp	D
Cysteine	Cys	C
Glutamic acid	Glu	E
Glutamine	Gln	Q
Glycine	Gly	G
Histidine	His	H
Isoleucine	Ile	I
Leucine	Leu	L
Lysine	Lys	K
Methionine	Met	M
Ornithine	Orn	O
Phenylalanine	Phe	F
Proline	Pro	P
Serine	Ser	S
Threonine	Thr	T
Tryptophan	Trp	W
Tyrosine	Tyr	Y
Valine	Val	V

Chapter 1

Protein-Protein Interactions as Therapeutic Targets

Section 1.2.2 of this Chapter contributed to a review article published in *Nature Chemistry*.¹

Protein-protein interactions (PPIs) mediate a number of essential cellular processes and their implication in numerous diseased states makes them desirable targets for therapeutic intervention. Inhibiting PPIs, however, was initially considered a daunting challenge, as it was unclear how to effectively and selectively target them using small molecules. Recent advances in the field have contributed to change the collective perception on PPIs and new strategies have been developed that are turning PPIs into more tractable targets. These strategies will be discussed later in this Chapter and have been recently reviewed.² PPI inhibitors must cover 800-1100 Å² of a protein surface and complement the projection of hydrophobic and charged domains on a relatively flat surface. PPIs are therefore very different from the more traditional enzyme-substrate kind of interaction where a small substrate binds in a well-defined cavity on the enzyme. In the latter case, structural features of the substrate or the cavity itself can guide the design of competitive inhibitors, whereas PPIs lack those defining features, which caused them to be considered undruggable until a few decades ago. PPIs bring into play electrostatic, hydrophobic and hydrophilic interactions, however studies have shown that hydrophobic interactions are generally the driving force for the formation of protein-protein complexes.³ Common methods to discover inhibitors of PPIs are: the investigation of peptides derived from short contiguous sequences at the interface (*e.g.* peptidomimetics)⁴ and the development of biopharmaceutical compounds that usually bind to PPI

surfaces *e.g.* monoclonal antibodies⁵ or polypeptide hormones.⁶ High throughput screening (HTS) has also been exploited to this end, but only showed limited success in identifying inhibitors of PPIs (*e.g.* the Nutlins).⁷ Other conventional methodologies used in drug discovery to identify lead compounds have also proven rather unsuccessful when applied to PPIs. These approaches are limited for several reasons.⁴ The relatively large and featureless interface makes it hard for a small molecule to be competitive and to achieve selective binding to an individual protein. Furthermore, the binding of protein partners often involves areas of the protein surfaces that are far apart and thus cannot be mimicked by simple synthetic peptides. Few “drug-like” small molecules have been identified from library screening as effective PPIs disruptors; however several starting compounds with K_d in the mid-micromolar range have been identified by HTS. Medicinal chemistry approaches have then improved the properties of these hits and generated compounds with K_d in the mid/low nanomolar range (this was the case for binders of IL-2, Bcl-xL, hDM2 and HPV E2).⁸ One reason for which HTS of existing libraries does not provide efficient PPI disruptors is that these libraries are the result of past research effort into GPCRs (G-Protein coupled receptors),^{9, 10} and more traditional, druggable targets. Despite these facts, intense research efforts have yielded successful approaches to the modulation of PPIs and examples of the inhibition of two protein partners with low molecular weight ligands have been reported, some of them are currently in clinical trials.⁷

The α -helix is the most prominent structural motif in proteins and as such is commonly found at protein-protein interfaces.^{11, 12} The α -helix was the first-described secondary structure discovered by Linus Pauling in 1951, after William Astbury’s pioneering studies at Leeds on the X-ray diffraction of keratin.¹³ This discovery constitutes one of the major breakthroughs in contemporary science. An ideal alpha helix consists of H-bonds between every i^{th} CO and $(i + 4)^{\text{th}}$ NH, with 3.6 residues per turn and a pitch of 5.4 Å, the contiguous arrays of hydrogen bonds giving rise to a rigid rod-like structure (Fig. 1.1).¹⁴ In many α -helix mediated PPIs, a few key residues located along one face of the helix insert deep in a cleft on the partner protein and are critical for binding. The existence of such “hot-spot residues” at the interface of two interacting proteins was first

evidenced by a mutagenesis study conducted by Clackson and Wells,¹⁵ and was more widely discussed by Stites in 1997.¹⁶

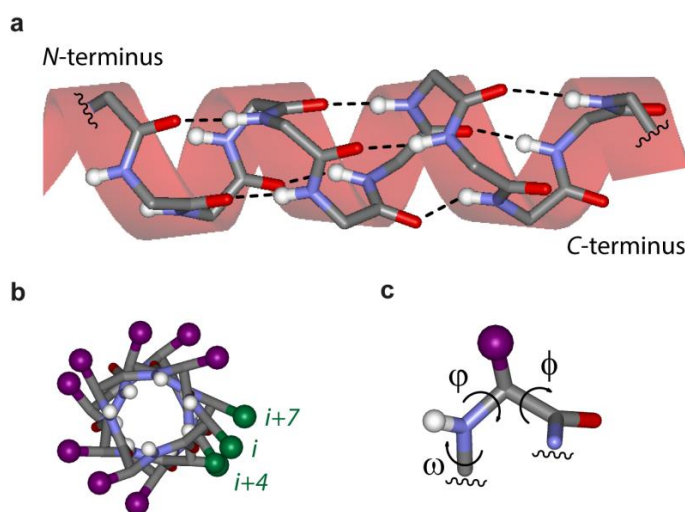


Figure 1.1 The alpha-helix. **a.** Intramolecular H-bond network within the α -helix (side chain atoms are omitted for clarity). **b.** View of an α -helix along the helical axis, the side chains are represented by purple balls, except for those at positions i , $i + 4$ and $i + 7$ which are represented in green. **c.** Torsion angles in polypeptide bonds.

The intrinsic properties of α -helices¹⁷ dictate that hot-spot residues located on the same helical face should be located at defined positions on the helix, namely i , $i + 3$ or $i + 4$, $i + 7$ or $i + 8$ etc. Mutagenesis studies have confirmed that this combination of residues is a recurrent pattern in a number of therapeutically relevant interactions, such as the gp41 protein, responsible for the fusion process enabling HIV infection,¹⁸ the p53/hDM2 interaction¹⁹⁻²² and the Bcl-2 family of interactions.²³⁻²⁵ These key oncogenic targets will be described in the next section. Designing a molecule that could mimic the spatial presentation of the key residues is an attractive strategy adopted by several research groups (Fig. 1.2).

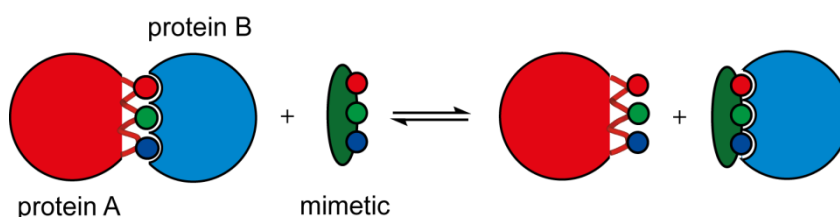


Figure 1.2 Disruption of an α -helix mediated PPI by a designed inhibitor replicating the spatial presentation of key binding residues.

Three main categories of mimetics arise: peptide-based scaffolds, proteomimetics²⁶ and small molecules; they will be described in the third section of this Chapter. The development of α -helix mimetics is a key field of research in the Wilson group. As illustrated in Fig. 1.2, the strategy is to design a scaffold that would mimic the spatial projection of key residues from protein A to achieve competitive binding with protein B, thereby allowing protein A to play a beneficial role. The p53/hDM2 and related p53/hDMX PPIs were chosen as starting points for this study, as they are suitable model targets to elaborate a general approach to the disruption of α -helix mediated PPIs.

1.1 Targets and insight into their biological context

1.1.1 The p53/hDM2 interaction

1.1.1.1 Generalities and structure of p53

p53 plays a pivotal role in the cell cycle, but also in a cell's defence against cancer, as a powerful growth suppressor and pro-apoptotic protein.²⁷ It was identified in 1979 by Lionel Crawford, David P. Lane, Arnold Levine and Lloyd Old and was named for its apparent molecular mass on SDS-PAGE: 53 kDa; however its real mass calculated from its amino acid residues is only 43.7 kDa. This difference is due to the high number of proline residues in the protein, which slow its migration in SDS-PAGE, making it appear heavier than it actually is.²⁸ The protein is 393 amino acids long and is constituted of six domains:

- the *N*-terminal transcription-activation domain (TAD), also known as activation domain 1 (AD1) which activates transcription factors and contains the hDM2 binding site (residues 1-42);
- the activation domain 2 (AD2) important for apoptotic activity (residues 43-63);
- the proline rich domain important for the apoptotic activity (residues 64-92);
- the central DNA-binding core domain (DBD, Fig. 1.3), which contains one zinc atom and several arginine amino acids (residues ~ 100-300). 90% of p53 mutations found in human cancers occur in this region which contains highly conserved domains;

- the homo-oligomerisation domain (OD, residues 307-355), consists of a β -strand followed by an α -helix necessary for dimerisation, as p53 is composed of a dimer of dimers. Tetramerisation is essential for the activity of p53 *in vivo*. The OD also includes a nuclear export signal (NES, residues 316-325);
- the C-terminal domain contains three nuclear localisation signals (NLS) and a non-specific DNA binding domain that binds to damaged DNA. This region is also involved in down regulation of DNA binding of the central domain (residues 356-393).

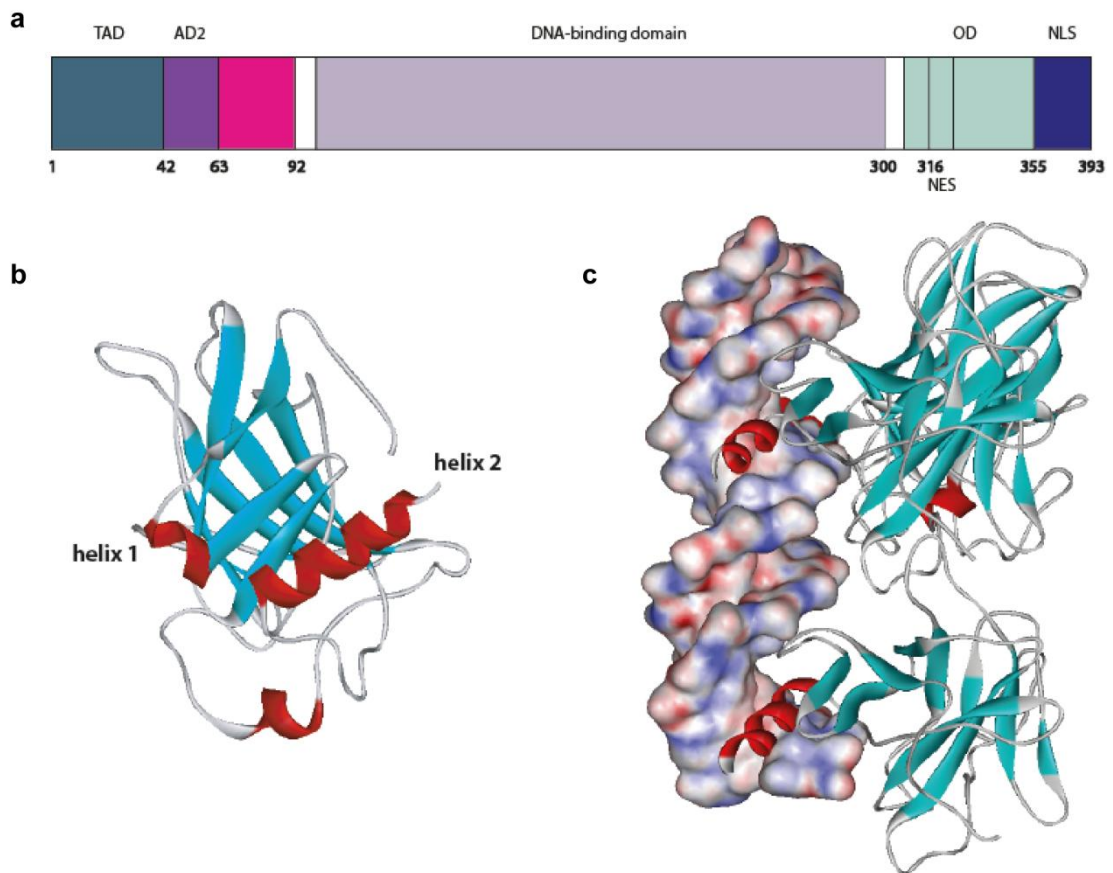


Figure 1.3 p53 directly binds DNA to exert its post-transcriptional activity. a. Domain structure of p53. **b.** 3D structure of the central DNA-binding domain of p53 (PDB ID: 3EXJ), helix 2 has the ability to bind to DNA. **c.** p53 core domain as an oligomer (ribbons) bound to DNA (surface), (PDB ID: 1TSR).

p53 plays a central role in cell cycle regulation. Its major role is to maintain the stability of the genome by preventing the multiplication of any cell whose DNA has undergone mutations, and it is thus involved in preventing cancer. p53 has

several anti-cancer functions: activation of DNA repair, inducing growth arrest by holding the cell cycle, or initiation of apoptosis if the DNA cannot be repaired. The TP53 gene, which encodes for p53 is affected in approximately half of all cases of human tumours, either by mutation or deletion.²⁹ Some mutant p53s can no longer bind to DNA, therefore p21 (a cyclin-dependant kinase inhibitor whose expression is tightly controlled by p53) cannot be produced and play its role as a stop-signal for cell division, which becomes uncontrollable, thus resulting in the formation of tumours.³⁰ Mutations that deactivate p53 in cancer usually occur in the DNA-binding domain, preventing the protein from binding to its target DNA sequences and activating the transcription of these genes.³¹ The p53 protein is activated in response to stressful stimuli such as DNA damage, hypoxia, spindle damage, nitric oxide, heat/cold shock, viral infection and oncogenic activation.³² Upon activation, the association between p53 and its negative regulator *hDM2* is abolished, the half-life of the protein is drastically increased, which induces its accumulation in the nucleus and a conformational change allows p53 to take on an active role as a transcription factor in these cells. The critical event leading to the activation of p53 is the phosphorylation of its *N*-terminal domain. This domain contains a large number of phosphorylation sites and is therefore one of the primary targets for protein kinases transducing stress signals. In the response phase, p53 activates the transcription of a large number of p53-regulated genes that are responsible for cell cycle arrest or apoptosis. If the cell cycle is arrested, the cell can trigger repair mechanisms, some of which are directly activated by p53. Genes involved in cell cycle arrest include *hDM2* and p21; and those involved in the intrinsic apoptotic pathway encode pro-apoptotic members of the Bcl-2 family such as Bax, Noxa B and Puma.³³ Once the repair is completed, the concentration of p53 returns to a normal level and the cell cycle resumes. If the cell is too damaged to be repaired, it then undergoes apoptosis. In this mechanism, the role of p53 is to activate the transcription of the Bax and Bak genes. Bax and Bak can then form oligomers, which perforate the mitochondrial membrane and allow cytochrome *c* to reach the cytoplasm, where it activates the caspase cascade, a key event in the process of apoptosis.³⁴ However, it is still unclear how and why some cells undergo apoptosis whilst others go through cell cycle arrest.

1.1.1.2 Structures and functions of *hDM2* and *hDMX*

As p53 mediates growth arrest and apoptosis under stressful conditions, it is essential to keep its activity under control during normal development. p53 is thus tightly regulated under both normal and stressful conditions by nuclear export and degradation *via* the ubiquitin-dependant proteasome pathway.^{35, 36} This degradation is mediated by interactions with two negative regulators: *hDM2* and *hDMX*. *mDM2* (murine double minute 2) designates the gene and the 491-amino acid long protein for which this gene codes in mice.²² The human homologue of this protein was later identified and is referred to as *hDM2*. *hDM2* is one of the major regulators of p53 and both proteins control one another's cellular levels. *hDM2* is also a responsive gene : its transcription can be activated by p53, thus when p53 is stabilised, the transcription of *hDM2* is also induced, resulting in higher *hDM2* protein levels. Increased *hDM2* levels regulate p53 activity in three ways:

- *hDM2* binds to the *N*-terminal domain of p53, blocking its transcriptional activity;
- *hDM2* induces nuclear export of p53;
- *hDM2* stimulates degradation of p53 via the E3 ubiquitin ligase - proteasome pathway : it covalently attaches ubiquitin to p53, marking it for proteasome degradation.

It was demonstrated that mice lacking the *mDM2* gene are embryonic-lethal (die early in development), but this lethality was fully rescued by deletion of p53, suggesting that the activity of p53 is regulated by *hDM2*.^{37, 38} *hDMX* (also known as *hDM4*) is a structural homologue of *hDM2* possessing 490 amino acid residues and shares the same arrangement of structural domains, except that *hDMX* lacks the ubiquitin-ligase function. Like *hDM2*, a knockout of *hDMX* in mice resulted in embryonic-lethality, and the double knockout of *hDMX* and p53 was shown to be viable.³⁹ *hDM2* and *hDMX* are directly involved in p53 functional inactivation in approximately 40% of tumours, making them attractive drug targets⁴⁰ and they both repress p53 transcriptional activity by binding to an amphiphilic helix of its *N*-terminal domain. Several lysine residues in the p53 *C*-terminus have been identified as the sites of ubiquitination. *hDM2* is capable of

auto-polyubiquitination, and in complex with p300, a cooperating E3 ubiquitin ligase, is capable of polyubiquitinating p53.³⁵ In this manner, *hDM2* and p53 are both members of a negative feedback control loop that keeps the level of p53 low in the absence of p53-stabilising signals. This loop can be interfered with by kinases and genes like p14arf when p53 activation signals including DNA damage are high. However, ubiquitination of p53 is reversible through a ubiquitin specific protease (HAUSP).⁴¹ This is one way by which p53 is stabilised in response to oncogenic insults. *hDMX* also binds to p53 and inhibits p53-dependent transcription. *hDMX* is overexpressed in 10-20% of various tumours, again resulting in the suppression of p53 activity.⁴²

In contrast to *hDM2*, *hDMX* cannot act as a ubiquitin ligase to control the stability of p53, but instead is mainly responsible for regulating its transcriptional activity.⁴³ As the loss of *hDM2* or *hDMX* leads to embryonic lethality,³⁷ their expression is necessary for regulation of p53 during normal development. On the other hand, the overexpression of *hDM2* abolishes the ability of p53 to induce cell cycle arrest and apoptosis.⁴⁴ An overexpression of *hDM2* is observed in 40-60% of human oestrogenic sarcomas and about 30% of soft tissues sarcomas, where wild type p53 is retained.⁴⁵ *hDM2* was initially validated as a drug target for antisense oligonucleotides, monoclonal antibodies and small peptides.^{46, 47} In antisense oligonucleotide therapy, the oligoDNA sequences are complementary to the DNA or RNA sequence of their target gene. Antisense oligonucleotides that inhibit expression of *hDM2* also demonstrate significant activation of p53, resulting in growth arrest and/or apoptosis in cancer cells. Some second generation antisense oligonucleotides displayed antitumor activity both *in vitro* and *in vivo*.⁴⁰ Acting synergistically in tumour cells, *hDM2* and *hDMX* have become two of the most attractive molecular targets for cancer therapy.⁴⁰

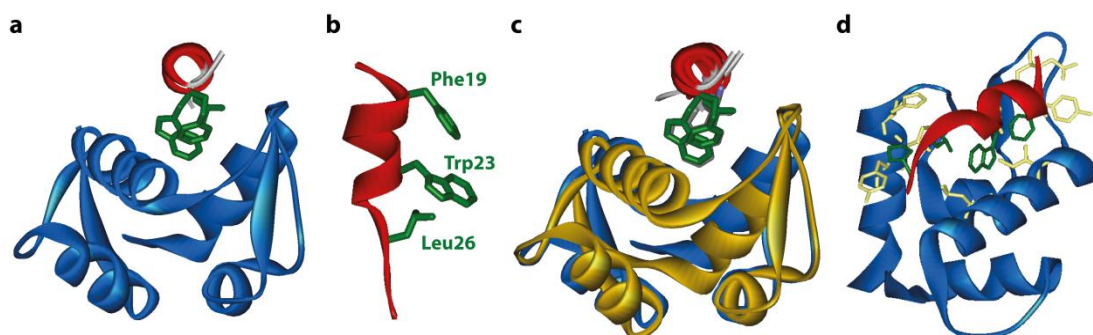


Figure 1.4 The p53/hDM2 and related p53/hDMX interactions. **a.** Structure of *hDM2* bound to p53 (PDB ID: 1YCR), the 3 key residues of p53 (green) insert deep into a hydrophobic cleft on *hDM2*. **b.** The native p53 helix. **c.** Overlay of the crystal structures of p53 bound to *hDM2* (blue, **a**) and *hDMX* (gold, PDB ID: 3DAC), highlighting the structural homology between the two proteins. **d.** Interfacial residues are shown for both p53 (green) and *hDM2* (yellow).

A crystal structure of p53 (residues 15-29) bound to the p53-binding domain of *hDM2* (residues 19-102) showed that p53 forms an amphiphilic α -helix interaction with a deep hydrophobic cleft on *hDM2*, where three key hydrophobic residues play an essential role in the binding : Phe19, Trp23 and Leu26 located at positions i , $i + 4$ and $i + 7$ of the p53 helix²² (Fig. 1.4). Since the loss or mutation of p53 function is associated with tumour growth, reactivating wild type (WT) p53 in tumours where its function has been suppressed by *hDM2* and related regulators has become an attractive approach for novel anticancer therapeutic strategies.²¹ This justifies the intensive search for a small molecule inhibitor that could disrupt the p53/*hDM2* interaction by specifically binding to this area, and release p53 which in turn would activate the p53 pathway. Recent structural studies revealed extensive similarity between the p53-binding site of *hDM2* and *hDMX* in overall folding and the shapes of their p53-binding pockets, however a few sequence differences result in a smaller hydrophobic cleft in *hDMX* that prevents efficient binding of some compounds that show a good affinity with *hDM2*.⁴⁸ In general, antagonists designed for *hDM2* inhibition are significantly less efficient against *hDMX*, which limits their potential as ‘drugs’.

1.1.2 The Bcl-2 family of interactions

1.1.2.1 Generalities and structure of the Bcl-2 family

Bcl-2 (B-cell lymphoma 2) designates a family of mammalian genes and the proteins they produce. 25 genes in the Bcl-2 family are known to date and the number of family members identified is constantly growing. They govern mitochondrial outer membrane permeabilisation (MOMP) and can be either pro-apoptotic (*i.e.* Bax, Bak, Noxa B, and Puma) or pro-survival (including Bcl-2 proper, Bcl-x_L and Mcl-1). The most well known Bcl-2 family members and their binding partners are reported in Table 1.1.

Table 1.1 Bcl-2 family members and their binding partners.

Sub-family	Protein name	Known binding partners (PDB ID indicated where applicable)
Anti-apoptotic members	Bcl-2	Bim (4B4S), Bid, Bad, Bax (2XAO), Puma, Bmf
	Bcl-x _L	Bim (3FDL, 1PQ1), Bad (2BZW), Puma, Bax (3PL7), Bak (2LP8), Bid, Bad (1G5J), Bmf
	Mcl-1	Noxa B (2NLA), Bim (2NL9), Puma (2ROC), Bax (3PK1), Noxa A (2ROD), Bim (3KJO), Puma, Bmf, Bid (2KBW)
	A1	Bim (2VM6), Puma (2VOF), Bak (2VOH), Bid (2VOI), Bmf (2VOG), Noxa B
	Bcl-w	Bim, Puma, Bid (1ZY3), Bad, Bmf, Bax
Multidomain Pro-apoptotic members	Bak	A1, Bcl-x _L , Bax, Bid
	Bax	Bak, Bcl-2, Bcl-w, Bcl-x _L , Mcl-1, Bid
BH3-only Pro-apoptotic members	Bim	Mcl-1, A1, Bcl-x _L , Bcl-w, Bcl-2
	Bad	Bcl-x _L , Bcl-w, Bcl-2
	Noxa B	Mcl-1, A1
	Bid	Bcl-w, Mcl-1, A1, Bcl-x _L , Bak (2M5B)
	Puma	A1, Mcl-1, Bcl-x _L , Bcl-w, Bcl-2
	Bmf	Bcl-2, A1, Bcl-x _L , Bcl-w, Mcl-1

The members of the Bcl-2 family share one or more of the four characteristic domains of homology entitled the Bcl-2 homology (BH) domains, named BH1, BH2, BH3 and BH4. These domains are known to be crucial for function, as deletion of these domains affects survival/apoptosis rates.⁴⁹⁻⁵¹ The Bcl-2 family

comprises three subfamilies that contain between one and four BH domains. The anti-apoptotic subfamily comprises proteins that conserve all four BH domains. The pro-apoptotic Bax-like subfamily lacks BH4 domains whereas another pro-apoptotic subfamily of proteins only have the BH3 domain, and are called the BH3-only proteins (Bad, Puma, Noxa B, etc.). The multi-domain Bcl-2 family members (anti-apoptotic and the Bax-like proteins) also share a C-terminal membrane-anchoring sequence and a similar 3D structure : an eight-helix bundle that creates a groove into which helical BH3-domain peptides bind.⁵² The sequence that determines whether the protein will carry out a pro-apoptotic or pro-survival function remains elusive. In a viable cell, the pro-apoptotic Bcl-2 family members Bax, Bak, and BH3-only proteins are antagonised by anti-apoptotic members. In response to an apoptotic stimulus, BH3-only members are activated and prevent anti-apoptotic Bcl-2 members from inhibiting pro-apoptotic members. In addition, they might directly induce a conformational change of Bax and Bak which subsequently oligomerise and insert into the mitochondrial outer membrane where they form pores either by themselves or by associating with the permeability transition pore complex (Fig. 1.5).⁵³

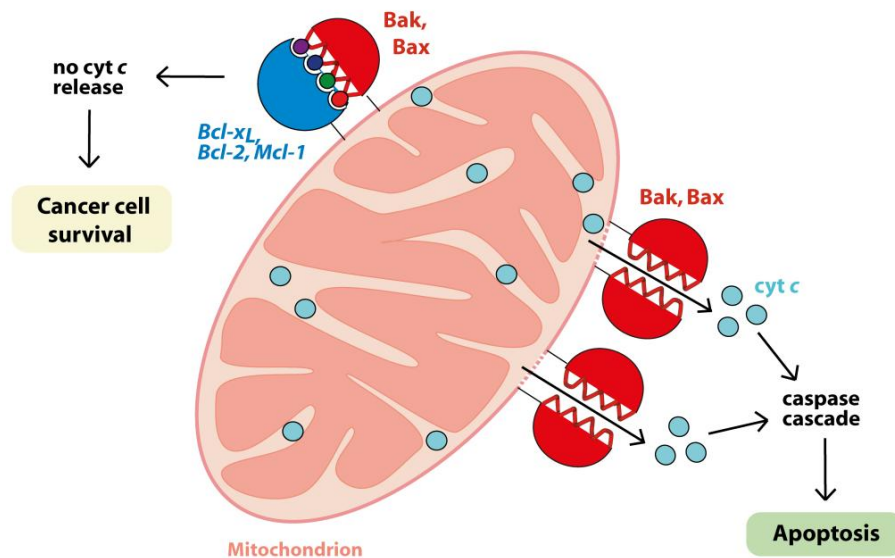


Figure 1.5 Role of the Bcl-2 proteins in the induction of apoptosis. In cancer cells where the apoptotic pathway is not impaired, the multidomain pro-apoptotic members (Bax and Bak, red) can oligomerise, thereby releasing cytochrome *c* from the mitochondrion and in turn trigger apoptosis. In cases where anti-apoptotic members (blue) are overexpressed, apoptosis is blocked and the cancer cell survives.

In consequence, apoptotic factors such as cytochrome *c* are released from the inner mitochondrial membrane into the cytosol, which contributes to the formation of the apoptosome and the subsequent activation of the caspase cascade and the induction of apoptotic cell death.²⁵

1.1.2.2 Pro-apoptotic members of the Bcl-2 family

Interactions between pro-survival and pro-apoptotic proteins govern cell-fate and the pro-apoptotic BH3-only proteins play a pivotal role in promoting apoptosis. Bak and Bax are both essential for apoptosis, given that cells in which they were both deleted are essentially resistant to apoptosis.^{54, 55} Various apoptotic stimuli induce expression and/or activation of specific BH3-only family members, which translocate to the mitochondria and initiate Bax/Bak-dependant apoptosis, however the “life/death switch” mechanism is still elusive. The binding profiles of the BH3-only proteins have been established, and their crystal structures in complex with their targets constituted a starting point for the design of the first inhibitors (Fig. 1.6). Subsequently, many non-natural BH3 sequences have been synthesised and showed new binding profiles, indicating that target-selective small molecule antagonists might be found.

Noxa B is one of the BH3-only pro-apoptotic members of the Bcl-2 family. It only shows weak pro-apoptotic activity on its own, but appears to be crucial in the mitochondrial Bcl-2-regulated pathway of apoptosis, by targeting the pro-survival protein Mcl-1 for proteasomal degradation. Studies showed that in certain tissues, Noxa B induction in response to DNA damage could occur in a p53-independant manner, and also suggested a possible tumour suppressor function for Noxa B independent of the p53 status of a cell.⁵⁶ Apoptosis induced by Noxa B is accompanied by cytochrome *c* release and subsequent caspase activation. No binding of Noxa B to pro-apoptotic Bak or Bax has been reported so far, suggesting that it inhibits anti-apoptotic members of the Bcl-2 family.⁵⁷

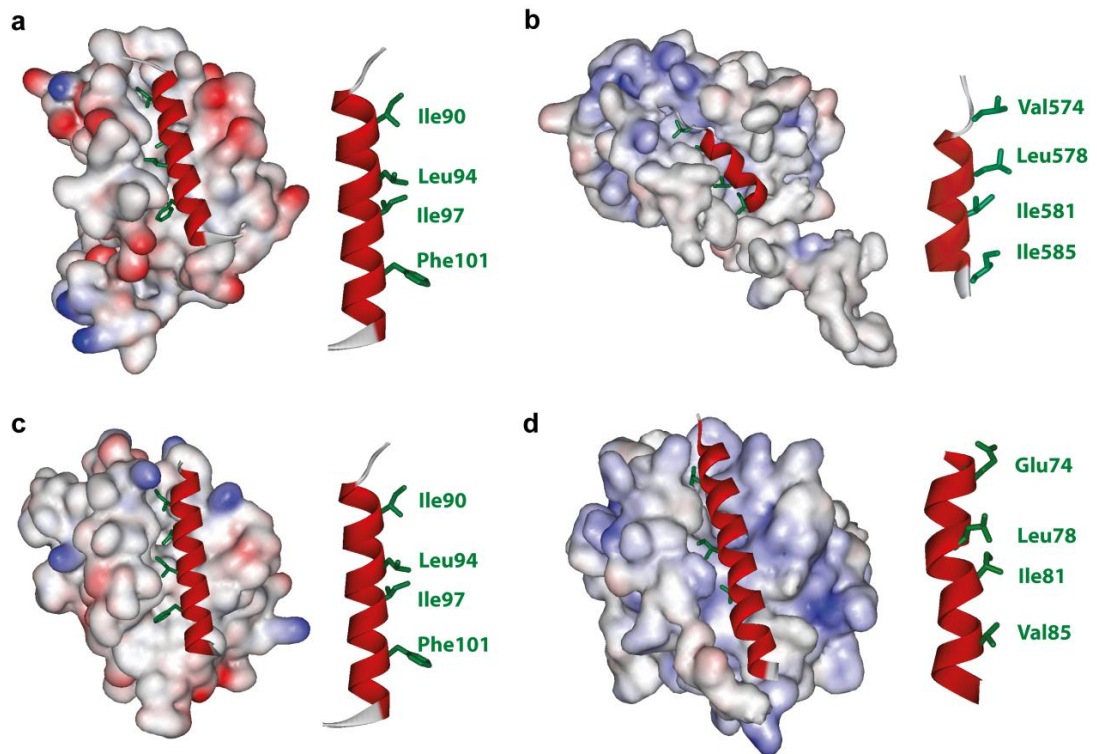


Figure 1.6 Crystal structures of pro-survival proteins (surface) with BH3 ligands (ribbons), key residues are represented in green. a. Bcl-x_L/Bim BH3 (PDB ID: 3FDL using Bcl-x_L 1-209 and deletion of residues 27-82). **b.** Bcl-x_L/Bak (PDB ID: 1BXL using Bcl-x_L 1-221). **c.** Mcl-1/Bim BH3 (PDB ID: 2NL9). **d.** Mcl-1/Noxa B (PDB ID: 2JM6, NMR structure).

Compared to other BH3-only proteins like Bim and Puma, which bind all survival Bcl-2 proteins with comparable affinities, Noxa B selectively binds to Mcl-1 (and A1 albeit with a lower affinity).⁵⁸ The possible involvement of Noxa B in oncogenesis is still under investigation, however its importance as a drug target became evident when analysing the efficiency of the BH3-mimetic ABT-737, mentioned in a later section of this chapter.

1.1.2.3 Pro-survival members of the Bcl-2 family

Many cancer cells overexpress the anti-apoptotic family members Bcl-2, Bcl-x_L and Mcl-1 to evade apoptosis.⁵² It has also been shown that overexpression of Bcl-2 can inhibit the potency of many currently available anticancer drugs by blocking the apoptotic pathway.⁵⁹ The anti-apoptotic Bcl-2 proteins block apoptosis by preventing BH3-only protein-induced oligomerisation of the pro-

apoptotic Bcl-2 family members Bax and/or Bak in mitochondrial outer membranes, which would otherwise lead to the efflux of cytochrome *c* and other mitochondrial intermembrane space proteins. The anti-apoptotic Bcl-2 proteins differentially bind to the BH3-only proteins. Some BH3-only proteins (for example Bid and Bim) interact with essentially all anti-apoptotic Bcl-2 proteins, whereas others (for example Noxa B) interact only with certain Bcl-2 family members.⁵⁶ Mcl-1 seems to have a different behaviour to the other anti-apoptotic proteins, as some studies reveal that Mcl-1 degradation during cell death is uniquely associated with the formation of the Mcl-1/Noxa B complex, whereas the Mcl-1/Bim or Mcl-1/Puma interactions lead to its stabilisation. Moreover, ABT-737 efficiently antagonises Bcl-2, Bcl-x_L and Bcl-w, but is ineffective in killing tumour cells expressing high levels of Mcl-1. Knockdown of Mcl-1 helped to restore the sensitivity to ABT-737 treatment in resistant colon and bladder cell lines.⁶⁰ The development of a Noxa B-like BH3 mimetic or a mimetic that also targets Mcl-1 is therefore highly desirable to overcome ABT resistance and should significantly increase treatment efficiency of current and novel treatment strategies against cancer.

1.2 Inhibition of α -helix mediated PPIs

Several approaches have been adopted by research groups to achieve inhibition of α -helix mediated PPIs by replicating the hot-spot residues involved in the binding event. These strategies can be divided into three categories according to the nature of the backbones they employ:

- **Type I** mimetics mimic the local topography of the structural motif; for example peptide backbone mimetics. The analogy is applicable at the atomic level.
- **Type II** mimetics are the functional mimetics, which are generally small non-peptide molecules that bind to the corresponding receptors. These functional mimetics need not mimic the structure of the original motifs.
- **Type III** mimetics are in general non-peptide scaffolds that serve as topographical mimetics, with their substituents mimicking the side-chains of important amino acid residues.

This section will be focused on inhibition of PPIs that involve binding through a single helical face, such as the p53/*hDM2*, p53/*hDMX*, gp41 fusion and Bcl-2 family of interactions. The discussion will therefore be limited to inhibitors that can mimic the i , $i + 4$ and $i + 7$ (and where applicable $i + 11$) positions of an α -helix.

1.2.1 Small molecule inhibitors

High throughput screening (HTS) has provided most of the small molecule inhibitors reported,^{61, 62} including the Nutlins⁷ – a series of compounds containing some of the most potent and clinically advanced inhibitors of the p53/*hDM2* interaction known to date.⁶³ Other potent inhibitors have been identified through structure-based design,^{63, 64} or a combination of screening methods and structure-based design.⁶⁵

1.2.1.1 Small molecule inhibitors of PPIs discovered by HTS

- A series of cis-imidazoline analogues known as the Nutlins were identified from a high-throughput screen by Vassiliev and co-workers at Roche.⁷ They are the first potent and selective small molecule inhibitors of the p53 – *hDM2* interaction, and represent the best characterised class of inhibitors to date. Nutlins bind to the p53-binding site of *hDM2* by mimicking the interaction with the three key residues. They display IC₅₀ values against p53/*hDM2* PPI in the range of 90-260 nM with eudismic ratios of 150-200 (quotient of activities of the enantiomers). Nutlins-1, 2 and 3 (compounds **1**, **2** and **3**, Fig. 1.7) were shown to have good cell permeability. Studies have shown that the Nutlins activate the p53 pathway in cancer cells, leading to cell cycle arrest, apoptosis and inhibition of tumour growth in mice.⁷ Compound **3** (Fig. 1.7) has been the most extensively studied. *In vivo* experiments with osteosarcoma SJS-1 tumour xenograft in nude mice demonstrated that this compound was well tolerated, inhibited 90% of tumour growth and caused tumour shrinkage. These studies provided the first *in vivo* proof-of-concept that activation of WT p53 by small molecule inhibitors of the p53/*hDM2* PPI is viable and may provide excellent therapeutic potential in cancer therapy.

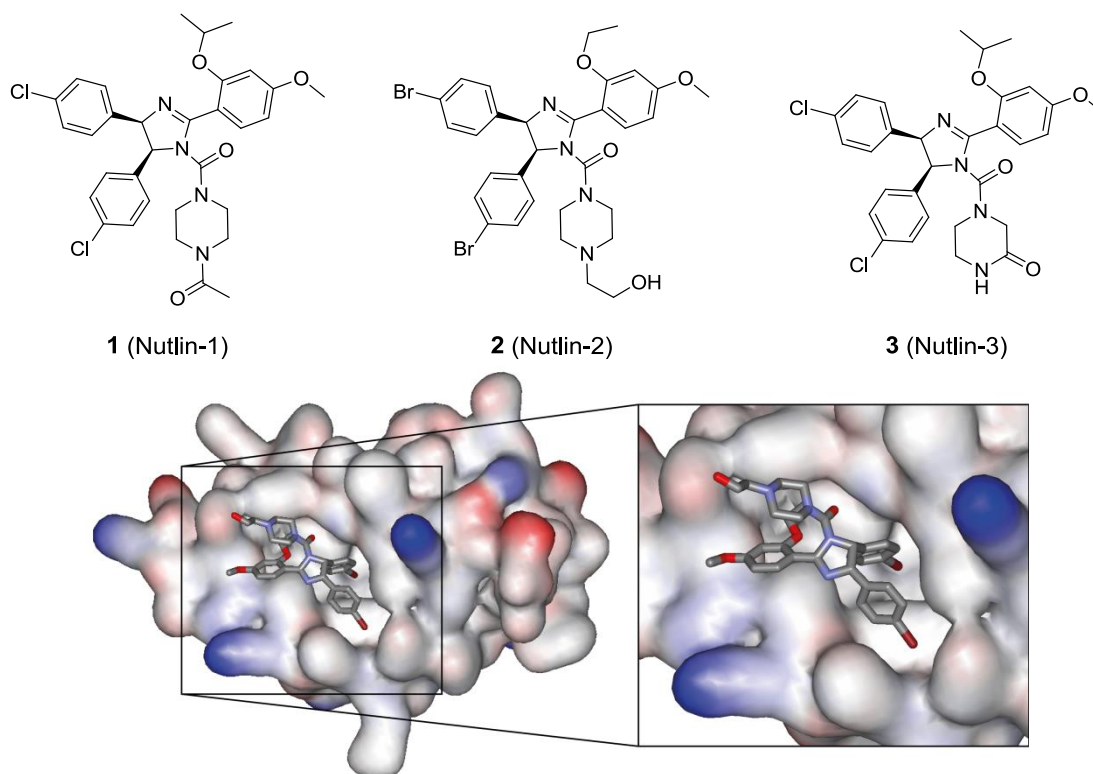


Figure 1.7 Structures of the Nutlin compounds (1, 2 and 3, active enantiomers) and crystal structure of Nutlin-2 bound to *hDM2* (PDB ID: 1RV1).⁷

Some studies showed that the Nutlins did not bind to *hDMX* and that overexpressed *hDMX* could block the ability of *cis*-imidazolines to induce apoptosis, thus limiting the clinical effectiveness of these inhibitors. However, combination therapy may be an effective way to overcome *cis*-imidazolines resistance in cancers with *hDMX* aberrations.⁶⁶ Clinical trials on the Nutlin compounds are still underway.⁶⁷

- Benzodiazepinediones⁶⁸ (BDP) are another well-documented series of p53/*hDM2* inhibitors that were discovered using HTS at Johnson and Johnson. They were found to decrease the proliferation of cancer cells. A co-crystal structure of *hDM2* with compound 4 (Fig. 1.8) showed that it projected its three phenyl rings into the p53 binding site of *hDM2* by mimicking the spatial arrangement of the p53 triad motif. However, this BDP exhibited poor pharmacokinetic properties and poor cellular permeability.

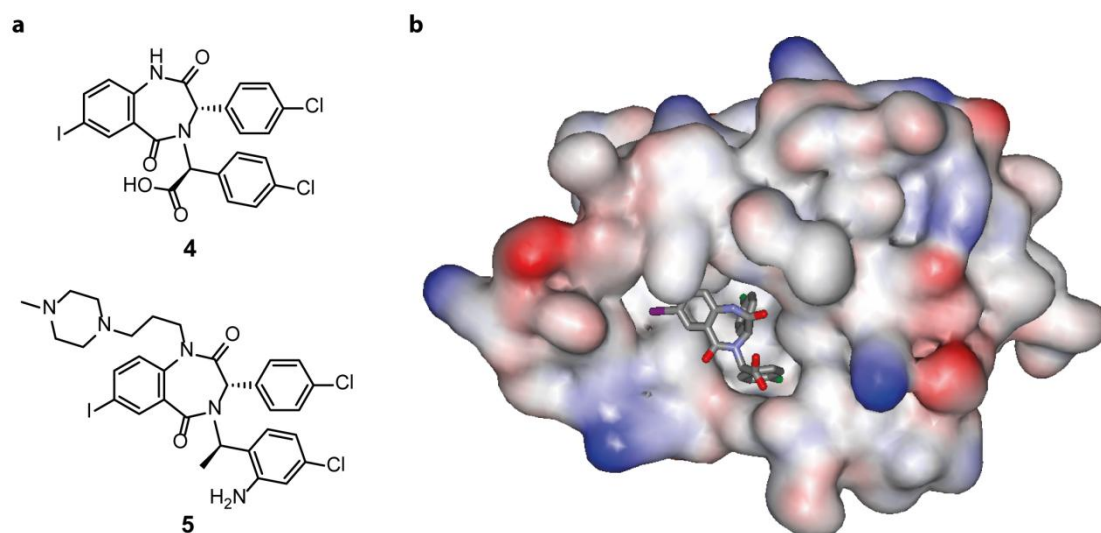


Figure 1.8 Benzodiazepinediones as inhibitors of the p53/hDM2 interaction. a. Structure of two BDP inhibitors (**4** and **5**) and **b.** Crystal structure of BDP inhibitor **4** in complex with hDM2 (PDB ID: 1T4E).⁶⁸

Further optimisation led to the BDP **5** which was studied in a combination therapy and was proved to enhance Doxorubicin activity *in vivo*.⁶⁹ 79% of tumour growth inhibition was achieved with a combination of both compounds at doses that were inactive alone. Moreover, the combination dosage resulted in reduced toxicity due to the lower dosages required. This supported *in vivo* evidence that a small molecule hMD2 antagonist may offer therapeutic benefit as a combination therapy.

Screening of natural products libraries yielded some Bcl-2 inhibitors:

- A prodigiosin (bipyrrole containing natural product) was identified in a screen of a library of natural products. Lead optimisation resulted in compound **6** (also known as Obatoclax, Fig. 1.9), which binds to Bcl-2, Bcl-x_L, Bcl-w and Mcl-1 with low-micromolar affinity.⁶² This compound was shown to disrupt the Bak/Mcl-1 complex.⁷⁰ *In vitro* and *in vivo* studies confirmed the activity of **6** as a single agent in multiple cancer cell lines. Several modes of action have been suggested for this compound and doubts remain over the utility of this compound as its biological activity appears non-specific.

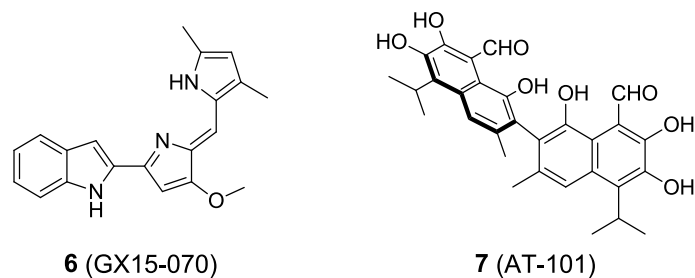


Figure 1.9 Structures of two natural product-derived Bcl-2 inhibitors.

- AT-101 (**7**, Fig. 1.9) is the development name for (-)-gossypol, a natural product derived from cotton plant and used in a wide range of therapeutic contexts. The active enantiomer was found to bind Bcl-2 ($K_i = 320$ nM), Bcl-x_L ($K_i = 480$ nM) and Mcl-1 ($K_i = 180$ nM).⁷¹ In studies conducted at Ascenta, AT-101 showed a similar cytotoxic potency to that of GX15-070 despite an approximately five fold tighter binding to Bcl-2 targets. As it displays good pharmacokinetic properties and manageable side effects, many gossypol derivatives have been developed.⁷²

1.2.1.2 Structure-based design of small molecule inhibitors of PPIs

Over the last decade, the explosion in the number of crystal structures that have been elucidated allowed several families of compounds to be developed to inhibit PPIs using structure-based design. The most potent/biologically active ones are described below:

- Compounds containing a spiro-oxindole scaffold were identified using structure-based drug design as inhibitors of the p53/hDM2 interaction. It has been shown that the oxindole ring mimics the side chain of Trp23, critical for binding to hDM2; and the hydrophobic- substituted spiropyrrolidine ring mimics the side chains of Phe19 and Leu26.⁷³ Primary optimisations of the first compounds obtained in this series led to compound **8** in Fig. 1.10, with a K_i of 86 nM in a fluorescence anisotropy-based assay. Further analysis of the crystal structure of p53/hDM2 revealed that the residue Leu22 was also critical for binding, which led to the inhibitor known as MI-63 (compound **9**, Fig. 1.10), with an improved K_i of 3 nM.⁷⁴ Despite its potent *in vitro* activity, compound **9** was unsuitable for *in vivo* evaluation due to a poor pharmacokinetic profile.

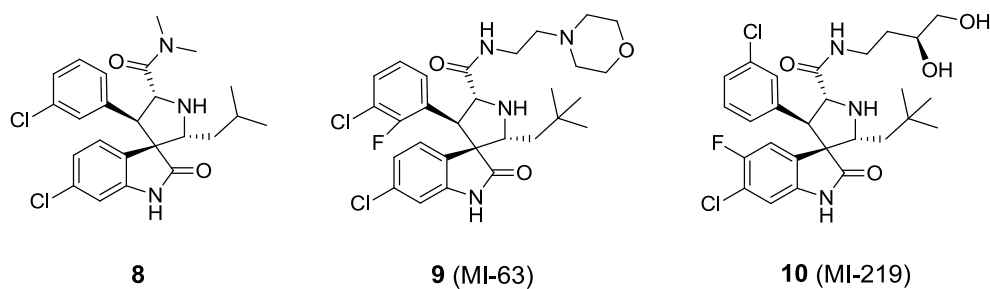


Figure 1.10 Spiro-oxindole inhibitors of the p53/hDM2 interaction.

Recently, extensive chemical optimisation of **9** yielded a modified analogue **10** (Fig. 1.10) containing a more solubilising side chain, with an improved pharmacokinetic profile and a K_i of 5 nM in the FA-based assay.⁶³

- **ABT-737 (11)**: Using SAR by NMR (Structure-Activity Relationship by Nuclear Magnetic Resonance), a proprietary technology developed by an Abbott team led by S. Fesik, Abbott researchers created three-dimensional maps of these proteins and discovered small molecules that bound tightly to the Bcl-2 family of proteins and demonstrated greater potency than any previously discovered compounds. This fragment screening allowed the development of ligands with high affinity for the hydrophobic groove of Bcl-x_L^{65, 75} (Fig. 1.11). The technique requires the screening of diverse fragments and identification of fragments that can simultaneously bind to proximal sites on the protein surface. Based on structural information, these fragments can be linked to produce a ligand whose binding affinity is theoretically the sum of the individual pieces⁷⁶ – providing that they can be linked in a way that allows the different moieties to bind in the same way as they do individually. Several ligands with low-nanomolar affinities have been developed through this method: A-385358, targeting Bcl-x_L (K_i = 0.8 nM) and Bcl-2 (K_i = 67 nM) displays cell-killing activity. Further studies and extensive chemical optimisation from A-385358 yielded compound **11** (ABT-737) which was reported to restore cell death to cancerous cells, thus inducing regression of solid tumours. Additionally, Abbott Bcl-2 family inhibitors were found to enhance the effects of chemotherapy and radiation in other types of cancer, such as non-small cell lung cancer.

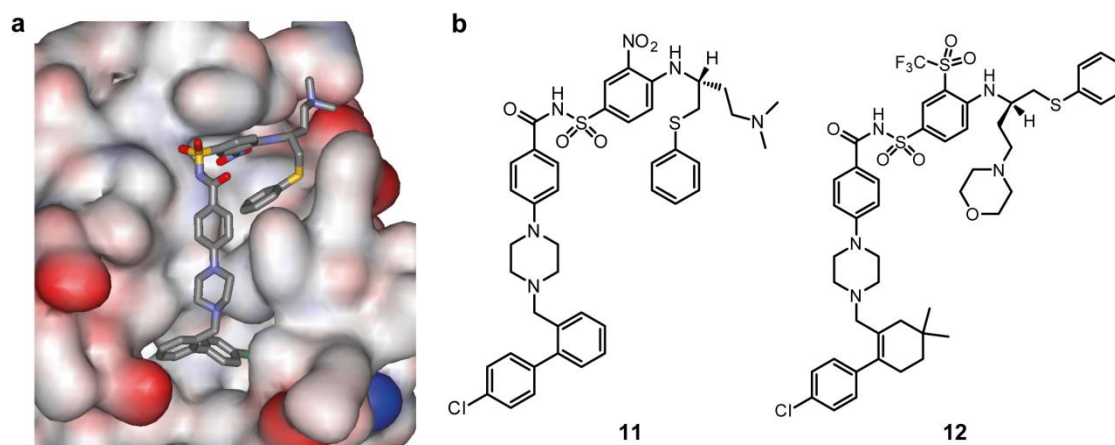


Figure 1.11 Abbott inhibitors of the Bcl-x_L/Bak interaction. **a.** Close up view of the crystal structure of **11** bound to Bcl-x_L (PDB ID: 2YXJ).⁷⁷ **b.** Structures of **11** (ABT-737) and **12**.

The linking process for this molecule proved difficult and required multiple synthetic strategies. Although fragment screening can identify the individual building blocks and their preferred binding orientation in the protein pocket, it can be challenging to link the moieties whilst maintaining the desired binding modes. Further modifications have resulted in a clinical candidate, **12** (ABT-263), which retains potency for Bcl-2, Bcl-x_L and Bcl-w and has a moderate oral bioavailability (F) in animal models (F = 20%).⁶³ This compound is currently in Phase II clinical trials.⁷⁸

1.2.2 Peptide inhibitors

Because of their large interacting surfaces, peptides offer the prospect of enhanced potency and high specificity in addition to a low toxicity. Early efforts to develop inhibitors of PPIs employed peptides that were directly derived from the native helical protein segments; however these presented rather poor cell penetration and were susceptible to proteolytic degradation. Most of the peptidic and peptidomimetic inhibitors of the p53/hDM2 interaction examined to date only bind hDM2 with affinities ranging from high nanomolar to low micromolar, and none is nearly as effective as the Nutlins (small molecule inhibitors developed by Roche, cf. Section 1.2.1) in tumour killing *in vitro*.^{7, 40} Numerous synthetic peptides, as well as natural product hDM2 inhibitors have been

identified; however, the most potent of these peptides only exhibited modest cellular activity due to poor cell permeability.^{79, 80} Several short peptides mimicking BH3-only proteins have been designed, but only displayed poor binding affinities to anti-apoptotic proteins probably due to a lack of helicity.⁸¹ Two main approaches to the stabilisation of a helical conformation are described in this section; they include constrained peptides made of natural α -amino acids, and the use of β -peptides⁸²⁻⁸⁶ and α/β -peptides,⁸⁷⁻⁹⁰ which display enhanced helicity and also offer the advantage of being stable against proteolytic degradation *in vitro* and *in vivo*.

1.2.2.1 Constrained peptides

The small difference (5–15 kcal/mol) in free energy between the folded and the unfolded states drives the equilibrium towards the formation of the folded structure. The contribution to this free energy is the result of the balance between enthalpic and entropic factors. Different strategies have been developed to stabilise peptides in a helical conformation, and are described in more details in the Wilson group's *Nature Chemistry* review.¹

- *α -Helix stabilisation by natural and non-natural amino acids:* Amino acids exhibit varied preferences for different secondary structures.⁹¹ Specific interactions between neighbouring side-chains (ion pairing or hydrophobic) can modulate the intrinsic propensities of various amino acids to stabilise or destabilise the helical structure.

- *Helix capping strategy:* Another strategy is the design of templates that can induce a particular conformation, when incorporated at the right position. In an α -helix, the first few residues at each terminus lack some intrahelical hydrogen bonds, thus only possessing limited helical character. The "helix capping"⁹² strategy refers to the stabilisation of the helical conformation within these terminal residues by introducing a template that forms a specific pattern of hydrophobic interactions and hydrogen-bonds.

- *Helix stabilisation by cross linking:* The induction of helicity by covalently cross linking the side-chains of otherwise unfolded peptide is an attractive

alternative for generating short and stable α -helical structures.⁹³ Several approaches have been developed, each of them making use of different cross-linking residues (both natural and unnatural), *i.e.* disulfide bridges, lactam bridges, hydrocarbon staples and hydrogen-bond surrogates (Fig. 1.12). These anchoring residues for cross-linking are in most cases inserted along a single helical face, ideally on the opposite side to where the hot-spot residues are located. The cross-link is therefore installed between residues at positions i and $i + 4$ or i and $i + 7$ depending on the length of the linker considered.

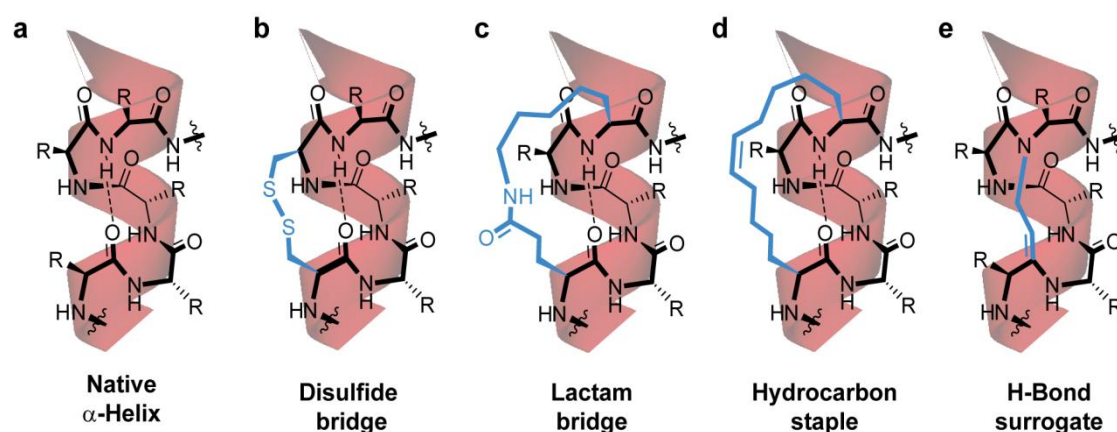


Figure 1.12 Covalent cross-linking strategies for the stabilisation of α -helical conformations (H-bonds are represented by a dashed line). **a.** Native α -helix. **b.** Disulfide bridge. **c.** Lactam bridge. **d.** Hydrocarbon staple. **e.** Hydrogen-bond surrogate.

- *Helix stabilisation via disulfide bridges* (Fig. 1.12b): Schultz *et al.* reported a short α -helical peptide stabilised by an intramolecular disulfide bond bridging the i and $i + 7$ residues.⁹⁴ Several other groups have investigated the use of disulfide bridges to stabilise α -helical peptides and inhibit PPIs,^{95, 96} but none of them were targeted to the p53/*hDM2* PPI or the Bcl-2 family of interactions and will therefore not be discussed in this manuscript.

- *Helix stabilisation via lactam bridges* (Fig. 1.12c): Rosenblatt and co-workers have initiated studies on lactam bridges as a method to stabilise α -helices.⁹⁷ The lactam link was installed between Lys and Asp at positions i and $i + 4$. As for the disulfide bridges, no helix stabilised *via* a lactam bridge was targeted to the model PPIs discussed in this manuscript and they will therefore not be described further.

- *Helix stabilisation via olefin metathesis* (Fig. 1.12d): Grubbs and co-workers inserted non natural amino acids bearing a side chain with a terminal alkene (*O*-allyl serines) into peptide sequences and demonstrated that cross-linking these residues *via* ring closing metathesis could yield peptides where the helical conformation is stabilised by the resulting macrocycle.⁹⁸ This strategy was slightly modified by Verdine and co-workers, who made use of α,α -disubstituted non natural amino acids instead of monosubstituted *O*-allyl serines. Disubstituted residues were already known to enhance helical propensity and were introduced in the sequence of p53 in place of two non-essential residues to yield a stabilized and potent inhibitor of the p53/*hDM2* PPI (Fig. 1.13a).⁹⁹ Korsmeyer and co-workers generated analogues of the Bid-BH3 peptide with staples at positions *i* and *i* + 4, and obtained peptides with enhanced α -helicity, improved biological activities (these stabilised helical peptides were shown to bind to Bcl-x_L) as well as resistance to proteases both *in vitro* and *in vivo*.¹⁰⁰

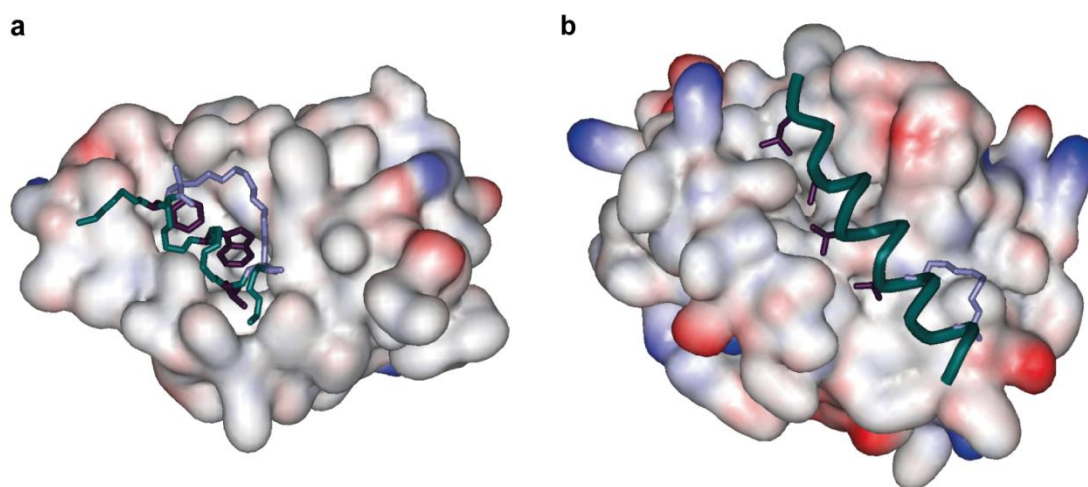


Figure 1.13 Crystal structures of stapled peptide inhibitors bound to their target proteins. a. Verdine's group stapled p53 peptide bound to *hDM2* (PDB ID: 3V3B)⁹⁹ and **b.** Walensky's stapled Mcl-1 peptide bound to Mcl-1 (PDB ID: 3MK8).¹⁰¹

The group also developed a series of ligands based on the Bid-BH3 domain that were shown to activate the pro-apoptotic protein Bax through direct binding.¹⁰² Later, the Walensky group designed a series of stapled peptides with high affinities towards Mcl-1 which were derived from the BH3 domain of Mcl-1 itself, rather than one of its known binding partners (Fig. 1.13b).¹⁰¹ Verdine and co-

workers have also used their disubstituted stapled peptide strategy to target the interaction between the transcription factor NOTCH 1 and its co-activator peptide MAML 1. This interaction plays a central role in the NOTCH signalling pathway involved in cell-fate determination. The authors have demonstrated that their peptides were able to achieve competitive binding to NOTCH 1 and *in vivo* studies also attributed them anti-leukaemic activity.¹⁰³ These studies also highlighted that constrained peptides could display good cell permeability and indicated a potential therapeutic window. In addition, this approach could be applied to other transcription factor complexes that were until then considered as chemically untractable. Recently, Walensky and co-workers used hydrocarbon double-stapling as a means to stabilise longer helical domains. These peptides presented improved antiviral activity compared to singly-stapled or natural peptides when tested for inhibition of the gp41 assembly. They also displayed enhanced resistance to proteases *in vitro* and *in vivo*, as well as evidence of oral bioavailability in mice.¹⁰⁴

- *Covalent hydrogen bond surrogates* (HBS, Fig. 1.12e): The α -helix is defined by a pattern of sequential ($i + 4 \cdots i$) hydrogen-bonds. Generally, hydrogen-bonds alone are weak and inadequate for stabilising short peptides into a well defined conformation. Replacement of hydrogen-bonds in α -helices with a covalent mimic and thus constraining the peptide to adopt an α -helical conformation was envisioned and developed by Satterthwait and co-workers.¹⁰⁵ Subsequently, Arora and co-workers have synthesized a highly helical HBS analogue of the Bak BH3 α -helix which displayed a K_d value of 69 nM against Bcl-x_L. Moreover, this peptide proved to be 60-fold more resistant to trypsin-mediated proteolysis than the linear analogue.¹⁰⁶ They then applied this strategy to the inhibition of gp41-mediated cell fusion, another HBS-helix derived from the C-terminal peptide from gp41 was shown to inhibit formation of the six-helix bundle with an IC₅₀ value of 43 μ M.¹⁰⁷

- *β -Turns as α -helix mimetics*: Robinson and co-workers designed and synthesised a series of β -turn cyclic peptides that mimic short α -helices. The β -hairpin structure is promoted by the presence of a D-Pro-L-Pro dipeptide

template.^{108, 109} Optimization of the mimetics lead to high affinity towards *hDM2*, with IC₅₀'s as low as 140 nM for compound **13** (Fig. 1.14).

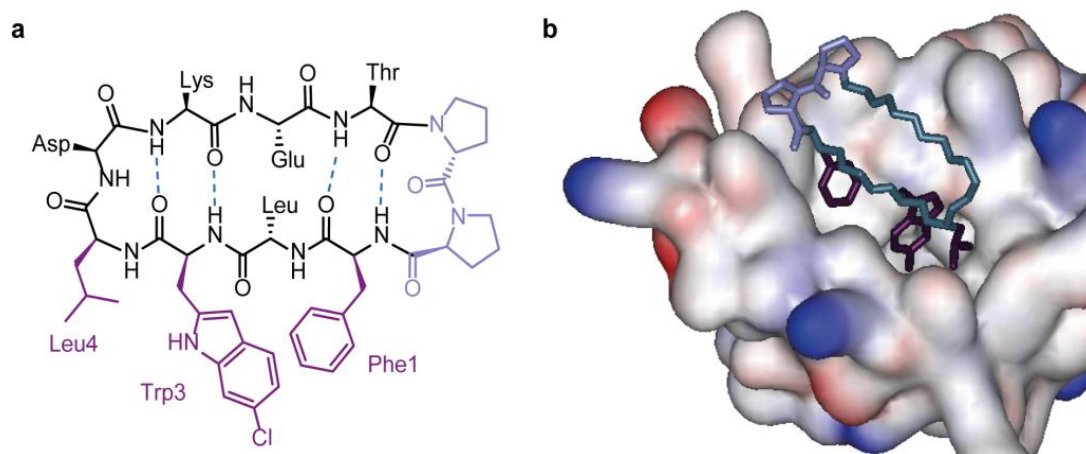


Figure 1.14 β -Hairpin inhibitor **13 of the p53/*hDM2* interaction.¹⁰⁹** **a.** Structure of **13**, proline residues are represented in light mauve, key interacting residues in dark purple (Phe1, 6-ClTrp3, Leu4). **b.** Close up view on the crystal structure of **13** bound to *hDM2* (PDB ID: 2AXI) with the same colour coding as in **a.**, the remaining backbone of the cyclic peptide in dark green, non-backbone atoms are omitted for clarity; *hDM2*₁₇₋₁₂₅ represented as a surface.

1.2.2.2 Foldamers adopting a helical conformation

The smallest backbone alteration of α -amino acids is the addition of a methylene unit (Fig. 1.15a,b). This minor backbone modification furnishes β -peptides which have an enhanced resistance to proteolysis and a more favorable pharmacodynamic profile than their natural counterparts.¹¹⁰ In most α -helix mediated PPIs, a small subset of residues located along one face of the helical binding partner accounts for most of the binding energy. The functional mimicry of α -helices by β - and mixed α/β -peptides therefore aims at mimicking the spatial presentation of this binding epitope while maintaining a stable helical conformation. Because the extra methyl group of β -amino acids introduces an additional degree of freedom and thus flexibility in the peptide backbone, it was initially thought that β -peptides would be entropically disfavored from adopting well defined folded states in solution.¹¹¹ However, in depth structural studies have shown that suitably substituted β -peptides possess a higher propensity to

fold into stable secondary structures than α -peptides,¹¹² making it possible to observe a defined structure within relatively short sequences.

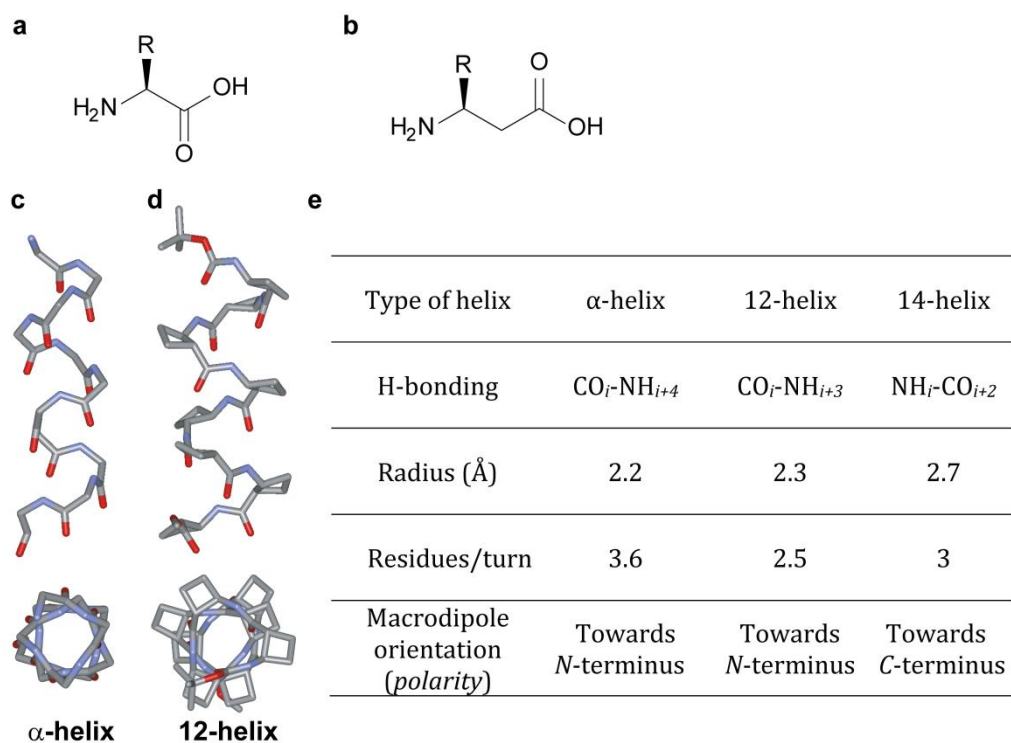


Figure 1.15 α - versus β -peptides: Comparison of the most common helical conformations accessible to natural peptides and foldamers. **a.** Structure of an α -amino acid. **b.** Structure of a β^3 -amino acid. **c.** Lateral and top views of the backbone of an α -helix (PBD ID: 2NLA). **d.** Lateral and top views of the backbone of a 12-helix stabilized by cyclobutane containing residues (CCDC ID: 742823). **e.** Table summarizing the characteristic properties of the α - 12- and 14-helices.

The correlation between β -amino acids substitution pattern and their folding preferences has been extensively reviewed.¹¹³ The best characterized secondary structures in β -peptides are the 14-helix and the 12-helix (named after the number of backbone atoms per hydrogen-bond ring, Fig. 1.15). Several such scaffolds have been targeted to the inhibition of PPIs.

Note: Using this nomenclature, the α -helix is also referred to as 4_{13} -helix, denoting a hydrogen bond between every carbonyl oxygen and the α -amino nitrogen of the 4th residue toward the *C*-terminus, and 13 atoms being involved in the ring.

- *Biologically active β -peptides:* Human cytomegalovirus (HCMV, alternatively known as herpesvirus-5) is a significant pathogen that can be life-threatening for immune-compromised patients. α -Peptides derived from the HCMV proteins gB and gH elicited poor inhibitory activity, hence Gellman and co-workers designed a series of β -peptides to mimic five key residues in the gB heptad repeat that are involved in the coiled coil formation that is crucial to viral entry.¹¹⁴ Assessment of a small library of compounds provided an inhibitor with an IC_{50} of 30 μ M, whereas α -peptide analogues were inactive at 100 μ M. These foldamers are proposed to target HCMV fusion machinery by adopting a 12-helical structure and mimicking the gB heptad repeat, thus blocking the helix bundle formation and HCMV infection.

The Schepartz group designed a β^3 -homodecamer targeting the p53/*hDM2* PPI whose 14-helical conformation was promoted by stabilization of the electrostatic macrodipole and intramolecular salt bridges.⁸⁵ The most potent compound achieved comparable affinity to that of the native peptide for *hDM2* (< 2.5 fold lower), displaying some selectivity towards the targeted interaction.¹¹⁵ Subsequent SAR studies improved potency by 10 fold through introduction of a 6-chloro- β^3 -amino acid analogue in place of the key W23 residue of p53.^{116, 117} Schepartz and co-workers also applied this approach to the identification of a β^3 -decapeptide inhibitor of gp41 fusion that achieved comparable affinity to that of most potent α -helical inhibitors ($K_d = 1.2 \mu$ M).⁸²

The selective transport of lipid through the brush-border membrane in the small intestine of mammals is mediated by two types of class B scavenger receptors (SR-BI and SR-BII).¹¹⁸ Inhibition of the cholesterol and fat absorption at this level has been demonstrated to occur through binding of an amphipathic α -helix motif to class B scavenger receptors. Whilst α -peptide inhibitors were inefficient in whole cell assays due to proteolysis, Seebach and co-workers demonstrated that amphipathic 14-helical β -peptide mimetics could be used to circumvent this degradation whilst retaining biological activity.¹¹⁹ Taken together, these results underscore the ability of 14-helical β -peptides to functionally mimic α -helices, despite having subtle structural differences and opposite macrodipole directions.

- *Mixed α/β -peptides as α -helix mimetics*: Gellman and co-workers sought to apply β - and α/β -foldamers to the inhibition of the Bcl-2 family of PPIs. Screening of over 200 peptides based on pure β - or α/β -backbones adopting different helical conformations failed to identify potent ligands for Bcl-x_L with the best compound identified, a 14/15-helical α/β -peptide, only exhibiting moderate inhibition of the Bcl-x_L/Bak interaction ($K_i = 4.2 \mu\text{M}$).⁸⁷ Building on these preliminary results, a potent chimeric inhibitor was designed in which an unnatural 14/15-helical portion was designed to mimic the *N*-terminal segment of Bak; whereas key side chains in the *C*-terminal region were replicated by an α -segment to give a nanomolar ligand for Bcl-x_L ($K_i = 2 \text{ nM}$),⁸⁷ proving that the α/β -14/15-helical backbone is suitable to mimic the presentation of hot-spot residues of an α -helix.

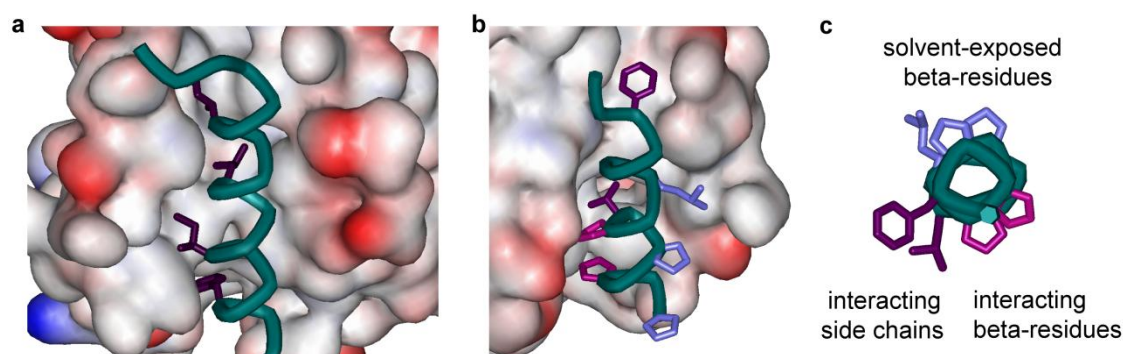


Figure 1.16 α/β -Peptide inhibitors of the Bcl-2 family. **a.** The pro-apoptotic protein Bim bound to Bcl-x_L (PDB ID: 3FDL). **b.** Chimeric Bim-mimetic ($\alpha/\beta + \alpha$)-peptide **14** binds Bcl-x_L similarly to natural BH3 domains and triggers cytochrome *c* release – leading to apoptosis (PDB ID: 3FDM). **c.** View of the α/β -foldamer along the helical axis (PDB ID: 3FDM).

A crystal structure of the most potent chimeric peptide mimicking the Bim-BH3 peptide **14** bound to Bcl-x_L was published shortly after (Fig. 1.16b).⁹⁰ Whilst this approach clearly resulted in the identification of potent inhibitors of PPIs, the work also highlighted that for some PPIs, simply presenting key side chains along one face of a helical scaffold may not be sufficient and that a more subtle matching of the α -helix may be necessary. The Gellman group therefore adapted the approach through sequence-based design of a Puma analogue – another pro-apoptotic member of the Bcl-2 family.⁸⁹ The strategy relies upon placement of α -

residues at some but not all positions within an α -helix to give a hybrid foldamer with enhanced stability and properties. The study of seven analogues containing the $\alpha\beta\alpha\alpha\alpha\beta$ repeat (placing the β -residues along one face of the helix and shown by X-ray crystallography to form helical structures) demonstrated that both the affinity and selectivity of hybrid peptides for Bcl-x_L and Mcl-1 are largely dependent on the position of the β -residues along the helix. The design and screening of these seven peptides identified a peptide which binds both Bcl-x_L and Mcl-1 ($K_i = 1$ nM and 150 nM respectively), and whose binding to Bcl-x_L is even tighter than that of the chimeric peptide obtained (see above) after screening of 200 peptides and structure-based optimisation. The first co-crystal structure between a sequence-based designed α/β -peptide mimicking Puma and Bcl-x_L revealed key geometrical parameters that the foldamer helix needs to reproduce in order to achieve tight binding.¹²⁰ Despite the introduction of six β -amino acids in the sequence, key contacts between the hot-spot residues of the native helix and Bcl-x_L were maintained, and the $\alpha\beta\alpha\alpha\alpha\beta$ heptad repeat gives rise to a more regular helix than any 1:1 α/β -peptide or chimeric foldamers. The success of the sequence based approach prompted the Gellman group to develop a two-step sequence based design of an α/β -peptide that prevents the formation of the six-helix bundle of the HIV membrane protein gp41 - a much longer and therefore challenging α -helical target.⁸⁸ Firstly, the same strategy as for the design of the Puma analogue was used: β^3 -residues were inserted into the α -sequence of the C-terminal heptad repeat domain (CHR) of gp41 to form $\alpha\beta\alpha\alpha\alpha\beta$ repeats. In the second step, selected β^3 -residues were replaced by cyclically constrained β -residues, to overcome the entropic penalty associated with the pre-organisation required for more flexible analogues. This approach allowed the structural and functional mimicry of 10 turns of an α -helical CHR domain (Fig. 1.17a-c), and the most potent peptide (**15**, $K_i = 9$ nM), represented a ~ 380 -fold improvement on the analogous acyclic α/β -peptide. This peptide also displayed an antiviral activity comparable to that of the native α -peptide and enhanced resistance to proteolysis (~ 280 fold).⁸⁸

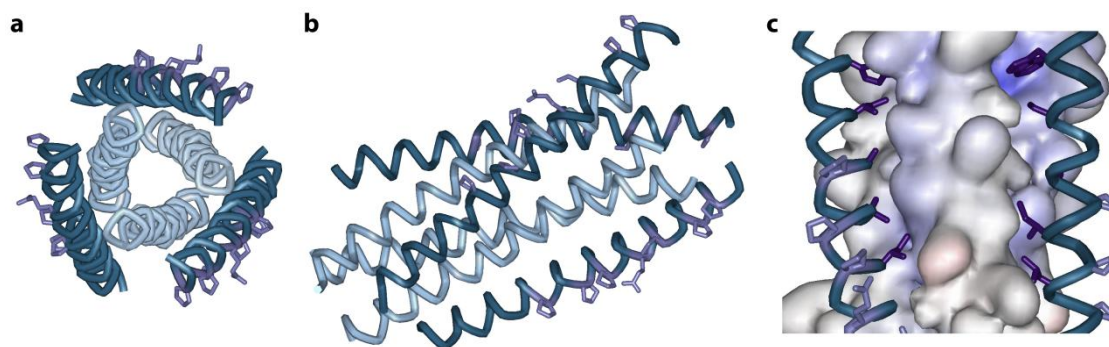


Figure 1.17 α/β -Foldamers applied to the inhibition of the gp41 fusion interaction. **a.** View along the helix bundle axis and **b.** lateral view of the six helix bundle formed by NHR α -peptides and the α/β -foldamers **15**, β -residues are colored in light purple. **c.** Close up view of α/β -inhibitor **15** bound to the NHR core helices, interfacial residues are represented in purple, β -residues are highlighted in light purple (PDB ID: 3G7A).

- *Other foldamers as α -helix mimetics:* In principle any abiotic backbone reproducing the α -helical conformation can be used as a template for inhibitor design. For instance Appella and co-workers used peptoids as inhibitors of p53/hDM2.¹²¹ These compounds were initially selected on the basis of their propensity to adopt a type II polyproline helical conformation and modelling studies that indicated a suitably functionalized peptoid could bind to hDM2 in this conformation. Although inhibitors were identified, the authors noted that the most potent compounds were less helical in the absence of protein than other compounds in the series that might have been expected to show greater potency as a consequence of being more helical. A subsequent study from the same group exploited *N*-acylpolyamine scaffold pre-organised into an active conformation through intramolecular hydrogen-bonding for inhibition of p53/hDM2.¹²² This elegant report illustrated that other secondary structures can recapitulate essential molecular recognition features of α -helices. Cyclic peptides containing Phe, Trp and Leu at positions 1, 3 and 4 of the sheet were found to project residues matched to the geometrical projection of Phe19, Trp23 and Leu26 in the p53 α -helix. Ultimately, low nM inhibitors of this interaction were identified using this approach. Benkovic and co-workers also investigated the use of cyclic peptides in the context of HIV fusion inhibition.¹²³ HIV propagation requires the recruitment of host proteins such as TSG101 to mediate its release from the plasma membrane of infected cells. It was thus thought that targeting the

interaction between Gag (a virally encoded protein that contains a tetrapeptide motif essential for the viral budding event) and TSG101 would offer a new approach for antiviral therapy that would circumvent the resistance of mutant forms of HIV. They assembled a library of cyclic peptides using a SICLOPPS methodology (Split Intein-mediated Circular Ligation of Peptides and Proteins)¹²⁴ then subjected it to a bacterial reverse two-hybrid screening. Hits identified were then chemically re-synthesised using SPPS (Solid Phase Peptide Synthesis) and tested for HIV budding inhibition in mammalian cells. Eventually, one Tat-tagged cyclic peptide was shown to inhibit viral budding with an IC₅₀ of 7 μM, demonstrating the therapeutic potential in this approach.¹²³ Overall the use of foldamers containing α-residues within contiguous sequences or as individual “mutations” to an α-amino acid backbone or use of completely abiotic backbones such as the peptoids represents a valid strategy for elaborating ligands with enhanced properties and the ability to selectively perturb PPIs. However due to subtle topological differences between such sequences and native α-helices, considerable iteration is still required to identify optimal ligands.

1.2.3 Proteomimetics

Despite the unfavorable features of protein surfaces for inhibitor design, a rational approach based on the role of secondary structure at the interface – and in particular the α-helix – is under intense investigation. The ability to design a scaffold to mimic the surface of an α-helix opens perspective for versatility: a unique scaffold could be used as a generic helical core mimic. Appropriate modifications of the side chains displayed and their spatial presentation could allow this single scaffold to be applied to the inhibition of several PPIs. This approach presents major advantages compared to the two previously described approaches: Type II mimetics lack versatility, meaning that for every single PPI a new inhibitor needs to be designed from scratch (either using HTS or structure-based design, cf. section 1.2.1). Type I mimetics are often designed after the sequence of the native helix, however the position, length and nature of the constraining element need to be optimized, and the synthesis of the required unnatural amino acids can be relatively complex. Considering that the hot-spot

residues for binding are often aligned along one helical face and located one helical turn apart, efforts have been devoted to develop synthetic blocks that could mimic the display of side chains separated by one helical turn. This way, mimicking the arrangement of side chains at positions i , $i + 4$ and $i + 7$ (or indeed $i + 11$) of an α -helix would only require 3 or 4 of these designed blocks. The proteomimetics approach could therefore benefit from a modular and expedient synthesis, as well as a more drug-like character due to their reduced molecular weight as compared to peptide mimetics. Different classes of designed proteomimetics have emerged and some have been shown to effectively act as α -helix mimetics and selectively disrupt targeted PPIs. The field of proteomimetics has been largely pioneered by Hamilton and co-workers; the terphenyl scaffold (Fig. 1.18) reported in 2001 was one of the first true helix mimetics.²⁶

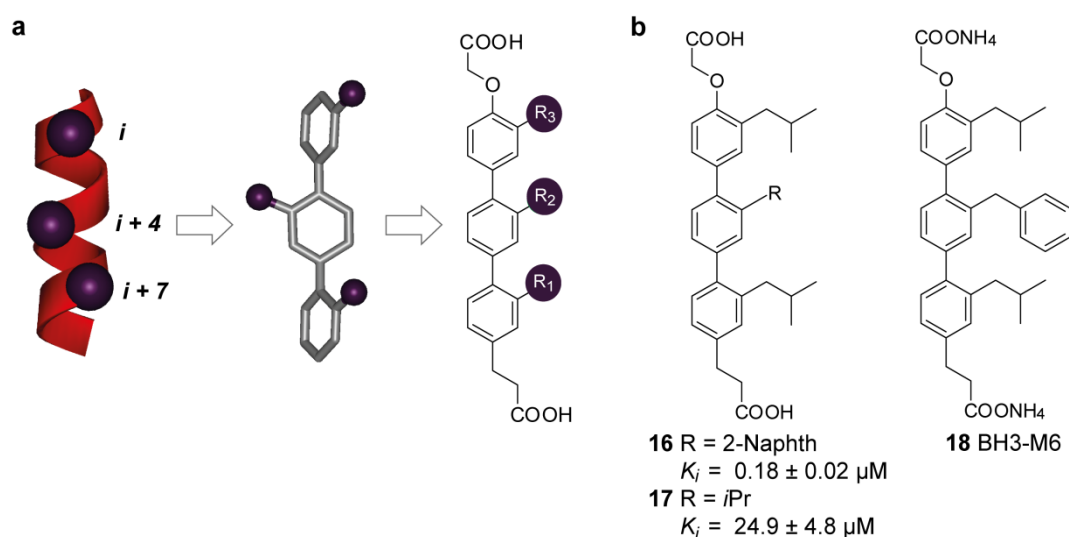


Figure 1.18 Terphenyl scaffold developed by the Hamilton group. **a.** The terphenyl scaffold allows mimicry of positions i , $i + 4$ and $i + 7$ of an α -helix. **b.** Terphenyl-based inhibitors: **16** was a Bcl-x_L binder, **17** inhibited the assembly of the gp41 core, **18** was initially tested against p53/hDM2 and was recently shown to act as a pan-Bcl inhibitor.

The terphenyl scaffold has been targeted to a number of therapeutically relevant PPI targets, including the p53/hDM2 and the Bcl-2/Bak interactions.¹²⁵ Substitution of this terphenyl scaffold at the *ortho* positions allows mimicry of the spatial arrangement of the i , $i + 4$ and $i + 7$ substituents of an α -helix, as shown in Figure 1.18a. Several terphenyl-based helix mimetics of p53 have been described

and others have been targeted to the inhibition of the hexameric coiled-coil assembly of gp41, for example terphenyl **17** (Fig. 1.18) displayed an IC_{50} value of $24.87 \pm 4.8 \mu\text{M}$,¹²⁶ again evidencing the versatility of this scaffold. Terphenyl-based structures were also applied to the mimicry of BH3-only proteins, which led to molecules with inhibition constants as low as 114 nM against the Bcl-x_L/Bak interaction, the critical residues for binding being: Val74, Leu78, Ile81 and Ile85. Terphenyl **16** (containing a 2-naphthyl side chain, Fig. 1.18) binds to hDM2 over 100-fold more strongly than its analogue with a 1-naphthylmethylene side chain and has a 14:82 fold selectivity over Bcl-x_L/Bcl-2.¹²⁵ This is consistent with the deeper pocket in hDM2 for Trp23 at the $i + 4$ position compared to the Leu78 pocket of Bcl-x_L or Bcl-2. These results confirm that the terphenyl scaffold can mimic the side chain-induced selectivity of α -helices. Compound **18** (Fig. 1.18b) presented a K_i value of $3.5 \pm 1.0 \mu\text{M}$ against the p53/hDM2 PPI¹²⁵ and was recently tested against the Bcl-2 family in a series of whole cell experiments, where it was renamed BH3-M6. The compound was shown to be a pan-Bcl-2 antagonist, as it was able to disrupt interactions between anti-apoptotic Bcl-x_L, Bcl-2, Mcl-1 and pro-apoptotic members Bax, Bak, Bim and Bad, both in cell free and in intact human cancer cells.¹²⁷ Several scaffolds have also been designed in an attempt to improve the poor solubility of the original terphenyl compounds. In 2003, the Hamilton group published the synthesis of a new trispyridylamide scaffold (Fig. 1.19a), which exhibited low micromolar affinities when tested against the Bcl-x_L/Bak PPI.¹²⁸ In this scaffold, bifurcated hydrogen bonds render the backbone planar and position the side chains on one side of the molecule, as confirmed by X-ray structures. Residues at positions i , $i + 4$ and $i + 7$ of an α -helix are however not located on a straight line; Ahn and co-workers therefore sought to slightly increase the backbone flexibility by replacing the pyridine rings with benzyl rings, thereby releasing the backbone from the constrain exerted by the bifurcated hydrogen bonds. Two examples of the resulting *O*-alkylated tris-benzamide scaffold have been prepared and will be investigated as potential glucagon antagonists.¹²⁹ The Wilson group developed a solution phase synthesis of *O*-alkylated aromatic oligoamide rods and extended the synthesis to the pentamer,¹³⁰ then demonstrated that this scaffold was suitable for α -helix mimicry as similar potency to the native peptide in disrupting the p53/hDM2 PPI

was achieved ($IC_{50} = 1.0 \mu\text{M}$ and $IC_{50} = 1.2 \mu\text{M}$ respectively).¹³¹ Hamilton and co-workers have also attempted to improve the solubility of their terphenyl scaffold by replacing the benzyl core with pyridine rings. The resulting terpyridine scaffold (Fig. 1.19c) presented an increased solubility but required a lengthy 15-step synthesis¹³² and has not been tested for binding yet.

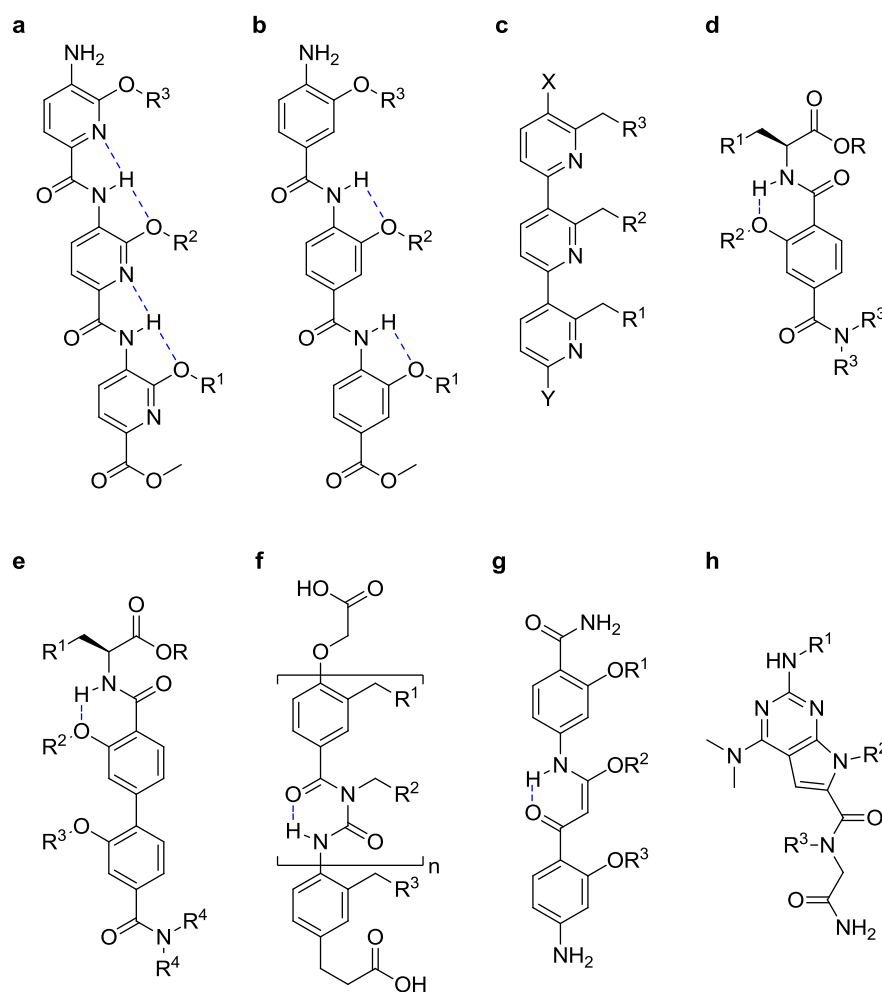


Figure 1.19 Proteomimetic scaffolds designed after the terphenyl scaffold. Hydrogen bonds are represented in blue. **a.** Trispyridylamide. **b.** 3-*O*-Alkylated oligobenzamide. **c.** Terpyridine. **d.** Terephthalamide. **e.** 4,4-Dicarboxamide. **f.** Oligobenzoylurea. **g.** Oligophenylenaminones. **h.** Pyrrolopyrimidine.

The next generations of scaffolds were designed to present both improved solubility and more modular syntheses: a series of terephthalamides^{133, 134} (Fig. 1.19d) achieved sub-micromolar inhibition of the Bcl-x_L/Bak interaction. Other attempts to increase the solubility of the scaffold have met limited success: Rebek

and co-workers have developed an oxazole-pyridazine-piperazine scaffold to reproduce the i , $i + 4$ and $i + 7$ residues of the Bak helix.¹³⁵ The use of heterocyclic rings was intended to enhance the solubility as the solvent-exposed face of the mimetic is rich in hydrogen-bond donors and acceptors. These however failed to overcome the potency of their terphenyl analogues. Families of 4,4-dicarboxamides¹³⁶ (Fig. 1.19e) and oligobenzoylureas¹³⁷ (Fig. 1.19f) were investigated as they offer the possibility to mimic an additional hot-spot residue from BH3-only proteins, however no improvement in affinity for the target proteins was reported ($K_i = 1.8 \pm 0.63 \mu\text{M}$ and $K_i = 2.4 \pm 0.3 \mu\text{M}$ respectively, against Bcl-x_L/Bak). Hamilton and co-workers have also developed an oligophenylaminone scaffold where the intramolecular H-bond places the three side chains along a single helical face (Fig. 1.19g), as predicted by modelling studies.¹³⁸ This scaffold presents the advantages of being synthetically accessible and proved to be amenable to longer oligomer synthesis. The group therefore sought to apply it to the mimicry of extended helices such as leucine-zippers (structural motifs in the DNA-binding region of transcription factor proteins). A compound was reported to structurally mimic 10 helical turns of a leucine zipper, as confirmed using X-ray crystallography, and this constitutes the longest proteomimetic characterized to date.¹³⁹ The biological activity of this series of compounds has however not yet been assessed.

The proteomimetic approach is highly desirable as it offers versatility: different interactions can be selectively targeted using a single scaffold only by changing the side chain appendage. Fully exploiting the potential of this strategy however requires building large libraries of compounds for screening and even though modular syntheses have been developed, only a few are amenable to library assembly. Several libraries of proteomimetics have been reported in solution phase, but fewer examples of solid phase assembled libraries have been described to date. Guy and co-workers have designed several scaffolds targeting the p53/hDM2 interaction *in silico* and identified an oligobenzamide scaffold as the most potent out of the 4 considered for synthesis. In this scaffold, side chains are directly attached to the benzyl rings *via* carbon-carbon bonds and assembly of over a hundred compounds in solution phase yielded low-micromolar inhibition of the target PPI.¹⁴⁰ The Boger group has recently reported another

solution phase synthesis of the *O*-alkylated oligobenzamide scaffold, targeted to the p53/hDM2 PPI.¹⁴¹ They then explored permutations of *C*- and *N*-terminal aromatic units with more flexible corresponding natural amino acids. The most potent compound ($IC_{50} = 8 \mu M$) contained two α -residues mimicking Phe19 and Leu26 and a middle aromatic residue bearing an indole side chain (Trp23 mimic). This compound then served as a template for an 8000-member library made of all the possible combinations of 20 *C*-terminal α -residues, 20 central aryl units containing proteinogenic side chains as well as unnatural analogues, and another 20 *N*-terminal α -residues. Testing and ranking of each side chain revealed that the most potent compound was, unsurprisingly, the one bearing side chains corresponding to the native p53 peptide, and which served as a template for this library.¹⁴¹

Although the assembly of libraries of compounds in solution has been exemplified by several research groups, fewer have been reported using solid phase synthesis (SPS). Oligobenzamide proteomimetic inhibitors constitute an attractive class of ligands for α -helix mediated PPI inhibition, as they exhibit predictable folding patterns imposed by the preferred conformation of the Aryl-NHCO-Aryl bond. They are also an attractive template for solid phase synthesis, as coupling and protecting strategies can be derived from those used in classical peptide synthesis. Recently, Lim and co-workers reported the solid phase assembly of a library of 900 compounds targeted to the p53/hDM2 and p53/hDMX interactions, based on a novel pyrrolopyrimidine scaffold (Fig. 1.19h). Biological assessment of 90 of these compounds in fluorescence anisotropy competition assays revealed dual inhibitors, with sub-micromolar inhibition constants against both targeted interactions. In addition, this scaffold presents enhanced aqueous solubility as compared to terphenyl-derived scaffolds, exhibits high cell-permeability and induces p53 level and activity in cells. The Kilbinger group reported the SPS of an *N*-alkylated oligobenzamide scaffold *via* acylation of secondary aromatic amines on a Wang resin support, extending the synthesis to the decamer.¹⁴² This scaffold had however not been applied to α -helix mimicry until a few years later when Wilson and co-workers published their manual solid phase methodology to assemble a library of 24 such compounds and identified

potent inhibitors of the p53/hDM2 interaction (Fig. 1.20, **19** presented an IC_{50} of $2.8 \mu\text{M}$ compared to the native peptide $IC_{50} = 1.2 \mu\text{M}$).¹⁴³

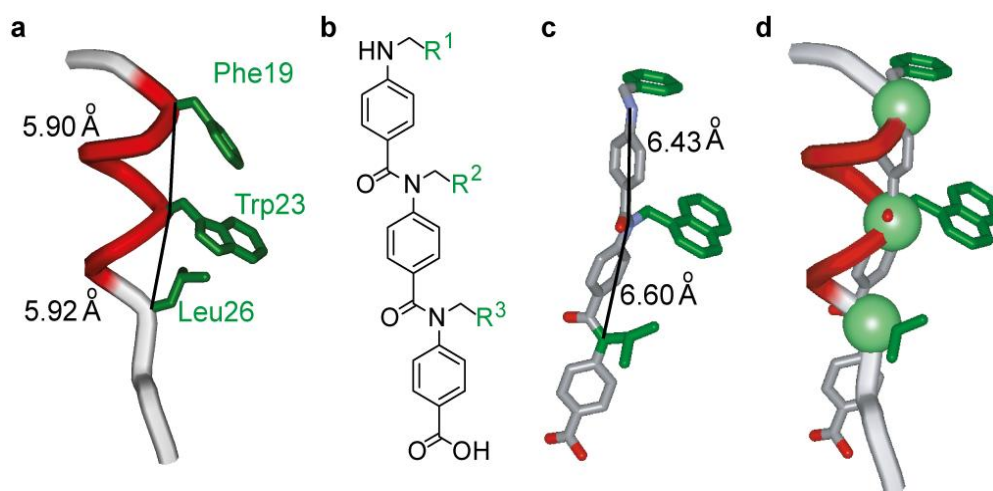


Figure 1.20 Wilson's *N*-alkylated oligobenzamide scaffold as a helix mimetic. a. hDM2 binding domain of p53. **b.** General structure of the *N*-alkylated oligobenzamides. **c.** Minimum energy conformation of one of the most potent compound produced so far with the *N*-alkylated scaffold. **d.** Overlay of the proteomimetic and a p53 peptide.

These encouraging results led to further synthetic developments, and notably the transposition of the SPS to an automated methodology using a CEM Liberty[®] microwave assisted peptide synthesiser¹⁴⁴ (cf. Chapter 2). This new methodology allowed the assembly of a large library of proteomimetics that were assessed against two model interactions: p53/hDM2 and Noxa B/Mcl-1 (cf. Chapter 3). In the event that co-crystal structures of these oligobenzamides with the target protein can be obtained, these will be used to guide the design of more potent inhibitors. Hits identified in the preliminary screening of the library can also be refined based on the SAR established from these assays, and selectivity enhanced *via* introduction of unnatural amino acids – this will be discussed in the next Chapters.

1.3 Project aims

As discussed in this chapter, intense efforts are directed towards the inhibition of PPIs, and several approaches have emerged. Small molecules have provided some of the most potent inhibitors so far, but only offer tailored answers to each PPI target. On the other hand, proteomimetics and foldamers present the prospect of a versatile approach to each class of PPIs. With this in view, the Wilson group has developed a scaffold to mimic the alignment of side chains that are critical to the binding of several α -helix mediated PPIs. This scaffold possesses the advantage of an accessible and modular synthesis. Previously within the group, a small library of *N*-alkylated oligobenzamides has been designed to disrupt the p53/*h*DM2 interaction, and was built using manual solid phase synthesis (SPS).¹⁴³ Preliminary binding studies using a fluorescence anisotropy assay suggested the scaffold to be suitable for α -helix mimicry: the most potent compound that was then identified displayed an IC₅₀ comparable to that of the native peptide.¹⁴³

The present work aimed at further investigating this *N*-alkylated oligobenzamide scaffold. This included the development of an automated methodology for SPS using a microwave assisted peptide synthesiser¹⁴⁴ that would allow the generation of a large library of compounds. The library was mainly focused on the p53/*h*DM2 PPI, although a small sub-library targeting the Bcl-2 family was also assembled. These libraries were to be tested in the previously used fluorescence anisotropy assay firstly against the model interactions (p53/*h*DM2 and p53/*h*DMX), then against the Bcl-2 family in order to establish the versatility of the scaffold. Further biophysical characterisation of the most potent compounds was to be acquired using techniques that have not yet been applied to this scaffold, and assessment of the cellular uptake was also envisioned.

Chapter 2

Microwave assisted solid phase synthesis of *N*-alkylated oligobenzamide α -helix mimetics

The work reported in this chapter formed the basis of the following publication:
K. Long, T. A. Edwards and A. J. Wilson, *Bioorg. Med. Chem.* 2013,
[dx.doi.org/10.1016/j.bmc.2012.09.053](https://doi.org/10.1016/j.bmc.2012.09.053).¹⁴⁴

Oligomers that adopt preferential conformations are named foldamers;^{112, 145-147} their stable and predictable folding into well-defined structures has been exploited in various areas of research. The relative synthetic accessibility of foldamers from monomer building blocks also confers adaptability, versatility, and the possibility to modify their inherent properties. These features make them attractive utensils to modulate biological processes.¹⁴⁸ Previously, the Wilson group reported the manual solid phase synthesis (SPS) of an *N*-alkylated aromatic oligoamide scaffold (Fig. 2.1) and demonstrated that it was suitable for α -helix mimicry through identification of low μ M inhibitors of the helix mediated p53/hDM2 interaction.¹⁴³ In its extended all *trans* conformation, substituents appended to the nitrogen atoms are displayed in such a manner as to match the spatial presentation of side chains located at the *i*, *i* + 4 and *i* + 7 positions of an α -helix. This subset of residues located along one helical face has been shown to be a recurrent pattern in α -helix mediated protein-protein interactions (PPIs),^{12, 147, 149} where they account for most of the binding energy and are referred to as 'hot-spot' residues.^{15, 16}

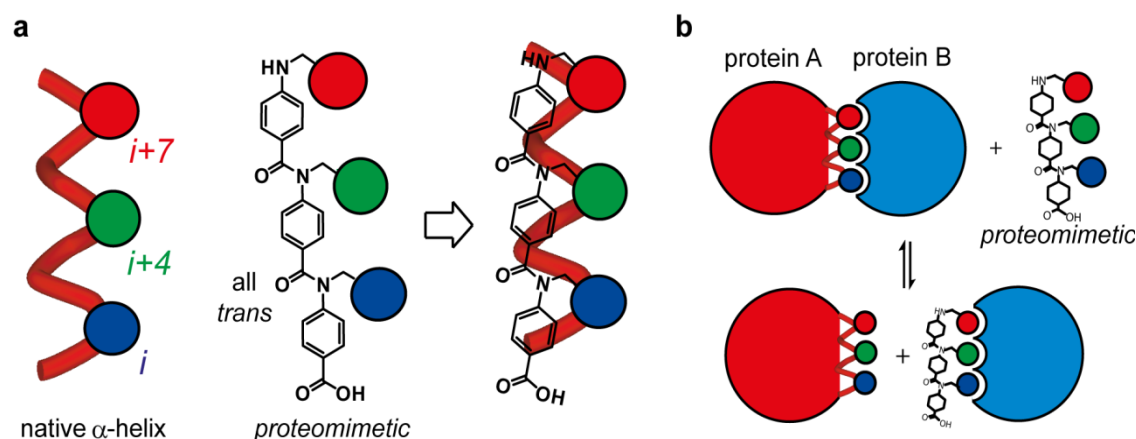


Figure 2.1 The *N*-alkylated oligobenzamide scaffold as a helix mimetic. **a.** Mimicry of the spatial presentation of residues i , $i + 4$, $i + 7$ (coloured circles) in an α -helix by our *N*-alkylated proteomimetic scaffold. **b.** Cartoon representing the exploitation of α -helix mimicry in achieving competitive inhibition.

PPIs possess features that largely differentiate them from more conventional enzyme-substrate interactions that are traditionally targeted by medicinal chemistry efforts.² Such interactions include the gp41 fusion protein, responsible for the fusion process enabling HIV infection;¹⁸ the interaction between p53 and its negative regulators *hDM2* and *hDMX* –p53’s function is inhibited by direct binding to *hDM2* and *hDMX* in about 10-15% of all cases of human cancers;¹⁹⁻²² and the Bcl-2 family of interactions²³⁻²⁵ involved in the regulation of apoptosis, a form of programmed cell death that is crucial during the development of multicellular organisms and in avoiding tumourigenesis. Although small molecule inhibitors^{4, 7, 63, 65, 126, 150} and constrained helical peptides^{102, 103, 151} or oligomers retaining the helical conformation¹⁵²⁻¹⁵⁴ have been used to target these and related PPIs, designing scaffolds that allow mimicry of key interfacial residues on an α -helix involved at a PPI interface offers considerable potential for the elaboration of generic approaches.¹⁴⁷ With this in mind, several such *proteomimetic*²⁶ scaffolds have been designed over the last decade; Hamilton’s terphenyl scaffold was the first true helix mimetic, displaying IC₅₀s in the micromolar range against several important PPI targets.^{26, 125, 126} Subsequently, several further scaffolds were described that were synthetically more accessible and presented more lead-like properties including the terephthalamide,¹³⁴ the 4,4-dicarboxamide,¹³⁶ and the oligobenzoylurea¹³⁷ templates amongst others.^{135, 138, 155, 156} Aromatic oligoamides¹⁵⁷ represent an attractive class of foldamers,^{128,}

129, 131, 136, 141, 158, 159 as their constitutive units can be easily prepared and then assembled into functional structures using modular syntheses. As they are somewhat similar to natural peptides in that they are made of amino acid subunits linked to one another by amide bonds, they are investigated as structural peptide mimetics. Although methods are already well-established for natural peptide synthesis, the assembly of aromatic oligomers has proven rather troublesome due to the reduced reactivity of the monomers as compared to natural amino acids, making assembly of screening libraries challenging.^{140, 141, 156} In order to achieve the objectives set out in this thesis, it was necessary to address this challenge. In the present chapter, we report an automated methodology for the preparation of *N*-alkylated aromatic oligoamides using a state of the art microwave assisted peptide synthesizer. This method provides enhanced yields and purities as well as reduced handling and coupling times. The tolerance of our coupling method towards functionalities encountered in proteinogenic amino acids is demonstrated, along with some more tailored, unnatural side chains.

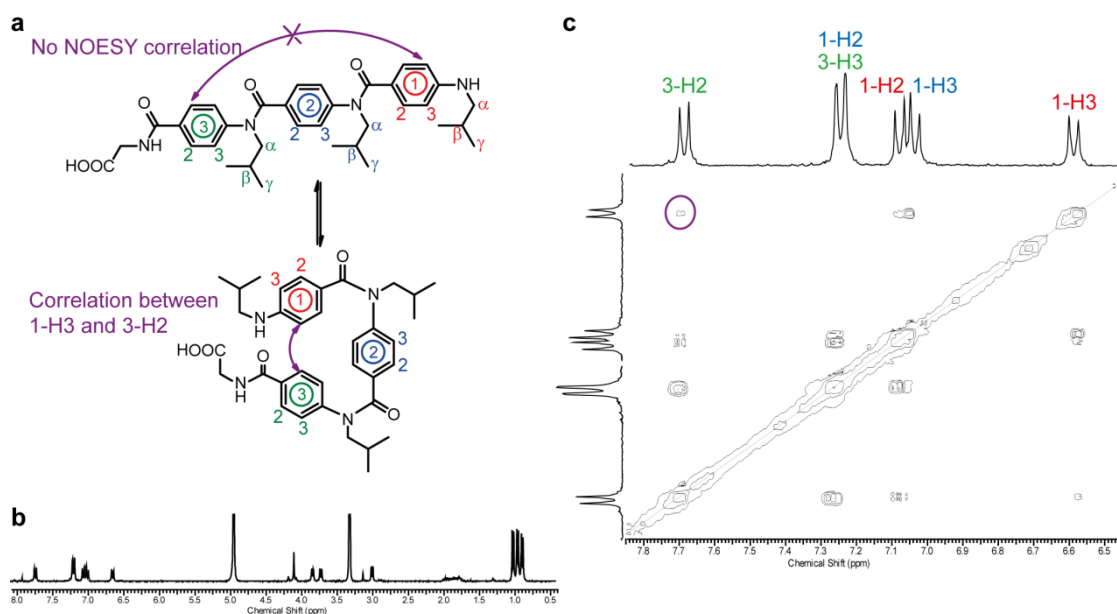


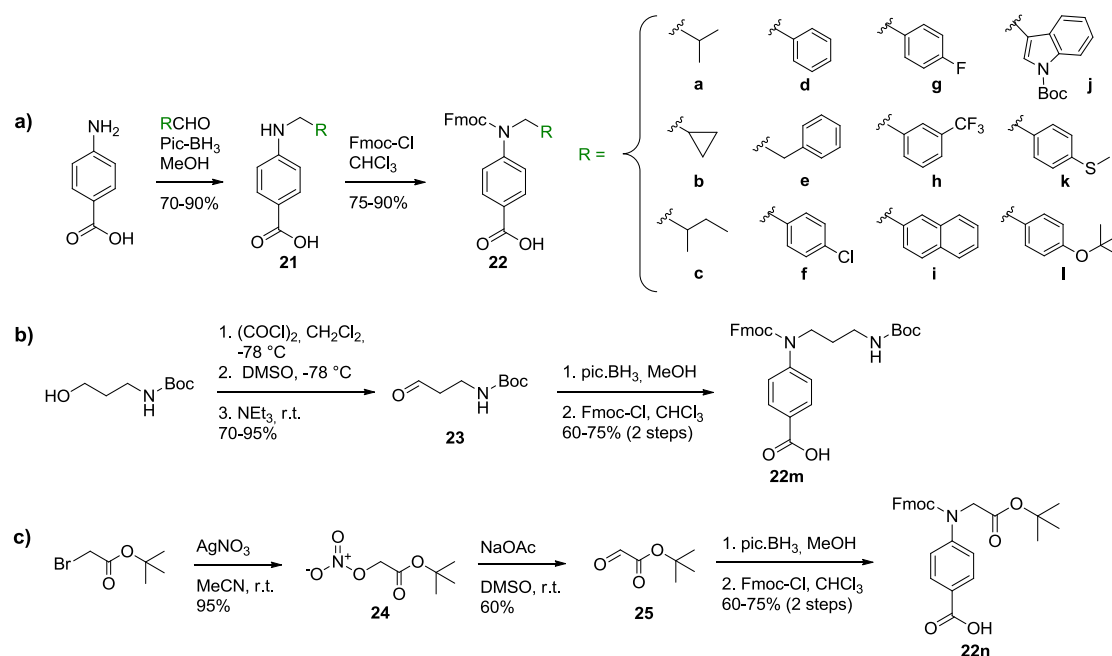
Figure 2.2 *N*-alkylated oligobenzamides preferentially adopt a *cis*-conformation in solution. **a.** The *cis-trans* equilibrium. **b.** $^1\text{H-NMR}$ of compound **20** (300 MHz, MeOD). **c.** Expansion on the aromatic region of the NOESY spectrum of compound **20** (300 MHz, MeOD); cross peaks between protons 1-H3 and 3-H2 illustrates the preference for the *cis*-conformer in methanol.

The preferred *cis* geometry of the amide bond in these molecules¹⁶⁰ (Fig. 2.2) has been shown to facilitate the cyclisation of such trimers,¹⁶¹ but it has also been demonstrated that the compounds may adopt the *trans* conformation (Fig. 2.1) upon binding to the target protein.

Our strategy for automated solid phase peptide synthesis (SPPS) of *N*-alkylated oligobenzamides centers on the use of a microwave assisted peptide synthesizer and the well established Fmoc strategy,¹⁶² providing orthogonality with side chain protecting groups. One of the key features of this oligoamide backbone is its synthetic accessibility. The scaffold is based on trimers of *N*-alkylated *p*-aminobenzoic acid units linked by sequentially installed amide bonds.

2.1 Monomer synthesis

In order to develop a method amenable to the generation of a library of diversely functionalized tribenzamides, a range of monomers **22a-n** was prepared following the previously reported route (Scheme 2.1a).¹⁴³



Scheme 2.1 Synthetic route to Fmoc protected building blocks. a. Synthesis of Fmoc protected *N*-alkylated *p*-aminobenzoic acid monomers from commercially available aldehydes. **b.** Preliminary Swern oxidation of ionic side chain. **c.** Synthetic route for the preparation of the aldehyde precursor of the acidic monomer.

Although the Wilson group's prior study confirmed that hydrophobic side chains were privileged for the design of inhibitors of the p53/*hDM2* interaction (and a considerable number of others),¹² we sought to incorporate the whole range of functionalities encountered in natural amino acids into the monomer set so as to scope the functional group tolerance of our method. In the case of amine containing side chains where the starting aldehydes were not commercially available, Swern oxidation¹⁶³ was performed on the parent alcohol (Scheme 2.1b), whilst one further side chain, containing an acidic functionality, was prepared using a different route (Scheme 2.1c).

2.2 Solid Phase Peptide Synthesis

Trimeric oligoamides **26-37** were built from sequential coupling of *N*-alkylated *p*-aminobenzoic acid monomers *via* SPS using the well established Fmoc strategy, widely employed in natural peptide synthesis.¹⁶² The previously reported SPS on this scaffold¹⁴³ was adapted for a CEM Liberty[®] automated microwave assisted peptide synthesizer. Experiments focused on the use of Wang resin preloaded with Gly as the solid support, although it should be noted that a limited number of experiments using unfunctionalized Wang resin were also performed. Direct loading onto the Wang resin however proved less efficient and robust than with the preloaded resin. The same protection strategy as for natural amino acid coupling was sought for the *N*-alkylated oligobenzamide scaffold so as to avoid the development of an entirely new permanent and semi-permanent protecting group strategy, hence the prime synthetic objective was to optimize amide bond formation; however the deactivated secondary aniline is significantly less nucleophilic than a primary amine. Coupling agents that are classically used in peptide synthesis (HCTU,¹⁶⁴ PyBOP,¹⁶⁵ TFFH,¹⁶⁶ EDCI,¹⁶⁷ DIC,¹⁶⁷ HOBt,¹⁶⁸ MSNT,¹⁶² etc.) proved inefficient when applied to the present scaffold under microwave heating (as had been the case in the earlier manual SPS study).¹⁶⁸ Initially, temperature and coupling time were set to 60 °C and 30 min respectively, and 4 eq. of monomer were used per coupling. Under these standard conditions (Table 2.1), all these reagents were able to load the aromatic monomers onto the Gly-preloaded Wang resin, but no dimer could be formed.

Previous studies on the solution phase synthesis of these trimers revealed that the monomers required activation as acyl chlorides in order for the coupling reaction to take place. Acyl chlorides of the monomers **22a-n** can be obtained by reaction with dichlorotriphenylphosphorane¹⁶⁹ (Cl_2PPh_3) at elevated temperatures, or with Ghosez's reagent¹⁷⁰ at room temperature. Both reagents were assessed under microwave heating conditions and optimal coupling conditions have been carefully determined. As the activation using the phosphorane required heating, both the monomer and the coupling agent had to be dissolved in the desired solvent and placed on the synthesizer's manifold; the acyl chloride was then obtained *in situ* within the reaction vessel. Under these unoptimized conditions, a respectable percentage of conversion could be obtained with a dimer/loaded monomer ratio of 65-35 (Table 2.1, Entry 7). Because Ghosez's reagent could generate the reactive species at room temperature, the acyl chloride could either be generated *in situ*, (Table 2.1, Entry 8) or obtained by preactivation (Table 2.1, Entry 9).

Table 2.1 Screening of activating agents under standard conditions (Single coupling, 60 °C, 30 min). % conversions estimated from the UV chromatograms of the crude cleavage product.

Entry	Activator	Solvent	Microwave method	Base	1 st residue loaded	% dimer
1	HCTU	DMF	Single, 60 °C, 30 min	DIPEA	Yes	0
2	PyBOP	CHCl_3	Single, 60 °C, 30 min	DIPEA	Yes	65%
3	TFFH	CHCl_3	Single, 60 °C, 30 min	/	Yes	10%
4	EDCI	CHCl_3	Single, 60 °C, 30 min	/	Yes	0
5	DIC	CHCl_3	Single, 60 °C, 30 min	/	Yes	0
6	MSNT	CHCl_3	Single, 60 °C, 30 min	/	Yes	0
7	Cl_2PPh_3	CHCl_3	Single, 60 °C, 30 min	/	Yes	65%
8	Ghosez	CHCl_3	Single, 60 °C, 30 min	NMI	Yes	25%
9	Preactiv. Ghosez	CHCl_3	Single, 60 °C, 30 min	NMI	Yes	50%

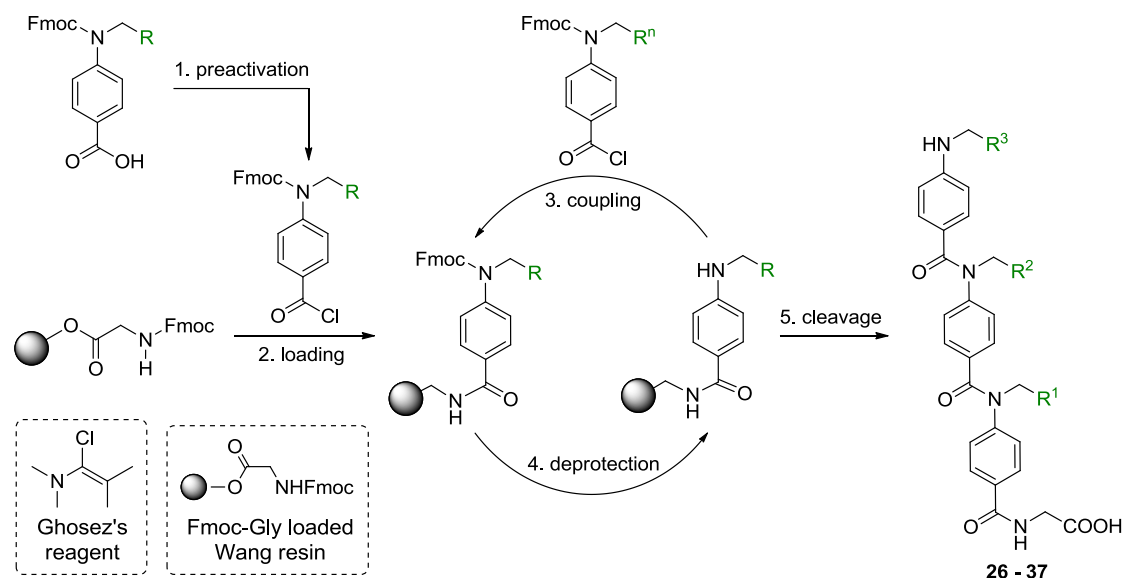
Due to the water sensitivity of these coupling agents and the low reactivity of the aniline towards acyl chlorides at room temperature, significant care was required to exclude water from the preactivation step and coupling reaction. At first, coupling was optimized for the formation of dimers using dichlorotriphenylphosphorane, as it is easier to handle than Ghosez's reagent. Again, the standard set of coupling conditions was used to allow the study of each parameter (base, solvent, temperature and coupling time) independently. Different solvents were tested, with the pre-requisite that all reagents should be soluble in the considered solvent. Single couplings in dioxane, tetrahydrofuran or dichloroethane provided no or low conversion to dimer, whereas conversions from 55 to 60% were obtained in chloroform or DMF. In DMF, conversion could be somewhat enhanced by raising the coupling temperature to 90 °C. Further optimization was carried out in parallel for both solvents (Table 2.2). Prolonging the coupling time to 45 min or 1 hour did not improve the conversion, but reducing the coupling time to 20 min was not detrimental either. Finally, switching to a double coupling improved conversion to the dimer from 60% with a single coupling to quantitative (Table 2.2, Entry 6).

Table 2.2 Optimisation of the coupling time using Cl₂PPh₃.

Entry	Activator	Solvent	Coupling	T (°C)	t	Base	% conversion
1	Cl ₂ PPh ₃	CHCl ₃	Single	60	30 min	/	Dimer - Monomer 55-45
2	Cl ₂ PPh ₃	CHCl ₃	Single	60	60 min	/	Dimer - Monomer 5-95
3	Cl ₂ PPh ₃	CHCl ₃	Single	60	20 min	/	Dimer - Monomer 60-40
4	Cl ₂ PPh ₃	DMF	Single	60	30 min	/	Dimer - Monomer 60-40
5	Cl ₂ PPh ₃	DMF	Single	60	20 min	/	Dimer- Monomer 60-40
6	Cl ₂ PPh ₃	DMF	Double	60	20 min	/	100% Dimer

Despite these encouraging preliminary results, dichlorotriphenylphosphorane proved to be unreliable from batch to batch and in subsequent studies on the functional tolerance of the method. Further studies on Ghosez's α -chloroamine

were then performed in chloroform. Under the optimized coupling conditions established with the first acylating agent (Table 2.2, Entry 6), complete conversion could also be obtained with the α -chloroamine. Couplings also proved to be much more reproducible than with dichlorotriphenylphosphorane and Ghosez's reagent was therefore established as the coupling reagent of choice for these monomers.



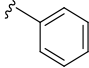
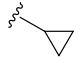
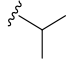
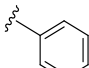
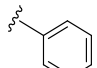
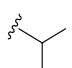
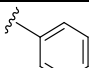
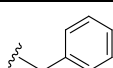
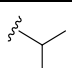
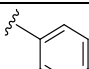
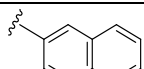
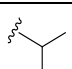
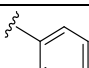
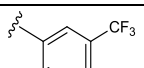
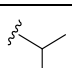
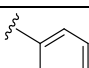
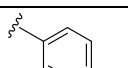
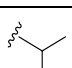
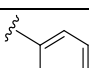
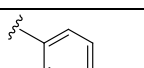
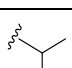
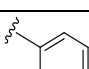
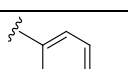
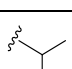
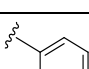
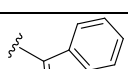
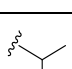
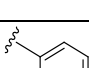
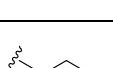
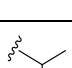
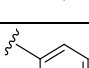
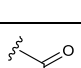
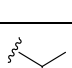
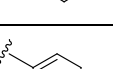
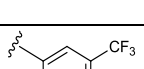
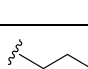
Scheme 2.2 Outline of procedure used for solid-phase synthesis of *N*-alkylated aromatic oligoamide α -helix mimetics. 1. Preactivation: Monomer (2×2.5 eq. to resin, 0.5 mmol) in anhydrous CHCl_3 (5.5 mL), pre-activated with Ghosez's reagent (0.95 eq. to the monomer, 0.48 mmol) for a minimum of 1 hour; 2. Loading: resin (0.1 mmol, 127 mg) swelled in 5 mL DMF, monomer loaded using a double coupling method (2×20 min, 60°C). In the case of acid labile side chain protecting groups, NaHCO_3 (solid, excess) can be added to the resin tube; 3. Coupling: same method as for the loading; 4. Deprotection: 20% piperidine in DMF, standard microwave method used (two cycles, 75°C , 3 min, cf. experimental section); 5. Manual cleavage: DCM-TFA (1-1, 0.7 mL), 2×20 min, r.t.

Further optimization of the coupling time, temperature, number of equivalents of monomer to the resin and solvent (Scheme 2.2) led to complete conversion to trimers in good yields. Because double couplings are required, using 4 eq. of monomer **22a-n** per coupling means that a large amount of monomer is consumed. After further optimization, the minimum number of equivalents of monomer to the resin was identified as 2.5 eq. per coupling, and the coupling time was maintained at 20 minutes. Standard microwave assisted deprotection

was used and didn't require any optimization. Including the wash cycles, this new method therefore yields trimers in 4 hours, which is a dramatic improvement on the 4 days previously required using the manual SPS method.¹⁴³ Although cleavage from the resin can be performed on the synthesizer, this would require additional and extensive washes of the reactor. We therefore chose to carry out the cleavages manually (cf. Experimental Section), which also allowed to optimize the productivity of the synthesizer. For side chains containing a reactive functionality that needs to be protected during the coupling, our strategy was to use acid-labile protecting groups. These protecting groups would thus remain untouched during the basic Fmoc deprotection step, but would be removed during acidic cleavage from the resin. During coupling however, one equivalent of hydrochloric acid is generated and this acidity could potentially deprotect the side chains. To quench this acidity, the presence of a base was required during coupling and the base tolerance of the present method was thus assessed. Firstly, *N*-methyl imidazole was tested, but this base presented the major inconvenience of being highly hygroscopic, thus requiring distillation and storage under strictly anhydrous conditions prior to use; the reagent was therefore considered incompatible with the microwave synthesizer. For this reason, a solid inorganic base seemed more reasonable and couplings were thus tested in presence of sodium bicarbonate, which was introduced in excess at the same time as the resin. Using a solid base presents the additional advantage that it is retained in the reaction vessel after each round of filtered washes following couplings and is therefore introduced only once, again minimizing entry points for water. The bicarbonate is readily removed by rinsing the resin with water prior to the cleavage step. It was then necessary to thoroughly test the functional group tolerance of the method by assembly of a small library. These studies were carried out in chloroform, as it is much less hygroscopic than DMF. The present library was designed to assess the ability of monomers **22a-n** to be coupled to another monomer already attached to the resin to form a dimer, as well as the ability of these dimers to couple to another activated monomer to provide trimers **26-37**. To obtain consistent data, the same monomers were used at the *N*- and *C*-termini for each trimer, respectively the benzyl **22d** and isobutyl **22a** monomers. The optimized coupling conditions afforded the desired trimers with

good conversion and yield (Table 2.3) and the crude material was in most cases more than 90% pure as observed on the LC-MS spectrum.

Table 2.3 Library of *N*-alkylated tribenzamides with the side chains sequence. Unless otherwise specified, the reported purity and yield correspond to crude compounds.

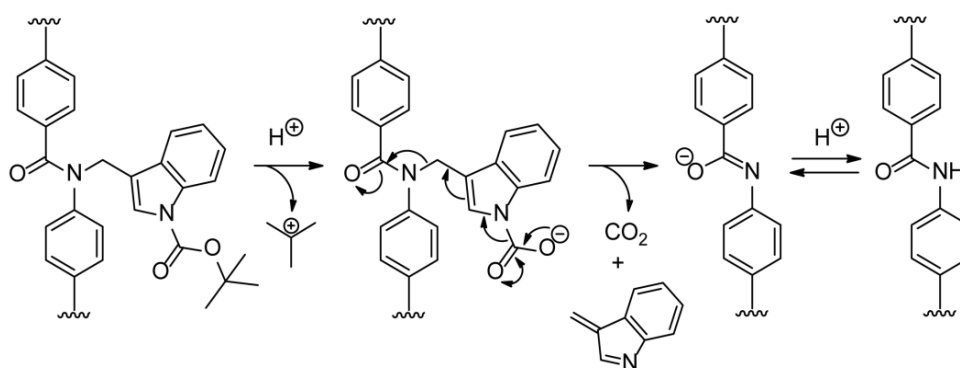
Trimer number	R ³	R ²	R ¹	Purity	Yield
26				85%	85%
27				95%	100%
28				~90%	~ 95%
29				70%	~ 90%
30				99%	100%
31				99% ^a (crude 80%)	7% ^a
32				80%	~ 85%
33				99% ^b (crude 75%)	22% ^b
34				~ 95% ^c	10%
35				99% ^a (crude 80%)	~ 6% ^a
36				99%	100%
37				99%	100%

^a Purified by precipitation.

^b Purified by MS-directed preparative HPLC

^c Purified by column chromatography

When the purity of the crude material was judged unsatisfactory, purification was attempted. Several methods were used including column chromatography, preparative TLC, preparative HPLC, mass directed preparative HPLC or precipitation, which improved purity but considerably affected the isolated yields of pure compounds. In the range of monomers that were submitted to coupling, the indole containing monomer **22j** was problematic, in agreement with previous observations.¹⁴³ LC-MS analysis of the cleavage product indicated that the coupling occurs, but that the indole functionality is lost, presumably due to acid catalyzed elimination of the Boc-protecting group during the TFA-cleavage step, followed by cascade elimination of the indole ring (Scheme 2.3).



Scheme 2.3 Cascade elimination of the indole functionality during acidic cleavage from the resin.

This issue was addressed by using milder conditions for the cleavage step. The cleaving cocktail was diluted from a 1-1 mixture of dichloromethane-TFA down to a 25%, then 10% TFA in dichloromethane solution (Table 2.4). Diluting the cleavage cocktail indeed solved the elimination issue, but the isolated product was then still Boc-protected. Adjusting the length of the cleavage also failed to yield the desired deprotected trimer, as it seemed impossible to reach a compromise between Boc-deprotection and preservation of the indole side chain. For side chains containing a functional group that is prone to elimination, it might be necessary to adjust cleavage mixture and cleavage time to achieve neat cleavage from the resin as well as complete deprotection whilst preserving the side chain. It was envisaged that the isolated Boc-protected trimer could be

selectively deprotected *via* thermolysis,¹⁷¹ however only eliminated indole was isolated under the reported conditions.

Table 2.4 Indole deprotection versus side chain elimination

Entry	Cleavage cocktail	Cleavage time	Observed products (LC-MS)
1	Neat TFA	30 min	Mostly eliminated indole
2	50% TFA in CH ₂ Cl ₂	30 min	Mostly eliminated indole
3	25% TFA in CH ₂ Cl ₂	10 min	Mostly Boc-protected trimer and traces of eliminated indole
4	10% TFA in CH ₂ Cl ₂	5 min	Mostly Boc-protected trimer
5	10% TFA in CH ₂ Cl ₂	10 min	Mostly Boc-protected trimer
6	10% TFA in CH ₂ Cl ₂	15 min	Mostly Boc-protected trimer
7	10% TFA in CH ₂ Cl ₂	30 min	Mostly eliminated indole

The library demonstrates the tolerance of this method towards: aliphatic chains and hence analogues of Ala, Val, Leu, Ile residues (trimers **26** and **37**, Table 2.1), aromatics analogues of Phe and halogenated aromatics (**27-31**), sulfur containing side chains (**32**), tyrosine analogues (**33**), tryptophan analogues (**34**), basic and acidic chains analogues of Lys, Asp and Glu (**35** and **36**). The incorporation of an aliphatic sulfur containing side chain (*i.e.* a Met analogue) was also investigated, but the synthesis and purification of the corresponding monomer was problematic, and its limited solubility in chloroform is potentially responsible for the inefficiency of the coupling. In the case of an imidazole bearing monomer (*i.e.* a His analogue), two protecting groups were considered, namely Boc and Trt, but in both cases the Fmoc protection step proved cumbersome and fully protected monomer was not isolated. Functional tolerance towards a few remaining proteinogenic side chains still remains to be demonstrated; notably proline, cysteine, arginine, asparagine/glutamine and histidine, however the method that has been developed is sufficiently powerful for exploration of SAR space. In addition, α -amino acids can be coupled to the *N*-terminus of the oligobenzamide,

rendering the approach entirely compatible with standard oligopeptide synthesis (noting that amino acids loaded to the resin demonstrate this feature for the *C*-terminus, Figure 2.2).

The robustness of the method towards synthesizing longer oligomers, which might allow the mimicry of longer helical domains, has also been investigated. The optimized coupling conditions described in Scheme 2.2 have been applied in this study, using ten rounds of deprotection-coupling cycles. Test cleavages on small aliquots of resin were performed at different stages. This LC-MS analysis was useful to determine whether the coupling step was complete or not, but was not accurate enough to quantify the decrease in coupling efficiency after the pentamer. Tetramers and a pentamer have been made with purity confirmed by NMR as well as HRMS (cf. Experimental section) and it has been possible to extend the synthesis as far as the decamer (Figure 2.3, compound **40**).¹⁴⁴

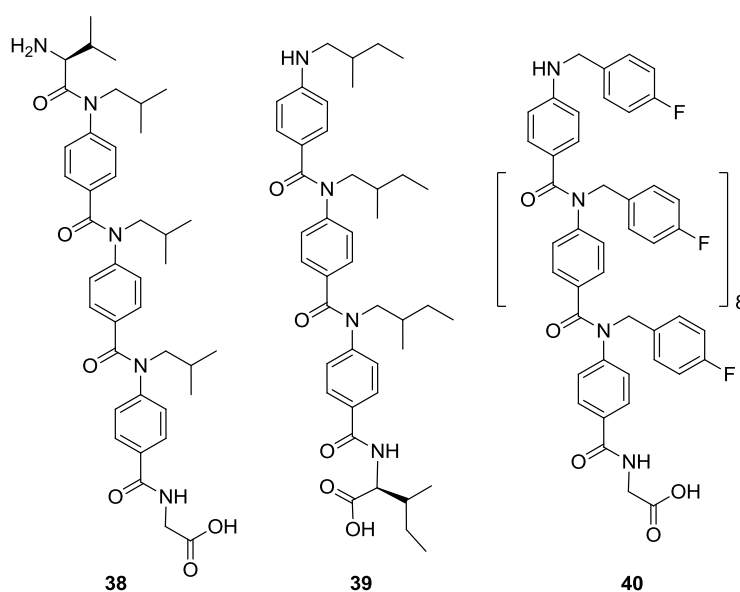


Figure 2.3 Extending the scope of the present SPS methodology. The method is compatible with natural amino acids both at the *N*- and *C*-terminus (compounds **38** and **39**) and can be extended to the synthesis of a decamer (**40**).

2.3 Conclusions

A robust automated SPS methodology has been established for the synthesis of *N*-alkylated oligobenzamides using a microwave assisted peptide synthesizer, allowing facile library generation of diversely functionalized compounds. A wide range of monomers has been prepared and incorporated into trimers to demonstrate the reproducibility and functional tolerance of our method. Side chains compatible with this method cover the whole range of hydrophobic side chains, which are the most commonly involved in PPI interfaces. Combinations of side chains give access to a wide variety of oligomers, and thus allow mimicry of numerous potential helix surfaces. The synthesis of oligomers up to the decamer has also been established, which broadens the range of possible applications for both this method and the present scaffold. Our ongoing efforts are directed towards the synthesis of a library and its screening against a diverse range of α -helix mediated PPIs.

Chapter 3

Testing the hypothesis: **Assembly and Screening of a library of proteomimetics**

As discussed in Chapter 1, targeting protein-protein interactions (PPIs) presents considerable therapeutic potential, as they regulate virtually every cellular process and are involved in a number of diseased states. Modulating them however constitutes a daunting challenge, given their intrinsic lack of defining features. Given the number of existing PPIs, a desirable approach would be to have adaptable and synthetically accessible lead molecules that can selectively target several PPIs *via* minor changes rather than tailoring a new chemical modulator from scratch for each PPI. A possible strategy would be to design compounds that are amenable to library assembly for screening. Intense research efforts have yielded several approaches to disrupt PPIs, though only a few are amenable to library generation.^{140, 141, 172} In the Wilson group, several oligobenzamide *proteomimetics* have been developed^{131, 143, 158} and in the case of the *N*-alkylated scaffold a modular solid phase synthesis (SPS) was established to build libraries of compounds. This methodology makes use of a state of the art microwave assisted peptide synthesiser and was described in Chapter 2. In the present chapter, the design, synthesis and biological testing of a library of 75 proteomimetics will be detailed. This library was mostly made of compounds targeted to the p53/*hDM2* and p53/*hDMX* interactions (cf. Chapter 1), but also contained a sub-library of compounds designed to disrupt the Bcl-2 family of interactions.

3.1 Targeting the p53/hDM2 interaction

3.1.1 The library

A 60-member library was generated using the SPS described in Chapter 2, which illustrated the robustness of the newly developed methodology. The set of monomers used in this library were mostly made of aromatic and aliphatic side chains, as shown in Figure 3.1.

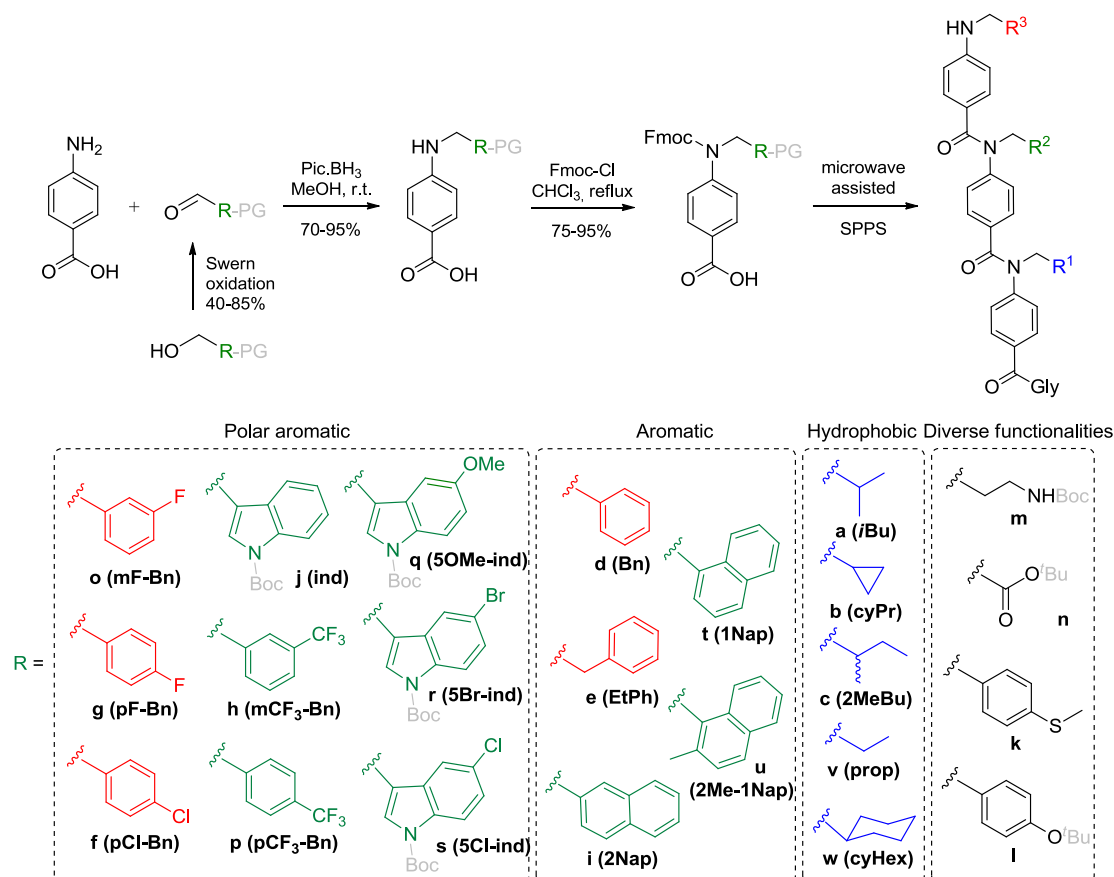
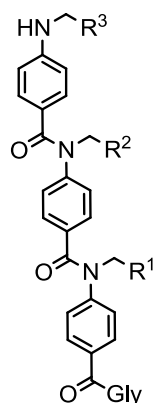


Figure 3.1 Monomer synthesis and set of monomers used in the library assembly using the automated SPS methodology described in Chapter 2. The monomers are colour-coded according to the p53 residues they are designed to mimic (red: Phe19 mimics, green: Trp23 mimics, blue: Leu26 mimics, grey: protecting groups that are removed during cleavage from the resin, named 'PG' in the synthetic scheme).

As described in the previous chapter, the first set of compounds was designed to assess the functional tolerance of the newly established coupling method and thus side chains R1 and R3 were fixed while all monomers were incorporated in the middle position. The library consisted of 60 trimers (Fig. 3.2), which were generally obtained in purities above 85-90% (judging from UV chromatograms

and NMR spectra). This was deemed as a high enough purity threshold for testing in the fluorescence anisotropy (FA) assay; considering that none of the purification methods tested was found to be efficient or high yielding (cf. Chapter 2). It was decided that when compounds with lower purities displayed good activities in the biophysical assay, they would be re-synthesised in order for the pure compound to be re-tested.



- | | | | |
|----|--|----|---|
| 26 | R ¹ = Bn, R ² = cyProp, R ³ = <i>i</i> Bu | 56 | R ¹ = Bn, R ² = <i>m</i> CF ₃ -Bn, R ³ = cyHex |
| 27 | R ¹ = Bn, R ² = Bn, R ³ = <i>i</i> Bu | 57 | R ¹ = cyProp, R ² = EtPh, R ³ = <i>m</i> F-Bn |
| 28 | R ¹ = Bn, R ² = EtPh, R ³ = <i>i</i> Bu | 58 | R ¹ = <i>m</i> F-Bn, R ² = EtPh, R ³ = cyProp |
| 30 | R ¹ = Bn, R ² = <i>m</i> CF ₃ -Bn, R ³ = <i>i</i> Bu | 59 | R ¹ = EtPh, R ² = <i>p</i> CF ₃ -Bn, R ³ = <i>i</i> Bu |
| 31 | R ¹ = Bn, R ² = <i>p</i> Cl-Bn, R ³ = <i>i</i> Bu | 60 | R ¹ = <i>p</i> F-Bn, R ² = cyHex, R ³ = Prop |
| 32 | R ¹ = Bn, R ² = <i>p</i> MeS-Bn, R ³ = <i>i</i> Bu | 61 | R ¹ = Bn, R ² = <i>i</i> Bu, R ³ = Bn |
| 33 | R ¹ = Bn, R ² = <i>p</i> OH-Bn, R ³ = <i>i</i> Bu | 62 | R ¹ = Bn, R ² = 2Naph, R ³ = cyProp |
| 36 | R ¹ = Bn, R ² = COOH, R ³ = <i>i</i> Bu | 63 | R ¹ = <i>p</i> Cl-Bn, R ² = 2Naph, R ³ = cyProp |
| 37 | R ¹ = <i>p</i> Cl-Bn, R ² = <i>m</i> CF ₃ -Bn, R ³ = 2Me-Bu | 64 | R ¹ = <i>m</i> CF ₃ -Bn, R ² = <i>m</i> CF ₃ -Bn, R ³ = Bn |
| 41 | R ¹ = <i>i</i> Bu, R ² = <i>p</i> CF ₃ -Bn, R ³ = <i>i</i> Bu | 65 | R ¹ = <i>p</i> Cl-Bn, R ² = <i>m</i> CF ₃ -Bn, R ³ = cyProp |
| 42 | R ¹ = Bn, R ² = 2Me-1Naph, R ³ = <i>i</i> Bu | 66 | R ¹ = <i>p</i> F-Bn, R ² = 2Naph, R ³ = Prop |
| 43 | R ¹ = EtPh, R ² = <i>p</i> Cl-Bn, R ³ = <i>i</i> Bu | 67 | R ¹ = 2Naph, R ² = <i>i</i> Bu, R ³ = Bn |
| 44 | R ¹ = <i>i</i> Bu, R ² = <i>p</i> F-Bn, R ³ = <i>i</i> Bu | 68 | R ¹ = <i>p</i> F-Bn, R ² = <i>p</i> F-Bn, R ³ = <i>i</i> Bu |
| 45 | R ¹ = Bn, R ² = <i>p</i> F-Bn, R ³ = <i>i</i> Bu | 69 | R ¹ = <i>p</i> F-Bn, R ² = <i>m</i> F-Bn, R ³ = <i>i</i> Bu |
| 46 | R ¹ = Bn, R ² = <i>m</i> F-Bn, R ³ = <i>i</i> Bu | 70 | R ¹ = Bn, R ² = <i>m</i> CF ₃ -Bn, R ³ = 2Me-Bu |
| 47 | R ¹ = Bn, R ² = 1Naph, R ³ = <i>i</i> Bu | 71 | R ¹ = Bn, R ² = <i>p</i> CF ₃ -Bn, R ³ = 2Me-Bu |
| 48 | R ¹ = Bn, R ² = prop-NH ₂ , R ³ = <i>i</i> Bu | 72 | R ¹ = <i>p</i> F-Bn, R ² = <i>m</i> CF ₃ -Bn, R ³ = 2Me-Bu |
| 49 | R ¹ = Bn, R ² = <i>p</i> F-Bn, R ³ = Prop | 73 | R ¹ = EtPh, R ² = <i>m</i> CF ₃ -Bn, R ³ = 2Me-Bu |
| 50 | R ¹ = <i>m</i> F-Bn, R ² = <i>m</i> CF ₃ -Bn, R ³ = <i>i</i> Bu | 74 | R ¹ = <i>p</i> Cl-Bn, R ² = <i>p</i> CF ₃ -Bn, R ³ = 2Me-Bu |
| 51 | R ¹ = <i>p</i> Cl-Bn, R ² = <i>m</i> CF ₃ -Bn, R ³ = <i>i</i> Bu | 75 | R ¹ = EtPh, R ² = <i>p</i> CF ₃ -Bn, R ³ = 2Me-Bu |
| 52 | R ¹ = <i>p</i> F-Bn, R ² = <i>m</i> CF ₃ -Bn, R ³ = <i>i</i> Bu | 76 | R ¹ = <i>p</i> Cl-Bn, R ² = <i>m</i> F-Bn, R ³ = 2Me-Bu |
| 53 | R ¹ = Bn, R ² = 5Br-Ind, R ³ = <i>i</i> Bu | 77 | R ¹ = <i>p</i> Cl-Bn, R ² = <i>p</i> Cl-Bn, R ³ = 2Me-Bu |
| 54 | R ¹ = Bn, R ² = cyHex, R ³ = <i>i</i> Bu | 78 | R ¹ = <i>p</i> F-Bn, R ² = <i>p</i> CF ₃ -Bn, R ³ = <i>i</i> Bu |
| 55 | R ¹ = Bn, R ² = EtPh, R ³ = Prop | 79 | R ¹ = <i>p</i> F-Bn, R ² = <i>p</i> CF ₃ -Bn, R ³ = cyProp |
| | | 80 | R ¹ = Bn, R ² = <i>m</i> CF ₃ -Bn, R ³ = Prop |
| | | 81 | R ¹ = cyHex, R ² = 2Naph, R ³ = EtPh |
| | | 82 | R ¹ = Bn, R ² = <i>m</i> CF ₃ -Bn, R ³ = cyProp |
| | | 83 | R ¹ = EtPh, R ² = <i>m</i> F-Bn, R ³ = <i>i</i> Bu |
| | | 84 | R ¹ = <i>p</i> Cl-Bn, R ² = <i>m</i> F-Bn, R ³ = <i>i</i> Bu |
| | | 85 | R ¹ = <i>p</i> Cl-Bn, R ² = <i>p</i> F-Bn, R ³ = <i>i</i> Bu |
| | | 86 | R ¹ = EtPh, R ² = <i>p</i> F-Bn, R ³ = <i>i</i> Bu |
| | | 87 | R ¹ = EtPh, R ² = 2Me-1Naph, R ³ = <i>i</i> Bu |
| | | 88 | R ¹ = <i>p</i> Cl-Bn, R ² = 2Naph, R ³ = <i>i</i> Bu |
| | | 89 | R ¹ = EtPh, R ² = 5Br-BocInd, R ³ = <i>i</i> Bu |
| | | 90 | R ¹ = EtPh, R ² = H, R ³ = <i>i</i> Bu |
| | | 91 | R ¹ = Bn, R ² = <i>p</i> CF ₃ -Bn, R ³ = <i>i</i> Bu |

Figure 3.2 The library of 60 proteomimetics targeting the p53/hDM2 interaction. The side chains are named using the nomenclature reported in Figure 3.1.

Monomers **q** and **s** (5-methoxy indole and 5-chloro indole respectively) have not been successfully included in the library, due to a technical limitation that was discussed in Chapter 2 (during acidic cleavage from the resin, the indole side chains were eliminated along with the Boc-deprotection), hence only limited amounts of these compounds - if any - were obtained in sufficient purity for preliminary testing. In one instance, a small amount of the desired unprotected Boc-indole trimer could be isolated (compound **53**) and on another occasion, some Boc-protected indole containing trimer was isolated (**89**). In order to yield a relatively focused library of p53 mimetics, the benzyl monomer was chosen as the *N*-terminal residue (Phe19 mimic) and the isobutyl monomer as the *C*-terminal one (Leu26 mimic). The next few compounds were then obtained by replacing one of the terminal side chains with a structural analogue, *i.e.* Bn was replaced with EtPh or a halogenated aromatic side chain whilst *i*Bu was replaced with a cyclopropyl ring or other aliphatic side chains. A few trimers with mismatched sequences were also prepared. The first 15 compounds were tested in a manual single point assay (cf. Section 3.1.2.2); these results were used to establish some structure-activity relationships which guided the design of the next series of compounds.

3.1.2 Biophysical evaluation of the library of oligobenzamides

Initially, it was planned that the library of oligobenzamides would be tested against both the p53/*hDM2* and the p53/*hDMX* interactions. I expressed His-*hDM2*₁₇₋₁₂₆ L33E with the assistance of Dr. A. Bartlett at the Astbury Centre for Structural Molecular Biology, following a procedure that was established previously in the group.¹³¹ As no *hDMX* clone was available, molecular cloning experiments were carried out in an attempt to obtain *hDMX* constructs containing different tags (cf. Experimental Section):

- His-*hDMX*: could be used in Fluorescence Anisotropy (FA) assays, the His-tag being useful for purification.
- His-Tev-GFP-PreS-*hDMX*: a *hDMX* construct that contains a removable fluorescent tag; the resulting protein could be used as such in FRET assays, or the GFP-tag could be cleaved *via* the PreS site (a recognition sequence that can be

specifically cleaved by a PreScission protease – a genetically engineered protease) to yield a non-fluorescent protein for FA assays.

- GST-*hDMX*: could be used in FA assays, GST is also known to enhance the solubility of other proteins.

- SUMO-*hDMX*: could be used in FA assays, crystallisation trials and is known to enhance the solubility of the protein.

Of all the attempts to prepare these constructs, the only recombinant DNA that was successfully prepared was His-Tev-GFP-PreS-*hDMX*₂₆₋₁₁₀, as confirmed by sequencing. Tev designates a recognition site that can be specifically cleaved by a TEV protease (from Tobacco Etch Virus); it is commonly used to remove affinity tags such as the His-tag from proteins following purification.¹⁷³ This construct would be suitable for future FRET assays as a fluorescent tag is attached to the protein, but not for the FA assay. Cleavage of the GFP-tag using PreScission protease was then attempted to obtain the non-fluorescent protein for FA assay, but the cleavage unexpectedly failed. This protein could thus not be used to screen the library, and time did not allow for further molecular cloning and construct investigation to be carried out at that point. Further efforts have been dedicated by the Edwards group (Dr. A. Bartlett and S. Hussain) towards obtaining a *hDMX* construct that would be suitable for use in fluorescence anisotropy assays. An additional non-fluorescent GST-*hDMX* construct was successfully produced and expressed, but it however proved to be relatively unstable. Only one compound could be tested using this protein, the results are presented in Section 3.3. The library has therefore only been assessed on the p53/*hDM2* interaction using a FA assay, first in single point, then in a competition assay that allowed a better quantification of the efficiency of the compounds.

3.1.2.1 The fluorescence anisotropy assay

The library was tested against p53/*hDM2* in a previously reported FA competition assay (Fig. 3.3).⁸⁵ In this assay, the change in anisotropy is measured upon displacement of a fluorescein-labelled p53 peptide from *hDM2* by the proteomimetic (Fig. 3.3). This assay is also employed by other research groups to test new potential inhibitors.^{29, 125, 174, 175} In order to determine the limits of anisotropy that can be observed in this assay, the binding of the native p53 tracer

to hDM2 was assessed. A serial dilution of the protein into the tracer (Fig. 3.3c) allowed the determination of the dissociation constant ($K_d = 164.4 \pm 10.8$ nM), which was in the range of values that were previously obtained in the group. A dose-response titration was also carried out with Nutlin-3a (which served as positive control in the experiments described thereafter) and provided an IC_{50} of 353.9 ± 6.59 nM (Fig. 3.3d), which was in the nanomolar range, as initially reported by Vassilev and co-workers using a surface plasmon resonance assay ($IC_{50} = 90$ nM).⁷

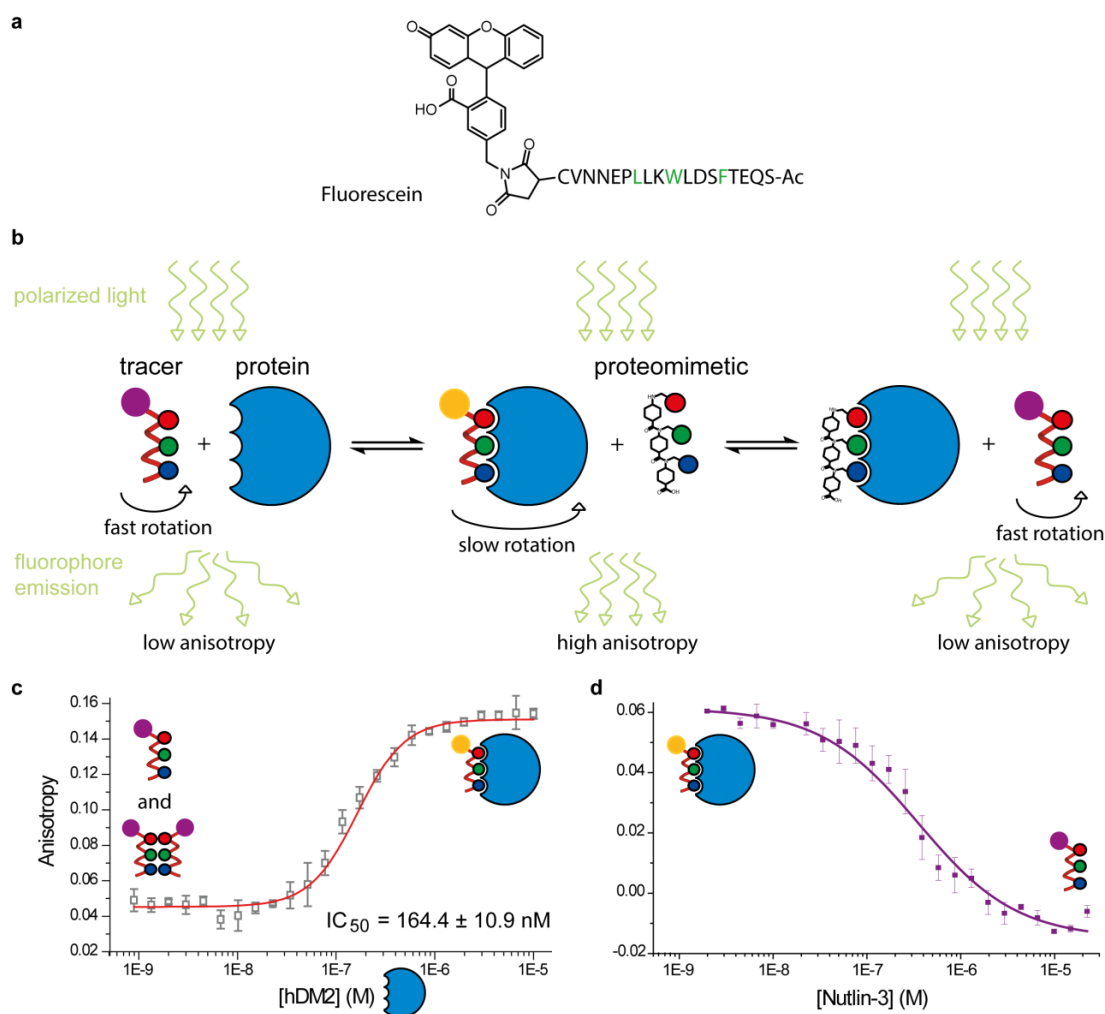


Figure 3.3 The fluorescence anisotropy assay. **a.** The p53 tracer (Flu-p53₁₅₋₃₁). **b.** At low concentrations of protein (His-hDM2₁₇₋₁₂₆ L33E) the tracer is free to tumble in solution: the directionality of the polarized excitation light is lost. At high concentrations of protein, the tracer is engaged in a much bigger complex: the tumbling is reduced hence an increase in anisotropy. At high concentrations of proteomimetic: the tracer is freed from its complex with the protein, the anisotropy decreases again. **c.** Direct titration of protein. **d.** Displacement assay using Nutlin-3a.

In this competition assay, the concentration of protein and tracer were kept constant (150 nM and 50 nM respectively) while the proteomimetic was serially diluted from 100 μ M down to 9 nM (cf. competition assay with Nutlin-3a, Fig. 3.3d). Previous experience with competition assays on this PPI within the group has revealed that the equilibrium taking place was not a simple two state competition and likely involved aggregation/interaction of the tracer with all other component present, as depicted in Figure 3.4. This complex equilibrium prevented the determination of K_d values. The fluorescently tagged p53 was not only interacting with *hDM2*, but also itself, as well as with the proteomimetic¹³¹ and the positive controls (unlabelled p53 and Nutlin-3a). These undesired interactions generated additional contributions to the overall anisotropy.

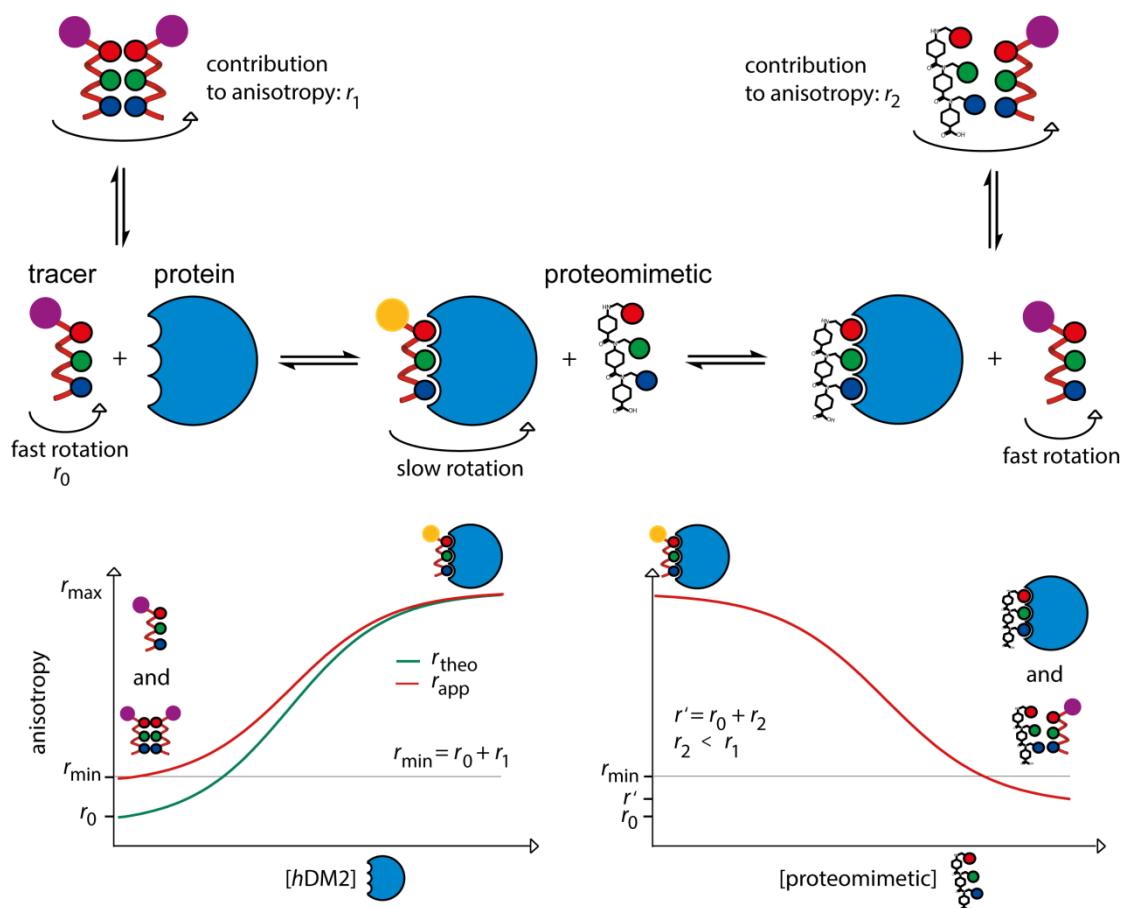


Figure 3.4 The equilibrium preventing K_d determination. In this assay, aggregation of the tracer during the direct titration (left plot, contribution to the anisotropy = r_1) prevents determination of r_0 (theoretic minimum anisotropy). Interaction of the tracer with the proteomimetic during the displacement assay (right plot, contribution to the anisotropy = r_2) precludes measurement of the expected end-point (r_{min}).

The minimum anisotropy r_{\min} was determined during the direct titration of the tracer by *hDM2*. It should correspond to a solution where the tracer would be completely free to tumble. But given that the tracer has been found to interact with itself (r_1), the anisotropy value at the beginning of the titration was actually above the theoretical value ($r_{\min} > r_0$). During the competition assay, the tracer was progressively displaced from the interaction, but the concentration of proteomimetic at the end point was much higher than the concentration of tracer. The probability to find the tracer aggregated with another tracer molecule was thus much lower than the probability for tracer-inhibitor complexes to form, and the latter species would bring a smaller contribution to the anisotropy (r_2).

3.1.2.2 Initial screening: manual single point assay

Considering the large number of compounds to be tested and the amount of protein that would be required to test all of them in a dose-response competition assay, a rapid screening of the library was necessary. This was designed as a relatively crude experiment which although unlikely to provide quantitative data, would allow establishment of a rough ranking of the compounds and identification of the most potent inhibitors in order to further test them in a full competition assay. Subsets of compounds were tested manually in a 96-well plate, where each compound was tested in triplicate and one blank was measured. This allowed screening 15 compounds per plate and the concentration of proteomimetic was fixed at 10 μM . A positive control known to bind the target protein was present on each plate, in the case of the p53/*hDM2* interaction, unlabelled p53 and Nutlin-3a (one of the most potent inhibitors of the p53/*hDM2* PPI known to date,⁷ cf. Chapter 1) was chosen and used as a reference to assess the potency of the *N*-alkylated tribenzamides. In the case of Nutlin-3a, a concentration of 10 μM effected displacement of the tracer; compounds that gave anisotropies values close to that of Nutlin-3a were thus likely to have IC_{50} values in the low micromolar/nanomolar range. Compounds that were not significantly displacing the tracer at this concentration were considered inactive.

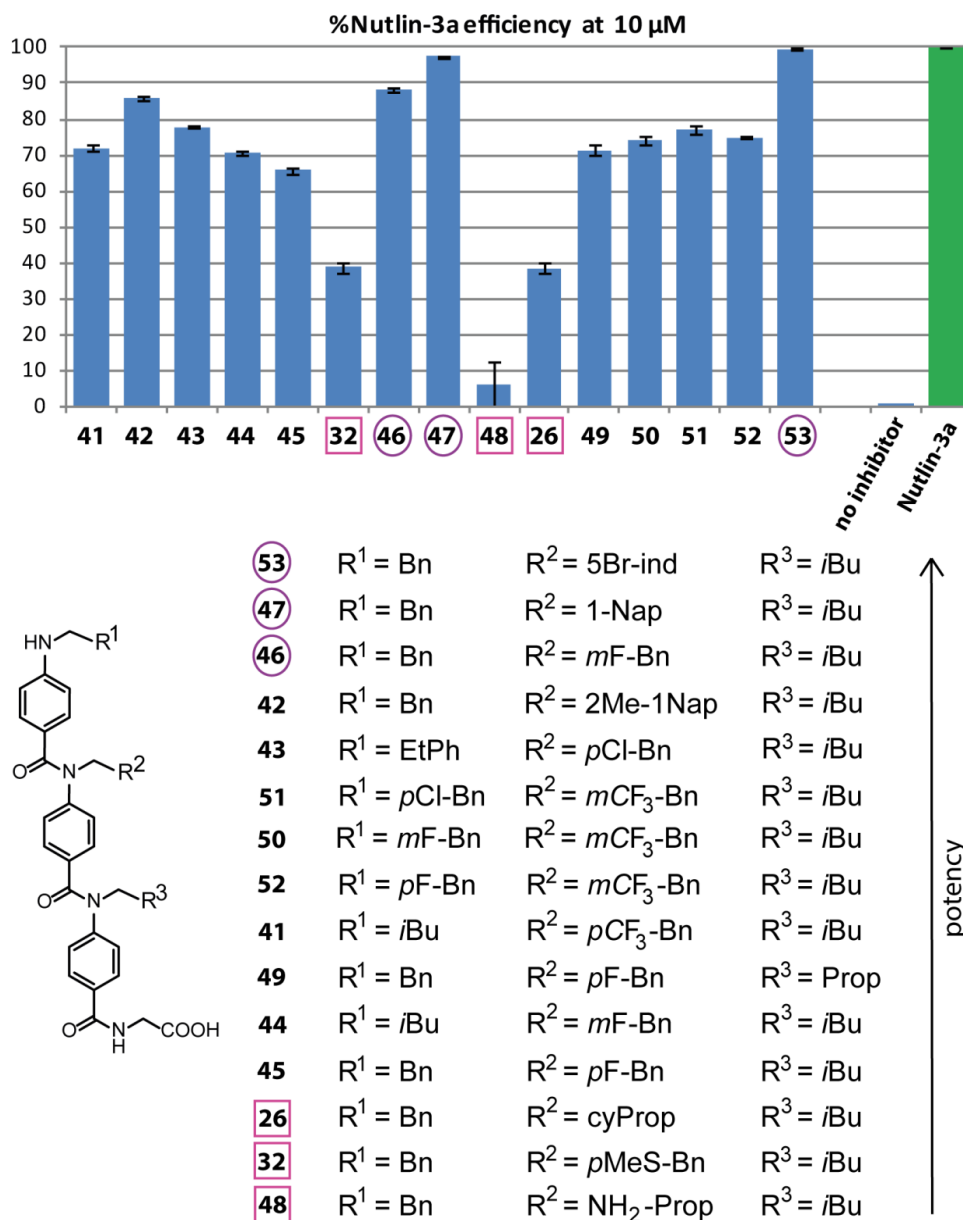


Figure 3.5 Results from a single point assay on the first subset of 15 compounds at 10 μ M, presented as a percentage of Nutlin-3a efficiency. In this assay, the positive control is Nutlin-3a (set to 100% efficiency) and the negative control is a well where the inhibitor is replaced with buffer (0% efficiency). The least active compound is **48**, and the most active ones are **46**, **47** and **53**.

In order to get data that is easily comparable between compounds tested on different plates, a relative efficacy compared to the positive control was calculated for each compound (the efficacy of the positive control was set to 100%) and the results are presented as a bar diagram. Results from this single point screening are reported in Figure 3.5; the relative efficiency of each

compound compared to Nutlin-3a was represented by a bar. From this initial screening, it appeared that these first 15 compounds presented a broad range of efficacies. Compounds **32**, **48** and **26** were poorly active against the target PPI (< 40% Nutlin-3a efficiency). These compounds all had suitable side chains to mimic Phe19 and Leu26, but a mismatched side chain at the Trp23 position (respectively: 4-methylthiobenzyl, 3-aminopropyl, and cyclopropyl). On the other hand, compounds **42**, **46**, **47** and **53** presented efficiencies above 85% of that from Nutlin-3a. These four compounds all possessed appropriate side chains to mimic the three p53 hot-spot residues, and in particular bulky aromatic residues in the middle position. These compounds, along with the least active **48** were then tested in a full competition assay; the resulting binding curves are overlaid in Figure 3.6. In the design of the next compounds, bulky aromatics as well as halogenated benzyl rings were thus prioritised.

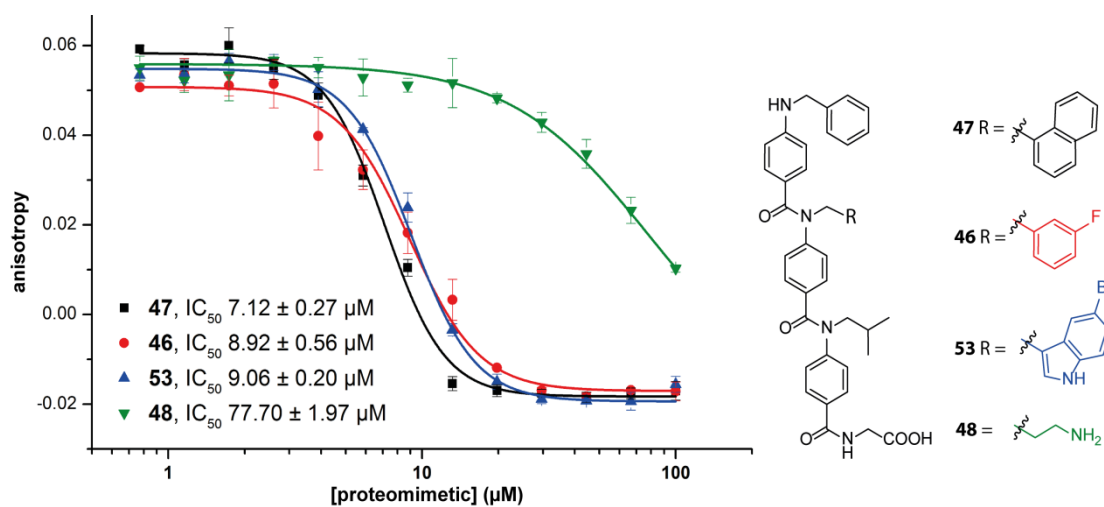


Figure 3.6 Dose-response curves for hits identified in the single point screening against p53/hDM2 (compounds **46**, **47**, **53**) along with the least potent compound in this series (compound **48**).

Compounds **46**, **47** and **53** had been tested on the same plate in the single point assay, and their %Nutlin-3a efficiencies were 88.2%, 97.3% and 99.6% respectively. The IC_{50} s determined in this competition assay did not confirm the preliminary ranking established from the single point assay, but rather that

compound **47** is the most potent one ($IC_{50} = 7.12 \pm 0.27 \mu\text{M}$, Fig. 3.6), followed by compound **46** ($IC_{50} = 8.92 \pm 0.56 \mu\text{M}$) and then compound **53** ($IC_{50} = 9.06 \pm 0.20 \mu\text{M}$). As a comparison, Nutlin-3a displayed an IC_{50} of $354 \pm 67 \text{ nM}$. These results suggest that the single point assay is not accurate enough to provide a definite ranking of compounds, but that it is a useful tool to identify the most potent compounds within a series. For compound **48**, which was identified as the least potent in the single point assay, the lower asymptote was not reached in the dose-response assay (Fig. 3.6, green curve). This means that even at $100 \mu\text{M}$, **48** was not able to completely displace the tracer from its interaction with *hDM2*. The binding curve was plotted using a fixed anisotropy corresponding to the lower plateau that should be reached upon complete displacement, which allowed measuring an apparent IC_{50} of $77.70 \pm 1.97 \mu\text{M}$.

The second set of compounds was tested on another 96-well plate; results from this single point screen are presented in Figure 3.7. Some of the compounds appeared to exceed the 100% efficiency set for the positive control in this assay - this was probably due to compound-tracer interactions. It is worth noting that among the most potent compounds from this series, the vast majority fitted the design rules: small aromatic ring in R1, bulky aromatic side chain in R2 and aliphatic side chain in R3. Less potent compounds generally presented mismatched side chains at the R2 position, whether aliphatic (**60**, **54**), hydrophilic (**36**), or polar aromatic (**33**).

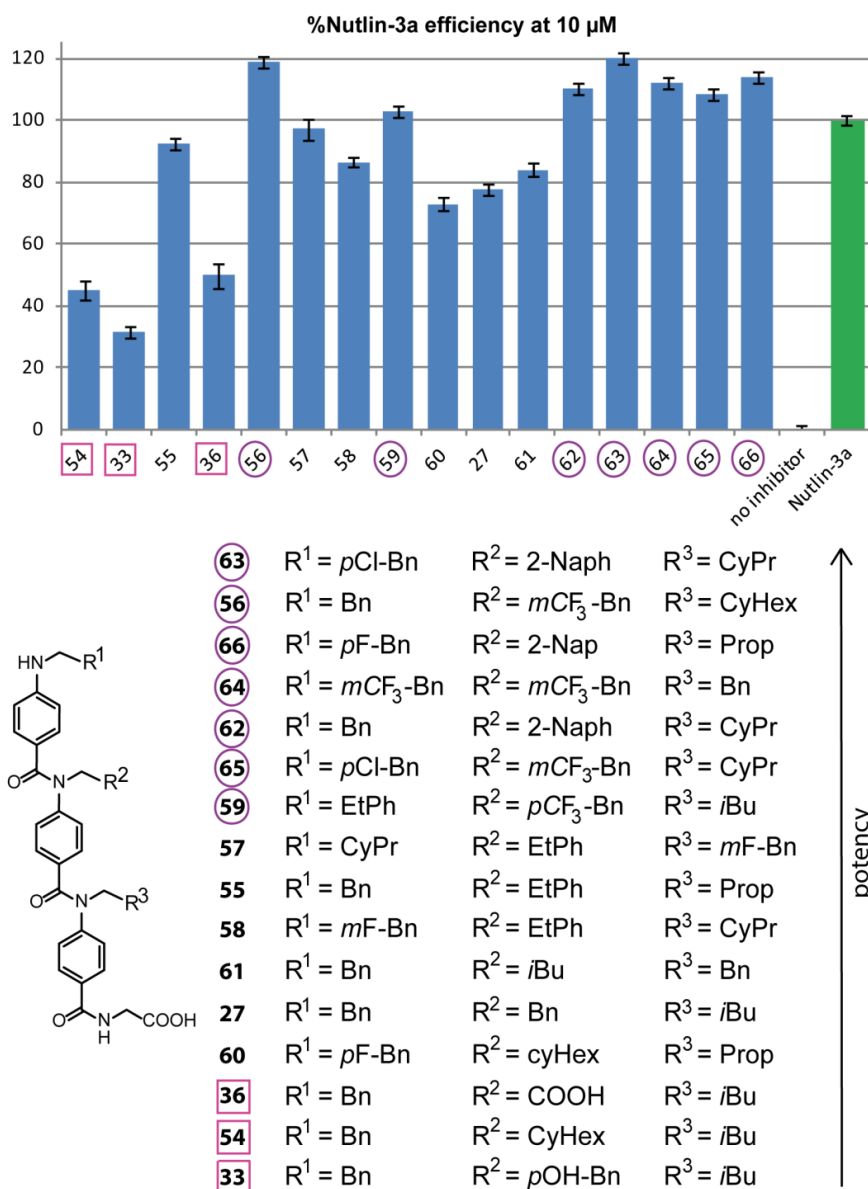


Figure 3.7 Single point screening on the second subset of 15 compounds. The most potent compounds were **56, 59, 62, 63, 64, 65, 66** (purple circles) and the least potent ones were **54, 33, 36** (pink squares).

Four hits from this subset, *i.e.* compounds **56, 62, 63, 66** as well as the least potent **33** were tested in a full competition assay. The resulting dose-response curves are presented in Figure 3.8. As expected, compounds that displayed more than 100% efficiency in the single point assay presented a lower IC₅₀ than Nutlin-3a when tested in the full competition assay. Compounds **57** and **58** displayed similar % efficiencies, suggesting that there was no significant impact of reversing the compound's macrodipole on the potency.

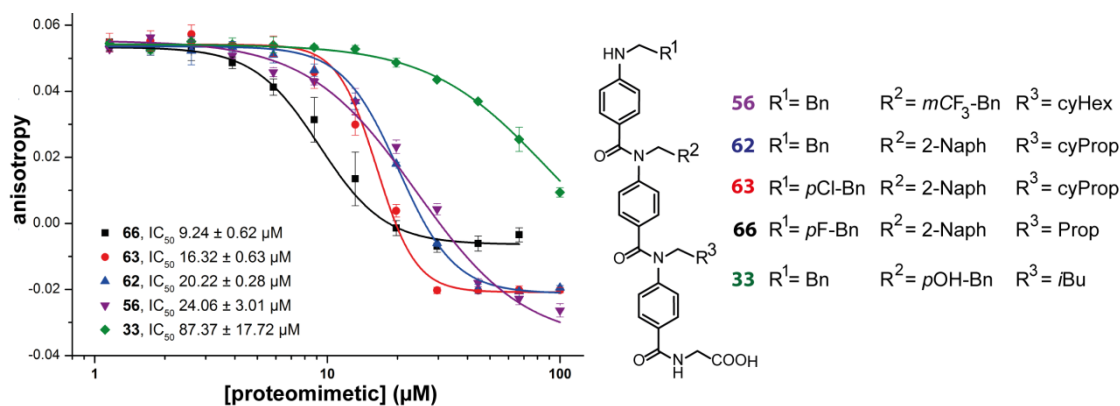


Figure 3.8 Dose-response curves for hits identified in the single point assay (compounds **56**, **62**, **63**, **66**) as well as for the least potent compound **33**.

As was the case for the first series of compounds, the real ranking of the compounds established in the competition assay did not reflect the one that was observed in the single point assay.

Results from the third subset of compounds (**60** – **77**, Fig. 3.9) suggested that compounds **60**, **67**, **69** and **70** were the least potent ones. Compounds **60** lacked an aromatic ring at the R2 position and **67** was a mismatched sequence, so they were both expected to be poorly active. It was thought that the other two compounds (**69** and **70**) would be good mimetics, as they display a side chain arrangement that matches that of the p53 hot-spots. Their poor efficiency was especially surprising when considering that **68** and **71** were two of the most potent ones, and only differed from **69** and **70** (respectively) by the position of the substituent of the benzyl at the R2 position. Compounds **71** to **77** all fitted the initial design rules (aromatic ring at R1, substituted aromatic ring at R2 and aliphatic chain at R3) and appeared to be efficient in this assay. This confirmed the design rule and validated the use of the 2-methylbutyl side chain as a Leu26 mimic but it also suggested that there might have been a problem with compounds **68** - **70** during the testing. Repeating the assay on compounds **60** and **67-71** confirmed the ranking, but the gap in efficiencies between **68/69** and **70/71** was reduced (%Nutlin-3a efficiencies were: 71%/56% and 51%/69% respectively and 25% for **67**, data in Appendix I).

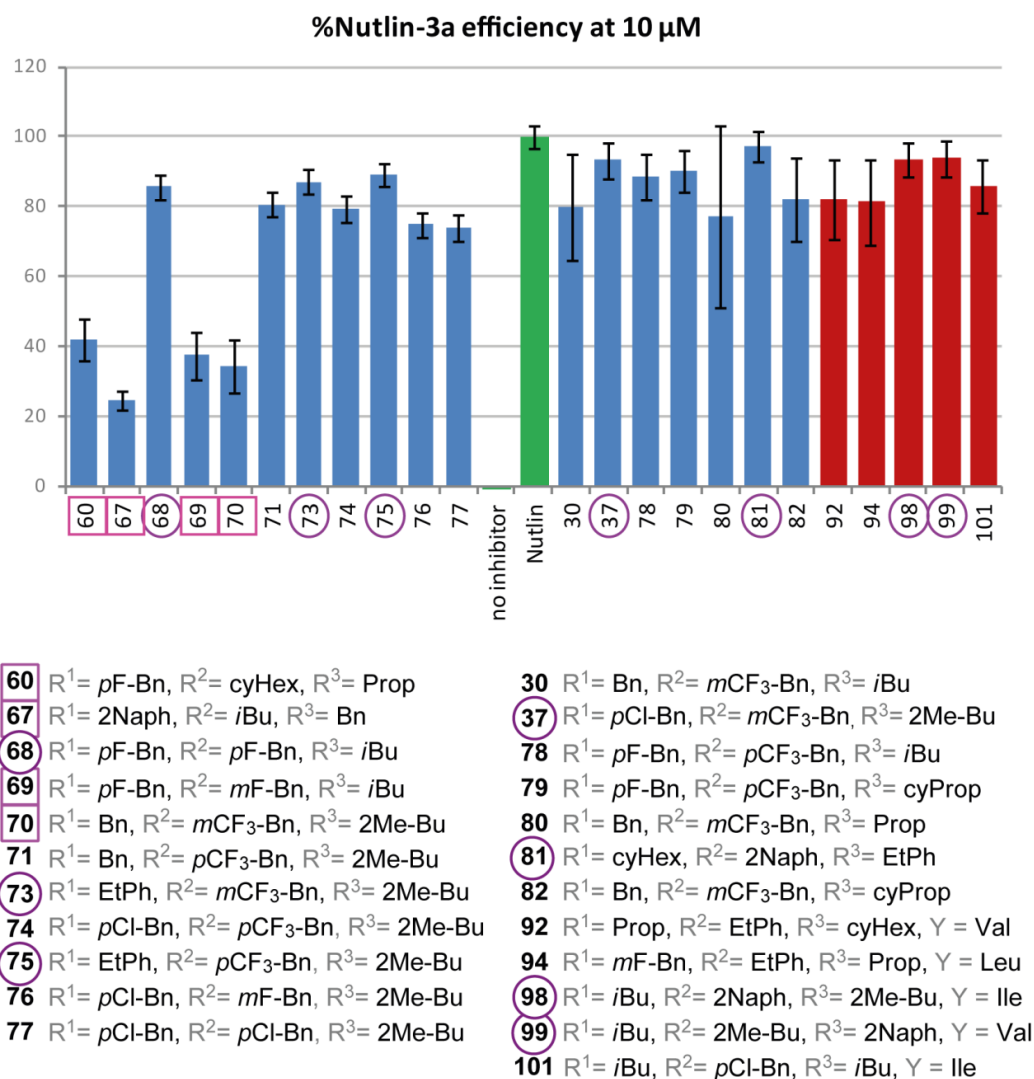


Figure 3.9. Results from single point screening on the third and fourth set of compounds against p53/hDM2, at 10 μ M. Sets of compounds reported on either side of the controls (no inhibitor and Nutlin-3a, green) have been tested together. Compounds in red (92-101) have an additional natural amino acid attached to their C-terminus (Y).

The influence of the position of the substituent on the benzyl ring at R2 was studied through comparison of compounds **68** and **69**. The single point screen indicated that **68** (*para*-substituted) was more active than the *meta*-substituted compound (86% for **68** against 37% for **69** in the first screening, ranking confirmed by repeating the experiment). Comparison of their binding curves revealed only a slight preference towards substitution at the *para* position, although the difference in affinity was relatively small (5 μ M, Fig. 3.10) and could be compound-dependent.

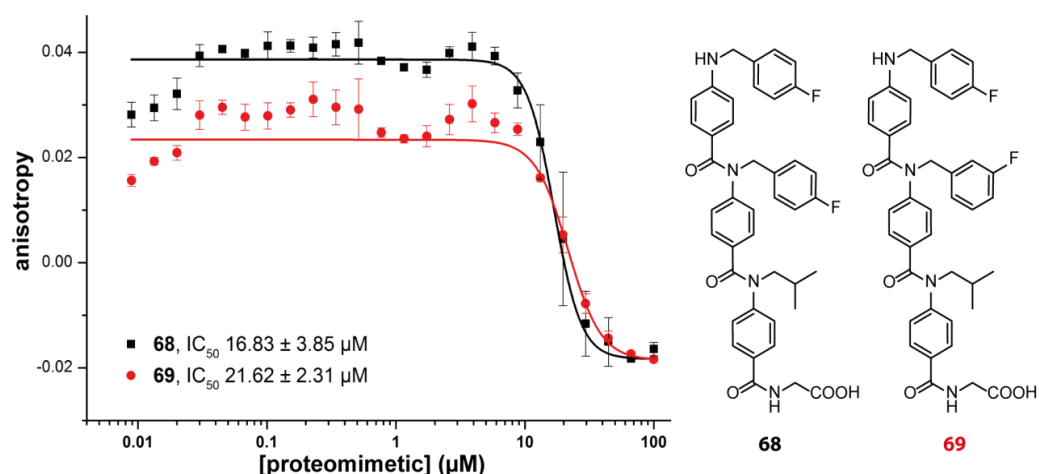


Figure 3.10. Comparing para (**68**) and meta (**69**) substitution on the benzyl ring at position R2. These compounds were tested on the Hamilton robot.

The fourth subset of compounds (**30**, **37**, **78-101**) presented more homogenous results, with efficiencies between 78-98%. The subset of compounds displaying 3 side chains (in blue, Fig. 3.9) was relatively focused, with bulky aromatics at the R2 position; most potent compounds included **37** and **81**. Interestingly, the last subset of hybrid compounds containing an additional α -residue displayed good activity despite presenting only one aromatic side chain out of four substituents. This confirmed that the presence of an aromatic ring at R2 was a sufficient condition for binding to *hDM2*. The most potent hybrid compounds were the two that contained the bulkiest substituent (2-naphthyl, **98**, **99**).

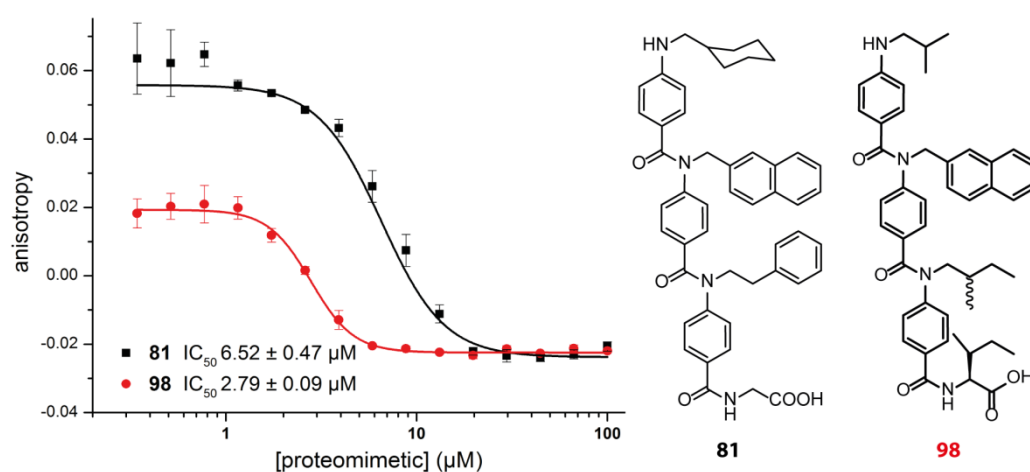


Figure 3.11. Dose-response curves for hits on the fourth subset of compounds (**78-101**). Compound **81** was tested in 96-well plates whereas **98** needed to be tested in 384-well plates, which explains the different titration start points.

The most potent tribenzamide **81** and the most potent hybrid oligoamide **98** were tested for dose-response (Fig. 3.11). Both displayed low micromolar IC₅₀s (6.52 ± 0.47 μM for **81**, 2.79 ± 0.09 μM for **98**). The anisotropy value at the start of the titration is different for these compounds because **98** was tested in a 384-well plate, whereas **81** was tested in a 96-well plate; however this should not affect the IC₅₀ value. It is worth noting that **60** had already been tested with the previous set of compounds (Fig. 3.7) and despite being one of the least active compounds then, it still displayed a ~68% efficiency (but the most active compounds from this screen displayed efficiencies above 100%). When re-tested with the third set of compounds (Fig. 3.9), **60** was again one of the least active compounds, this time displaying a 40% efficiency. This illustrated that although the raw values extracted from these assays – and therefore the relative ranking of compounds - were not necessarily reproducible, hits and inactive compounds could still be reliably identified.

Taking together observations from all these separate single point experiments, it appeared that testing all the compounds in one single experiment could potentially improve the accuracy and representativeness of the results. Using different batches and stocks of reagents indeed introduced some variability into this assay. Different batches of tracer will present different behaviours towards aggregation and protein stocks prepared on separate occasions were likely to present slight fluctuations in concentration and protein folding, especially if the stocks were made with different batches of buffer. It therefore seemed necessary to test the compounds under the exact same assay conditions, and considering the time required to plate manually a set of 15 compounds, this would only be achievable using an automated method.

3.1.2.3 Automated single point screening of the library

It appeared that the reproducibility of the assay was variable for compounds tested separately – and therefore using different protein and tracer solutions. In order to maximize the accuracy of the results, an automated method was developed by Dr. C. J. Empson to test the library in single point on a Hamilton Star

Microlab robot. This method allowed for the whole library to be tested within 3 hours and made use of 384-well plates, which helped reduce the consumption of protein and tracer. No reproducible conditions could be found for the single point on the robot using 384-well plates, and the broad range of relative efficiencies that corresponded to previously identified hits indicated that results from this automated screening failed to reproduce results from the initial screens carried out manually in 96-well plates. Results from the automated screening of the library were thus not exploitable (cf. Appendix II). Performing the assay manually in 96-well plates however presented two drawbacks: it was highly time consuming, and used a lot of material. A method could be developed to carry out the assay on 96-well plates on the robot, which would make it more time-efficient, but this has not been attempted as it would have consumed a large amount of reagents for information that was already available. It might however be worth considering for screening against other PPI targets in the future.

3.2 Targeting the Bcl-2 family of interactions

As mentioned in Chapter 1, the interactions between pro- and anti-apoptotic members of the Bcl-2 family involve 4 key binding residues. The two main interactions targeted in this study were the Bcl-2/Bak and the Mcl-1/Noxa B interactions, as is the case for the other interactions within this family, the hot-spot residues involved in the binding are mostly aliphatic (Fig. 3.12a-c). The Hamilton group reported that in the case of the Bcl-x_L/Bak interaction, only 3 consecutive hot-spot residues from Bak needed to be mimicked in order to achieve competitive binding to Bcl-x_L,¹⁷⁶ and mimicking the fourth key residue using an alternative scaffold even proved to be detrimental to the activity,^{136, 137} although it is not excluded that the loss of potency might be due to the scaffold itself. For the purposes of this study we chose to adapt the *N*-alkylated oligobenzamide scaffold so as to mimic all four key side chains. Both sub-libraries were then tested against both targets, in order to study the versatility and selectivity of each scaffold.

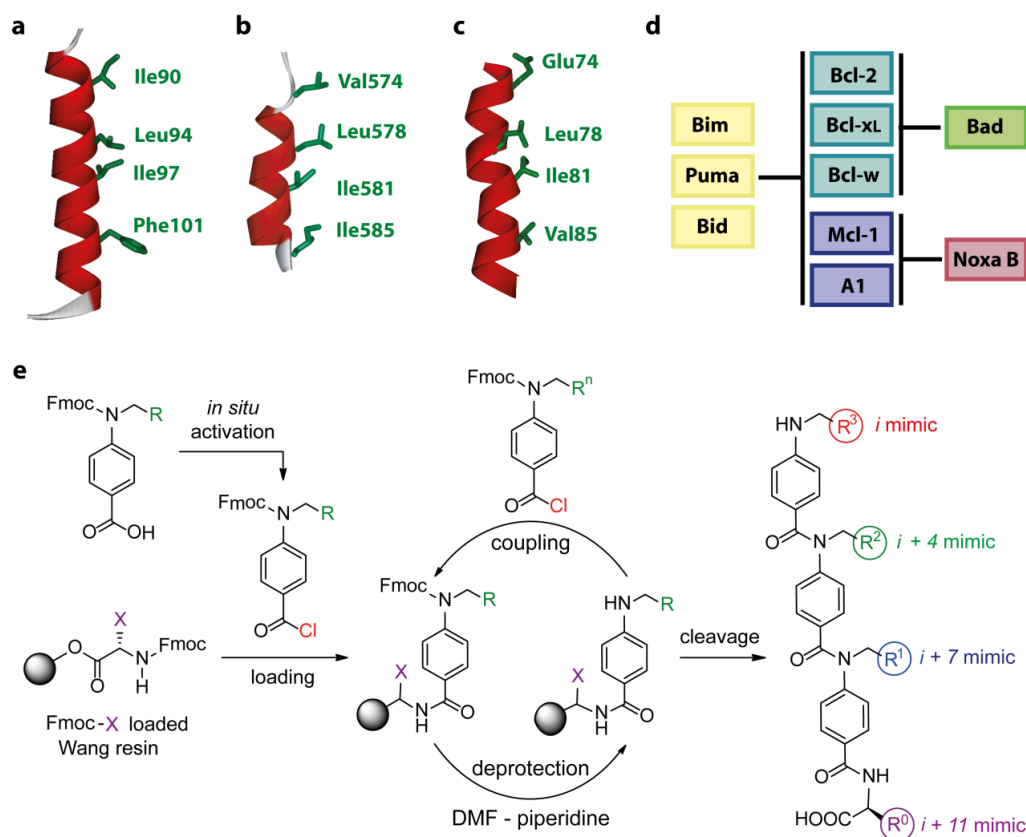
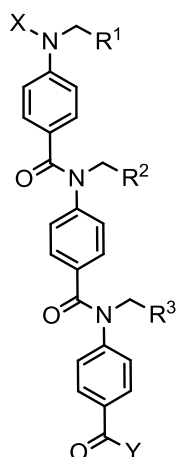


Figure 3.12 Targeting the Bcl-2 family: model interactions and SPS strategy. **a.** The Bim helix (PDB ID: 1PQ1). **b.** The Bak helix involved in binding to Bcl-x_L (PDB ID: 1BXL). **c.** The Noxa B helix involved in binding to Mcl-1 (PDB ID: 2JM6). **d.** Binding profiles for the main Bcl-2 family members. **e.** SPS scheme leading to proteomimetics displaying 4 side chains.

As mentioned in Chapter 2, the library of trimers targeting the p53/hDM2 PPI was built on solid phase, using a Wang resin pre-loaded with Gly. It was envisaged that this SPS methodology could directly be transposed to the synthesis of proteomimetics displaying 4 key side chains by simply using a resin pre-loaded with a different α -amino acid (Fig. 3.12e). This approach yielded proteomimetics where three hot-spot residues would be mimicked by the aromatic building blocks, whereas the fourth one would be mimicked by the α -residue preloaded on the resin. Given that the pro-apoptotic members of the Bcl-2 family are mostly made of combinations of aliphatic residues, monomers bearing an aliphatic side chain were prioritised in this library (Fig. 3.13).



- 92** R¹= Prop, R²= EtPh, R³= cyHex, X = H, Y = Val
93 R¹= Prop, R²= cyHex, R³= Prop, X= H, Y = Ile
94 R¹= *m*F-Bn, R²= EtPh, R³= Prop, X= H, Y = Leu
95 R¹= 2Me-Bu, R²= 2Me-Bu, R³= 2Me-Bu, X = H, Y = Ile
96 R¹= *i*Bu, R²= *i*Bu, R³= *i*Bu, X = Val, Y = Gly
97 R¹= *i*Bu, R²= 2Me-Bu, R³= 2Me-Bu, X = H, Y = Ile
98 R¹= *i*Bu, R²= 2Naph, R³= 2Me-Bu, X = H, Y = Ile
99 R¹= *i*Bu, R²= 2Me-Bu, R³= 2Naph, X = H, Y = Val
100 R¹= *i*Bu, R²= 2Me-Bu, R³= *p*Cl-Bn, X = H, Y = Val
101 R¹= *i*Bu, R²= *p*Cl-Bn, R³= *i*Bu, X = H, Y = Ile
102 R¹=COOH, R²= 2Me-Bu, R³= *i*Bu, X = H, Y = Val
103 R¹=COOH, R²= 2Me-Bu, R³= 2Me-Bu, X = H, Y = Val
104 R¹= *i*Bu, R²= 2Me-Bu, R³= *i*Bu, X = H, Y = Asp
105 R¹= 2Me-Bu, R²= 2Naph, R³= 2Me-Bu, X = H, Y = Ile
106 R¹= *i*Bu, R²= *i*Bu, R³= *i*Bu, X = H, Y = Gly
107 R¹= *i*Bu, R²= *i*Bu, R³= 2Naph, X = H, Y = Leu

Figure 3.13 Library of proteomimetics bearing 4 side chains and targeted to the Bcl-2 family of interactions.

A few unnatural side chains were also explored, as Hamilton and co-workers reported a terphenyl bearing a 2-naphthyl side chain at the *i* + 4 position to be one of their most potent Bcl-x_L/Bak inhibitors ($K_i = 114$ nM).¹⁷⁶ The library of Bcl inhibitors is represented in Figure 3.13. Most of the library members were made of three aromatic monomers followed by a natural amino acid at the C-terminus, except for **96**, which had an additional α -valine at the N-terminus. This compound illustrated the compatibility of the methodology with natural systems.

3.2.1 Testing against the Mcl-1/Noxa B interaction

The versatility of the *N*-alkylated oligobenzamide scaffold was then studied. At first, two PPIs that are part of the Bcl-2 family of interactions were envisaged, and the corresponding proteins and tracers were prepared by two post-doctoral members of the group (molecular cloning and expression of Mcl-1₁₇₂₋₃₂₇ and Bcl-x_{L1-209}: Dr. A. Bartlett; synthesis of FITC-Noxa B₆₈₋₈₇ and carboxyfluorescein-Ahx-Bid₈₀₋₉₉: Dr. P. Prabhakaran, Flu-Ahx-Bad₁₀₃₋₁₂₈ was purchased from Peptide Science Research Ltd.). The versatility of the developed proteomimetic scaffold was thus only studied on the Mcl-1/Noxa B interaction, and an isolated

compound was tested against the p53/hDMX PPI. Conditions for the Mcl-1/Noxa B assay were optimized. A direct titration of the tracer by the protein was performed and led to the determination of a K_d value of 32.46 ± 1.14 nM, which was in agreement with values reported in the literature.¹⁷⁷ Conditions for the displacement assay using the unlabelled Noxa B peptide were optimized in a joint effort (with D. J. Yeo and V. Azzarito) and provided an IC_{50} of 704 ± 35 nM, using 150 nM protein and 50 nM tracer. No workable assays have been produced yet for the interaction of Bcl-x_L with Bad and Bid peptides and these PPIs were therefore not investigated within the context of this study. As discussed earlier, it was of crucial importance to test the compounds in the same conditions in order to obtain reliable and exploitable data. The whole library of oligobenzamides was thus subjected to a single point screen using the automated method described in the previous Section, as these assay conditions might be suitable for this particular interaction.

3.2.1.1 Single point assay against the Mcl-1/Noxa B PPI

In this assay, an unlabelled Noxa B peptide was used as the positive control. Screening against this target interaction was carried out on the Hamilton Star Microlab robot, using the same method as for the screening against p53/hDM2. Results for the screening of the whole library in this assay are presented as a bar diagram (Fig. 3.14). These results indicate that five oligoamides seemed to be active against the target PPI: compounds **72**, **89**, **98**, **100**, and **105** displayed between 25 and 60% Noxa B efficiency. Although this might not seem like a very high threshold to select potent compounds, the four most potent ones (**72**, **89**, **98** and **105**) were tested in a full competition assay. It is worth noting that a considerable number of compounds displayed anisotropy values that exceeded that of the fully bound tracer (wells containing only protein, tracer and buffer). This was attributed to the DMSO, as a concentration of 10% was present in the test wells, whereas the negative control (wells only containing protein and tracer) did not contain any. At this concentration, it is possible that the viscosity of the solution and the structure of the protein itself were affected; both of which could affect the resulting anisotropy.

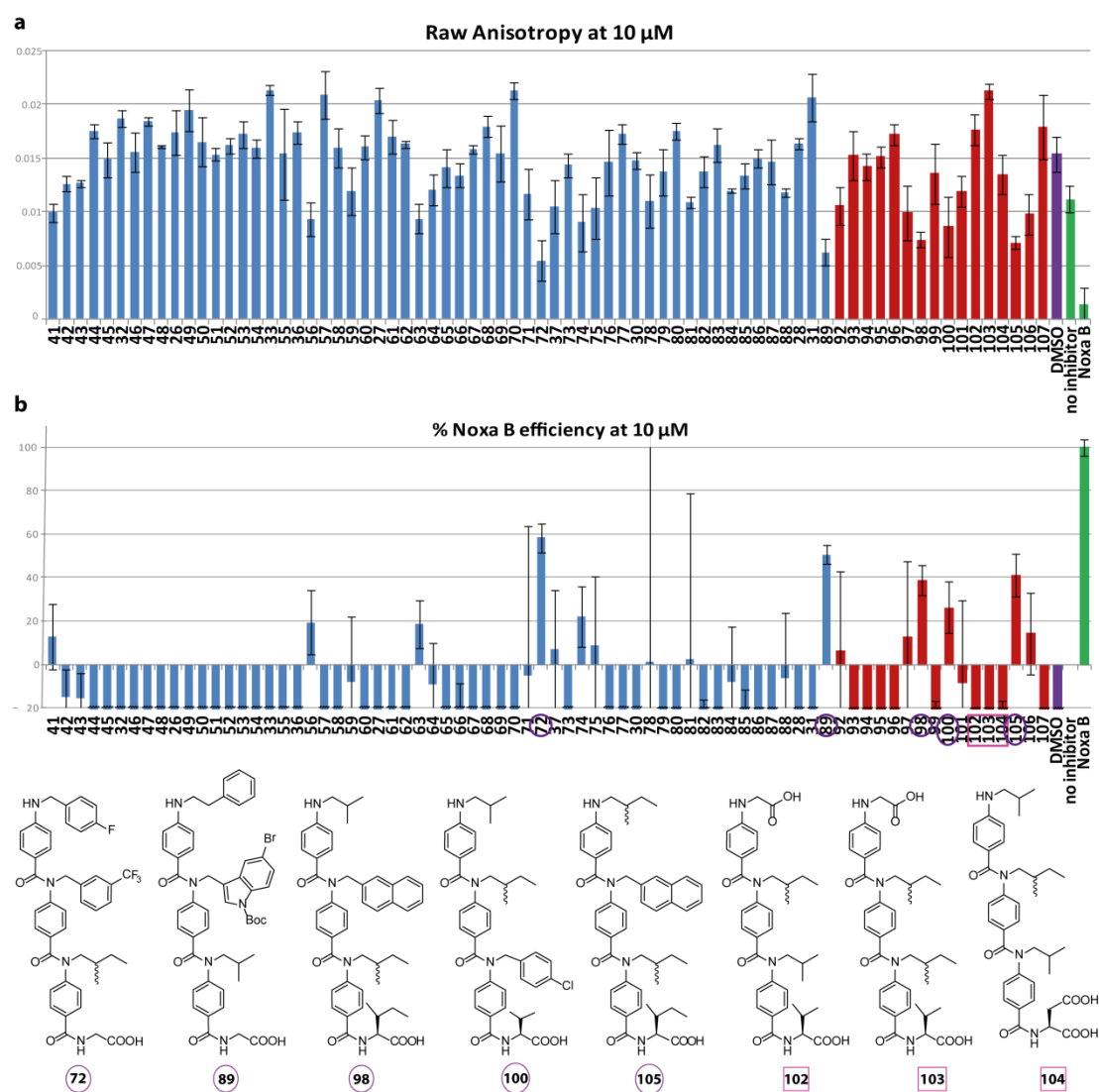


Figure 3.14 Results from the single point screening of the library against Mcl-1/Noxa B. Blue: results for compounds initially designed to target p53/hDM2 and containing only 3 side chains; red: sub-library targeting the Bcl-2 family; green: controls. **a.** Raw anisotropies are reported for each compound tested at 10 μM . **b.** Results presented as a percentage of Noxa B efficiency – most of the compounds exhibited negative efficiencies due to their unexpectedly high anisotropy values (scale limited to -20%).

Although for some of the compounds the error over the three repeats was significant, all the compounds identified as hits presented acceptable errors (Fig. 3.14b). Considering that the amount of protein available was a limiting factor, it was decided that this assay would not be repeated, as the resulting data was still exploitable, and was confirmed by further competition assays.

3.2.1.2 Competition assays against the Mcl-1/Noxa B PPI

Using the optimized conditions (150 nM protein, 50 nM tracer), the 'hits' identified in the single point assay as well as some of the less potent compounds were tested (Fig. 3.15).

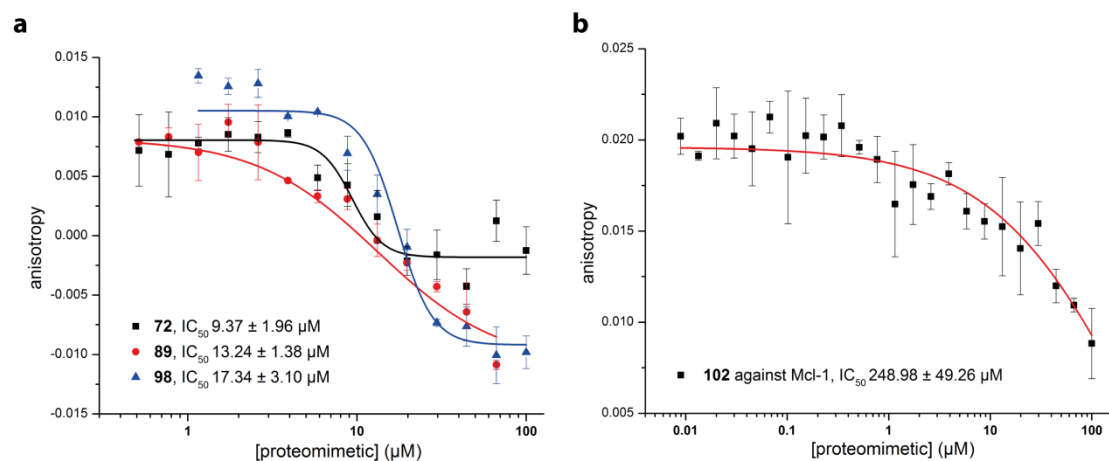


Figure 3.15 Compounds tested against Mcl-1 in a dose-response assay (structures in Fig. 3.14). **a.** Hits from the single point screening. **b.** Dose-response curve for **102**.

These assays allowed the identification of low micromolar inhibitors of the Noxa B/Mcl-1 interaction: compound **72**, IC₅₀ = 9.37 ± 1.9 μM; **89**, IC₅₀ = 13.24 ± 1.4 μM and **98**, IC₅₀ = 17.34 ± 3.1 μM. Compounds **102**, **103** and **104** (cf. Fig. 3.14 for structures) which were specifically designed to mimic Noxa B turned out to be amongst the least active compounds of the library, with **102** displaying an apparent IC₅₀ = 245 ± 49.3 μM. This might be due to the proteomimetic not being able to display the acidic side chain the same way as the native Noxa B helix. As was the case for inactive compounds in the case of the p53/hDM2 PPI, the lower asymptote was not reached for **102**, meaning that a concentration of 100 μM was not high enough to displace the fluorescent Noxa B from the interaction with Mcl-1. This result however confirmed predictions of the single point screening. It is worth noting that two of the most potent compounds against p53/hDM2 were also amongst the best inhibitors of the Noxa B/Mcl-1 PPI (although **89** only weakly inhibited this PPI). Furthermore, among the sub-library that was initially designed to inhibit the Bcl-2 family of PPIs, the most potent compounds all

included an aromatic side chain. The selectivity of the oligobenzamide scaffold was further investigated, using data from both single point screenings and additional competition assays. The results are discussed in the next Section.

3.3 Selectivity of the scaffold

Hits from each of the single point screening were tested in dose-response competition assay on both the p53/hDM2 and the Noxa B/Mcl-1 interactions, in order to study the selectivity of the scaffold and its possible use in a general approach to the disruption of α -helix mediated PPIs. The results for compounds against both targets are presented in Figure 3.16. Some compounds including **72**, **98** and **105** have been found to inhibit both the p53/hDM2 and Noxa B/Mcl-1 PPIs. **98** inhibited p53/hDM2 with an IC_{50} of $2.79 \pm 0.13 \mu\text{M}$ and Noxa B/Mcl-1 with an IC_{50} of $17.34 \pm 3.1 \mu\text{M}$ (Fig. 3.16c) whilst **72** inhibited p53/hDM2 with an IC_{50} of $3.05 \pm 0.22 \mu\text{M}$ and Noxa B/Mcl-1 with an IC_{50} of $12.82 \pm 2.44 \mu\text{M}$ (Fig. 3.16e). Compound **47** which was one of the initial hits against p53/hDM2 (IC_{50} of $7.12 \pm 0.26 \mu\text{M}$) had been predicted by the single point screening to be inactive against Noxa B/Mcl-1. The competition assay revealed **47** also inhibited this second PPI (IC_{50} of $9.18 \pm 2.7 \mu\text{M}$ against Noxa B/Mcl-1, Fig. 3.16d). Taken together, these results suggest that these compounds may be acting as non-specific inhibitors, which may be explained by the general hydrophobicity of the scaffold and side chains required.

Compound **89** containing a Boc-protected bromoindole however acted as a specific p53/hDM2 inhibitor (20-fold selectivity for p53/hDM2 with an IC_{50} of $0.67 \pm 0.06 \mu\text{M}$). Although this Boc-trimer was not the initially desired unprotected compound, it was decided that it should be included in the testing phase, as this additional Boc-group might provide a better fit within the binding pocket. It is not excluded that this additional hydrophobic group might just bring some additional hydrophobic and non-specific interactions. Other potent inhibitors of the p53/hDM2 PPI have been tested against Noxa B/Mcl-1 and generally displayed lower affinities for the second PPI, but none was as selective as **89**.

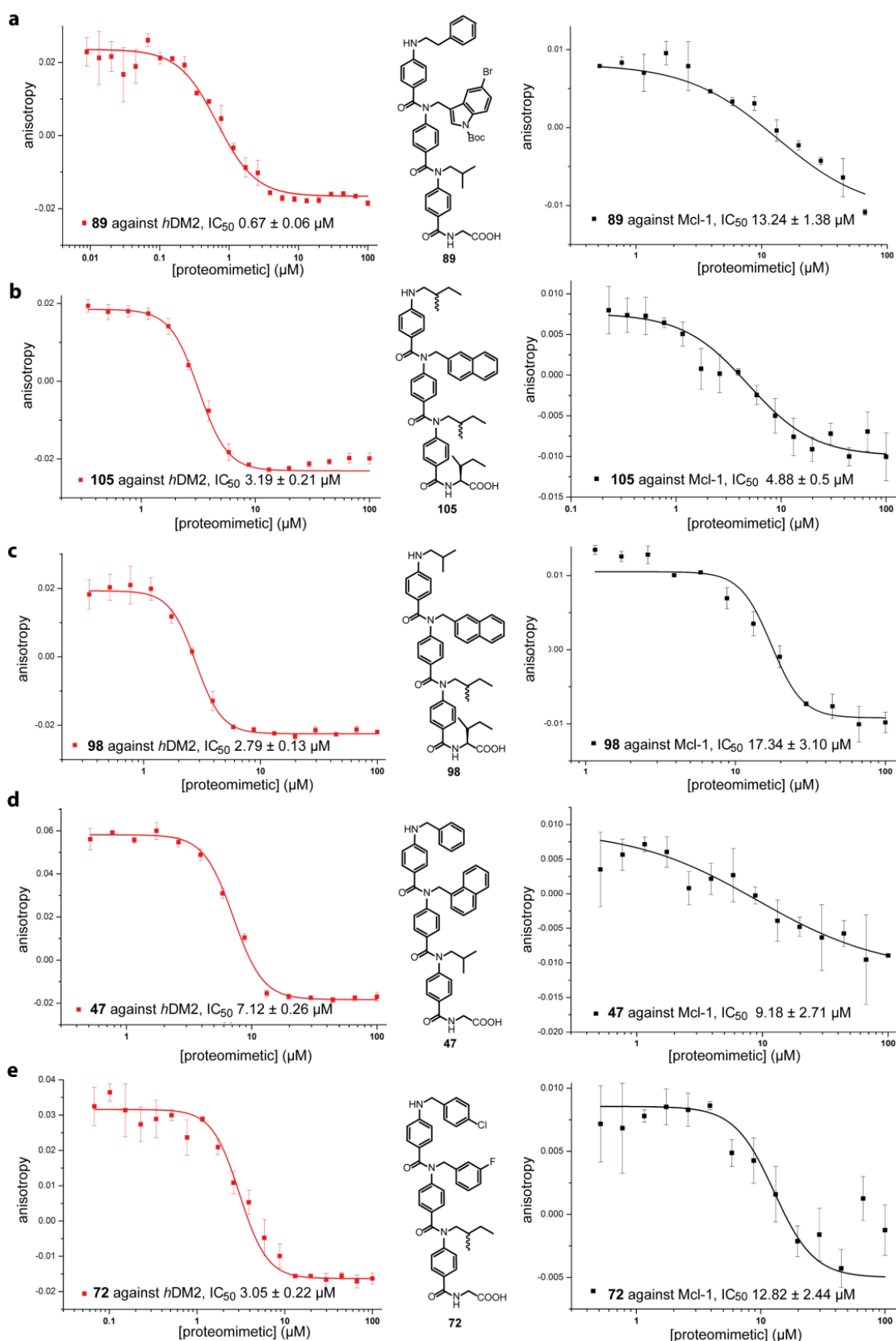


Figure 3.16 Assessment of the selectivity of the *N*-alkylated oligobenzamide scaffold (in red: against p53/*hDM2*, in black: against Noxa B/Mcl-1). a. Compound 89. b. Compound 105. c. Compound 98. d. Compound 47. e. Compound 72.

From the subset of compounds tested on both targets, four of the most potent ones (**72**, **89**, **98**, **105**) presented IC_{50} s below 3 μ M against p53/hDM2. Two of them included two aromatic side chains matching Phe19 and Trp23 from. The other two compounds were initially designed to target the Bcl-2 family but included a naphthyl ring at the R2 position (**98** and **105**). This confirmed that the presence of a substituted aromatic ring at the R2 position was a prerequisite for activity, and that the presence of a fourth aliphatic side chain in the sequence might lead to enhanced activities.

It is worth noting that the most potent inhibitor of Noxa B/Mcl-1 was the one that presented four side chains, three of which were aliphatic (**105**, $IC_{50} = 4.88 \pm 0.5 \mu$ M). This suggested that the scaffold designed was suitable for mimicry of BH3-only peptides. Compounds **47**, **72** and **89** which presented two aromatic substituents out of a total of three side chains, were slightly less active against Noxa B/Mcl-1 (IC_{50} s ranging from 9 to 13 μ M), suggesting that for this scaffold, the mimicry of four side chains enhanced the binding affinity for Mcl-1. Compound **102**, which possessed a side chain arrangement matching that of the native Noxa B helix was inactive against Noxa B/Mcl-1, and displayed poor activity against the p53/hDM2 PPI (IC_{50} of $245 \pm 49.3 \mu$ M against Noxa B/Mcl-1 and $28.1 \pm 0.33 \mu$ M against p53/hDM2, cf. Appendix III). No specific Mcl-1 binder has been identified yet.

The selectivity of the oligobenzamide scaffold was also assessed against the p53/hDMX interaction. As mentioned earlier in this Chapter, Dr. A. Bartlett and S. Hussain from the Edwards group had successfully expressed a GST-hDMX protein, and have tested the most potent inhibitor of the p53/hDM2 that had been identified at that time (compound **47**, $IC_{50} = 7.12 \pm 0.27 \mu$ M). The corresponding dose-response curve (Fig. 3.17) provided an IC_{50} value of $18.81 \pm 0.96 \mu$ M against p53/hDMX.

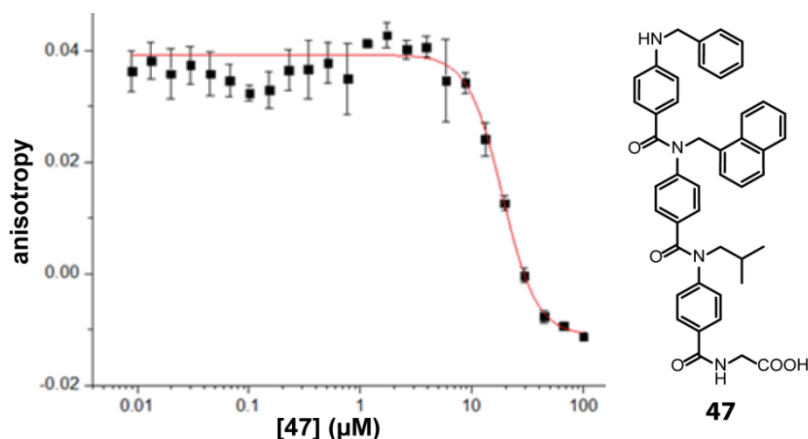


Figure 3.17 Preliminary testing against the p53/hDMX PPI. Compound **47**, one of the most potent p53/hDM2 inhibitors (IC_{50} $7.12 \pm 0.27 \mu\text{M}$) identified in this study displayed an IC_{50} of $18.81 \pm 0.96 \mu\text{M}$ against p53/hDMX.

Although this IC_{50} was higher than that against p53/hDM2, it illustrated that **47** was a non-specific inhibitor of all three targeted PPIs (p53/hDM2: $7.12 \mu\text{M}$, p53/hDMX $18.8 \mu\text{M}$, Noxa B/Mcl-1: $9.2 \mu\text{M}$). The higher IC_{50} against p53/hDMX could be explained by the shallower binding cleft in hDMX (Nutlin-3a which displays a low nanomolar IC_{50} against p53/hDM2 is inactive against p53/hDMX).⁷ It is probable that screening of the whole library against this PPI would provide some more efficient and specific inhibitors, especially those which possess a smaller aromatic ring at R2. The GST-hDMX fusion protein was however found to be highly unstable, so **47** was the only compound that could be tested against this PPI. Current efforts are dedicated to the isolation of a more stable construct that would allow further investigation of this PPI.

3.4 Proteolytic studies

One of the oligobenzamides (**99**) was selected as a representative member of the library to undergo proteolytic studies against a range of proteases. The experiment was carried out by Dr. P. Prabhakaran. As expected, the oligobenzamide displayed resistance to all tested proteases, and when tested against the non-selective proteinase K, only the C-terminal α -amino acid was cleaved. This demonstrates the enhanced resistance of aromatic amide bonds towards proteolysis, a highly desirable feature for testing in a biological context. The results are summarized in Figure 3.18.

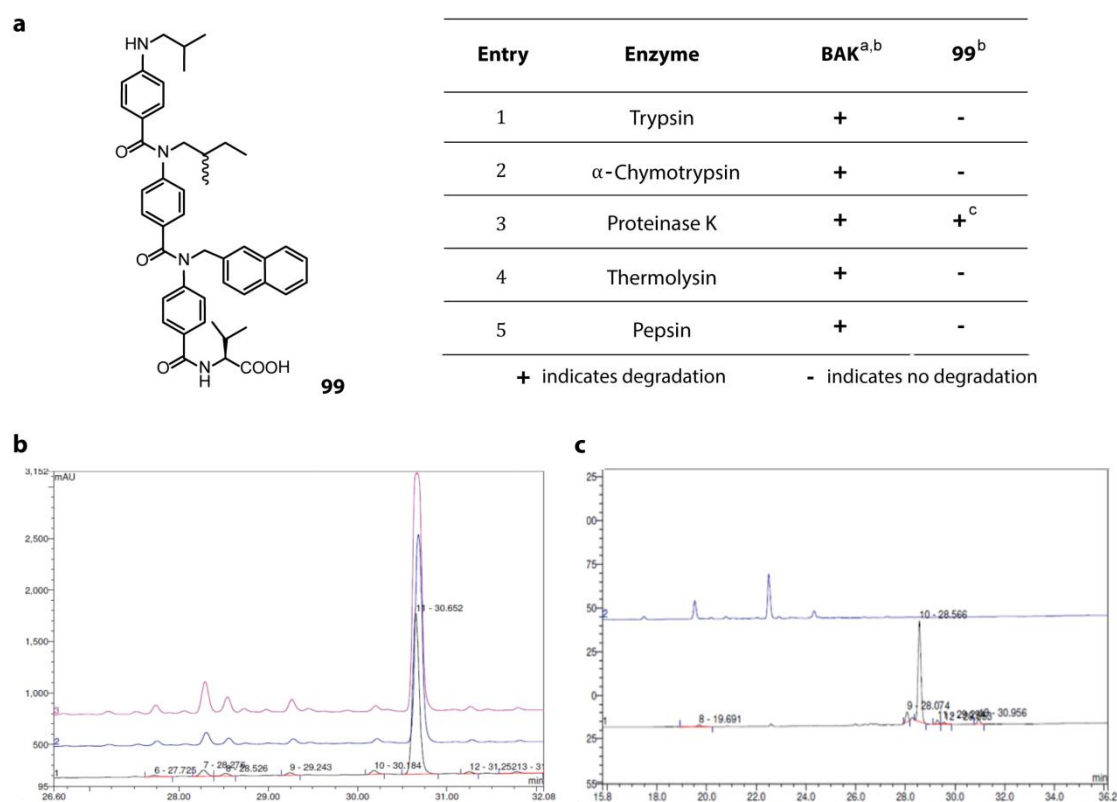


Figure 3.18 Proteolytic study on compound 99. **a.** Structure of the compound and table summarizing the result from proteolytic studies against 5 proteases; ^a measured in buffer and in a mixture of buffer and DMSO, ^b tested in a mixture of buffer and DMSO (29%), ^c only the C-terminal α -residue was cleaved by proteinase K (data not included), none of the aromatic amide bonds were cleaved. **b.** Analytical HPLC traces of **99** (black), after treating with α -chymotrypsin (pink) and Trypsin (blue) for 15 minutes at r. t. **c.** Analytical HPLC traces of Bak (black), and after treating with α -chymotrypsin (blue) for 15 minutes at r. t.

3.5 Cell assays

A limited number of whole cell experiments were carried out on a selection of 40 oligobenzamides. The compounds were tested by Dr. H. Martin and in collaboration with Dr. D. C. Tomlinson (Leeds Institute of Molecular Medicine and Astbury Centre, University of Leeds) using immunofluorescence techniques on the U2OS cell line, which is a human osteosarcoma cell line expressing WT p53. These cells were thus suitable to assess whether the inhibitors were able to restore p53 function in cells, as this could result in the activation of the p53 pathway and in turn trigger cell death by apoptosis.^{21, 26, 178} U2OS cells were exposed to 2 doses of each compound (5 and 10 μM), and the response was monitored at two time points (24 h and 48 h). Parameters observed included the number of cells, the percentage of abnormal cells (looking at alteration in the cell and nucleus size and brightness, DAPI was used to stain the nuclei) and the percentage of histone H3 positive cells (looking at mitotic arrest or delay). Cross-analysis of the results allowed some preliminary observations. Three compounds that showed decreased H3 staining and increased cell size were likely to induce cell cycle arrest/delay in the G1 phase (**44**, **55**, **96**). Compounds that displayed increased H3 staining were likely to induce cell cycle arrest/delay in the M phase (**37**). Results from this preliminary screening did not allow a definite conclusion as to whether the compounds were actually penetrating the cells, as they only seemed to display an effect at the highest dose and exposure time (10 μM , 48 h). This may suggest that the compounds display a general cytotoxicity, and this possibility will need to be investigated in future experiments (such as MTT assays). Different compounds have however been found to generate different effects on the cell cycle arrest, number of cells, size and shape of cells and nuclei, which suggested that these might be able to penetrate the cell. Fluorescence microscopy images of cells exposed to **42** and **97** showed a difference in cells shapes and density and suggested that they might be inducing apoptosis (Fig. 3.19), although the evidence is not clear-cut and will need further confirmation. From the set of 40 compounds tested in the cell assay, only 17 were identified as 'hits' in the single point FA screen, and conversely, not all the 'hits' have been tested in cells so definite conclusions cannot be drawn at that stage.

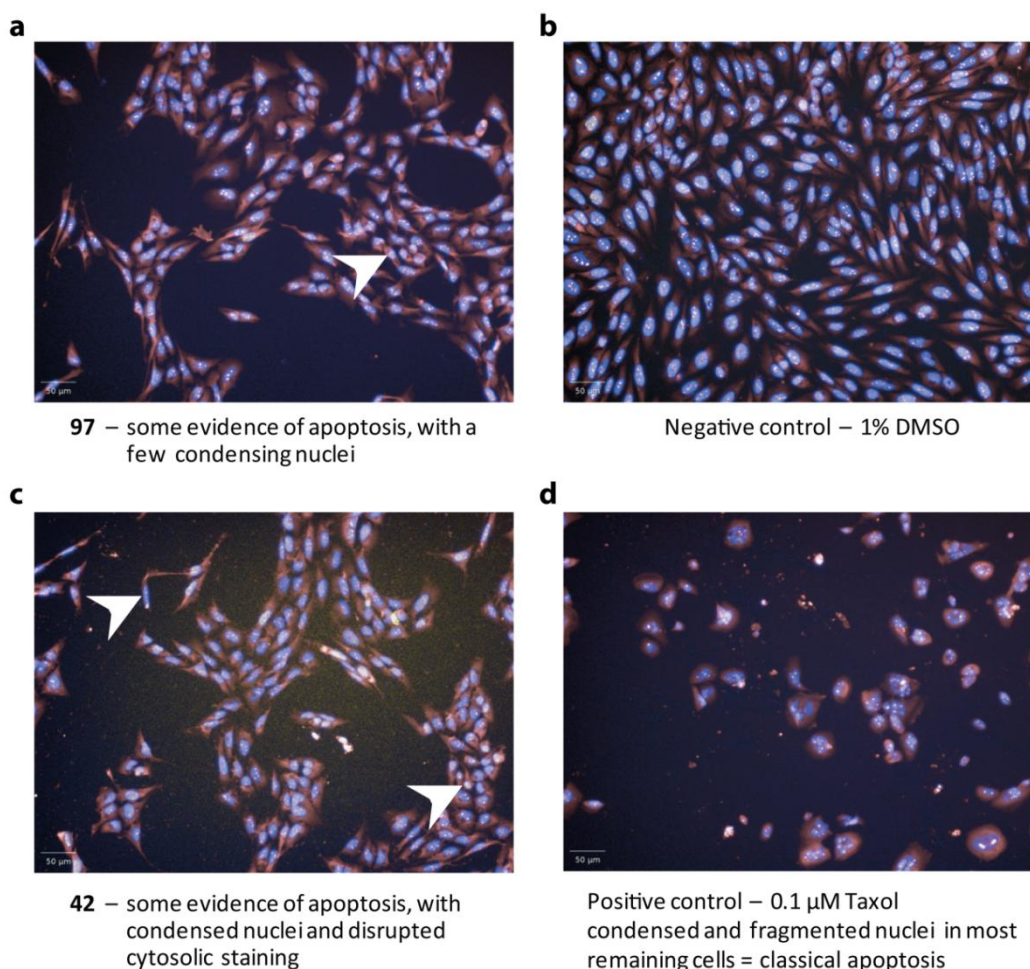


Figure 3.19 Fluorescence microscopy images showing limited evidence of apoptosis. **a.** Compound **97**. **b.** Negative control = 1% DMSO. **c.** Compound **42**, seemed to cause nuclei condensation and disruption of the cytosolic staining. **d.** Positive control = 0.1 μM Taxol.

Compounds that seemed potentially active in these cell assays which had not been identified as hits in the preliminary single point screen were tested in a dose-response assay against p53/hDM2 (Fig. 3.20). Out of these 6 compounds, five presented IC_{50} values between 8.9 and 15.65 μM (**37**, **42**, **44**, **55**, and **97**) and one was inactive (**96**, cf. Fig. 3.20 for IC_{50} s). Although these results do not demonstrate that these compounds can actually penetrate cells to trigger apoptosis, they show that the compounds are relatively potent inhibitors of p53/hDM2. This suggests that if they do penetrate cells, then it is plausible that they will exert their inhibitory role. Compound **96**, which displayed some

evidence of cellular activity but was inactive in the FA competition assay, might have been identified as a false positive in the cell assay.

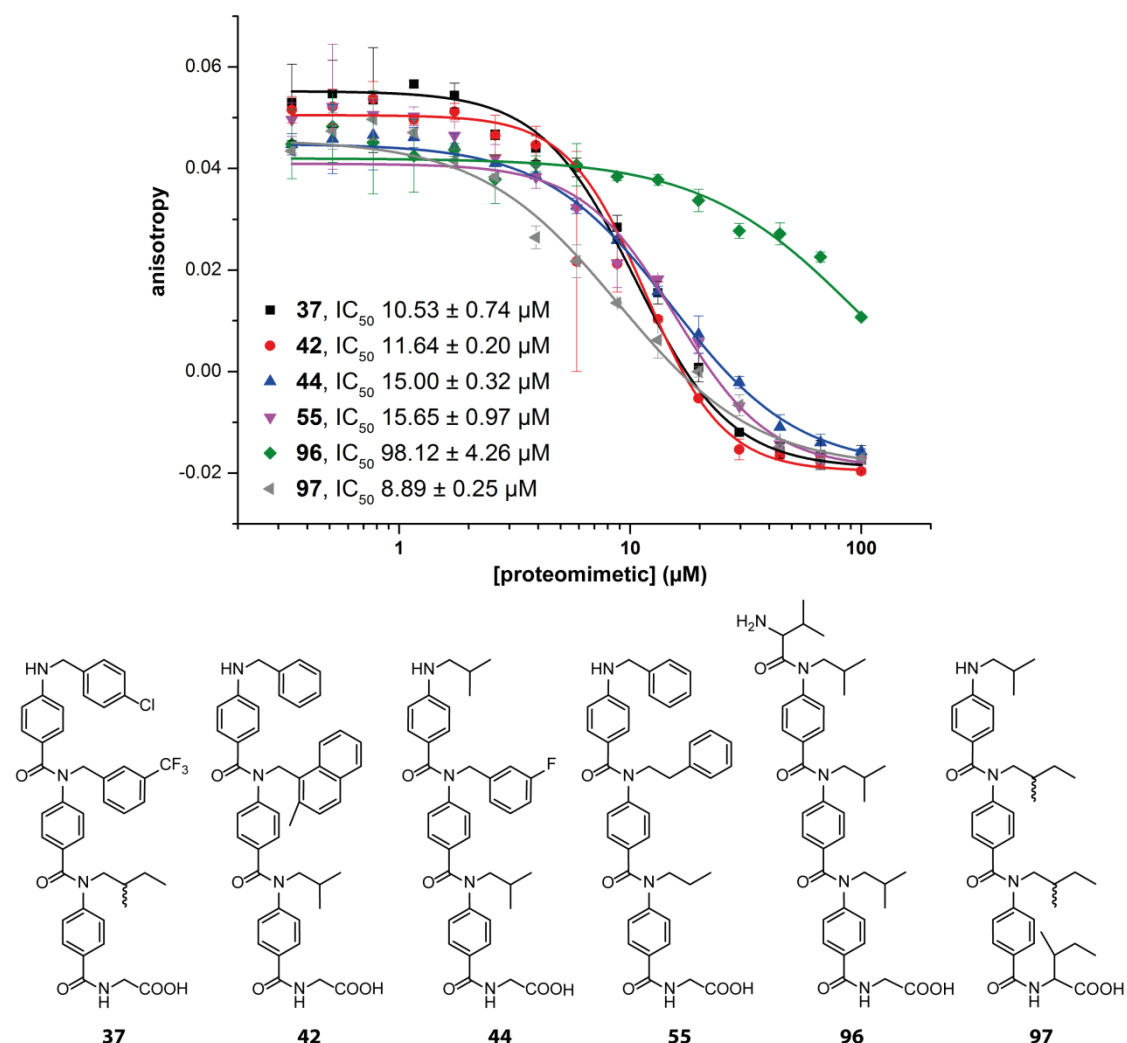


Figure 3.20 Dose-response curves on compounds that appeared to be potentially active in cell assays. Compounds 44, 55, 96 were likely to induce cell-cycle arrest/delay in the G1 phase; compound 37 was likely to induce cell-cycle arrest/delay in the M phase; compounds 42 and 97 displayed limited evidence of apoptosis in the high content screening.

As these preliminary observations were encouraging, further experiments will be carried out in the near future in order to investigate more deeply the cellular activity of the entire library of oligobenzamides. Additional cytotoxicity assays will also be carried out by collaborators. Recent studies in U2OS cells have revealed that Nutlin-3a was inducing cytoskeletal rearrangement, decreasing the

formation of lamellipodia (cytoskeletal actin extension of the cell that is crucial for motility) and consequently decreasing cell migration and invasion, in addition to holding the cell cycle in the G1 phase.¹⁷⁹ Results from initial cell studies on Nutlin-3a conducted by Vassilev and co-workers could not be used as a reference for this study as they were using different cell lines (SJSa, HCT116 and RKO).⁷ Disrupting the p53/hDM2 PPI would also include other phenotypes including p53 stabilization, upregulation of downstream proteins including Bax, but these would not be observable with the set of techniques available for this study. Inhibitors of the Bcl-2 family of interactions (ABT-737,⁷⁷ binding to Bcl-2 and Bcl-x_L and Obatoclax,⁶² binding to Mcl-1) both seemed to induce formation of autophagosomes as well as inducing apoptosis *via* caspase-3 activation in the U2OS cell line.^{180, 181} In future experiments, each compound will therefore be monitored for: autophagy status (using anti-LC3 antibody),^{180, 181} caspase-3 activation, changes to the cytoskeleton and overall cytotoxicity.

3.6 Discussion

Protein-protein interactions have become highly desirable targets for therapy, however classically used approaches to modulate PPIs have only met with limited success. It seems that appropriate tools to modulate these unconventional interactions are still to be developed. As a vast proportion of PPIs are mediated by an α -helix, which is a very well characterized protein secondary structure; this type of interactions represent a common starting point for study. The present study aimed at disrupting α -helix mediated PPIs by using an oligobenzamide scaffold as a mimetic of the helical core. Using such a scaffold to display side chains in an arrangement that replicates that of the native helix is an attractive approach as it opens the perspective of versatility: using a single scaffold to target several PPIs. Two PPIs served as a model for studying the target selectivity/specificity of the *N*-alkylated oligoamide scaffold: p53/hDM2 and Noxa B/Mcl-1. In an attempt to establish design rules for a generic approach to α -helix mediated PPI disruption, two libraries of oligobenzamides were assembled. The first library was made of 60 trimers and targeted to the p53/hDM2 interaction; it therefore contained combinations of aromatic and aliphatic side

chains. Unnatural substituents such as halogenated aromatic rings have been incorporated in an attempt to enhance the potency and selectivity of these compounds towards the targeted PPI. The second sub-library was designed to disrupt the Bcl-2 family of interactions by mimicking the BH3 domains involved in the binding and therefore contained mostly aliphatic side chains. The interaction of BH3 proteins with their binding partners however involves four key side chains. For this 16-member library, the SPS methodology was therefore transposed to a Wang resin pre-loaded with an α -residue corresponding to the fourth hot-spot residue of the native helix instead of glycine. Both libraries were tested in a fluorescence anisotropy assay against model PPIs, first in a single point screen in order to identify the most active compounds, and then these hits were tested in a full competition assay to determine IC_{50} s. The manual screening against p53/hDM2 reliably lead to hit identification and whilst testing subsets of compounds, several low-micromolar inhibitors have been identified and used to establish basic SARs. These SARs confirmed that bulky aromatics at the R2 position were a prerequisite for activity. This was illustrated by the low micromolar IC_{50} s measured for compounds that were initially designed to target the Bcl-2 family such as **98** and **105**, which only display one aromatic ring, and present an aliphatic chain in place of the key Phe19 residue of p53. The most potent inhibitor of p53/hDM2 identified was compound **89**, a trimer containing a Boc-protected 5-bromoindolyl side chain at R2 ($IC_{50} = 0.67 \pm 0.06 \mu\text{M}$). The biological relevance of compound **89** however needs to be questioned, as the Boc group may be cleaved under biological conditions. Ideally, the corresponding unprotected compound should also be tested, but this was precluded by the technical limitations discussed previously, which meant that the Boc group could not be removed without resulting in the elimination of the indole ring. **53**, which was the only indole-containing compound for which some Boc-deprotected product could be isolated, displayed an IC_{50} value of $9.06 \pm 0.20 \mu\text{M}$. Compounds **89** and **53** can however not be directly compared, as their R1 substituent were different (phenethyl and benzyl, respectively) and they were tested on separate occasions.

It appeared that the amount of reagents used as well as the handling time could be reduced by adapting the assay to an automated methodology. This was

also likely to enhance the accuracy and comparability of the results, and could potentially allow the establishment of a relative ranking of the compounds. The whole library was thus subjected to an automated single point screen where all the compounds could be tested at once. Transposing the assay to an automated method however proved more challenging than initially expected, and no reproducible conditions have been found yet. Screening against the Mcl-1/Noxa B PPI using the automated assay proved more fruitful, and allowed the identification of 5 hits. When tested in a full competition assay, four of them presented IC₅₀s in the low micromolar range (<10 μM). Within the whole library, a few dual inhibitors have been identified (**47**, **72**), along with specific p53/hDM2 inhibitors such as **89**, however no specific Mcl-1 binder has been identified yet. Interestingly, compounds **102** – **104** which had side chains specifically designed to mimic those of Noxa B were among the least active compounds of the library. This might be due to the proteomimetic not being able to display the acidic side chain the same way as the native Noxa B helix. A longer linker might be needed for the acidic side chain to reach into the binding pocket in Mcl-1 and make the required interactions with neighbouring residues. This illustrates that despite the structural data available to help the design of inhibitors, further research efforts are required in order to gain a better understanding of how PPIs can be interfered with.

3.7 Summary and conclusions

In summary, a library of 75 compounds (divided into two sub-libraries) has been assembled using the newly developed microwave assisted SPS methodology¹⁴⁴ reported in Chapter 2, which further illustrates its robustness and efficiency. Testing this library against two PPIs (p53/hDM2 and Noxa B/Mcl-1) using a fluorescence anisotropy assay led to the identification of inhibitors with IC₅₀s in the low micromolar range, whether specific (**89**), or dual inhibitors (**105**, **47**, **72** and **98**). Although *N*-alkylated oligobenzamide inhibitors did not display unprecedented potencies against the model interactions, low micromolar inhibition was attained, and this study demonstrated that target selectivity could be achieved. Given its synthetic accessibility, this scaffold is suitable for further

Chapter 3: Assembly and screening of a library of proteomimetics

studies, including the assembly of a larger library targeting the Bcl-2 family, with a view to identify some specific Mcl-1 or Bcl-x_L binders. In addition, the proteolytic stability of these aromatic oligoamides was confirmed against a panel of enzymes - proteinase K seemed to be able to cleave the terminal α -amino acid off, but left the aromatic amides untouched. Preliminary cell assays on half of the library of oligobenzamides provided encouraging results, suggesting that some of the compounds might be able to penetrate the cells and trigger apoptosis. Further cellular investigation on the entire library will be carried out in order to gain a better insight into their cellular behaviour.

Chapter 4

Solid phase synthesis and biological evaluation of oligoureas as α -helix mimetics

The work described in this chapter relates to a short term scientific mission (STSM) that results from a collaboration between the Wilson group (University of Leeds) and the Guichard group (Institut Européen de Chimie et Biologie, IECB, Université de Bordeaux, France). The synthetic work was carried out over 2 months at the IECB, whilst the biological evaluation of the compounds was done in Leeds. This STSM was funded by COST (European Cooperation in Science and Technology).

Over the last decade, inhibition of protein-protein interactions (PPIs) has become a distinct field of research and α -helix mimicry represents an intensely explored route towards this goal. In order to circumvent natural peptides' intrinsic susceptibility to proteolytic degradation, new peptide backbone mimetics were sought.¹⁸²⁻¹⁸⁴ As mentioned in Chapter 1, a variety of strategies have been reported to stabilize helical structures in α -peptides, and a number of non-natural foldamers have also been shown to act as α -helix mimetics. In this context, oligoureas have received increasing attention as they are inherently resistant to proteolysis¹⁸⁵ and are structurally very similar to γ -peptides. Several solid phase syntheses (SPS) have been reported after K. Burgess' initial methodology using phthaloyl-isocyanates as activated building blocks in 1995.^{186, 187} The following year, Schultz published an alternative method using an azide to mask the *N*-terminal amine and a nitrophenyl carbamate as the activating group.¹⁸⁸ Liskamp and co-workers have then transposed this methodology to the Fmoc system.¹⁸⁹ The Guichard group has been developing an SPS methodology using succinimidyl carbamates as the activating moiety. These carbamates

combine excellent stability with high reactivity and are therefore attractive activating groups. Their first method made use of Fmoc protection for the *N*-terminal amine, and the monomer synthesis started from β^3 -amino acids.¹⁹⁰ The synthesis was then adapted to use the more widely available α -residues as starting material¹⁹¹ (either Boc- Z- or Fmoc-protected) and finally in 2012, this methodology was adapted to microwave assisted SPS¹⁹² – this will be described in Section 2 of this Chapter. The Guichard group has also reported most of the structural characterisation of oligoureas to date.¹⁹³⁻¹⁹⁷ They have investigated the use of oligoureas as antibacterial agents^{198, 199} and foldamers,^{194, 197} studied their self assembling properties²⁰⁰ and exploited them as anion transporters,²⁰¹ but their potential as α -helix mimetics and inhibitors of PPIs has not yet been studied. This collaborative project was thus aimed at combining the knowledge and expertise of the Guichard and Wilson groups to develop oligourea scaffolds and apply them to the disruption of the p53/*hDM2* PPI.^{21, 22} The synthetic strategy to access these oligoureas was already established and made use of a recently published microwave assisted SPS.¹⁹² A small library of oligoureas was assembled at the IECB, and then tested in the same fluorescence anisotropy (FA) assay^{85, 125, 131} as the oligobenzamides, in Leeds (cf. Section 4).

4.1 Oligoureas as α -helix mimetics

The α -helix is the most prominent secondary structure found in proteins and is often found at the interface between two interacting proteins. Manipulating these α -helix mediated interactions by replicating the helical structure has thus been a major concern in modern chemical biology. Several approaches to generate stable helical conformations have emerged, using different building blocks and stabilizing strategies (cf. Chapter 1, section 1.2). Certain building blocks are the primary focus of investigation; these include natural or engineered α -amino acids, longer homologues such as β - and γ -amino acids, cyclic aliphatic and aromatic residues.^{84, 99, 157, 202, 203} The use of non-natural residues is also expected to provide the resulting oligomer with additional proteolytic stability, which is one of the main limitations of natural peptides. Among linear amino acids, the 2-azido-2-substituted ethyl carbamate monomers described in this Chapter are

closer to γ -amino acids as they result from the formal replacement of the α -carbon in the γ -residue by a nitrogen atom to generate the urea function. This additional nitrogen atom provides oligoureas with enhanced helix stability due to a greater backbone conformational restriction and additional intramolecular hydrogen bonds (Fig. 4.1a).

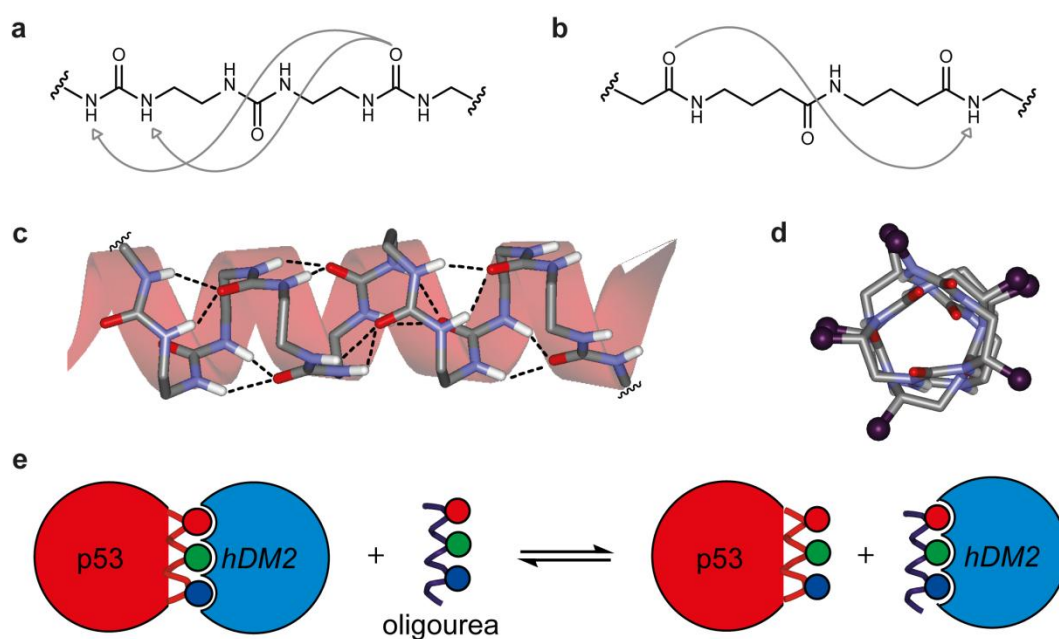


Figure 4.1 Oligourea scaffold as a helix mimetic. **a.** The bifurcated H-bond pattern in N,N'-linked oligoureas. **b.** The H-bond pattern in γ -peptides. **c.** The dense network of bifurcated H-bonds in the oligourea stabilizes the helical conformation (side chains atoms are omitted for clarity). **d.** View of the oligourea backbone along the helical axis, side chains are represented by purple balls. **e.** Using the oligourea backbone as a helix mimetic to disrupt the p53/hDM2 PPI.

Oligoureas were first described as peptide backbone mimics in 1995 by K. Burgess and co-workers.^{186, 187} Oligomers made of more than five residues have previously been shown by the Guichard group to adopt a 2.5 helical conformation that is reminiscent of the 2.6 helical structure found in γ^4 -peptides.^{193, 194} The urea linkage is particularly interesting as it shares some structural features with amide bonds: rigidity, planarity, polarity and H-bonding ability. The oligourea backbone also allows the projection of side chains along a single helical face, as illustrated in Figure 4.1d. Their use as peptidomimetics therefore is the focus of significant interest.

4.1.1 Design and preliminary modelling studies

The ability of oligoureas to mimic α -helices was to be tested against the model p53/hDM2 interaction. Different substitution patterns of the oligoureas were investigated in order to obtain the best possible match between the projections of the key side chains in both scaffolds. Preliminary modelling studies using Maestro 9.0.7 were conducted in order to determine which positions of the oligoureas should be considered as anchoring residues for the side chains designed to mimic the hot-spot residues in p53. In this study, crystal structures of oligoureas **108** - **110** have been superimposed onto the crystal structure of the native p53 peptide (Fig. 4.2). RMSD (Root Mean Square Deviation) values have been calculated to estimate the geometrical match between the positions of the α -carbons of the hot-spot residues in p53 and backbone atoms from the oligourea (highlighted in yellow in Fig. 4.2), arranged into different substitution patterns. The oligourea scaffold that provided the lowest RMSD value should theoretically have been the most appropriate to mimic the p53 helix. The modelling studies presented in this Chapter have been performed by V. Azzarito in Leeds, using crystal structures previously elucidated by the Guichard group.¹⁹⁵ Three different oligourea crystal structures have been modelled against the p53 helix (Fig. 4.2a) and the results are summarized in Figure 4.2b-j. The crystal structure examined in Figure 4.2b-d was that of an octamer capped at the *N*-terminus (**108**) with key side chains at positions 2, 5 and 8. When overlayed onto the p53 helix, this scaffold presented an attractive RMSD of 0.7968, however this was a relatively long sequence, and assembling a library of octamers would have been both material and time consuming. The next scaffold (Fig. 4.2e-g) envisaged was a tetramer and also provided an interesting RMSD value. In this case, residues 1, 2 and the capping element on residue 4 were considered for key lateral chain appendage. Substitution at the *C*-terminal oligourea amine could however only be attained by solution phase synthesis, as the SPS methodology used in this project resulted in unsubstituted ureas at the *C*-terminus. This scaffold, which would have required a relatively lengthy and time consuming synthesis in solution phase was thus left aside.

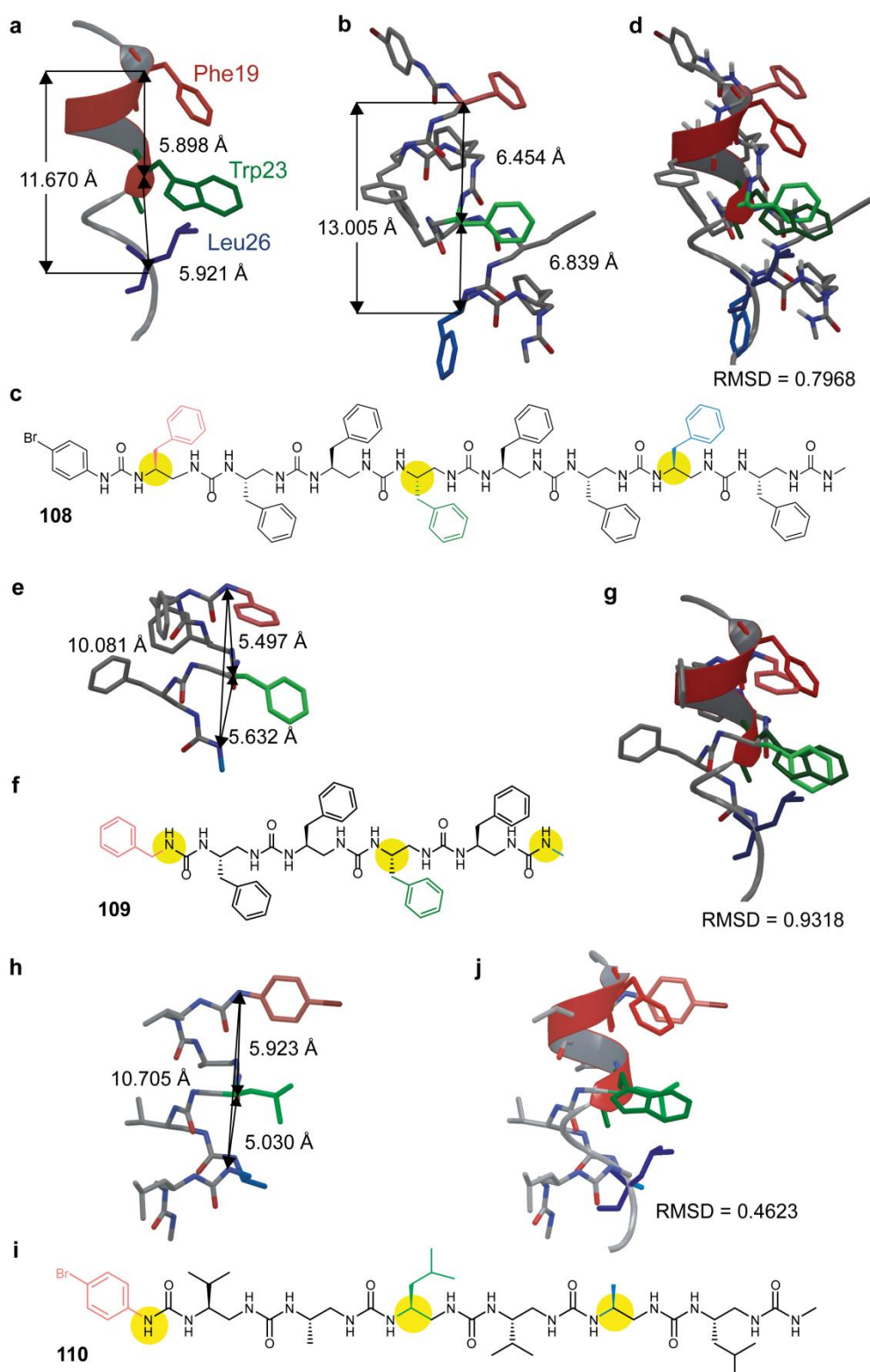


Figure 4.2 Preliminary modelling studies. Atoms from the oligourea backbone considered for RMSD calculation are highlighted in yellow. **a.** Crystal structure of the native p53 helix (residues 15-31). **b.e.h.** Crystal structures of oligoureas **108**, **109** and **110** elucidated by the Guichard group. **c.f.i.** Corresponding linear structures. **d.g.j.** Overlay of crystal structures **b.e.h.** with that of p53, with calculated RMSD values.

Hexamer **110** (Fig. 4.2h-j) with anchoring points at residues 2, 4 and capped 6 presented the best RMSD value (0.4623) among the different substitution patterns investigated and was therefore chosen as a starting point for the synthesis of a small library of oligourea helix mimetics.

4.2 Synthesis

A small library of oligoureas has been assembled using a methodology recently reported by the Guichard group.¹⁹² In this method, activated monomers are coupled on a solid support under microwave heating. For each monomer, the terminal amide group is activated for nucleophilic substitution as a succinimidyl carbamate, whereas the terminal primary amine was masked as an azide group (Fig. 4.3). Because the azide reduction proved to be more efficient under Staudinger conditions,¹⁹² the solid support used in this synthesis needed to be compatible with aqueous conditions – the resin should possess adequate swelling properties in water, a NovaPEG Rink amide resin was therefore chosen.

4.2.1 Building blocks synthesis

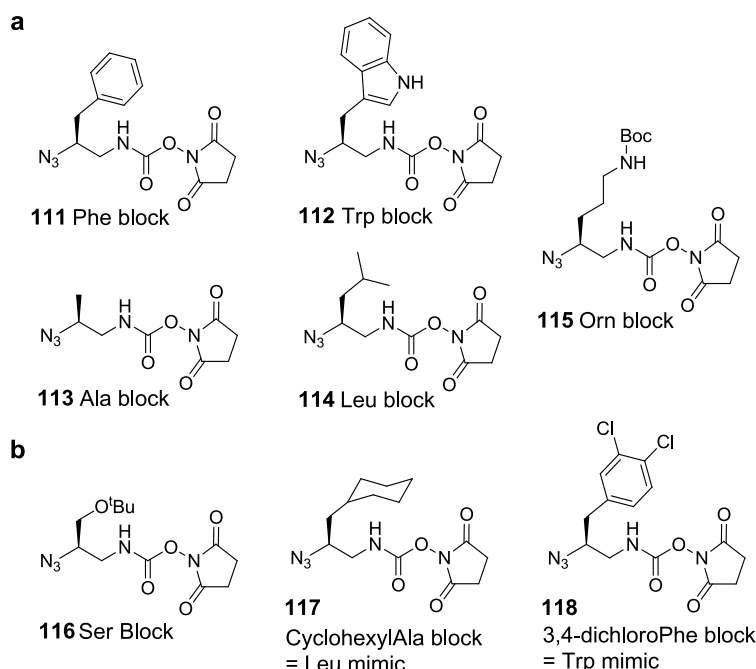
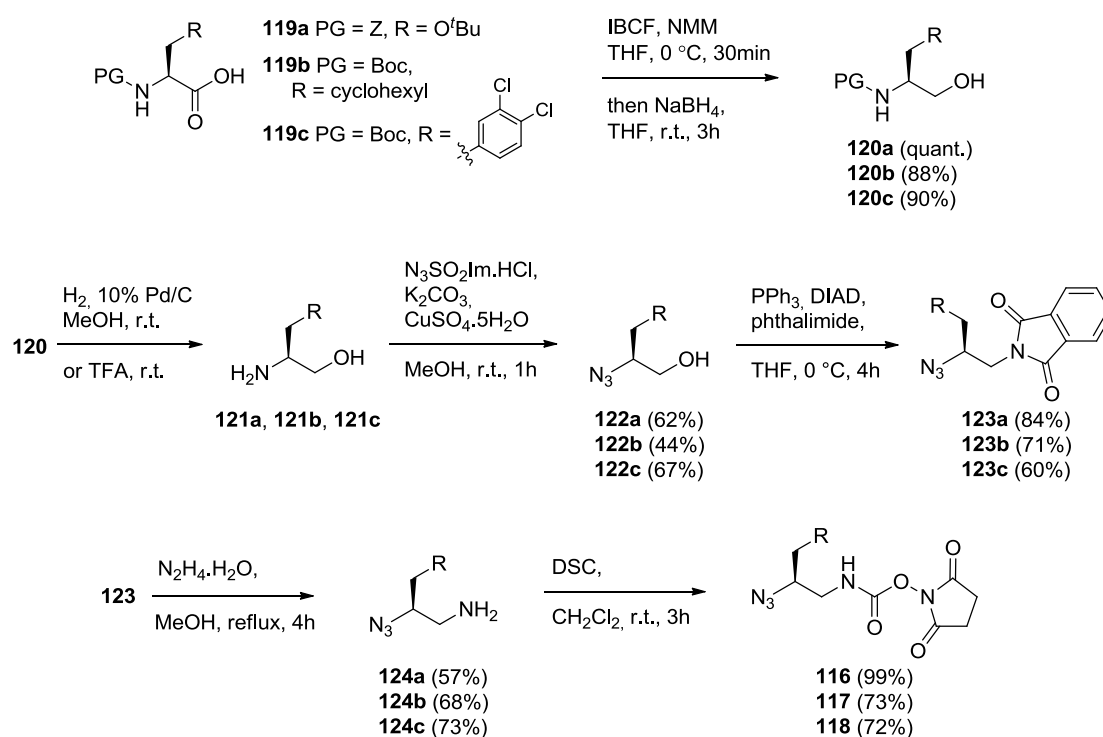


Figure 4.3 Monomers used for the synthesis of oligoureas. a. Monomers previously made available **111 - 115. b.** Monomers bearing unnatural side chains synthesised during the STSM, **116 - 118.**

Due to the time constraints imposed on this STSM and to ensure the best use of this time in order to assemble the target library of oligoureas, a few building blocks (**111** – **115**, Fig. 4.3a) had previously been synthesised by Dr. K. Pulka (Guichard group), so that the solid phase assembly of oligomers could start straight away. Three additional building blocks were also prepared as part of the project. Unnatural side chains (**116** – **118**, Fig. 4.3b) were chosen in order to introduce some more diversified mimics of p53's hot-spot residues. The synthetic route to these monomers was recently reported¹⁹² and is described in Scheme 4.1.



Scheme 4.1 Synthetic route to azido-carbamate building blocks.

The synthesis started from commercially available α -amino acids and led to the activated azido-succinimidyl carbamates **116** - **118** in 6 steps. Firstly, the carboxylic acid was reduced to the corresponding alcohol **120** *via* formation of an asymmetric anhydride using isobutyl chloroformate (IBCF). The amine was then deprotected then converted to the azide **122** using N₃SO₂Im.HCl²⁰⁴– this azide transfer agent had to be prepared beforehand. The alcohol was then converted to

a phthalimide **123** under Mitsunobu conditions¹⁸⁷ and subsequently reduced to the primary amine **124**. Nucleophilic attack of the primary amine onto disuccinimidyl carbamate eventually led to the activated monomers **116** - **118**. Three new blocks were successfully prepared with varying overall yields: 34% for the Serine analogue, 12% for the cyclohexylalanine block and 18% for the dichlorophenylalanine block. Throughout the rest of the Chapter, these succinimidyl (2-azido-2-substituted ethyl) carbamate monomers (or the corresponding moiety within an oligourea sequence) will be referred to as the name of the natural amino acid they were designed to mimic, preceded by a 'U', hence the serine analogue **116** will be referred to as ^USer, etc.

4.2.2 Solid phase synthesis of oligoureas

In order to mimic the native p53 helix and potentially achieve competitive binding with the target protein *hDM2*, several oligourea scaffolds were designed, resulting from different arrangements of the hot-spot residues. For each substitution pattern on pure oligourea backbones, two examples have been synthesised in order to study the effect of the overall macrodipole of the oligourea on its stability and binding efficiency. One of the derivatives is capped at the *N*-terminus, whilst the other one has its *N*-terminus being left as a free amine (Fig. 4.4a,b). The macrodipole effect was also studied through a substitution pattern where the Trp mimic was introduced at position 4 instead of 3 (Fig. 4.4c), which could potentially induce the mimetic to bind in the opposite orientation within the *hDM2* binding cleft. Some hybrid scaffolds with α - or γ -amino acids attached to one or both termini have also been envisaged (Fig. 4.4d-f), as they can introduce more flexibility that might lead to a better fit of the inhibitor into the targeted binding cleft. The oligourea indeed gives rise to a compact cylindrical core, maintained by a dense hydrogen bonding network that might benefit from some additional flexibility. For hybrid scaffolds made of oligoureas bearing an α -amino acid at the *N*-terminus, no capping was performed and the oligomer was left with a free terminal amine. A series of 11 oligoureas (**125** - **135**) was prepared using the previously reported methodology, using a CEM Discovery microwave reactor.

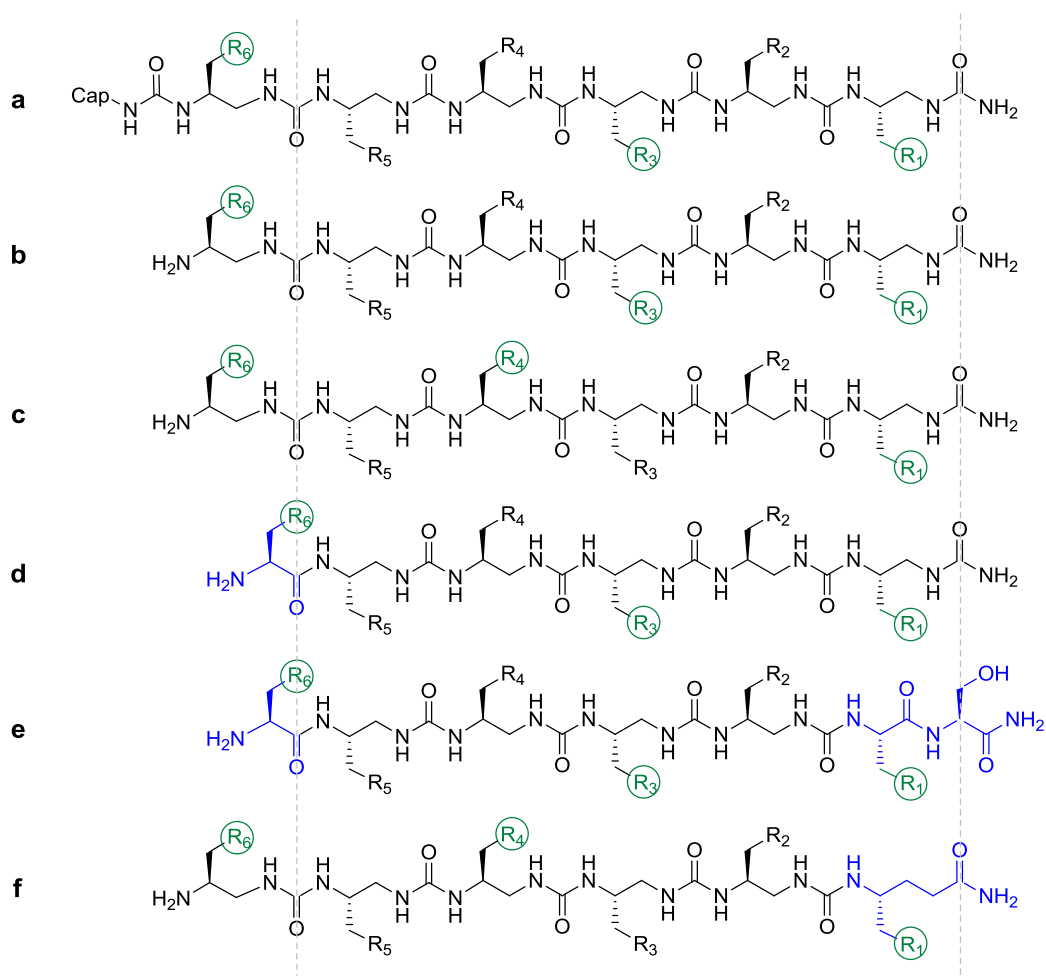


Figure 4.4 Oligourea and hybrid scaffolds designed for the mimicry of the p53 helix. a. Pure oligourea scaffold with i , $i + 2$ and $i + 5$ substitution pattern and capped N -terminus. **b.** Same oligourea with free N -terminus. **c.** Pure oligourea scaffold with i , $i + 3$ and $i + 5$ substitution pattern. **d.** Mixed oligourea-amide scaffold with an α -amino acid at the $i + 5$ position. **e.** Same hybrid scaffold with two additional α -residues at the C -terminus, one of them mimicking the i position. **f.** Hybrid oligourea scaffold with a γ -residue mimicking the i position.

Crude yields were relatively low (25-60%) and after cleavage, the crude oligomers were subjected to purification by HPLC (preparative or semi-preparative). These purifications were usually relatively low yielding ($\sim 10\%$) and in some cases the amount of pure material collected (less than 1 mg) did not allow characterisation and preliminary binding assays to be carried out. It was then decided to double the amount of resin used in SPS. Two possible explanations arise for these low yields: the loading of the first azido-carbamate onto the resin was incomplete, or the reduction of the azide into the primary

amine under Staudinger conditions was not complete. Incomplete loading would not be detectable on the HPLC chromatogram but would result in a low crude yield; whereas incomplete azide reduction would lead to the isolation of oligomers of different lengths after cleavage from the resin, which would show on the HPLC chromatogram. These low yields could also be due to a combination of both factors, although completion of each step (coupling and reduction) was checked using a chloranil test. Crude HPLC chromatograms indicated that in most cases the SPS was clean, although in some instances the product was contaminated with shorter oligomers. In order to push the loading of the first residue to completion, a double coupling of 30 minutes with 2 equivalents of monomer to the resin was carried out, and for the next residues a double coupling of 15 minutes using 1.5 equivalent of monomer was maintained. An alternative to the Staudinger azide reduction reported in the literature was also investigated, using TCEP (Tris(2-carboxyethyl)phosphine hydrochloride) as the reducing agent. This reagent was reported to achieve complete reduction of an azide group at room temperature after 2 hours and offered the additional advantage to be solid and thus less susceptible to oxidation, which was the case for the trimethylphosphine. It appeared however, that reduction of these azides on solid support using TCEP under standard microwave conditions was unsuccessful, so reduction of the azides using trimethylphosphine was resumed. By using a new batch of this reducing agent, the yield and purity of the synthesis were in general improved.

Straight after purification, oligourea **125** was sent to Leeds for testing, as the resulting data would guide the design of the next examples to be synthesized. This first compound was tested by Dr. A. Bartlett (Wilson/Edwards group) and the result is presented in Figure 4.6. This suggested that oligourea **125** (Fig. 4.6a) was indeed binding to *hDM2*, although the compound presented limited solubility in the assay conditions. It was then reasoned that in the next examples, the non-interacting phenylalanine mimic at position 5 would be replaced by a solubilising residue such as Orn or Ser. Table 4.1 summarizes the sequences of oligoureas that were synthesized, as well as the crude and isolated yields.

Table 4.1 The library of oligoureas. Oligourea residues are preceded by a U , natural residues are preceded by α , hot-spot residues mimicking those of p53 are in green, the capping elements are indicated in purple.

Scaffold	Sequence	Cpd	Crude yield	Isolated yield*
	<i>iPr</i> - U F- U F- U A- U W- U Orn- U L	125	13 mg 25%	2 mg 3.8%
	<i>iPr</i> - U F- U Orn- U A- U W- U Orn- U L	126	32 mg 43%	1.9 mg 2.6%
	U F- U Orn- U A- U W- U Orn- U L	127	35 mg 49%	2.2 mg 3%
Cap- U F- U X- U X- U W- U X- U L	<i>iPr</i> - U F- U S- U A- U W- U Orn- U L	131	71.2 mg 82%	5.8 mg 6.7%
	U F- U S- U A- U W- U Orn- U L	132	64.1 mg 70.7%	1.0 mg 1.1%
	<i>iPr</i> - U F- U Orn- U A- U W- U S- U L	133	44.1 mg Quant.	3.6 mg 8.1%
	U F- U Orn- U A- U W- U S- U L	134	28.3 mg 66%	2.0 mg 4.7%
Cap- U F- U X- U L- U W- U X- U L	<i>iPr</i> - U F- U S- U L- U W- U Orn- U L	135	68 mg 75%	5 mg 5.5%
	U F- U X- U W- U X- U X- U L	128	13 mg 28%	1.3 mg 4%
	α F- U X- U X- U W- U X- U L	129	29.6 mg 67%	3.2 mg 7.4%
α F- U X- U X- U W- U X- α L- α S	α F- U Orn- U A- U W- U Orn- α L- α S	130	20.7 mg 45%	0.3 mg 0.65%

* Yield of isolated material after preparative (or semi-preparative) HPLC purification; oligoureas **129-135** were purified by Dr. Casassus (Guichard group).

As mentioned previously in this section, the relatively low crude yields obtained for the first few oligoureas prompted for the SPS to be scaled up, so the consumption of monomer was higher than initially planned. The synthesis of this library used up all of the Leu and Trp monomers, and as it was envisaged that the collaboration would continue after this STSM, it was decided that new batches of these monomers would be synthesized during the last weeks of the mission in Bordeaux, while Dr. Casassus (Guichard group) would purify the last 7 oligoureas (**129 - 135**) and send them to Leeds for testing.

Because some of the monomers had been entirely used, the variant where the key Phe residue is introduced as the capping element on residue 6 and the hybrid scaffold containing a C-terminal γ -residue could not be investigated. These two scaffolds constitute important directions for future investigation on this project.

4.3 Biophysical evaluation

The small library of oligoureas was assessed using the previously reported FA assay used to assess *N*-alkylated oligobenzamides,^{85, 125, 131} cf. Chapter 3. The change in fluorescence anisotropy is measured upon displacement of the probe by the oligourea (Fig. 4.5). The protein used in this assay (His-*hDM2*₁₇₋₁₂₆) has been expressed in-house at the Astbury Centre as part of this research project (cf. Experimental section).

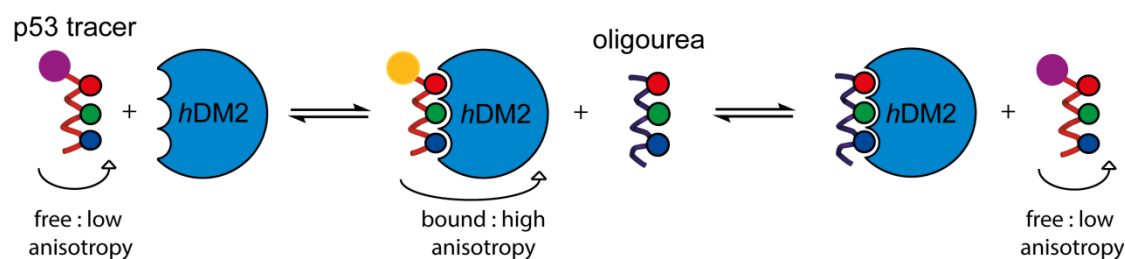


Figure 4.5 Cartoon representation of the fluorescence anisotropy (FA) assay. Firstly, the tracer is titrated with the target protein and fluorescence anisotropy increases upon binding to this much larger entity. The oligourea is then added and competitively binds to the target protein: the fluorescence anisotropy decreases as the tracer becomes free to tumble in solution again.

Previous experience with FA assays on oligobenzamides has revealed that undesired interactions of the p53 tracer with itself as well as with the oligobenzamides were precluding determination of a K_d value. The existence of a potential interaction of the oligoureas with the tracer was thus investigated. The results are reported in the Appendix IV. From this experiment, no evidence of interaction between the oligourea and the tracer could be observed.

4.3.1 Competition assay on the original oligourea

The first oligoureas were tested under the same conditions as the oligobenzamides: a fluorescence anisotropy competition assay where the concentration of oligourea is serially diluted from 100 μ M down to 9 nM in triplicate.

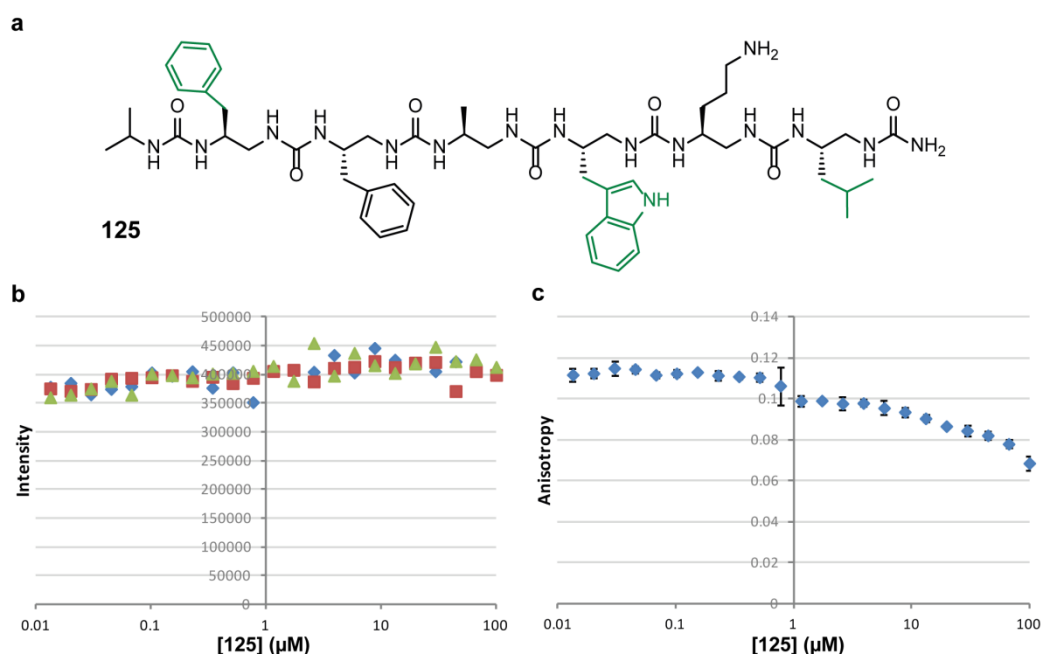


Figure 4.6 Results from the FA competition assay on the first synthesized oligourea. **a.** Structure of the first synthesized oligourea **125**. **b.** Intensities for all three replicates are plotted against the concentration of **125**. **c.** Average anisotropy versus concentration in oligourea.

The competition assay on compound **125** suggested that it was binding to *hDM2* in the micromolar range, although the binding curve (Fig. 4.6c) did not clearly present the characteristic sigmoidal shape that is expected for ligands that are potent inhibitors of the targeted interaction. From this set of data, it was however not possible to quantify the binding, as the anisotropy did not present the expected lower plateau that is usually reached at high concentrations of inhibitor. The fact that this curve did not present a clear sigmoidal shape also prevented extraction of an IC_{50} value. While testing this first oligourea it was noted that the compound presented a limited solubility in the conditions of the assay. The next oligomers were therefore designed with additional solubilising side chains.

4.3.2 Competition assays – an attempt to automation

Due to the lack of apparent reproducibility of the manual assay on the first few compounds, it was decided that the library would be tested using an automated method. Assays on the Hamilton Microlab Star robot made use of 384-well plates, thus reducing the amount of reagents used, in addition to being automated. Anisotropy plots for five oligoureas tested both on the robot and manually are reported in Figure 4.7. Results from assays conducted on the robot were however not faultless, as the overall intensity across the plate was not constant as it should be but rather presenting the same distinctive pattern (Fig. 4.7a). This defect also affected the anisotropy, masking the plateau that should be observed at the lowest concentrations in oligourea. This was attributed to sticking of the compounds to the pipette tips that are used on the robot (different tips were used in the manual assay). Optimizing this automated method would require the usage of a large amount of tips, as well as making the method much longer, which was not deemed as a good compromise. Figure 4.7 indicates that with the exception of compound **128**, better results can be obtained when the assay is carried out manually.

Whilst acceptable results had previously been obtained with the oligobenzamide series of compounds on the robot; it appeared more challenging to acquire exploitable data on the oligourea series. The oligoureas were thus re-tested manually, and eventually presented binding curves with more usual shapes; these results are presented thereafter. With the exception of **125**, all the oligoureas were soluble in the conditions required for the FA assay. It is worth noting that within the range of inhibitor concentration studied (100 μ M – 9 nM), in most cases the tracer was not fully displaced from its complex with *hDM2*. This is translated on the binding curves presented in Figure 4.7 by the absence of a lower plateau for the anisotropy.

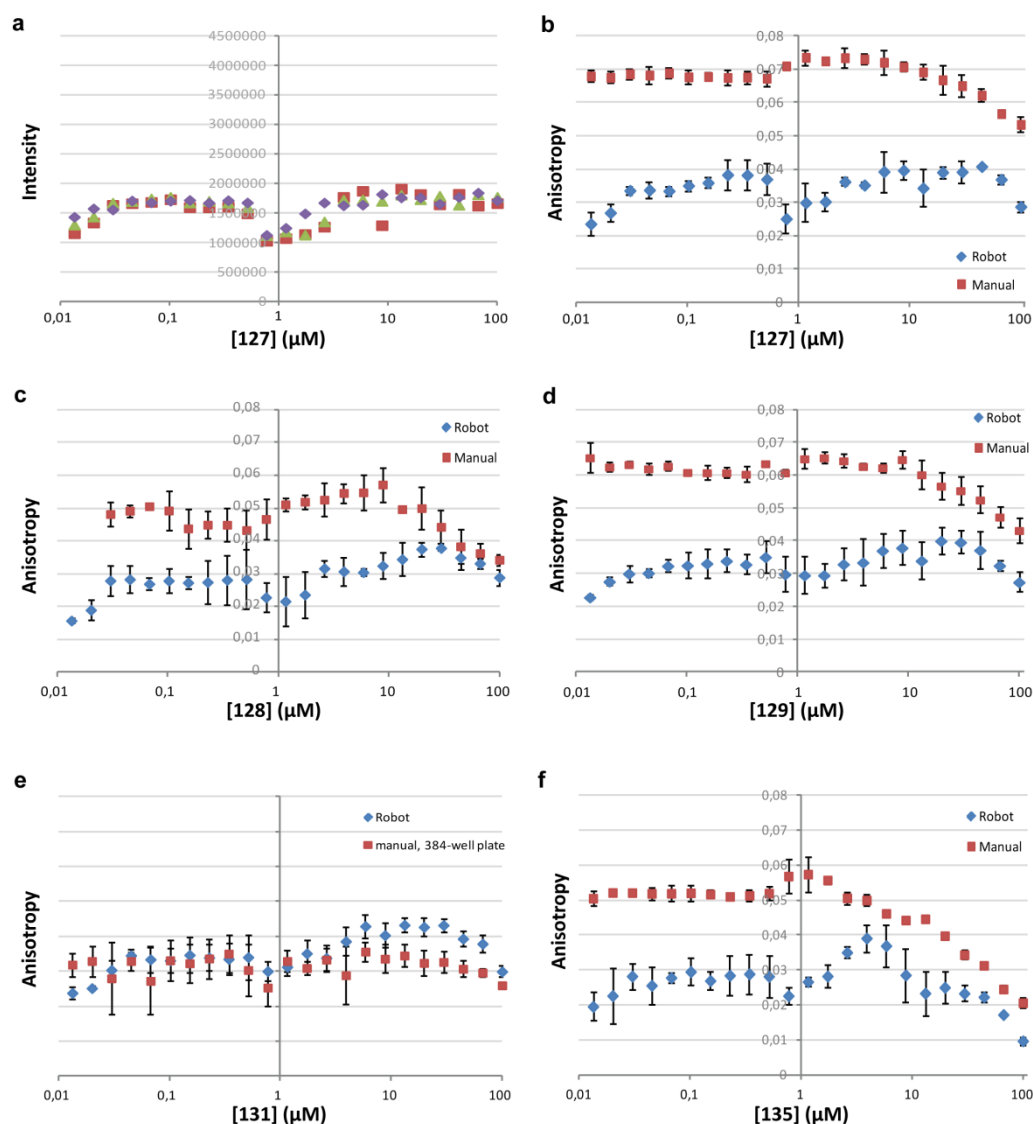


Figure 4.7 Comparing results from FA assays conducted on the robot to assays carried out manually. Anisotropy plots for compounds tested in both methods are overlaid. **a.** Distinctive intensity plot typically obtained on the robot, here with compound **127**. **b.** Oligourea **126**. **c.** Oligourea **128**. **d.** Oligourea **129**. **e.** Oligourea **131**. **f.** Oligourea **135**.

It was thought that the first few compounds tested had a low binding affinity for the target protein, but screening of the whole library revealed that none of the oligoureas presented a complete binding curve (cf. Section 3.2). For the purposes of this study, binding curves were fit in Origin 8.6 using a fixed minimum, which corresponded to the lower plateau of anisotropy reached in the displacement assay using the unlabelled p53 peptide. If the oligoureas had been able to fully displace the tracer from the interaction, then the anisotropy should indeed have

returned to this value. Using this fitting parameter allowed the determination of apparent IC_{50} values that were then used as a tool to establish a preliminary comparison of the compounds. For the best inhibitors identified, efforts will then be devoted to the obtention of a full binding curve, in order to determine IC_{50} values.

4.3.2 Establishment of Structure-Activity Relationships

Derivatives **126** and **127** were then prepared, with the Phe \rightarrow Orn replacement at position 5. An improvement in solubility was noted with these compounds and results from FA assays are reported in Figure 4.8. This substitution pattern Phe-Orn-Ala-Trp-Orn-Leu then became the standard pattern and the next oligoureas were designed to study the effect of modifications to this standard on the binding affinity.

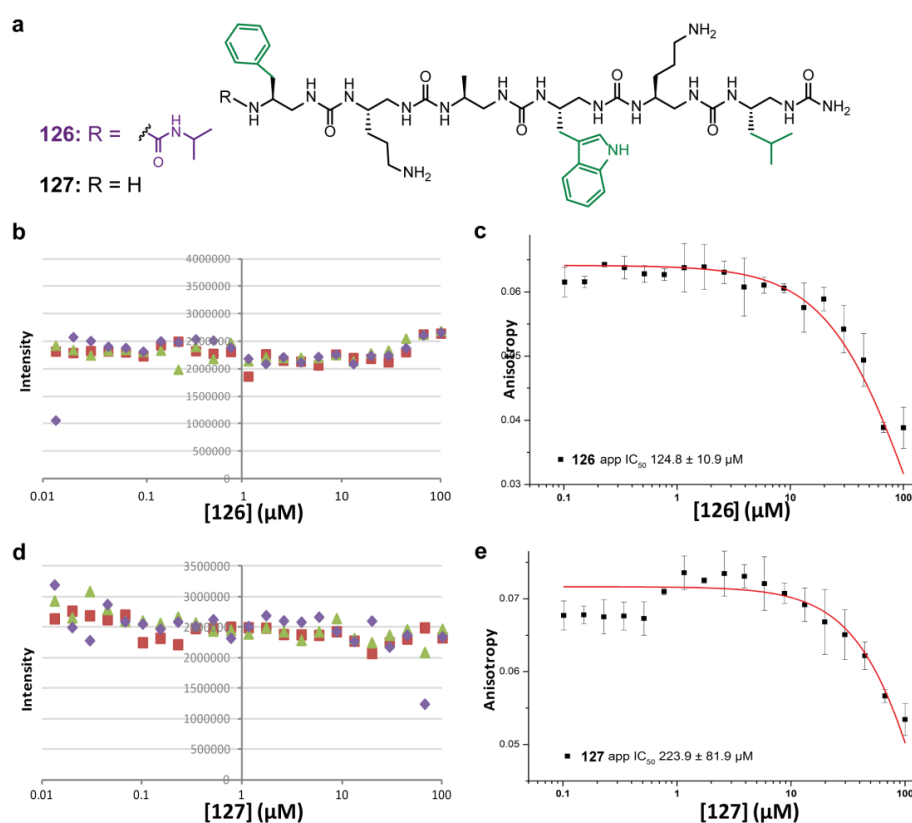


Figure 4.8 Results from the FA competition assay on oligoureas containing an additional solubilizing Orn residue. a. Structure of the oligoureas: **126** was capped at the *N*-terminus with isopropyl isocyanate (purple) and **127** was left as a free amine. **b, c.** Intensity and average anisotropy of compound **126**, the experiment was carried out on the Hamilton robot. **d, e.** Intensity and average anisotropy of compound **127**, the experiment was carried out manually.

Compound **126** was tested on the robot, and the corresponding intensity curves present the usual shape, whereas the intensities for compound **127** tested manually displayed a flat intensity profile. Fitting in Origin 8.6 using a fixed lower plateau suggested that both compounds were poor inhibitors, although the capped analogue **126** seemed to be relatively more potent (apparent IC_{50} of $124.8 \pm 10.9 \mu\text{M}$ against 223.9 ± 81.9 for **127**).

The next compounds synthesised aimed at studying the effect of the macrodipole on the binding affinity. The Phe5 \rightarrow Orn replacement was maintained, but Trp3 was swapped with Ala4, meaning that the key residues were in positions $i, i + 3$ and $i + 5$ of the oligourea backbone. Results from the FA assay on the free amine analogue are reported in Figure 4.9.

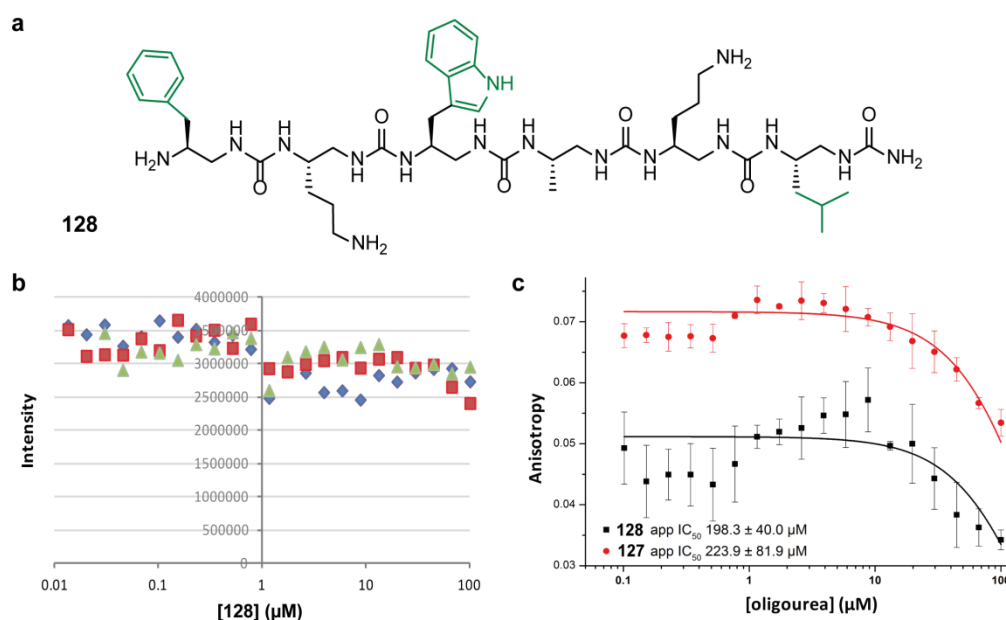


Figure 4.9 Effect of the macrodipole orientation on binding: the $i, i + 3$ and $i + 5$ substitution pattern. a. Structure of the oligoureas: **128**. b. Comparison to the analogue oligourea with the ‘standard’ $i, i + 2$ and $i + 5$ pattern.

The comparison of binding curves for compound **128** and **127** showed that placing the Trp at position 3 rather than 2 makes no difference in terms of inhibition (cf. Fig. 4.9) and **128** was equally inactive. This might be explained by the fact that reversing the oligourea macrodipole did not affect the binding, or that the oligourea might still bind in the same orientation, due to induced-fit of the protein around the Trp side chain.

Next was the replacement of the key U Phe residue at position 6 by its natural α -amino acid analogue, yielding the hybrid oligomer **129** (Fig. 4.10). The α -residue was introduced as an Fmoc-amino acid, and the coupling was carried out in presence of PyBOP as the coupling agent, under the same microwave conditions as for *N*-succinimidyl carbamates. The final Fmoc-deprotection was carried out manually, without microwave heating. In this case, because the sequence was terminated by a natural amino acid, the oligomer was just left as a free amine and no capped analogue was prepared. The replacement of the key interacting U Phe residue by its natural analogue somewhat weakens the natural oligourea H-bonding network, as one *N*-terminal bifurcated H-bond is missing. It was thought that this could potentially be favourable to the binding event, as additional flexibility was brought to the terminus, which could lead to a better fit of the side chain within the binding pocket on the surface of *hDM2*. On the other hand, the hybrid scaffold displays a shorter distance between the U Trp and α -Phe in the hybrid scaffold as compared to that between U Trp and U Phe (Fig. 4.4d and b respectively), which might be either beneficial or detrimental to the binding.

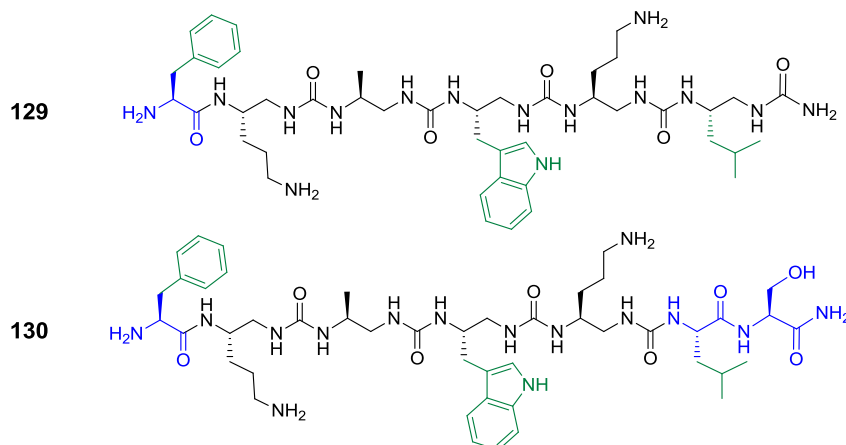


Figure 4.10 Structures of hybrids oligoureas 129 and 130 (Binding curves in Appendix V).

Judging from the FA results (Appendix V), the replacement of the U Phe for its natural analogue did not have a dramatic effect on the binding (**129**, apparent $IC_{50} = 177.8 \pm 61.4 \mu M$ against $223.8 \pm 81.8 \mu M$ for the all-oligourea analogue **127**). It has been noted from the literature that several crystal structures of the p53 helix had an additional serine residue immediately following Leu26 at the *C*-

terminus and it was thought that this residue might be beneficial for crystal formation. The analogue of compound **129** with an α -Leu and an additional α -Ser at the C-terminus was thus synthesized, resulting in hybrid oligourea **130** (Fig. 4.10). **130** displayed an apparent IC_{50} of $263.4 \pm 31.3 \mu M$, which showed that replacing the key Leu residue by its natural counterpart and adding an extra amino acid at the C-terminus was somewhat detrimental to the binding. Compounds **127** and **130** presented similar apparent IC_{50} s, which indicated that the simultaneous replacement of both terminal key residues in the initial designed scaffold by their α -amino acid analogues did not result in a significant change in the binding of the oligourea to *hDM2*. Hybrid scaffolds containing α -residues were therefore not investigated further.

The next two oligoureas prepared contained an all-oligourea backbone, to study the effect of the Orn5 \rightarrow Ser replacement. Serine was chosen as it displayed a shorter chain as Orn but should still play a solubilising role. Comparison of binding curves for **131** and **132** (Appendix V) did not reveal a significant difference in binding affinity between the capped and free compounds. Changing Orn5 for a Ser at position 5 did not affect the binding affinity either, as shown by comparison of **131** with **127** (**131**, apparent IC_{50} of $224.3 \pm 45.5 \mu M$ and **127** apparent IC_{50} of $223.8 \pm 81.8 \mu M$ Appendix V).

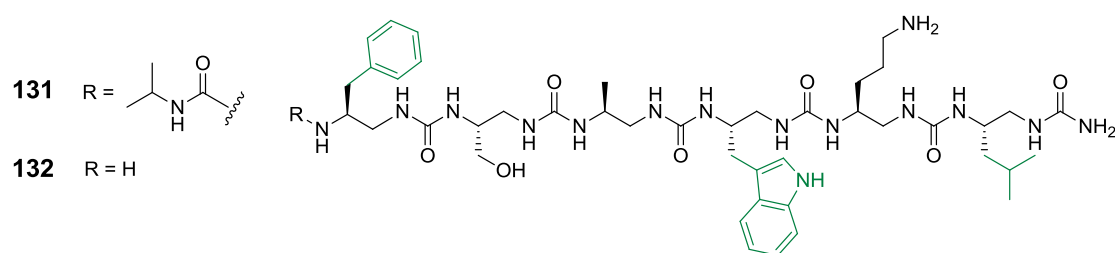


Figure 4.11 Structures of oligoureas 131 (capped) and 132 (uncapped).

Inverting the Orn and Ser residues at position 2 and 5 yielded the pair of oligoureas **133** and **134**. The capped analogue **133** seemed to present a lower IC_{50} as the uncapped oligourea (Fig. 4.12c), suggesting that in this case the capped analogue was binding to the target protein with a higher affinity, although the large error on the IC_{50} value for **134** precluded a definitive conclusion. When

comparing this capped oligomer with **131**, its analogue with inverted positions for Orn and Ser, it appeared that placing Ser at position 2 and Orn at position 5 resulted in a significant increase in affinity for *hDM2* (apparent IC_{50} of $42.9 \pm 4.3 \mu\text{M}$ for **133** and $224.3 \pm 45.5 \mu\text{M}$ for **131**). This might be due to a reduced steric hindrance with the Ser residue, or to additional H-bonding to interfacial residues of *hDM2*.

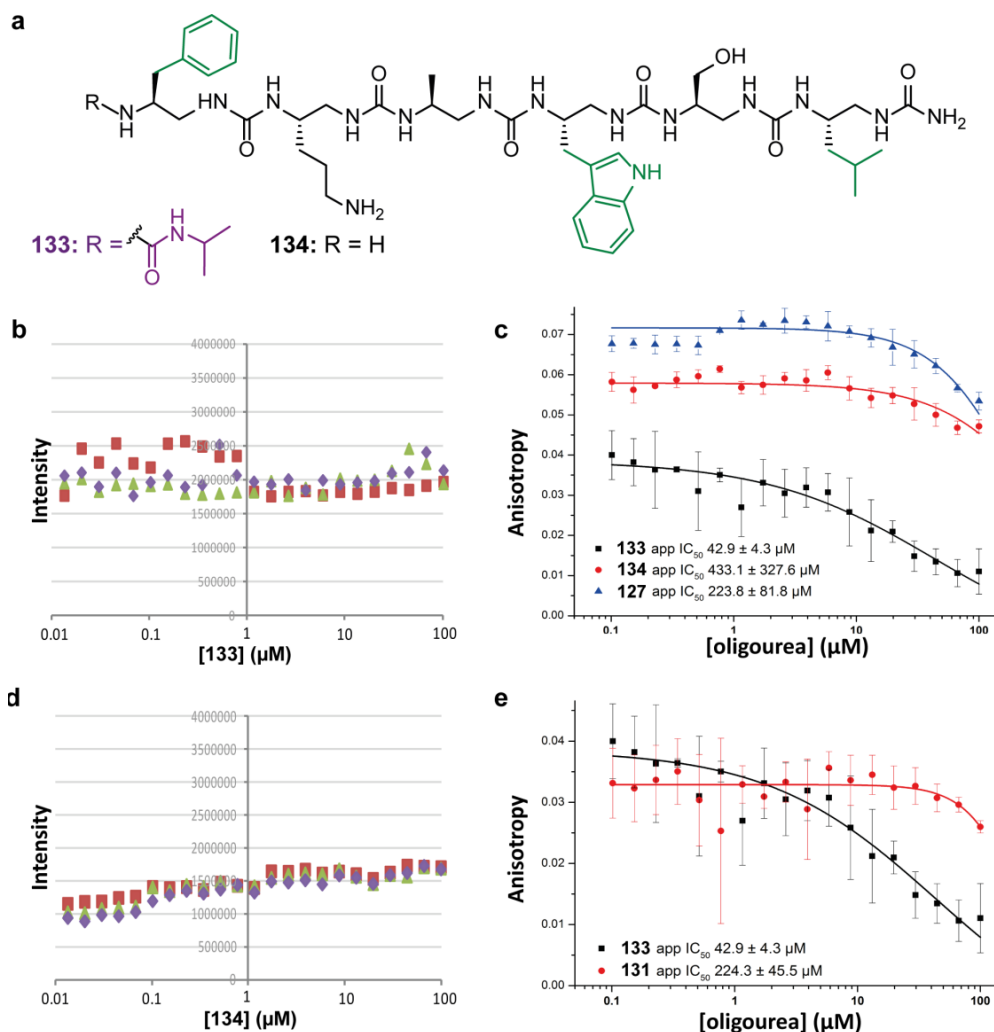


Figure 4.12 Swapping positions of Orn and Ser. **a**. Structure of oligoureas **133** and **134**. **b**. **d**. Intensity plots for **133** and **134** respectively. **c**. Overlay of binding curves for compounds **133**, **134** and **127**. **e**. Overlay of binding curves for compounds **133**, and **131**.

The last oligourea synthesised saw its Ala residue replaced by a Leu, which had been reported to be a ‘secondary’ hot-spot residue for the binding of p53 to

hDM2.^{205, 206} Due to the low amount of monomers left, only the capped variant of this oligomer was prepared (Fig. 4.13).

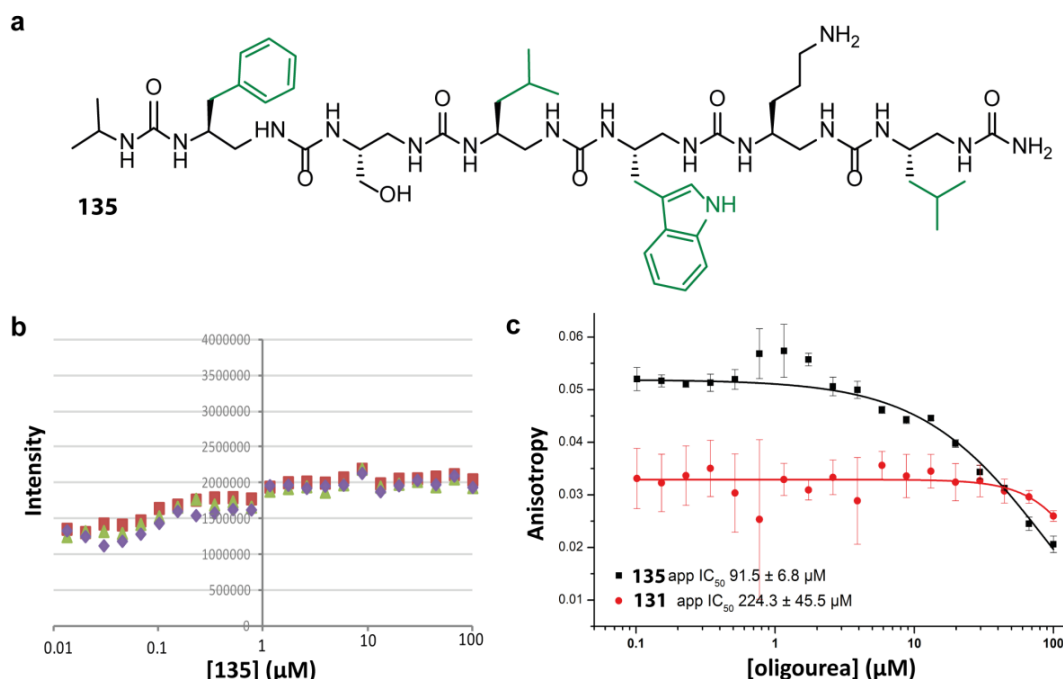


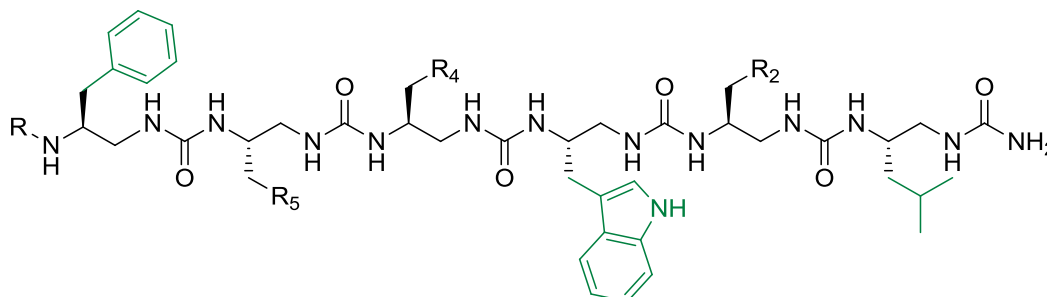
Figure 4.13 Introducing an additional key residue: the Leu22 mimic. **a.** Structure of oligourea **135** with the 4 key interacting side chains in green. **b.** Intensity plots for **135**. **c.** Overlay of binding curves for **135** and **131**.

Comparing the data to that obtained for compound **131** (containing an ^UAla in place of the ^ULeu4 mimic), it appeared that the introduction of this additional Leu mimic was indeed beneficial to the binding (apparent IC₅₀ value lowered by ~130 μM, cf. Fig. 4.13). This suggested that the oligourea scaffold was suitable for the mimicry of two consecutive residues of an α -helix.

At first, the library was tested in a manual assay using 96-well plates, then as the amount of some of the oligoureas was precluding further tests to be carried out, the assay was moved to 384-well plates. Although the 384-well plates proved to be more technically challenging to use, this allowed reducing by a third the amount of oligourea needed per assay. Table 4.2 summarizes all the results obtained from the library of oligoureas that was synthesized. The compounds

were compared pairwise in order to extract Structure-Activity Relationships (SAR) that will guide the design of future generations of oligourea helix mimetics.

Table 4.2 Summary of the design of the library of oligoureas and Structure-Activity Relationships established based on FA assay results.



Compounds compared	Modification	Effect
125 vs 126	$^U\text{Phe5} \rightarrow \text{Orn}$	Enhanced solubility No real improvement in activity
126 vs 127	<i>N</i> -term capping	Both compounds are weak inhibitors
127 vs 128	$^U\text{Trp3} \leftrightarrow ^U\text{Ala4}$	Potential inversion of the macrodipole: No marked effect
127 vs 129	$^U\text{Phe6} \rightarrow \alpha\text{Phe6}$	Replacement of the key Phe by its α -analogue: No marked effect
129 vs 130	$^U\text{Leu1} \rightarrow \alpha\text{Leu-Ser}$	α -Residues at both termini: No marked effect
131 vs 132	<i>N</i> -term capping	No marked effect
132 vs 127	$^U\text{Orn5} \rightarrow ^U\text{Ser}$	No marked effect
133 vs 134	<i>N</i> -term capping	The capped analogue 133 is significantly more active
134 vs 127 133 vs 126	$^U\text{Orn2} \rightarrow ^U\text{Ser}$	Slight preference for Ser over Orn at position 2
133 vs 131	Orn \leftrightarrow Ser	Preference for the Ser2-Orn5 over the Orn2-Ser5 combination
135 vs 131	$^U\text{Ala4} \rightarrow ^U\text{Leu}$	Significant increase in affinity upon addition of the additional key Leu22 mimic

Efforts have then been focused on obtaining the entire binding curve for the two most potent oligoureas, compounds **133** and **135**, in order to quantify their potency in terms of IC_{50} . It was reasoned that lowering the concentration of protein should shift the IC_{50} towards lower values, however when the assay was carried out with 50 nM of protein (a third of the initial concentration), the lower plateau was still not reached with 100 μ M inhibitor (cf. Appendix VI). Because the tracer was never fully displaced from the interaction even at the highest concentrations in oligoureas, it was not excluded that the drop in anisotropy was due to non specific interactions, however the observations made in this chapter are only preliminary, and will need further investigation to ascertain that the oligoureas are indeed able to compete away the tracer – even if only weakly. In order to support the hypothesis that the binding event was taking place, some structural studies were carried out and are described in the next section.

4.4 Conformational investigation of oligourea **133**

Compound **133** was identified as the potentially most active compound in the series, but no full binding curve could be obtained, which suggests that the drop in anisotropy could just be due to non-specific binding of the compound at high concentrations. Further structural evidence was therefore sought in order to support the hypothesis that the oligoureas were indeed binding into the targeted hydrophobic cleft of *hDM2*. The helicity of **133** was then confirmed by circular dichroism (CD) and the result is reported in Figure 4.14. Oligourea **133** presented an ECD signature with a maximum in the positive molar ellipticity at ~ 203 nm, indicative of the expected 2.5-helical folding in MeOH.

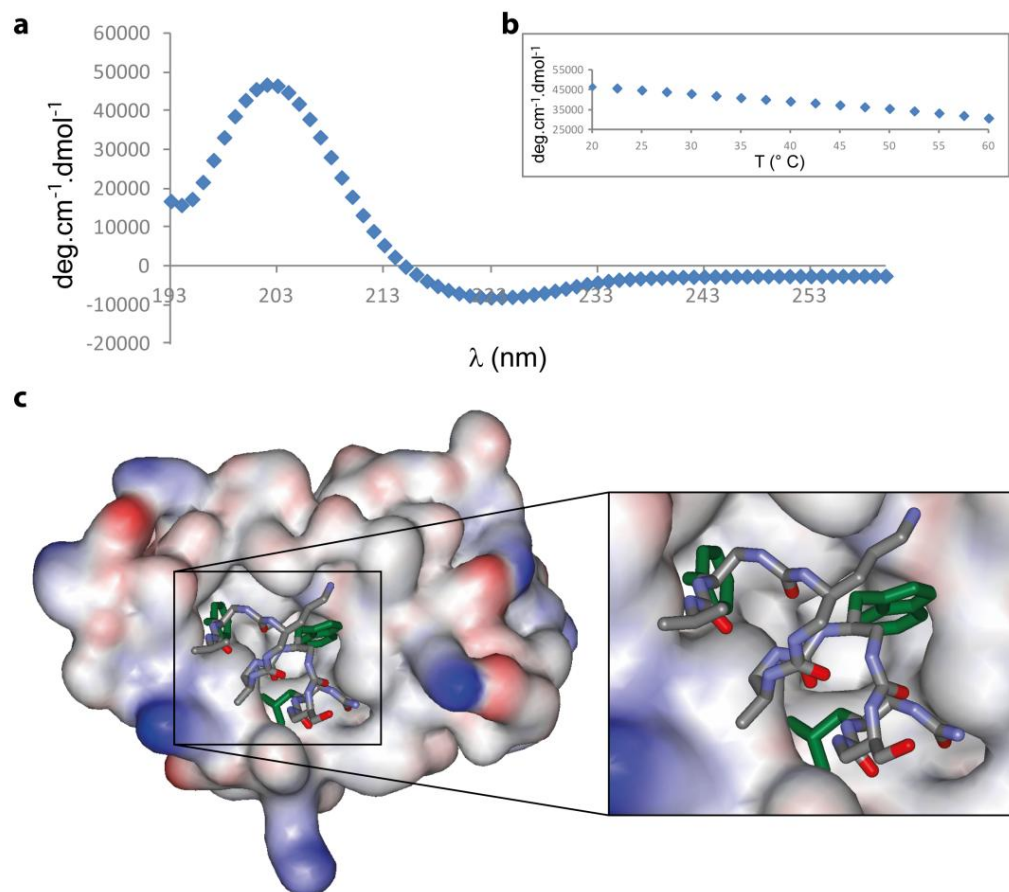


Figure 4.14 Investigating the helicity of oligourea 133 and potential binding to *hDM2*. **a.** CD spectrum recorded in MeOH at room temperature at a concentration of 0.2 mM. The maximum at 203 nm is indicative of 2.5 helix formation. **b.** CD Temperature scan of **133** in MeOH for $\lambda = 203$ nm. **c.** Manual docking of **133** onto the crystal structure of *hDM2* (from PDB ID: 1YCR).

This CD pattern of **133** in MeOH was not sensitive to increase in temperature (Fig. 4.14b). The intensity of the maximum at 203 nm recorded between 20 and 65 °C decreased only slowly upon temperature increase, following a linear trend and no melting was observed in the temperature range studied. A conformational search was performed on **133** and the lowest energy conformation was manually docked into the p53-binding cleft of *hDM2* (Fig. 4.14c). This illustrated that the oligourea could be accommodated into this binding pocket, and all three key interacting residues could indeed be oriented towards the inside of the binding cleft without any major steric clash. Taken together, these results suggest that oligourea **133** indeed adopted a 2.5-helical conformation required to obtain the alignment of key side chains along one helical face. The manual docking

experiment also showed that the oligourea should in theory be able to bind into the targeted cleft on *hDM2*.

4.5 Target selectivity

The library of oligoureas has also been screened in a single point assay against the Mcl-1/Noxa B interaction,^{177, 207} in order to study their selectivity. Results from this single point screening are reported in Figure 4.15.

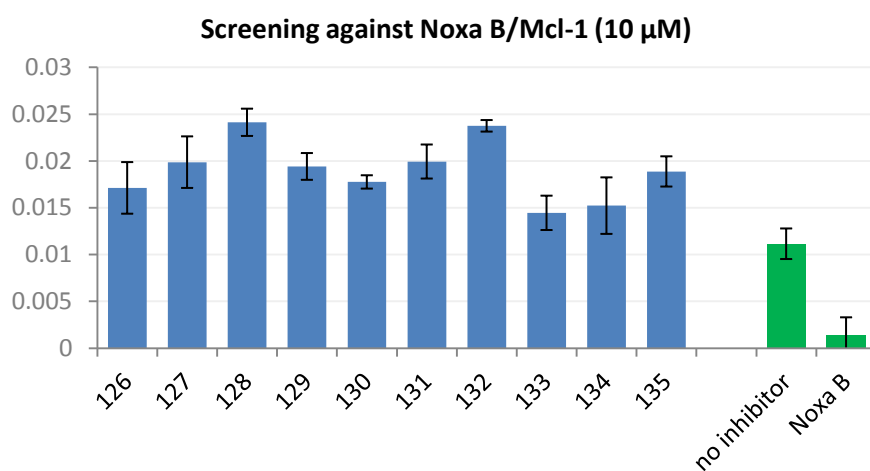


Figure 4.15 Investigating the target selectivity of the library of oligoureas: single point screening against the Mcl-1/Noxa B PPI.

The result from this screening shows that none of the oligoureas is active against the Mcl-1/Noxa B PPI: the designed inhibitors (and most importantly compounds **133** and **135**) are therefore p53/*hDM2* specific. As the library of oligoureas was tested in the same assay as the *N*-alkylated oligobenzamides (cf. Chapter 3), the anisotropies measured here were also higher than that of the negative control. As explained in the previous chapter, this was due to the fact that the test wells contained 10% DMSO whereas the control wells did not. DMSO could have either affected the viscosity of the solution, or the structure of the protein or binding cleft itself, thus altering the binding of the inhibitor.

4.6 Conclusions and future work

A library of 11 oligoureas has been assembled using a microwave assisted solid phase methodology. Testing of this library in a fluorescence anisotropy competition assay against the p53/*hDM2* interaction allowed the establishment of basic SAR. It seems that effect of the *N*-terminal capping is variable from one sequence to another, in agreement with previously reported results.¹⁹⁷ Ser and Orn have both been investigated as solubilising side chains, and it appeared that their respective position could actually affect the binding, possibly through interaction with neighboring side chains in the *hDM2* binding cleft. The last oligourea (**135**) also displayed a Leu22 mimic, which made it one of the two most potent p53/*hDM2* inhibitors of this library (along with compound **133**). Using the SAR from these preliminary experiments, a next generation of oligourea inhibitors was designed, they combine the features described above: Ser at position 2, the additional Leu4 mimic, Orn at position 5 (Fig. 4.16). Along with these designed scaffolds, other initially foreseen examples could not be investigated due to time restrictions, such as the hybrid oligourea/ γ -peptide (Fig. 4.16c) and variants of **133** and **135** bearing the dichlorophenylalanine and cyclohexylalanine side chains (Fig. 4.16e-g). Whilst manually docking the oligourea, it was also observed that the Phe side chain was not reaching into the binding pocket as deeply as it could. It seemed that shortening the distance between this Phe and the preceding Orn residue might provide a better fit. This would correspond to the analogue where the oligourea is capped with benzyl isocyanate, which had already been envisaged. It was also reasoned (from Fig. 4.14c) that replacing Ala by an acidic residue such as Asp might provide an additional ionic interaction with the neighbouring negatively charged domain on the surface of *hDM2*. Towards the *C*-terminus, it seemed that replacing the Leu for a Val residue might provide a better fit, as the Leu presented minor steric clashes with the surface of *hDM2*. The synthesis and biophysical evaluation of these new designed oligoureas (including ITC experiments in order to obtain more information on the thermodynamics of the binding) form the future work on this project.

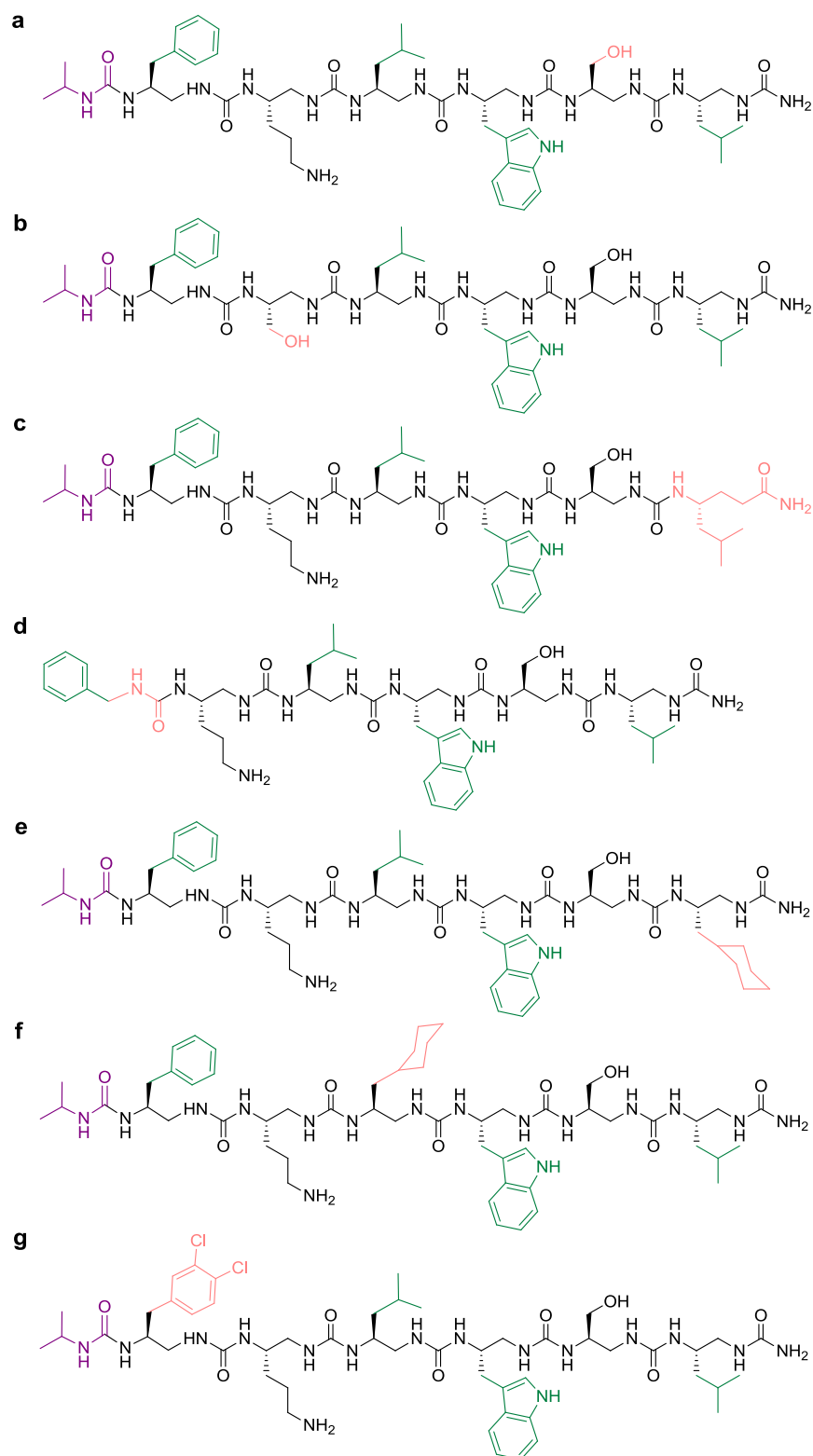


Figure 4.16 The next generation of oligourea. The suggested modifications are coloured in pink. **a.** Capped and uncapped variants of **135** with a Ser in position 2. **b.** Variants of **135** with a Ser in positions 2 and 5. **c.** Analogue of scaffold **a**. using a γ -residue as the Leu1 mimic. **d.** Analogue of scaffold **a**. capped with benzyl isocyanate as the Phe mimic. **e.** and **f.** Analogues of **a**. including cyclohexyl rings as mimics of Leu1 and Leu4. **g.** Analogue of **a**. including the dichlorophenyl monomer as the Phe mimic.

Chapter 5

Thesis summary and Future directions

α -Helix mediated PPIs are the primary focus of intense research efforts, as they are involved in the development of diseases such as HIV and cancer and therefore present a considerable therapeutic potential. Although small molecules have provided some of the most potent inhibitors so far, they only offer tailored answers; for each PPI target the design of inhibitors has to start from scratch. Considering the number of PPIs that involve binding through an α -helix, an attractive strategy would be to use a generic scaffold to mimic the helical core, and side chain appendages to mimic the hot-spot residues that are critical for the interaction. Foldamers and proteomimetics are two approaches that use this strategy. While foldamers are usually peptide-based and actually mimic the helical secondary structure, proteomimetics only replicate the spatial projection of the key side chains from the helix. Both approaches have yielded versatile scaffolds able to disrupt distinct PPIs. In this context, an automated SPS has been developed that allowed the assembly of a library of *N*-alkylated oligobenzamides. In previous studies, this scaffold was demonstrated to be a potent helix mimetic and also presented an accessible and modular synthesis. The newly developed methodology made use of a state of the art microwave assisted peptide synthesiser, and allowed facile library generation of diversely functionalized compounds. The oligomer assembly was compatible with a variety of side chains and could be extended to a decamer; the number of possible combinations thus meant that a wide range of potential helix surfaces could be mimicked. A few proteinogenic side chains proved more troublesome, whether during the monomer synthesis, or during the oligomer assembly – these will require further

investigation. The set of monomers compatible with the method however allowed SAR study on the model interactions chosen for this project. The robustness of the method was illustrated by the assembly of a 75-member library of tribenzamides. This library was divided into two sub-libraries, each designed to target one of the model PPIs: p53/hDM2 and Noxa B/Mcl-1. The library was tested in a fluorescence anisotropy competition assay, first in single point for hit identification and then dose-response assay on these hits provided IC₅₀ values that served as a basis for SAR studies. Manually screening the library proved cumbersome and an attempt has been made to adapt the assay to an automated method. In addition to being less time-consuming, this would also reduce the amount of reagents used. Automating the assay was however not as straightforward as anticipated and further optimization will be required to produce a workable assay. The manual screening nevertheless provided reliable hit identification, from which potent inhibitors of both interactions were identified, with IC₅₀s in the low micromolar range. Preliminary testing of dual inhibitor **47** against p53/hDMX suggested that this compound could be a non-specific inhibitor. It is not excluded that other hits might also owe their apparent potency to their hydrophobicity, giving rise to non-specific binding within the hydrophobic cleft of their target protein. A selectivity study however revealed that up to 20-fold selectivity could be attained (compound **89**); these studies therefore brought the first piece of evidence for the versatility of this scaffold. Efforts are currently ongoing within the group towards obtaining a co-crystal structure of an oligoamide bound to hDM2. This would not only establish whether these compounds are actually selective inhibitors or not, but would also serve as a guide for the design of future generations of compounds. Furthermore, the proteolytic stability of these aromatic oligoamides was established against a panel of proteases and a preliminary high content screening suggested that some of the compounds might be able to penetrate the cells and trigger apoptosis, although this will need to be confirmed by further experiments. Future investigations will include testing this library of oligobenzamides against different PPIs, *e.g.* interactions involving the Bcl-x_L antiapoptotic protein and further experiments against p53/hDMX. These will require additional molecular biology work, and setting up workable assays with these proteins. The studied

interactions will also be characterised using other biophysical methods, including ITC. This would circumvent the intrinsic limitations of the FA assay which precluded the determination of dissociation constants. Further cellular investigation on the entire library will also be carried out by collaborators in order to confirm observations and hypotheses from the initial cell assays.

A collaboration with the Guichard group (IECB, Université de Bordeaux, France) was established, and as a part of this PhD a 2-month scientific mission was carried out, for which independent funding was obtained from the European COST Action CM0803, Functional peptidomimetic foldamers: from unnatural amino acids to self-assembling nanomaterials. This collaboration aimed at applying oligoureas to helix mimicry, and testing them in the FA assay developed at Leeds. A small library of oligoureas has been assembled using a microwave assisted SPS. Testing this library against the p53/hDM2 interaction allowed the establishment of basic SAR and identified 2 potential inhibitors. This joint research project will continue with the design of a second generation of oligoureas based on the SAR from these preliminary experiments. Their synthesis and biophysical evaluation form the future work on this project.

During this PhD, two scaffolds have been investigated for α -helix mimicry – the *N*-alkylated oligobenzamide scaffold, and the *N,N'*-linked oligourea scaffold. Two other *O*-alkylated scaffolds are also being investigated within the group; their potential as helix mimetics has been established and further biophysical assessment is currently ongoing. Once thorough SAR studies have been carried out on these scaffolds, the study of hybrid scaffolds will be envisaged. This could potentially lead to the identification of inhibitors with improved potencies and selectivities

Chapter 6: Experimental section

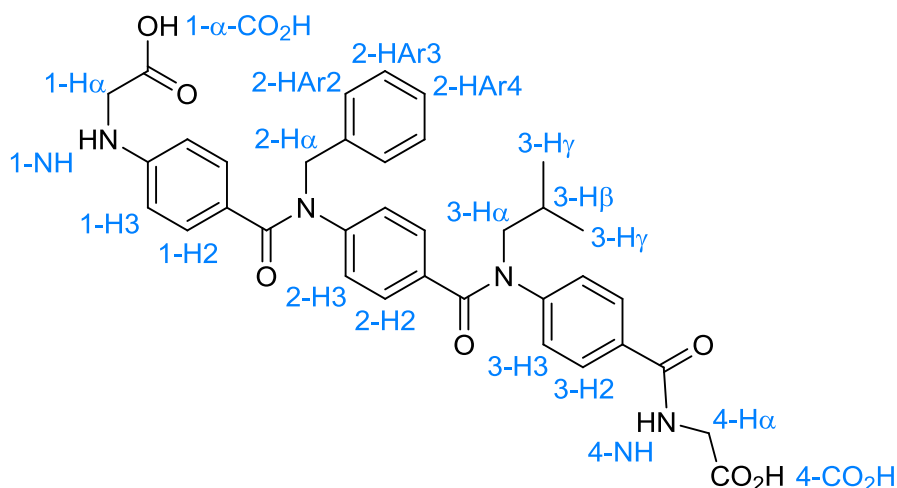
General considerations

All reagents were obtained from Aldrich, Alfa Aesar, Acros or Fluka and used without further purification. All solvents used were HPLC grade. Analytical TLC was performed using 0.2 mm silica gel 60 F₂₅₄ pre-coated aluminium sheets (Merck) and visualised using UV irradiation or, in the case of amine intermediates, by staining with a ninhydrin solution. Flash column chromatography was carried out on silica gel 60 (35 to 70 micron particles, FluoroChem). Solvent ratios are described where appropriate. Solvents were removed under reduced pressure using a Büchi rotary evaporator at diaphragm pump pressure. Samples were freed of remaining traces of solvents under high vacuum. ¹H and ¹³C NMR spectra were measured on a Bruker DPX300 or a Bruker Avance 500 spectrometer using an internal deuterium lock. Chemical shifts are reported in parts per million (ppm) downfield from TMS in δ units and coupling constants are given in hertz (Hz). Coupling constants are reported to the nearest 0.1 Hz. TMS is defined as 0 ppm for ¹H NMR spectra and the centre line of the triplet of CDCl₃ was defined as 77.10 ppm for ¹³C NMR spectra. When describing ¹H NMR data the following abbreviations are used; s = singlet, d = doublet, t = triplet, q = quartet, m = multiplet. Melting points were determined using a Griffin D5 variable temperature apparatus and are uncorrected. Microanalyses were obtained on a Carlo Erba Elemental Analyser MOD 1106 instrument, found composition is reported to the nearest 0.05%. Infrared spectra were recorded on a Perkin-Elmer FTIR spectrometer and samples analysed as solids (unless stated). Mass spectra (HRMS) were recorded in house using a Micromass GCT Premier, using electron impact ionisation (EI) or a Bruker Daltonics micrOTOF, using electron spray ionisation (ES). LC-MS experiments were run on a Waters Micromass ZQ spectrometer, samples ionised by electrospray and analysed by a time-of-flight mass spectrometer, or a Bruker Daltonics HCTUltra™ series spectrometer. All experiments were run through a C18 column on an acetonitrile–water gradient (typically 0–95% acetonitrile over 3 min). A representative example of each synthetic procedure is provided with all examples described in the ESI.

Numbering system

To simplify the numbering and NMR assignment of our trimers, we have devised a new sequential nomenclature, where each of the monomer building blocks is considered separately. The monomers are numbered from 1 to 3 starting from the N-terminal, and the glycine is numbered 4. Within each monomer, the numbering is the same: the carbons from the aminobenzoic acid are numbered using the standard system (the aromatic carbon bearing the carboxylic acid is C1, the one bearing the amine is C4). Then, the lateral chain is numbered: the carbon attached to the nitrogen is the C α , and the numbering of the aliphatic part of the side chain continues with C β , etc. In the case of aromatic side chains, the aromatic carbons are numbered CAr1, CAr2, etc. The numbering of the protons is calqued on the carbon numbering. To differentiate each individual carbon/proton, the monomer number is added as a prefix to the carbon/proton number.

The same nomenclature is applied to the Fmoc-protected monomers, and the protons corresponding to the Fmoc system are differentiated by the prefix F. The protons from the CH₂ group will therefore be numbered FH α , the neighbouring CH will be FH β , and the aromatic Fmoc protons are numbered FH2 to FH5.



6.1 Assembling a library of *N*-alkylated oligobenzamides (Chapters 2 and 3)

6.1.1 Monomer building blocks

Compounds **21a, d, i, j, m, v, 22a, d, i, j, m, v** and **23** have been previously reported and fully characterised (Campbell, F., Plante, J. P., Edwards, T. A., Warriner, S. L. & Wilson, A. J. *N*-alkylated oligoamide α -helical proteomimetics. *Org. Biomol. Chem.* **8**, 2344-2351, DOI: 10.1039/c001164a (2010). These compounds were re-synthesised and the characterisation matched the previously reported data.

4-(Cyclopropylmethylamino)benzoic acid **21b**

4-Aminobenzoic acid (1.95 g, 14.3 mmol), cyclopropane carboxaldehyde (1.00 g, 14.3 mmol) and picoline-borane complex (1.68 g, 15.7 mmol) were stirred at room temperature in methanol (50 mL) for 14 hours. A white precipitate formed. The precipitate was filtered and dried under high vacuum to yield the desired compound (0.85 g, 31%) as a colourless powder; R_F 0.20 (hexane – ethyl acetate 1-1); (Found: C, 69.10; H, 6.85; N, 7.20%; $C_{11}H_{13}NO_2$ requires: C, 69.09; H, 6.85; N, 7.32%); δ_H (500 MHz, MeOD) 0.28 (m, 2H, $H_{\gamma/\gamma'}$), 0.57 (m, 2H, $H_{\gamma'/\gamma}$), 1.12 (m, 1H, H_{β}), 3.04 (d, 2H, $J = 6.7$ Hz, H_{α}), 6.63 (d, 2H, $J = 8.8$ Hz, H_3), 7.79 (d, 2H, $J = 8.8$ Hz, H_2); δ_C (75 MHz, DMSO- d_6) 3.47, 10.36, 46.80, 110.68, 116.54, 131.09, 152.63, 167.49; ν_{max}/cm^{-1} (solid state) = 3375 – 3403 (NH), ~3000 (COOH), 1736 (C=O), 1360 (C-N), 1216 (C-O); ESI-HRMS found m/z 192.1023 $[M+H]^+$ $C_{11}H_{14}NO_2$ requires 192.1019.

4-((((9H-Fluoren-9-yl)methoxy)carbonyl)(cyclopropylmethyl)amino)benzoic acid **22b**

To a refluxing solution of 4-(cyclopropylmethylamino)benzoic acid **21b** (0.85 g, 4.4 mmol) in tetrahydrofuran (8 mL) was added dropwise a solution of Fmoc-chloride (1.21 g, 4.7 mmol) in tetrahydrofuran (5 mL). The reaction mixture was then stirred at reflux overnight. The solvents were evaporated, then the residue was purified by Flash column chromatography (*Biotage, 50g SNAP cartridge, Mobile phase* : dichloromethane – methanol gradient) to yield pure target material (1.20 g, 66%) as an off-white amorphous solid; R_F 0.47 (40% hexane in

ethyl acetate); δ_{H} (300 MHz, CDCl_3) 0.05-0.10 (m, 2H, $\text{H}\gamma/\gamma'$), 0.38-0.44 (m, 2H, $\text{H}\gamma'/\gamma$), 0.85-0.97 (m, 1H, $\text{H}\beta$), 3.53 (d, 2H, $J = 7.3$ Hz, $\text{H}\alpha$), 4.12 (t, 1H, $J = 6.2$ Hz, $\text{FH}\beta$), 4.50 (d, 2H, $J = 6.2$ Hz, $\text{FH}\alpha$), 7.20-7.31 (m, 6H, FH_4 , FH_5 , H_3), 7.37 (t, 2H, $J = 7.3$ Hz, FH_3), 7.71 (d, 2H, $J = 7.2$ Hz, FH_2), 8.09 (d, 2H, $J = 8.7$ Hz, H_2); δ_{C} (75 MHz, CDCl_3) 3.69, 10.21, 47.11, 54.66, 67.38, 119.93, 124.87, 126.96, 127.33, 127.66, 127.69, 131.07, 141.35, 143.69, 146.94, 155.01, 171.41; $\nu_{\text{max}}/\text{cm}^{-1}$ (solid state) = ~ 3013 (COOH), 1738 (CO), 1365 (C-N), 1217 (C-O); ESI-HRMS found m/z 412.1552 $[\text{M-H}]^- \text{C}_{26}\text{H}_{22}\text{NO}_4$ requires 412.1554.

4-((2-Methylbutyl)amino)benzoic acid **21c**

4-Aminobenzoic acid (3.00 g, 21.8 mmol), 2-methylbutyraldehyde (2.3 mL, 21.8 mmol) and picoline-borane complex (2.64 g, 24.7 mmol) were stirred at room temperature in methanol (60 mL) for 14 hours. The reaction mixture was then acidified with 1N hydrochloric acid ($\sim \text{pH } 4$) and extracted with ethyl acetate (2×100 mL). The combined organic layers were washed with brine (50 mL), dried over magnesium sulphate, filtered, concentrated and dried under high vacuum to yield the desired compound (4.51 g, 100%) as a colourless powder; R_{F} 0.22 (hexane – ethyl acetate 1-1); δ_{H} (300 MHz, MeOD) 0.96 (t, 3H, $J = 7.6$ Hz, $\text{H}\delta$), 0.98 (t, 3H, $J = 6.6$ Hz, $\text{H}\epsilon$), 1.22 (m, 1H, $\text{H}\gamma$), 1.54 (m, 1H, $\text{H}\gamma'$), 1.69 (m, 1H, $\text{H}\beta$), 2.93 (dd, 1H, $J_1 = 13.0$ Hz, $J_2 = 7.3$ Hz, $\text{H}\alpha$), 3.08 (dd, 1H, $J_1 = 13.0$ Hz, $J_2 = 6.3$ Hz, $\text{H}\alpha'$), 6.57 (d, 2H, $J = 8.9$ Hz, H_3), 7.78 (d, 2H, $J = 8.9$ Hz, H_2); δ_{C} (75 MHz, MeOD) 11.72, 17.77, 28.31, 35.60, 50.11, 111.89, 117.65, 132.78, 154.86, 170.89; $\nu_{\text{max}}/\text{cm}^{-1}$ (solid state) = 3375 – 3403 (NH), ~ 3000 (COOH), 1736 (C=O); ESI-HRMS found m/z 208.1325 $[\text{M+H}]^+ \text{C}_{12}\text{H}_{18}\text{NO}_2$ requires 208.1332.

4-(((9H-Fluoren-9-yl)methoxy)carbonyl)(2-methylbutyl)amino)benzoic acid **22c**

To a refluxing solution of **21c** (4.51 g, 21.8 mmol) in chloroform (50 mL) was added dropwise a solution of Fmoc-chloride (5.63 g, 24.0 mmol) in chloroform (10 mL). The reaction mixture was then stirred at reflux overnight and turned yellow. The solvents were evaporated, then the residue was purified by Flash column chromatography (*Stationary phase* : silica, 50 g; *Mobile phase* : hexane – ethyl acetate gradient). The resulting solid was then crystallised (diethyl ether – hexane) to yield pure target material (5.42 g, 58%) as colourless crystals; R_{F} 0.48

(40% hexane in ethyl acetate); δ_{H} (300 MHz, CDCl_3) 0.68 (d, 3H, $J = 6.3$ Hz, H ϵ), 0.71 (t, 3H, $J = 7.3$ Hz, H δ), 0.93 (m, 1H, H γ), 1.21 (m, 1H, H γ'), 1.36 (m, 1H, H β), 3.44 (m, 2H, H α), 4.05 (t, 1H, $J = 5.8$ Hz, FH β), 4.47 (d, 2H, $J = 5.8$ Hz, FH α), 7.08 (d, 2H, $J = 8.5$ Hz, H3), 7.16 (t, 2H, $J = 7.5$ Hz, FH4), 7.25 (d, 2H, $J = 7.5$ Hz, FH5), 7.30 (t, 2H, $J = 7.5$ Hz, FH3), 7.65 (d, 2H, $J = 7.5$ Hz, FH2), 7.97 (d, 2H, $J = 8.5$ Hz, H2); δ_{C} (125 MHz, CDCl_3) 11.04, 16.57, 26.60, 33.49, 47.27, 55.49, 67.14, 119.92, 124.78, 124.79, 126.96, 126.98, 127.65, 131.00, 141.41, 143.71, 146.88, 155.25, 171.10; $\nu_{\text{max}}/\text{cm}^{-1}$ (solid state) = ~ 3000 (COOH), 1712 (C=O); ESI-MS found m/z 452.0 [M+Na] $^+$; ESI-HRMS found m/z 430.2009 [M+H] $^+$ $\text{C}_{27}\text{H}_{28}\text{NO}_4$ requires 430.2013.

4-(Phenethylamino)benzoic acid **21e**

4-Aminobenzoic acid (5.84 g, 42.6 mmol), phenylacetaldehyde (5.0 mL, 42.6 mmol) and picoline-borane complex (5.02 g, 46.9 mmol) were stirred at room temperature in methanol (130 mL) for 14 hours. The solvent was removed under reduced pressure and the pH of the oily residue was adjusted to 4 by addition of 1N HCl and the mixture was placed in an ice bath to afford the target compound as off-white crystals (6.79 g, 66%); R_{F} 0.48 (hexane – ethyl acetate 1-1); m.p. 128-130 °C; (Found: C, 74.35; H, 6.30; N, 5.65%; $\text{C}_{15}\text{H}_{15}\text{NO}_2$ requires: C, 74.67; H, 6.27; N, 5.81%); δ_{H} (300 MHz, CDCl_3) 2.96 (t, 2H, $J = 6.9$ Hz, H β), 3.50 (t, 2H, $J = 6.9$ Hz, H α), 6.60 (d, 2H, $J = 8.7$ Hz, H3), 7.23-7.31 (m, 3H, HAr3, HAr4), 7.34-7.38 (m, 2H, HAr2), 7.95 (d, 2H, $J = 8.7$ Hz, H2); δ_{C} (75 MHz, CDCl_3) 35.23, 44.34, 111.61, 117.42, 126.68, 128.75, 132.39, 138.66, 152.30, 172.19 (missing 1 ^{13}C resonance); $\nu_{\text{max}}/\text{cm}^{-1}$ (solid state) = 3378 (NH), ~ 3028 (COOH), 1739 (CO), 1365 (C-N), 1217 (C-O); ESI-HRMS found m/z 242.1172 [M+H] $^+$ $\text{C}_{15}\text{H}_{16}\text{NO}_2$ requires 242.1176.

4-((((9H-Fluoren-9-yl)methoxy)carbonyl)phenethylamino)benzoic acid **22e**

To a refluxing solution of 4-(benzylmethylamino)benzoic acid **21e** (2.29 g, 9.5 mmol) in chloroform (30 mL) was added dropwise a solution of Fmoc-chloride (2.58 g, 9.9 mmol) in chloroform (10 mL). The reaction mixture was then stirred at reflux overnight. The solvents were evaporated, then the residue was crystallised from neat methanol to yield the pure target material (1.22 g, 28%) as colourless crystals; R_{F} 0.32 (hexane – ethyl acetate 1-1); (Found: C, 77.45; H, 5.45;

N, 3.00%; C₃₀H₂₅NO₄ requires: C, 77.74; H, 5.44; N, 3.02%); δ_{H} (300 MHz, MeOD) 2.62 (t, 2H, $J = 6.7$ Hz, H β), 3.73 (t, 2H, $J = 6.7$ Hz, H α), 4.14 (t, 1H, $J = 5.1$ Hz, FH β), 4.63 (d, 2H, $J = 5.1$ Hz, FH α), 6.92-6.98 (m, 4H, H₃, HAr₂), 7.15-7.24 (m, 3H, HAr₃, HAr₄), 7.27 (t, 2H, $J = 7.5$ Hz, FH₄), 7.38 (t, 2H, $J = 7.4$ Hz, FH₃), 7.43 (d, 2H, $J = 7.4$ Hz, FH₅), 7.76 (d, 2H, $J = 7.4$ Hz, FH₂), 7.86 (d, 2H, $J = 8.6$ Hz, H₂); δ_{C} (75 MHz, MeOD) 33.80, 46.68, 50.89, 66.28, 120.04, 124.77, 126.20, 126.27, 126.94, 127.53, 128.02, 128.27, 128.61, 129.80, 138.23, 140.84, 143.66, 145.39, 153.95, 166.74; $\nu_{\text{max}}/\text{cm}^{-1}$ (solid state) = ~3005 (COOH), 1738 (CO), 1365 (C-N), 1217 (C-O); ESI-HRMS found m/z 462.1728 [M-H]⁻ C₃₀H₂₄NO₄ requires 462.1711.

4-((4-Chlorobenzyl)amino)benzoic acid **21f**

4-Aminobenzoic acid (2.00 g, 14.6 mmol), 4-chlorobenzaldehyde (2.10 g, 14.6 mmol) and picoline-borane complex (1.87 g, 17.5 mmol) were stirred at room temperature in methanol (20 mL) for 14 hours. A white precipitate formed. The reaction mixture was filtered, and the precipitate was dried under high vacuum to yield the desired compound (3.03 g, 70%) as colourless crystals; R_{F} 0.35 (ethyl acetate – hexane 1-1); m.p. 214-216 °C; (Found: C, 64.25; H, 4.60; N, 5.20%; C₁₄H₁₂ClNO₂ requires: C, 64.25; H, 4.62; N, 5.35%); δ_{H} (300 MHz, MeOD) 4.28 (s, 2H, H α), 6.49 (d, 2H, $J = 9.0$ Hz, H₃), 7.20-7.26 (m, 4H, HAr₂-HAr₃), 7.66 (d, 2H, $J = 9.0$ Hz, H₂); δ_{C} (75 MHz, CDCl₃) 47.34, 112.77, 118.98, 129.88, 130.06, 132.99, 133.96, 139.93, 154.44, 170.99; $\nu_{\text{max}}/\text{cm}^{-1}$ (solid state) = 3426 (NH), ~3000 (COOH), 1738 (CO); ESI-HRMS found m/z 262.0633 [M+H]⁺ C₁₄H₁₃ClNO₂ requires 262.0629.

4-(((9H-Fluoren-9-yl)methoxy)carbonyl)(4-chlorobenzyl)amino)benzoic acid **22f**

To a refluxing solution of 4-(chlorobenzyl)aminobenzoic acid **21f** (1.66 g, 6.4 mmol) in tetrahydrofuran (15 mL) was added dropwise a solution of Fmoc-chloride (1.81 g, 7.0 mmol) in tetrahydrofuran (5 mL). The reaction mixture was then stirred at reflux overnight. The solvents were evaporated, then the target material was precipitated from tetrahydrofuran – hexane to yield a white amorphous solid (2.90 g, 94%); R_{F} 0.45 (7% methanol in dichloromethane); δ_{H} (300 MHz, MeOD) 4.13 (t, 1H, $J = 4.9$ Hz, FH β), 4.67 (d, 2H, $J = 4.9$ Hz, FH α), 4.69 (s, 2H, H α), 6.90–6.95 (m, 4H, H₃ and HAr₂), 7.18–7.26 (m, 4H, HAr₃ and FH₄),

7.34 (t, 2H, $J = 7.5$ Hz, FH3), 7.38 (d, 2H, $J = 7.5$ Hz, FH5), 7.74 (d, 2H, $J = 7.5$ Hz, FH2), 7.82 (d, 2H, $J = 8.5$ Hz, H2); δ_c (75 MHz, MeOD) 48.58, 53.71, 68.18, 120.96, 125.80, 127.75, 128.10, 128.74, 129.61, 129.80, 130.27, 131.45, 134.19, 137.43, 142.79, 145.04, 146.63, 156.69, 169.05; $\nu_{\max}/\text{cm}^{-1}$ (solid state) = ~ 3010 (COOH), 1739 (CO), 1365 (C-N), 1216 (C-O); ESI-HRMS found m/z 482.1167 [M-H]⁻ C₂₉H₂₁ClNO₄ requires 482.1165.

4-((4-Fluorobenzyl)amino)benzoic acid **21g**

4-Aminobenzoic acid (3.83 g, 27.9 mmol), 4-fluorobenzaldehyde (3.0 mL, 27.9 mmol) and picoline-borane complex (3.58 g, 33.5 mmol) were stirred at room temperature in methanol (90 mL) for 14 hours. A white precipitate formed. The reaction mixture was filtered, and the filtrate acidified (\sim pH 4) with 1N hydrochloric acid to induce further precipitation. The combined precipitates were dried under high vacuum to yield the desired compound (4.98 g, 73%) as a colourless powder; R_F 0.30 (5% methanol in dichloromethane); (Found: C, 68.30; H, 4.90; N, 5.65%; C₁₄H₁₂FNO₂ requires: C, 68.56; H, 4.93; N, 5.71%); δ_H (300 MHz, DMSO-d₆) 4.32 (d, 2H, $J = 6.0$ Hz, H α), 6.59 (d, 2H, $J = 8.9$ Hz, H3), 7.06 (t, 1H, $J = 6.0$ Hz, NH), 7.12-7.19 (m, 2H, HAr2), 7.34-7.41 (m, 2H, HAr3), 7.64 (d, 2H, $J = 8.9$ Hz, H2); δ_c (75 MHz, DMSO-d₆) 45.05, 111.15, 114.92, 115.20, 117.21, 128.97, 131.04, 135.51, 152.21, 167.41; $\nu_{\max}/\text{cm}^{-1}$ (solid state) = 3426 (NH), ~ 3015 (COOH), 1736 (CO), 1365, 1216; ESI-HRMS found m/z 244.0771 [M-H]⁻ C₁₄H₁₁FNO₂ requires 244.0779.

4-(((9H-Fluoren-9-yl)methoxy)carbonyl)(4-fluorobenzyl)amino)benzoic acid **22g**

To a refluxing solution of 4-(fluorobenzyl)aminobenzoic acid **21g** (4.04 g, 16.3 mmol) in tetrahydrofuran (50 mL) was added dropwise a solution of Fmoc-chloride (4.44 g, 17.2 mmol) in tetrahydrofuran (10 mL). The reaction mixture was then stirred at reflux overnight. The solvents were evaporated, then the residue was purified by column chromatography (*Stationary phase*: silica, *Mobile phase*: 1% to 10% methanol in dichloromethane). The product was then crystallised from dichloromethane-hexane to yield pure target material (7.00 g, 92%) as colourless crystals; R_F 0.45 (10% methanol in dichloromethane); m.p. 142-143 °C; δ_H (300 MHz, CDCl₃) 4.04 (t, 1H, $J = 6.2$ Hz, FH β), 4.52 (d, 2H, $J = 6.2$

Hz, FH α), 4.69 (s, 2H, H α), 6.85 (t, 2H, J = 8.7 Hz, HAr2), 6.92 (d, 2H, J = 8.6 Hz, H3), 6.96 (t, 2H, J = 7.7 Hz, HAr3), 7.14 (t, 2H, J = 7.4 Hz, FH3), 7.22 (d, 2H, J = 7.4 Hz, FH4), 7.29 (t, 2H, J = 7.4 Hz, FH2), 7.63 (d, 2H, J = 7.4 Hz, FH1), 7.91 (d, 2H, J = 8.6 Hz, H2); δ_c (75 MHz, CDCl₃) 47.16, 53.08, 67.48, 115.34, 115.63, 119.97, 124.76, 126.69, 127.01, 127.71, 129.35, 129.46, 131.05, 132.81, 141.37, 143.51, 146.35, 155.05, 171.01; $\nu_{\max}/\text{cm}^{-1}$ (solid state) = ~3067 (COOH), 1681 (CO), 1272); ESI-HRMS found m/z 466.1469 [M-H]⁻ C₂₉H₂₁FNO₄ requires 466.1460.

4-((3-(Trifluoromethyl)benzyl)amino)benzoic acid **21h**

4-Aminobenzoic acid (3.00 g, 21.9 mmol), 3-trifluoromethylbenzaldehyde (3.00 mL, 21.9 mmol) and picoline-borane complex (2.57 g, 24.1 mmol) were stirred at room temperature in methanol (20 mL) for 14 hours. A white precipitate formed. The reaction mixture was filtered, and the filtrate acidified with 1N hydrochloric (~15 mL) acid to induce further precipitation. The combined precipitates were dried under high vacuum to yield the desired compound (4.41 g, 68%) as a colourless powder; R_f 0.43 (ethyl acetate – hexane 1-1); δ_H (500 MHz, CDCl₃) 4.48 (s, 2H, H α), 6.61 (d, 2H, J = 8.7 Hz, H3), 7.52-7.58 (m, 2H, HAr5-HAr6), 7.66 (d, 1H, J = 7.5 Hz, HAr4), 7.71 (s, 1H, HAr2), 7.79 (d, 2H, J = 8.7 Hz, H2); δ_c (75 MHz, CDCl₃) 47.67, 112.94, 119.39, 121.60, 125.14, 125.19, 130.71, 132.30, 132.70 (q), 133.11, 142.82, 154.43, 171.02; $\nu_{\max}/\text{cm}^{-1}$ (solid state) = 3458 (NH), ~3000 (COOH), 1670 (CO), 1100-1275 (CF₃); ESI-MS m/z 296 [M+H]⁺; ESI-HRMS found m/z 294.0755 [M-H]⁻ C₁₅H₁₁F₃NO₂ requires 294.0747.

4-(((9H-Fluoren-9-yl)methoxy)carbonyl)(3-(trifluoromethyl)benzyl)amino)benzoic acid **22h**

To a refluxing solution of **21h** (0.79 g, 2.7 mmol) in tetrahydrofuran (4 mL) was added dropwise a solution of Fmoc-Cl (0.77 g, 2.9 mmol) in tetrahydrofuran (4 mL). The reaction mixture was stirred at reflux for 14 hours. The solvents were evaporated and the residue was crystallised (tetrahydrofuran – hexane) to yield the target compound (0.40 g, 27%) as colourless crystals; R_f 0.29 (2% methanol in dichloromethane); δ_H (500 MHz, CDCl₃) 4.11 (t, 1H, J = 5.6 Hz, FH β), 4.60 (d, 2H, J = 5.6 Hz, FH α), 4.84 (s, 2H, H α), 7.05 (d, 2H, J = 8.9 Hz, H3), 7.20 (t, 2H, J = 7.5 Hz, FH4), 7.22-7.28 (m, 3H, ArCH), 7.32-7.37 (m, 4H, ArCH), 7.49 (d, 1H, J = 8.0 Hz, HAr4), 7.68 (d, 2H, J = 7.5 Hz, FH2), 7.97 (d, 2H, J = 8.9 Hz, H2); δ_c (75 MHz, CDCl₃)

47.53, 53.75, 68.07, 120.38, 124.67, 124.89, 125.11, 126.81, 127.43, 127.69, 128.15, 129.60, 131.20, 131.31 (q), 131.55, 138.54, 141.76, 143.85, 146.64, 155.49, 171.66 (missing 1 ^{13}C resonance); $\nu_{\text{max}}/\text{cm}^{-1}$ (solid state) = ~ 3000 (COOH), 1690 (CO), 1120-1280 (CF_3); ESI-MS m/z 540 $[\text{M}+\text{Na}]^+$; ESI-HRMS found m/z 516.1450 $[\text{M}-\text{H}]^-$ $\text{C}_{30}\text{H}_{21}\text{F}_3\text{NO}_4$ requires 516.1428.

4-(4-Methylthiobenzylamino)benzoic acid **21k**

4-Aminobenzoic acid (0.79 g, 5.7 mmol), 4-methylthiobenzaldehyde (1.0 mL, 5.7 mmol) and picoline-borane complex (0.67 g, 6.31 mmol) were stirred at room temperature in methanol (20 mL) for 14 hours. The solvent was evaporated to 10 mL and the resulting mixture was acidified ($\sim\text{pH}$ 4) with 1N hydrochloric acid then left to crystallise to yield the desired compound (1.24 g, 79%) as white crystals; R_{F} 0.37 (40% hexane in ethyl acetate); m.p. 191-193 $^{\circ}\text{C}$; (Found: C, 65.60; H, 5.55; N, 5.10%; $\text{C}_{15}\text{H}_{15}\text{NO}_2\text{S}$ requires: C, 65.91; H, 5.53; N, 5.12%); δ_{H} (300 MHz, $\text{DMSO}-d_6$) 2.44 (s, 3H, SMe), 4.29 (d, 2H, $J = 6.2$ Hz, $\text{H}\alpha$), 6.58 (d, 2H, $J = 8.7$ Hz, H3), 7.05 (t, 1H, $J = 6.2$ Hz, NH), 7.22 (d, 2H, $J = 8.3$ Hz, HAr2), 7.29 (d, 2H, $J = 8.3$ Hz, HAr3), 7.65 (d, 2H, $J = 8.7$ Hz, H2); δ_{C} (75 MHz, $\text{DMSO}-d_6$) 14.81, 45.33, 111.15, 117.12, 126.07, 127.80, 131.03, 136.13, 136.26, 152.27, 167.42; $\nu_{\text{max}}/\text{cm}^{-1}$ (solid state) = 3356 (NH), ~ 3016 (COOH), 1737 (CO), 1365 (C-N), 1216 (C-O); ESI-HRMS found m/z 272.0747 $[\text{M}-\text{H}]^-$ $\text{C}_{15}\text{H}_{14}\text{NO}_2\text{S}$ requires 272.0751.

4-(((9H-Fluoren-9-yl)methoxy)carbonyl)(4-methylthiobenzylamino)benzoic acid **22k**

To a refluxing suspension of 4-(methylthiobenzylamino)benzoic acid **21k** (1.10 g, 4.0 mmol) in chloroform (12 mL) was added dropwise a solution of Fmoc-chloride (1.10 g, 4.2 mmol) in chloroform (5 mL). The reaction mixture was then stirred at reflux overnight. The solvent was removed under reduced pressure and the residue was precipitated from dichloromethane – hexane to afford the title compound as an off-white amorphous solid (1.13 g, 60%); R_{F} 0.25 (ethyl acetate – hexane 1-1); δ_{H} (300 MHz, $\text{DMSO}-d_6$) 2.42 (s, 3H, MeS), 4.00 (t, 1H, $J = 5.6$ Hz, FH β), 4.52 (d, 2H, $J = 5.6$ Hz, FH α), 4.86 (s, 2H, H α), 6.90 (d, 2H, $J = 8.4$ Hz, H3), 7.05-7.13 (m, 4H, HAr2, HAr3), 7.27 (t, 2H, $J = 7.5$ Hz, FH4), 7.37-7.45 (m, 4H, FH3, FH5), 7.73 (d, 2H, $J = 8.4$ Hz, H2), 7.88 (d, 2H, $J = 7.4$ Hz, FH2); δ_{C} (75 MHz, $\text{DMSO}-d_6$) 14.51, 46.72, 53.82, 66.57, 120.03, 124.88, 125.76, 126.14, 126.93, 127.54,

127.82, 129.72, 131.45, 133.77, 136.83, 140.85, 143.58, 149.76, 166.65, 171.86; $\nu_{\text{max}}/\text{cm}^{-1}$ (solid state) = ~3016 (COOH), 1738 (CO), 1365 (C-N), 1217 (C-O); ESI-HRMS found m/z 518.1390 $[\text{M}+\text{Na}]^+$ $\text{C}_{30}\text{H}_{25}\text{NaNO}_4\text{S}$ requires 518.1397.

4-(4-*tert*-Butoxybenzylamino)benzoic acid **211**

4-Aminobenzoic acid (0.77 g, 5.6 mmol), 4-*tert*-butoxybenzaldehyde (1.00 g, 5.6 mmol) and picoline-borane complex (0.69 g, 6.2 mmol) were stirred at room temperature in methanol (20 mL) for 14 hours. A white precipitate formed. The reaction mixture was filtered, and the filtrate acidified with 1N hydrochloric acid (~15 mL) to induce further precipitation. The combined precipitates were dried under high vacuum to yield the desired compound (1.14 g, 68%) as a colourless powder; R_F 0.37 (40% hexane in ethyl acetate); (Found: C, 71.90; H, 7.10; N, 4.70%; $\text{C}_{18}\text{H}_{21}\text{NO}_3$ requires: C, 72.22; H, 7.07; N, 4.68%); δ_{H} (300 MHz, DMSO- d_6) 1.27 (s, 9H, *t*Bu), 4.27 (d, 2H, $J = 5.2$ Hz, H α), 6.60 (d, 2H, $J = 9.0$ Hz, H3), 6.93 (d, 2H, $J = 8.4$ Hz, HAr2), 6.99 (t, 1H, $J = 5.2$ Hz, NH), 7.25 (d, 2H, $J = 8.4$ Hz, HAr3), 7.64 (d, 2H, $J = 9.0$ Hz, H2); δ_{C} (75 MHz, CDCl_3) 29.25, 47.62, 79.07, 112.01, 117.97, 124.89, 128.55, 132.77, 133.35, 152.84, 155.23, 172.85; $\nu_{\text{max}}/\text{cm}^{-1}$ (solid state) = 3427 (NH), ~2969 (COOH), 1736 (CO); ESI-MS m/z 322.1 $[\text{M}+\text{Na}]^+$; ESI-HRMS found m/z 322.1420 $[\text{M}+\text{Na}]^+$ $\text{C}_{18}\text{H}_{20}\text{NaNO}_3$ requires 322.1414.

4-(((9H-Fluoren-9-yl)methoxy)carbonyl)(4-*tert*-butoxybenzylamino)benzoic acid **221**

To a refluxing suspension of 4-(*tert*-butoxybenzylamino)benzoic acid **211** (1.12 g, 3.7 mmol) and sodium bicarbonate (0.47 g, excess) in tetrahydrofuran (15 mL) was added dropwise a solution of Fmoc-chloride (1.06 g, 4.1 mmol) in tetrahydrofuran (5 mL). The reaction mixture was then stirred at reflux overnight. The solvents were evaporated and the product was then purified by Flash column chromatography (ethyl acetate – hexane gradient) to yield pure target material (1.10 g, 57%) as a white amorphous solid; R_F 0.27 (ethyl acetate – hexane 1-1); δ_{H} (500 MHz, MeOD) 1.32 (s, 9H, *t*Bu), 4.16 (t, 1H, $J = 5.0$ Hz, FH β), 4.67 (d, 2H, $J = 5.0$ Hz, FH α), 4.88 (s, 2H, H α), 6.85 (d, 2H, $J = 8.4$ Hz, HAr2), 6.91 (d, 2H, $J = 8.1$ Hz, HAr3), 6.94 (d, 2H, $J = 7.6$ Hz, H3), 7.25 (t, 2H, $J = 7.5$ Hz, FH4), 7.37 (t, 2H, $J = 7.2$ Hz, FH3), 7.42 (d, 2H, $J = 7.2$ Hz, FH5), 7.76 (d, 2H, $J = 7.4$ Hz, FH2), 7.83 (d, 2H, $J = 7.6$ Hz, H2); δ_{C} (75 MHz, MeOD) 26.17, 48.57, 53.97, 68.22,

81.66, 120.94, 125.17, 125.84, 128.00, 128.09, 128.73, 129.52, 129.77, 131.37, 133.65, 142.78, 145.08, 155.88, 156.78, 169.12 (missing 1 ^{13}C resonance); $\nu_{\text{max}}/\text{cm}^{-1}$ (solid state) = \sim 3004 (COOH), 1736 (CO), 1365 (C-N), 1216 (C-O); ESI-HRMS found m/z 544.2092 $[\text{M}+\text{Na}]^+$ $\text{C}_{33}\text{H}_{31}\text{NaNO}_5$ requires 544.2094.

4-(2-*tert*-Butoxy-2-oxoethylamino)benzoic acid **21n**

tert-Butyl-2-(nitrooxy)acetate **24**: To stirred a solution of *tert*-butylbromoacetate (1.51 mL, 8.8 mmol) in dry acetonitrile (20 mL), under a N_2 atmosphere, was added silver nitrate (3.00 g, 11.6 mmol). The solution was stirred in the dark at room temperature for 72 h. The reaction mixture was filtered, concentrated and extracted between Et_2O (3 x 50 mL) and water (50 mL). The combined organic fractions were dried (Na_2SO_4) and concentrated and target material isolated (1.26 g, 7.0 mmol, 80%) as a colourless oil.

tert-Butyl-2-oxoacetate **25**: To a stirred solution of *tert*-butoxycarbonylmethyl nitrate (1.16 g, 6.5 mmol) in anhydrous dimethylsulfoxide (20 mL), under N_2 , was added sodium acetate (0.54 g, 6.6 mmol). The reaction mixture was stirred at room temperature for 30 min. The reaction mixture was then poured into brine (150 mL) and extracted with CH_2Cl_2 (6 x 50 mL). The combined organic fractions were washed with saturated NaHCO_3 (100 mL) and brine (100 mL), dried (Na_2SO_4) and concentrated and crude target material isolated as a yellow oil. The resultant crude product was taken directly and immediately onto the next step without purification.

4-Aminobenzoic acid (0.75 g, 5.5 mmol) and *tert*-butyl 2-oxoacetate (0.72 g, 5.5 mmol) were stirred in methanol (30 mL) at room temperature for 2 h, prior to addition of picoline-borane complex (0.85 g, 7.9 mmol) and left to stir overnight. The reaction mixture was concentrated and target material precipitated from methanol/water. Target material was isolated (0.69 g, 2.7 mmol, 49%) as a pale cream crystalline solid; m.p. 176-177 $^\circ\text{C}$; R_{F} 0.25 (20% Et_2O in dichloromethane); δ_{H} (300 MHz, MeOD) 1.48 (s, 9H, *t*Bu), 3.88 (s, 2H, CH_2), 6.60 (d, 2H, $J = 9.1$ Hz, ArCH), 7.82 (d, 2H, $J = 9.2$ Hz, ArCH); δ_{C} (75 MHz, MeOD) 28.7, 46.9, 83.2, 112.9, 119.8, 133.1, 154.2, 171.0, 172.3; $\nu_{\text{max}}/\text{cm}^{-1}$ (solid state) = 3406 (NH), \sim 2900 (COOH), 1731, 1668 (CO); HRMS calculated for $\text{C}_{13}\text{H}_{18}\text{NO}_4$ $[\text{M}+\text{H}]^+$ 252.1230, found 252.1231; ESI-HRMS found m/z 274.1051 $[\text{M}+\text{Na}]^+$ $\text{C}_{13}\text{H}_{17}\text{NNaO}_4$ 274.1050.

4-(((9H-Fluoren-9-yl)methoxy)carbonyl)(2-*tert*-butoxy-2-oxoethyl)amino)benzoic acid 22n

To a refluxing solution of 4-(2-*tert*-butoxy-2-oxoethylamino)benzoic acid (0.50 g, 1.6 mmol) and sodium hydrogencarbonate (0.67 g, excess) in chloroform (20 mL) was added dropwise a solution of Fmoc chloride (0.62 g, 2.4 mmol) in chloroform (20 mL) over 2 h. The reaction mixture was then stirred at reflux for a further 20 h. Excess sodium hydrogencarbonate was filtered off and column chromatography (*Stationary Phase*: Silica, 100 g; *Mobile Phase*: dichloromethane to 20% diethyl ether in dichloromethane) yielded pure target material (0.41 g, 0.9 mmol, 54%) as an amorphous solid; m.p. 76-77 °C; R_F 0.22 (20% diethyl ether in dichloromethane); δ_H (500 MHz, $CDCl_3$) 1.46 (s, 9H, *t*Bu), 4.16 (broad s, 1H, FH β), 4.27 (broad s, 2H, H α), 4.50 (d, 2H, $J = 6.7$ Hz, FH α), 7.23-7.37 (m, 8H, ArCH), 7.72 (d, 2H, $J = 8.1$ Hz, ArCH), 8.07 (d, 2H, $J = 8.4$ Hz, ArCH); δ_C (75 MHz, $CDCl_3$) 28.0, 47.0, 52.4, 68.1, 82.4, 120.0, 124.9, 126.4, 127.0, 127.7, 131.1, 132.4, 141.3, 143.5, 146.8, 154.8, 168.2, 169.4; ν_{max}/cm^{-1} (solid state) = ~3000 (broad, COOH), 1736, 1715, 1690, 1605 (CO); ESI-HRMS found m/z 474.1924 [M+H]⁺ C₂₈H₂₈NO₆ requires 474.1911, found m/z 491.2190 [M+NH₄]⁺ C₂₈H₃₁N₂O₆ requires 491.2177, found m/z 496.1721 [M+Na]⁺ C₂₈H₂₇NNaO₆ requires 496.1731.

4-(3-Fluorobenzylamino)benzoic acid 21o

4-Aminobenzoic acid (3.88 g, 28.3 mmol), 3-fluorobenzaldehyde (3.0 mL, 28.3 mmol) and picoline-borane complex (3.33 g, 31.1 mmol) were stirred at room temperature in methanol (90 mL) for 14 hours. A white precipitate formed. The reaction mixture was filtered, and the filtrate acidified (~pH 4) with 1N hydrochloric acid then left to crystallise to yield the desired compound (4.10 g, 59%) as colourless crystals; R_F 0.37 (40% hexane in ethyl acetate); m.p. 170-172 °C; (Found: C, 68.20; H, 4.95; N, 5.75%; C₁₄H₁₂FNO₂ requires: C, 68.56; H, 4.93; N, 5.71%); δ_H (300 MHz, DMSO-*d*₆) 4.36 (d, 2H, $J = 6.1$ Hz, H α), 6.59 (d, 2H, $J = 8.9$ Hz, H₃), 7.03-7.20 (m, 4H, NH, HAr₂, HAr₃, HAr₅), 7.34-7.41 (m, 1H, HAr₄), 7.66 (d, 2H, $J = 8.9$ Hz, H₂); δ_C (75 MHz, DMSO-*d*₆) 45.05 (CH₂), 111.15 (ArC-H₃), 114.92 (ArC-HAr₄), 115.20 (ArC-HAr₂), 117.21 (ArC-HAr₆), 128.97 (ArC-HAr₅), 131.04 (ArC-H₂), 135.51 (ArC-COOH), 152.21 (ArC-F), 159.52 (ArC-CH₂), 160.73

(ArC-NH), 167.41 (COOH); $\nu_{\max}/\text{cm}^{-1}$ (solid state) = 3427 (NH), \sim 3002 (COOH), 1736 (CO), 1365 (C-N), 1216 (C-O); ESI-HRMS found m/z 244.0788 [M-H]⁻ C₁₄H₁₁FNO₂ requires 244.0779.

4-(((9H-Fluoren-9-yl)methoxy)carbonyl)(3-fluorobenzylamino)benzoic acid 22o

To a refluxing solution of 3-(fluorobenzylamino)benzoic acid **21o** (2.61 g, 10.6 mmol) in tetrahydrofuran (40 mL) was added dropwise a solution of Fmoc-chloride (2.89 g, 11.2 mmol) in tetrahydrofuran (10 mL). The reaction mixture was then stirred at reflux overnight. The solvents were evaporated, then the residue was purified by column chromatography (*Stationary phase*: silica, *Mobile phase*: dichloromethane–hexane 1-1 then neat dichloromethane then 3% methanol in dichloromethane) to afford the target material as a white solid (3.41 g, 69%); R_F 0.45 (7% methanol in dichloromethane); (Found: C, 73.75; H, 4.75; N, 2.95%; C₂₉H₂₂FNO₄ requires: C, 74.51; H, 4.74; N, 3.00%); δ_H (300 MHz, CDCl₃) 4.12 (t, 1H, J = 5.8 Hz, FH β), 4.60 (d, 2H, J = 5.8 Hz, FH α), 4.80 (s, 2H, H α), 6.84 (m, 2H, HAr₄, HAr₆), 6.93 (m, 1H, HAr₅), 7.07 (d, 2H, J = 8.6 Hz, H₃), 7.18–7.24 (m, 3H, HAr₂, FH₄), 7.29 (d, 2H, J = 7.2 Hz, FH₅), 7.36 (t, 2H, J = 7.5 Hz, FH₃), 7.70 (d, 2H, J = 7.5 Hz, FH₂), 7.98 (d, 2H, J = 8.6 Hz, H₂); δ_C (125 MHz, CDCl₃) 47.17 (CH-CH₂), 53.29 (CH₂), 67.63 (CH₂-CH), 114.45 (ArC-HAr₄), 114.62 (ArC-HAr₂), 119.97 (ArC-FH₂), 124.74 (ArC-H₃), 126.38 (ArC-HAr₆), 127.04 (ArC-FH₃), 127.74 (ArC-FH₅), 130.14 (ArC-FH₄), 130.21 (ArC-COOH), 131.07 (ArC-HAr₅), 139.70 (ArC-H₂), 141.38 (ArC-F₁), 143.50 (ArC-F₆), 146.42 (ArC-CH₂), 160.07 (ArC-N), 161.95 (COO-N), 163.91 (ArC-F), 171.07 (COOH); $\nu_{\max}/\text{cm}^{-1}$ (solid state) = \sim 3016 (COOH), 1739 (CO), 1365 (C-N), 1216 (C-O); ESI-HRMS found m/z 466.1476 [M-H]⁻ C₂₉H₂₂FNO₄ requires 466.1460.

4-((4-(Trifluoromethyl)benzyl)amino)benzoic acid 21p

4-Aminobenzoic acid (3.00 g, 21.9 mmol), 4-trifluoromethylbenzaldehyde (3.00 mL, 21.9 mmol) and picoline-borane complex (2.57 g, 24.1 mmol) were stirred at room temperature in methanol (20 mL) for 14 hours. A white precipitate formed. The reaction mixture was filtered, and the filtrate acidified with 1N hydrochloric acid (\sim 15 mL) to induce further precipitation. The combined precipitates were dried under high vacuum to yield the desired compound (3.91 g, 61%) as a

colourless powder; R_F 0.40 (10% methanol in dichloromethane); m.p. 181-182 °C; δ_H (500 MHz, $CDCl_3$) 4.51 (s, 2H, $H\alpha$), 6.49 (d, 2H, $J = 9.1$ Hz, H3), 7.47 (d, 2H, $J = 7.5$ Hz, HAr2), 7.63 (d, 2H, $J = 7.5$ Hz, HAr3), 7.92 (d, 2H, $J = 9.1$ Hz, H2); δ_C (125 MHz, $CDCl_3$) 50.19 (CH_2), 115.46 (ArC-H3), 121.82 (ArC-COOH), 129.32 (ArC-HAr3), 130.51 (ArC-HAr2), 131.55 (ArC-CF₃), 133.14 (q, CF₃), 135.69 (ArC-H2), 148.53 (ArC-CH₂), 156.98 (ArC-NH), 173.62 (COOH); ν_{max}/cm^{-1} (solid state) = 3414 (NH), ~3000 (COOH), 1690 (CO), 1120-1180 (CF₃); ESI-MS m/z 296 $[M+H]^+$; ESI-HRMS found m/z 294.0755 $[M-H]^-$ C₁₅H₁₁F₃NO₂ requires 294.0747.

4-(((9H-Fluoren-9-yl)methoxy)carbonyl)(4-(trifluoromethyl)benzyl)amino)benzoic acid 22p

To a refluxing solution of **21p** (3.91 g, 13.3 mmol) in tetrahydrofuran (60 mL) was added dropwise a solution of Fmoc-Cl (3.78 g, 14.7 mmol) in tetrahydrofuran (20 mL). The reaction mixture was stirred at reflux for 14 hours. The solvents were evaporated and the residue was crystallised (tetrahydrofuran - dichloromethane) to yield the target compound (6.50 g, 91%) as yellow crystals; R_F 0.37 (ethyl acetate - hexane 1-1); m.p. 144-145 °C; (Found: C, 69.3; H, 4.3; N, 2.6; C₃₀H₂₂F₃NO₄ requires: C, 69.6; H, 4.2; N, 2.7%); δ_H (500 MHz, $CDCl_3$) 4.11 (t, 1H, $J = 5.1$ Hz, FH β), 4.64 (d, 2H, $J = 5.1$ Hz, FH α), 4.82 (s, 2H, $H\alpha$), 7.06 (d, 2H, $J = 8.4$ Hz, H3), 7.14 (d, 2H, $J = 7.9$ Hz, HAr2/3), 7.21 (t, 2H, $J = 7.4$ Hz, FH4), 7.30 (d, 2H, $J = 7.4$ Hz, FH5), 7.37 (t, 2H, $J = 7.5$ Hz, FH3), 7.50 (d, 2H, $J = 7.9$ Hz, HAr3/2), 7.69 (d, 2H, $J = 7.5$, FH2), 7.97 (d, 2H, $J = 8.4$, H2); δ_C (125 MHz, $CDCl_3$) 47.58 ($\underline{C}H-CH_2$), 53.76 (CH_2), 67.92 ($\underline{C}H_2-CH$), 120.40 (ArC-FH2), 125.09 (ArC-H3), 126.00 (ArC-HAr3), 126.05 (ArC-FH3), 126.58 (ArC-COOH), 127.45 (ArC-FH5), 128.02 (ArC-FH4), 128.16 (ArC-HAr2), 129.95 (q, CF₃), 130.35 (ArC-CF₃), 131.54 (ArC-H2), 141.54 (ArC-CH₂), 141.79 (ArC-F6), 143.83 (ArC-F1), 146.75 (ArC-N), 155.42 (N $\underline{C}OO-CH_2$), 171.68 (COOH); ν_{max}/cm^{-1} (solid state) = ~3000 (COOH), 1710 (CO), 1230-1120 (CF₃); ESI-MS m/z 540 $[M+Na]^+$; ESI-HRMS found 516.1435 m/z $[M-H]^-$ C₃₀H₂₁F₃NO₄ requires 516.1428.

tert-butyl 5-methoxy-3-formyl-1H-indole-1-carboxylate 23q

To a stirred suspension of 5-methoxy-1H-indole-3-carboxaldehyde (0.50 g, 2.8 mmol) in dichloromethane (20 mL) was added Boc-anhydride (0.65 g, 3.0 mmol), followed by triethylamine (0.44 mL, 3.1 mmol). The resulting mixture was stirred

at room temperature under a nitrogen atmosphere for 40 hours. The solvent was evaporated to afford a brown oil from which the title compound was precipitated using methanol to afford a cream amorphous solid (0.57 g, 2.1 mmol, 72%); R_F 0.45 (ethyl acetate - hexane 1-1); δ_H (300 MHz, DMSO- d_6) 1.65 (s, 9H, tBu), 3.81 (s, 3H, OMe), 7.05 (dd, 1H, $J_1 = 9.1$ Hz, $J_2 = 2.6$ Hz, H7), 7.62 (d, 1H, $J = 2.6$ Hz, H4), 7.99 (d, 1H, $J = 9.1$ Hz, H6), 8.63 (s, 1H, H2), 10.05 (s, 1H, CHO); δ_C (75 MHz, DMSO- d_6) 27.49 (CH₃-C), 55.31 (O-CH₃), 85.40 (OC-CH₃), 103.45 (ArC-H4), 114.63 (ArC-H6), 115.80 (ArC-H7), 120.40 (ArC-CO), 126.51 (ArC-H2), 129.71 (ArC-C-CO), 138.55 (ArC-N), 148.25 (NCOO-*t*Bu), 156.68 (ArC-OCH₃), 187.11 (CO); ESI-HRMS found m/z 298.1036 [M+Na]⁺ C₁₅H₁₇NaNO₄ requires 298.1050.

4-(((5-Methoxy-1H-indol-3-yl)methyl)amino)benzoic acid 21q

4-Aminobenzoic acid (0.28 g, 2.1 mmol), **23q** (0.57 g, 2.1 mmol) and picolineborane complex (0.23 g, 2.2 mmol) were stirred at room temperature in methanol (10 mL) for 14 hours. The solvent was evaporated and the product was isolated by slow precipitation from chloroform - diethylether, then dried under high vacuum to yield the desired compound (0.62 g, 75%) as a colourless solid; R_F 0.27 (10% methanol in dichloromethane); δ_H (300 MHz, DMSO- d_6) 1.60 (s, 9H, tBu), 3.79 (s, 3H, OMe), 4.42 (d, 2H, $J = 5.7$ Hz, H α), 6.69 (d, 2H, $J = 8.8$ Hz, H3), 6.93 (dd, 1H, $J_1 = 8.8$ Hz, $J_2 = 2.7$ Hz, HAr7), 6.97 (t, 1H, $J = 5.7$ Hz, NH), 7.26 (d, 1H, $J = 2.5$ Hz, HAr4), 7.63 (s, 1H, HAr2), 7.67 (d, 2H, $J = 8.8$ Hz, H2), 7.90 (d, 1H, $J = 8.8$ Hz, HAr6); δ_C (75 MHz, DMSO- d_6) 27.65 (CH₃-C), 55.41 (CH₂), 64.89 (O-CH₃), 83.49 (C-CH₃), 102.53 (ArC-HAr4), 111.14 (ArC-H3), 112.98 (ArC-HAr6), 115.43 (ArC-CH₂), 117.12 (ArC-HAr7), 118.21 (ArC-COOH), 124.24 (ArC-HAr2), 129.44 (ArC-N), 130.19 (ArC-C-CH₂), 131.03 (ArC-H2), 148.97 (NCOO-*t*Bu), 152.33 (ArC-O), 155.40 (ArC-NH), 167.44 (COOH); ν_{max}/cm^{-1} (solid state) = 3381 (NH), ~3016 (COOH), 1738 (CO), 1365 (C-N), 1217 (C-O); ESI-MS m/z 419.5 [M+Na]⁺; ESI-HRMS found m/z 395.1598 [M-H]⁻ C₂₂H₂₃N₂O₅ requires 395.1612.

4-(((9H-Fluoren-9-yl)methoxy)carbonyl)(5-methoxy-1-(*tert*-butoxycarbonyl)-1H-indol-3-yl)methyl)amino)benzoic acid 22q

To a refluxing suspension of **21q** (0.50 g, 1.3 mmol) and NaHCO₃ (0.21 g, excess) in tetrahydrofuran (10 mL) was added dropwise a solution of Fmoc-Cl (0.33 g, 1.3 mmol) in tetrahydrofuran (3 mL). The reaction mixture was stirred at reflux for

1.5 hour. The excess bicarbonate was filtered then the solvent was evaporated and the product was isolated by slow precipitation from chloroform - diethylether (0.27 g, 34%) as a white solid; R_F 0.25 (ethyl acetate - hexane 1-1); δ_H (300 MHz, DMSO- d_6) 1.56 (s, 9H, *t*Bu), 3.67 (s, 3H, OMe), 4.19 (t, 1H, $J = 6.1$ Hz, FH β), 4.52 (d, 2H, $J = 6.1$ Hz, FH α), 4.96 (s, 2H, H α), 6.87 (d, 1H, $J = 2.2$ Hz, HAr4), 6.92 (dd, 1H, $J_1 = 8.8$ Hz, $J_2 = 2.5$ Hz, HAr6), 7.12 (d, 2H, $J = 8.2$ Hz, FH5), 7.15 (t, 2H, $J = 7.2$ Hz, FH4), 7.30-7.36 (m, 5H, FH3, H3, HAr2), 7.78 (d, 2H, $J = 8.2$ Hz, FH2), 7.79 (d, 2H, $J = 8.8$ Hz, H2), 7.86 (d, 1H, $J = 8.6$ Hz, HAr7); δ_C (75 MHz, DMSO- d_6) 27.58 ($\underline{C}H_3$ -C), 44.21 ($\underline{C}H_2$ -N), 46.45 ($\underline{C}H$ - $\underline{C}H_2$), 55.08 ($\underline{C}H_3$ -O), 67.05 ($\underline{C}H_2$ -CH), 83.69 (\underline{C} - $\underline{C}H_3$), 101.99 (ArC-HAr4), 113.16 (ArC-HAr6), 115.50 (ArC- $\underline{C}H_2$), 116.56 (ArC-HAr7), 119.97 (ArC-FH2), 124.77 (ArC-H3), 124.97 (ArC-HAr2), 126.50 (ArC-COOH), 126.82 (ArC-FH3), 127.49 (ArC-FH5), 128.39 (ArC-FH4), 129.23 (ArC-NCOO t Bu), 129.71 (ArC-C- $\underline{C}H_2$), 129.81 (ArC-H2), 140.71 (ArC-F6), 143.51 (ArC-F1), 144.71 (ArC-N), 148.77 (ArC-NCOOCH $_2$), 154.29 (ArC-O), 155.34 ($\underline{C}OO$ - $\underline{C}H_2$), 166.70 (COOH); ν_{max}/cm^{-1} (solid state) = \sim 3016 (COOH), 1738 (CO), 1365 (C-N), 1217 (C-O); ESI-MS m/z 617.3 [M-H] $^-$; ESI-HRMS found m/z 617.2284 [M-H] $^-$ C $_{37}$ H $_{33}$ N $_2$ O $_7$ requires 617.2293.

***t*-butyl 5-bromo-3-formyl-1*H*-indole-1-carboxylate 23r**

To a stirred suspension of 5-bromo-1*H*-indole-3-carboxaldehyde (1.00 g, 4.5 mmol) in dichloromethane (20 mL) was added Boc-anhydride (1.02 g, 4.7 mmol), followed by triethylamine (0.7 mL, 4.9 mmol). The resulting mixture was stirred at room temperature under a nitrogen atmosphere for 20 hours. A white precipitate was formed. The reaction mixture was filtered and the solid was dried under high vacuum to afford the title compound (1.45 g, 4.5 mmol, quant.) as a white amorphous solid; R_F 0.65 (ethyl acetate - hexane 1-1); (Found: C, 51.90; H, 4.25; N, 4.25; Br, 24.75; C $_{14}$ H $_{14}$ BrNO $_3$ requires: C, 51.87; H, 4.35; N, 4.32; Br, 24.65%); δ_H (300 MHz, MeOD) 1.64 (s, 9H, *t*Bu), 7.44 (dd, 1H, $J_1 = 9.0$ Hz, $J_2 = 3.0$ Hz, H7), 7.96 (d, 1H, $J = 9.0$ Hz, H6), 8.15 (s, 1H, H2), 8.38 (d, 1H, $J = 3.0$ Hz, H4), 9.99 (s, 1H, H9); δ_C (75 MHz, DMSO- d_6) 27.48 ($\underline{C}H_3$ -C), 85.99 (\underline{C} - $\underline{C}H_3$), 117.04 (ArC-Br), 117.09 (ArC-HAr7), 119.54 (ArC-CO), 123.52 (ArC-HAr4), 127.37 (ArC-HAr2), 128.53 (ArC-C-CO), 134.14 (ArC-HAr6), 139.22 (ArC-N), 187.12 (COOH), (1 ^{13}C resonance missing); ν_{max}/cm^{-1} (solid state) = 1738 (CO), 1365 (C-N), 1217

(C-O); ESI-HRMS found m/z 346.0051 $[M+Na]^+$ $C_{14}H_{14}BrNaNO_3$ requires 346.0049.

4-(((5-bromo-1-(tert-butoxycarbonyl)-1H-indol-3-yl)methyl)amino)benzoic acid 21r

4-Aminobenzoic acid (0.59 g, 4.3 mmol), **23r** (1.40 g, 4.3 mmol) and picolineborane complex (0.53 g, 5.0 mmol) were stirred at room temperature in methanol (20 mL) for 14 hours. The solvent was evaporated and the product was precipitated from chloroform, then dried under high vacuum to yield the desired compound (1.72 g, 89%) as a white powder; R_F 0.25 (10% methanol in dichloromethane); δ_H (300 MHz, MeOD) 1.67 (s, 9H, *t*Bu), 4.48 (s, 2H, H α), 6.71 (d, 2H, $J = 8.8$ Hz, H3), 7.44 (dd, 1H, $J_1 = 8.9$ Hz, $J_2 = 2.1$ Hz, HAr7), 7.63 (s, 1H, HAr2), 7.81 (d, 2H, $J = 8.8$ Hz, H2), 7.84 (d, 1H, $J = 2.1$ Hz, HAr4), 8.05 (d, 1H, $J = 8.9$ Hz, HAr6); δ_C (75 MHz, DMSO- d_6) 27.85 ($\underline{C}H_3$ -C), 54.92 ($\underline{C}H_2$), 84.86 (\underline{C} -CH $_3$), 111.15 (Ar \underline{C} -H3), 116.48 (Ar \underline{C} - $\underline{C}H_2$), 117.13 (Ar \underline{C} -Br), 118.37 (Ar \underline{C} -HAr7), 119.38 (Ar \underline{C} -COOH), 124.76 (Ar \underline{C} -HAr4), 125.39 (Ar \underline{C} -HAr2), 128.14 (Ar \underline{C} -C-CH $_2$), 130.62 (Ar \underline{C} -H2), 132.03 (Ar \underline{C} -HAr6), 133.49 (Ar \underline{C} -N), 148.71 (N-COO), 152.12 (Ar \underline{C} -NH), 168.62 (COOH); ν_{max}/cm^{-1} (solid state) = 3398 (NH), ~1747 (COOH), 1364 (C-N), 1216 (C-O); ESI-MS m/z 467.1 $[M+Na]^+$.

4-(((9H-Fluoren-9-yl)methoxy)carbonyl)(5-bromo-1-(tert-butoxycarbonyl)-1H-indol-3-yl)methyl)amino)benzoic acid 22r

To a refluxing suspension of **21r** (0.83 g, 1.8 mmol) and NaHCO $_3$ (0.31 g, excess) in tetrahydrofuran (60 mL) was added dropwise a solution of Fmoc-Cl (0.53 g, 2.1 mmol) in tetrahydrofuran (8 mL). The reaction mixture was stirred at reflux for 2 hours. The excess bicarbonate was filtered then the solvent was evaporated and the product was isolated by column chromatography (ethyl acetate - hexane) followed by slow precipitation from chloroform - diethylether (0.41 g, 33%) as a pale yellow amorphous solid; R_F 0.25 (ethyl acetate - hexane 1-1); δ_H (300 MHz, CDCl $_3$) 1.64 (s, 9H, *t*Bu), 4.13 (t, 1H, $J = 6.2$ Hz, FH β), 4.58 (d, 2H, $J = 6.2$ Hz, FH α), 4.89 (s, 2H, H α), 7.11 (d, 2H, $J = 8.2$ Hz, H3), 7.18 (t, 2H, $J = 7.4$ Hz, FH4), 7.25 (d, 2H, $J = 7.4$ Hz, FH5), 7.26-7.28 (m, 1H, HAr4), 7.32 (t, 2H, $J = 7.4$ Hz, FH3), 7.42 (dd, 1H, $J_1 = 8.9$ Hz, $J_2 = 1.9$ Hz, HAr7), 7.48 (s, 1H, HAr2), 7.61 (d, 2H, $J = 7.5$ Hz, FH2), 7.99 (d, 1H, $J = 7.4$ Hz, HAr6), 8.01 (d, 2H, $J = 8.2$ Hz, H2); δ_C (75 MHz, CDCl $_3$)

28.14 ($\underline{\text{C}}\text{H}_3\text{-C}$), 29.73 ($\underline{\text{C}}\text{H}_2$), 46.99 ($\underline{\text{C}}\text{H-CH}_2$), 67.73 ($\underline{\text{C}}\text{H}_2\text{-CH}$), 77.24 ($\underline{\text{C}}\text{-CH}_3$), 105.00 ($\text{Ar}\underline{\text{C}}\text{-CH}_2$), 115.94 ($\text{Ar}\underline{\text{C}}\text{-Br}$), 116.17 ($\text{Ar}\underline{\text{C}}\text{-HAr7}$), 116.73 ($\text{Ar}\underline{\text{C}}\text{-FH2}$), 119.90 ($\text{Ar}\underline{\text{C}}\text{-HAr4}$), 122.16 ($\text{Ar}\underline{\text{C}}\text{-H3}$), 124.66 ($\text{Ar}\underline{\text{C}}\text{-HAr2}$), 124.78 ($\text{Ar}\underline{\text{C}}\text{-FH3}$), 126.93 ($\text{Ar}\underline{\text{C}}\text{-COOH}$), 127.62 ($\text{Ar}\underline{\text{C}}\text{-FH5}$), 127.67 ($\text{Ar}\underline{\text{C}}\text{-FH4}$), 131.07 ($\text{Ar}\underline{\text{C}}\text{-C-CH}_2$), 131.25 ($\text{Ar}\underline{\text{C}}\text{-H2}$), 141.28 ($\text{Ar}\underline{\text{C}}\text{-HAr6}$) 141.37 ($\text{Ar}\underline{\text{C}}\text{-N-COO}^t\text{Bu}$), 142.70 ($\text{Ar}\underline{\text{C}}\text{-F6}$), 143.47 ($\text{Ar}\underline{\text{C}}\text{-F1}$), 149.13 ($\text{Ar}\underline{\text{C}}\text{-N-CH}_2$), 154.25 (COO^tBu), 154.88 (NCOO-CH_2), 170.39 (COOH); $\nu_{\text{max}}/\text{cm}^{-1}$ (solid state) = \sim 3027 (COOH), 1750 (CO), 1364 (C-N), 1216 (C-O); ESI-MS m/z 665.3 [M-H]; ESI-HRMS found m/z 665.1291 [M-H] $\text{C}_{36}\text{H}_{30}\text{BrN}_2\text{O}_6$ requires 665.1293.

***tert*-butyl 5-chloro-3-formyl-1*H*-indole-1-carboxylate 23s**

To a stirred suspension of 5-chloro-1*H*-indole-3-carboxaldehyde (1.00 g, 5.6 mmol) in tetrahydrofuran (20 mL) was added Boc-anhydride (1.28 g, 5.9 mmol), followed by triethylamine (0.9 mL, 6.2 mmol). The resulting mixture was stirred at room temperature under a nitrogen atmosphere for 20 hours. A white precipitate was formed. The reaction mixture was filtered and the solid was dried under high vacuum to afford the title compound (0.87 g, 3.1 mmol, 56%) as a white amorphous solid; R_F 0.55 (ethyl acetate - hexane 1-1); (Found: C, 60.15; H, 4.95; N, 4.85; Cl, 12.75; $\text{C}_{14}\text{H}_{14}\text{ClNO}_3$ requires: C, 60.11; H, 5.04; N, 5.01; Cl, 12.67%); δ_{H} (300 MHz, DMSO-d_6) 1.66 (s, 9H, *t*Bu), 7.49 (dd, 1H, $J_1 = 9.0$ Hz, $J_2 = 2.5$ Hz, H7), 8.09 (d, 1H, $J = 9.0$ Hz, H6), 8.11 (d, 1H, $J = 2.5$ Hz, H4), 8.74 (s, 1H, H2), 10.06 (s, 1H, H9); δ_{C} (75 MHz, DMSO-d_6) 27.47 ($\underline{\text{C}}\text{H}_3\text{-C}$), 85.96 ($\underline{\text{C}}\text{-CH}_3$), 116.62 ($\text{Ar}\underline{\text{C}}\text{-HAr7}$), 119.65 ($\text{Ar}\underline{\text{C}}\text{-CO}$), 120.49 ($\text{Ar}\underline{\text{C}}\text{-HAr4}$), 125.83 ($\text{Ar}\underline{\text{C}}\text{-HAr6}$), 126.85 ($\text{Ar}\underline{\text{C}}\text{-HAr2}$), 128.97 ($\text{Ar}\underline{\text{C}}\text{-Cl}$), 133.79 ($\text{Ar}\underline{\text{C}}\text{-C-CO}$), 139.32 ($\text{Ar}\underline{\text{C}}\text{-N}$), 147.97 (N-COO), 187.05 (CO); $\nu_{\text{max}}/\text{cm}^{-1}$ (solid state) = 1738 (CO), 1365 (C-N), 1216 (C-O); ESI-HRMS found m/z 302.0548 [M+Na] $^+$ $\text{C}_{14}\text{H}_{14}\text{ClNaNO}_3$ requires 302.0554.

4-(((5-chloro-1-(*tert*-butoxycarbonyl)-1*H*-indol-3-yl)methyl)amino)benzoic acid 21s

4-Aminobenzoic acid (0.43 g, 3.1 mmol), **23s** (0.87 g, 3.1 mmol) and picolineborane complex (0.37 g, 3.4 mmol) were stirred at room temperature in methanol-dichloromethane (2-1, 10 mL) for 20 hours. The solvent was evaporated and the product was precipitated from chloroform, then dried under high vacuum to yield the desired compound (0.80 g, 67%) as a colourless

powder; R_F 0.37 (ethyl acetate - hexane 1-1); δ_H (300 MHz, DMSO- d_6) 1.61 (s, 9H, *t*Bu), 4.44 (d, 2H, $J = 5.8$ Hz, H α), 6.69 (d, 2H, $J = 8.8$ Hz, H3), 6.98 (t, 1H, $J = 5.8$ Hz, NH), 7.36 (dd, 1H, $J_1 = 8.9$ Hz, $J_2 = 2.1$ Hz, HAr7), 7.66 (d, 2H, $J = 8.8$ Hz, H2), 7.76 (s, 1H, HAr2), 7.85 (d, 1H, $J = 2.1$ Hz, HAr4), 8.01 (d, 1H, $J = 8.9$ Hz, HAr6); δ_C (75 MHz, DMSO- d_6) 27.60 ($\underline{C}H_3$ -C), 54.89 ($\underline{C}H_2$), 84.24 (\underline{C} -CH $_3$), 111.15 ($\underline{A}rC$ -H3), 116.18 ($\underline{A}rC$ -CH $_2$), 117.23 ($\underline{A}rC$ -HAr7), 117.87 ($\underline{A}rC$ -COOH), 119.37 ($\underline{A}rC$ -HAr4), 124.36 ($\underline{A}rC$ -HAr6), 125.34 ($\underline{A}rC$ -HAr2), 127.14 ($\underline{A}rC$ -Cl), 130.72 ($\underline{A}rC$ -C-CH $_2$), 131.03 ($\underline{A}rC$ -H2), 133.43 ($\underline{A}rC$ -NCOO), 148.72 (\underline{N} -COO), 152.18 ($\underline{A}rC$ -NH), 167.42 (COOH); ν_{max}/cm^{-1} (solid state) = 3398 (NH), \sim 3016 (COOH), 1747 (CO), 1364 (C-N), 1216 (C-O).

4-(((9H-Fluoren-9-yl)methoxy)carbonyl)(5-chloro-1-(*tert*-butoxycarbonyl)-1*H*-indol-3-yl)methyl)amino)benzoic acid 22s

To a refluxing suspension of **21s** (0.27 g, 0.7 mmol) and NaHCO $_3$ (0.11 g, excess) in tetrahydrofuran (7 mL) was added dropwise a solution of Fmoc-Cl (0.18 g, 0.7 mmol) in tetrahydrofuran (2 mL). The reaction mixture was stirred at reflux for 2 hours. The excess bicarbonate was filtered then the solvent was evaporated and the product was isolated by column chromatography (ethyl acetate - hexane) followed by slow precipitation from chloroform - diethylether (0.26 g, 71%) as a pale yellow amorphous solid; R_F 0.25 (ethyl acetate - hexane 1-1); δ_C (500 MHz, DMSO- d_6) 1.56 (s, 9H, *t*Bu), 4.19 (t, 1H, $J = 5.8$ Hz, FH β), 4.56 (d, 2H, $J = 5.8$ Hz, FH α), 4.93 (s, 2H, H α), 7.07 (d, 2H, $J = 7.7$ Hz, H3), 7.15 (t, 2H, $J = 7.3$ Hz, FH4), 7.31 (d, 2H, $J = 7.7$ Hz, FH5), 7.33-7.36 (m, 4H, ArCH), 7.41 (d, 1H, $J = 1.8$ Hz, HAr4), 7.75 (d, 2H, $J = 8.2$ Hz, FH2), 7.76 (d, 2H, $J = 8.8$ Hz, H2), 7.97 (d, 1H, $J = 8.2$ Hz, HAr7); δ_C (125 MHz, DMSO- d_6) 27.55 ($\underline{C}H_3$ -C), 43.93 ($\underline{C}H_2$), 46.55 ($\underline{C}H$ -CH $_3$), 66.94 ($\underline{C}H_3$ -CH), 84.42 (\underline{C} -CH $_3$), 103.35 ($\underline{A}rC$ -CH $_2$), 106.93 ($\underline{A}rC$ -HAr7), 116.23 ($\underline{A}rC$ -HAr4), 124.48 ($\underline{A}rC$ -FH2), 124.69 ($\underline{A}rC$ -H3), 125.91 ($\underline{A}rC$ -HAr2), 126.37 ($\underline{A}rC$ -Cl), 126.80 ($\underline{A}rC$ -FH3), 127.11 ($\underline{A}rC$ -COOH), 127.33 ($\underline{A}rC$ -FH5), 128.35 ($\underline{A}rC$ -FH4), 129.80 ($\underline{A}rC$ -C-CH $_2$), 130.19 ($\underline{A}rC$ -H2), 131.04 ($\underline{A}rC$ -HAr6), 133.23 ($\underline{A}rC$ -N-COO t Bu), 140.65 ($\underline{A}rC$ -F6), 143.53 ($\underline{A}rC$ -F1), 144.57 ($\underline{A}rC$ -N-CH $_2$), 148.50 (COO t Bu), 154.29 (N- $\underline{C}OOCH_2$), 166.64 (COOH); ν_{max}/cm^{-1} (solid state) = \sim 3016 (COOH), 1738 (CO), 1365 (C-N), 1217 (C-O); ESI-HRMS found m/z 621.1804 [M -H] $^-$ C $_{36}$ H $_{30}$ ClN $_2$ O $_6$ requires 621.1798.

4-(((Naphthalen-1-yl)methyl)amino)benzoic acid 21t

4-Aminobenzoic acid (0.88 g, 6.4 mmol), 1-naphthaldehyde (1.00 g, 6.4 mmol) and picoline-borane complex (0.82 g, 7.7 mmol) were stirred at room temperature in methanol (20 mL) for 14 hours. A white precipitate formed. The precipitate was filtered and dried under high vacuum to yield the desired compound (1.35 g, 70%) as a colourless amorphous solid; R_F 0.65 (10% methanol in dichloromethane); δ_H (300 MHz, DMSO- d_6) 4.78 (d, 2H, $J = 5.4$ Hz, H α), 6.70 (d, 2H, $J = 8.5$ Hz, H3), 7.08 (t, 1H, $J = 5.4$ Hz, NH), 7.44-7.49 (m, 2H, ArCH), 7.55-7.59 (m, 2H, ArCH), 7.67 (d, 2H, $J = 8.5$ Hz, H2), 7.86 (d, 1H, $J = 6.6$ Hz, ArCH), 7.97 (d, 1H, $J = 7.5$ Hz, HAr2/4), 8.12 (d, 1H, $J = 8.1$ Hz, HAr4/2); δ_C (75 MHz, DMSO- d_6) 44.52 (CH $_2$), 111.43 (ArC-H3), 117.50 (ArC-COOH), 123.92 (ArC-H), 125.42 (ArC-H), 125.81 (ArC-H), 126.18 (ArC-H), 126.7 (ArC-H), 127.89 (ArC-H), 128.90 (ArC-H), 131.42 (ArC-H2), 131.51 (ArC), 133.77 (ArC), 134.53 (ArC-CH $_2$), 152.90 (ArC-NH), 167.87 (COOH); ν_{max}/cm^{-1} (solid state) = 3423 (NH), ~3000 (COOH), 1658 (CO); ESI-MS m/z 300 [M+Na] $^+$; ESI-HRMS found m/z 278.1184 [M+H] $^+$ C $_{18}$ H $_{16}$ NO $_2$ requires 278.1176.

4-(((9H-Fluoren-9-yl)methoxy)carbonyl)(naphthalen-1-yl)methyl)amino)benzoic acid 22t

To a refluxing solution of **21t** (1.30 g, 4.3 mmol) in tetrahydrofuran (10 mL) was added dropwise a solution of Fmoc-Cl (1.18 g, 4.6 mmol) in tetrahydrofuran (10 mL). The reaction mixture was stirred at reflux for 15 hours. The solvent was then removed under reduced pressure and the residue purified by column chromatography (30% ethyl acetate in hexane) to afford the title compound as a white amorphous solid (1.89 g, 87%); R_F 0.27 (ethyl acetate - hexane 1-1); δ_H (300 MHz, CDCl $_3$) 4.08 (t, 1H, $J = 6.3$ Hz, FH β), 4.55 (d, 2H, $J = 6.3$ Hz, FH α), 5.34 (s, 2H, H α), 7.08-7.13 (m, 3H, ArCH), 7.09 (d, 2H, $J = 8.1$ Hz, H3), 7.17 (d, 2H, $J = 7.2$ Hz, ArCH), 7.24-7.32 (m, 3H, ArCH), 7.51-7.55 (m, 2H, ArCH), 7.61 (d, 2H, $J = 7.5$ Hz, ArCH), 7.75 (d, 1H, $J = 8.1$ Hz, ArCH), 7.83-7.89 (m, 1H, ArCH), 7.92 (d, 2H, $J = 8.3$ Hz, H2), 7.93-8.00 (m, 1H, ArCH); δ_C (75 MHz, CDCl $_3$) 47.44 (CH-CH $_2$), 52.12 (CH $_2$), 68.25 (CH $_2$ -CH), 120.31 (ArC-FH2), 123.52 (ArC-H3), 125.17 (ArC-COOH), 125.71 (ArC-H), 126.01 (ArC-H), 126.358 (ArC-H), 126.41 (ArC-H), 126.95 (ArC-H), 127.30 (ArC-H), 127.34 (ArC-H), 128.04 (ArC-H), 128.77 (ArC-H),

129.27 (ArC-H), 131.29 (ArC-H2), 131.37 (ArC), 132.41 (ArC), 134.17 (ArC-CH₂), 141.66 (ArC-F6), 143.88 (ArC-F1), 146.28 (ArC-N), 155.41 (N-COO), 171.74 (COOH); ESI-HRMS found m/z 500.1854 [M+H]⁺ C₃₃H₂₆NO₄ requires 500.1862.

4-(((2-Methylnaphthalen-1-yl)methyl)amino)benzoic acid **21u**

4-Aminobenzoic acid (0.81 g, 5.9 mmol), 2-methyl-1-naphthaldehyde (1.00 g, 5.9 mmol) and picoline-borane complex (0.72 g, 6.8 mmol) were stirred at room temperature in methanol (20 mL) for 14 hours. A white precipitate formed. The reaction mixture was filtered, and the filtrate acidified with 1N hydrochloric acid (~10 mL) to induce further precipitation. The combined precipitates were dried under high vacuum to yield the desired compound (1.60 g, 94%) as a colourless powder; R_F 0.65 (10% methanol in dichloromethane); m.p. 209-211 °C; δ_H (300 MHz, DMSO-d₆) 2.52 (s, 3H, CH₃), 4.61 (s, 2H, H α), 6.55 (br s, 1H, NH), 6.78 (d, 2H, J = 8.9 Hz, H3), 7.43 (d, 1H, J = 8.4 Hz, HAr3), 7.46-7.56 (m, 2H, HAr6-HAr7), 7.73 (d, 2H, J = 8.9 Hz, H2), 7.85 (d, 1H, J = 8.4 Hz, HAr4), 7.92 (d, 1H, J = 7.8 Hz, HAr5/8), 7.97 (d, 1H, J = 8.4 Hz, HAr8/5); δ_C (75 MHz, DMSO-d₆) 19.92 (C \underline{H}_3), 40.64 (C \underline{H}_2), 111.27 (ArC-H3), 117.36 (ArC-COOH), 124.04 (ArC-H), 125.23 (ArC-H), 126.86 (ArC-H), 128.14 (ArC-H), 128.62 (ArC-H), 129.43 (ArC-H), 131.01 (ArC-H2), 131.45 (ArC), 132.38 (ArC), 135.37 (ArC-CH₂), 153.07 (ArC-NH), 167.94 (COOH); ν_{max}/cm^{-1} (solid state) = 3373 (NH), ~3000 (COOH), 1738 (CO); ESI-MS m/z 314 [M+Na]⁺; ESI-HRMS found m/z 292.1332 [M+H]⁺ C₁₉H₁₈NO₂ requires 292.1327.

4-(((9H-Fluoren-9-yl)methoxy)carbonyl)((2-methylnaphthalen-1-yl)methyl)amino)benzoic acid **22u**

To a refluxing solution of **21u** (1.60 g, 5.5 mmol) in tetrahydrofuran (10 mL) was added dropwise a solution of Fmoc-Cl (1.50 g, 5.8 mmol) in tetrahydrofuran (10 mL). The reaction mixture was stirred at reflux for 15 hours. The solvents were evaporated and the residue crystallized from a mixture of tetrahydrofuran – hexane to yield the target compound as pale yellow crystals (2.43 g, 83%); R_F 0.53 (10% methanol in dichloromethane); m.p. 183-185 °C; δ_H (500 MHz, CDCl₃) 2.07 (s, 3H, CH₃), 4.03 (t, 1H, J = 6.5 Hz, FH β), 4.49 (d, 2H, J = 6.5 Hz, FH α), 5.38 (s, 2H, H α), 6.70 (d, 2H, J = 8.5 Hz, H3), 7.05 (d, 1H, J = 8.5 Hz, ArCH), 7.11-7.14 (m, 4H, ArCH), 7.27-7.31 (m, 2H, ArCH), 7.41 (t, 1H, J = 7.0 Hz, FH3/4), 7.48-7.51 (m,

1H, ArCH), 7.60-7.64 (m, 3H, ArCH), 7.75 (d, 1H, $J = 8.0$ Hz, ArCH), 7.80 (d, 2H, $J = 8.5$ Hz, H₂), 8.15 (d, 1H, $J = 8.5$ Hz, ArCH); δ_c (125 MHz, CDCl₃) 19.97 (CH₃), 46.21 (CH-CH₂), 47.06 (CH₂-N), 67.76 (CH₂-CH), 119.87 (ArC-FH₂), 119.97 (ArC-H₃), 123.78 (ArC-COOH), 124.86 (ArC-H), 125.02 (ArC-H), 126.93 (ArC-H), 127.63 (ArC-H), 128.17 (ArC-H), 128.55 (ArC-H), 128.63 (ArC-H), 128.85 (ArC-H), 130.67 (ArC-H), 132.44 (ArC-H₂), 132.65 (ArC-CH₃), 135.92 (ArC-CH₂), 141.29 (ArC-F₆), 143.60 (ArC-F₁), 144.96 (ArC-N), 155.22 (N-COO), 171.25 (COOH); $\nu_{\max}/\text{cm}^{-1}$ (solid state) = ~ 3000 (COOH), 1738 (CO); ESI-MS m/z 536 [M+Na]⁺; ESI-HRMS found m/z 512.1879 [M-H]⁻ C₃₄H₂₆NO₄ requires 512.1867.

4-(Cyclohexylmethylamino)benzoic acid **21w**

4-Aminobenzoic acid (1.50 g, 10.9 mmol), cyclohexanaldehyde (1.3 mL, 10.9 mmol) and picoline-borane complex (1.35 g, 12.0 mmol) were stirred at room temperature in methanol (60 mL) for 14 hours. A white precipitate formed. The reaction mixture was filtered, and the filtrate acidified with 1N hydrochloric acid (\sim pH 4) to induce further precipitation. The combined precipitates were dried under high vacuum to yield the desired compound (2.09 g, 82%) as a white powder; R_f 0.48 (40% hexane in ethyl acetate); (Found: C, 71.90; H, 8.25; N, 6.00%; C₁₄H₁₉NO₂ requires: C, 72.07; H, 8.21; N, 6.00%); δ_H (500 MHz, MeOD) 1.03 (dd, 2H, $J_1 = 11.7$ Hz, $J_2 = 2.6$ Hz, H γ), 1.21-1.36 (m, 3H, H δ , H ϵ), 1.63 (m, 1H, H β), 1.72 (d, 1H, $J = 11.1$ Hz, H ϵ'), 1.78 (d, 2H, $J = 12.9$ Hz, H δ'), 1.87 (d, 2H, $J = 11.7$ Hz, H γ'), 3.01 (d, 2H, $J = 6.8$ Hz, H α), 6.59 (d, 2H, $J = 8.9$ Hz, H₃), 7.79 (d, 2H, $J = 8.9$ Hz, H₂); δ_c (75 MHz, MeOD) 27.15 (CH δ), 27.71 (CH ϵ), 32.31 (CH γ), 38.70 (CH β), 50.70 (CH α), 111.98 (ArC-H₃), 117.55 (ArC-COOH), 132.77 (ArC-H₂), 154.83 (ArC-NH), 170.87 (COOH); $\nu_{\max}/\text{cm}^{-1}$ (solid state) = 3417 (NH), ~ 3015 (COOH), 1738 (CO), 1365 (C-N), 1217 (C-O); ESI-MS m/z 232 [M-H]⁻; ESI-HRMS found m/z 234.1484 [M+H]⁺ C₁₄H₂₀NO₂ requires 234.1489.

4-(((9H-Fluoren-9-yl)methoxy)carbonyl)(cyclohexylmethyl)amino)benzoic acid **22w**

To a refluxing solution of 4-(cyclohexylmethylamino)benzoic acid **21w** (2.09 g, 8.9 mmol) in tetrahydrofuran (30 mL) was added dropwise a solution of Fmoc-chloride (2.65 g, 9.9 mmol) in tetrahydrofuran (5 mL). The reaction mixture was then stirred at reflux overnight. The solvents were evaporated, then the residue

was purified by column chromatography (*Stationary phase* : silica; *Mobile phase* : ethyl acetate–hexane 2-3 to neat ethyl acetate) then crystallised from dichloromethane–hexane to yield the pure target material (2.33 g, 57%) as colourless platelets; R_F 0.25 (ethyl acetate–hexane 2-3); m.p. 150-152 °C; (Found: C, 75.50; H, 6.30; N, 3.10%; $C_{29}H_{29}NO_4$ requires: C, 76.46; H, 6.42; N, 3.07%); δ_H (500 MHz, $CDCl_3$) 0.72-0.84 (m, 2H, H γ), 1.04-1.12 (m, 3H, H δ , H ϵ), 1.35 (m, 1H, H β), 1.52 (d, 2H, $J = 12.3$ Hz, H δ'), 1.51-1.66 (m, 3H, H γ' , H ϵ'), 3.46 (d, 2H, $J = 7.0$ Hz, H α), 4.12 (t, 1H, $J = 5.6$ Hz, FH β), 4.56 (d, 2H, $J = 5.6$ Hz, FH α), 7.15 (d, 2H, $J = 8.1$ Hz, H3), 7.24 (t, 2H, $J = 7.4$ Hz, FH4), 7.34 (d, 2H, $J = 7.4$ Hz, FH5), 7.38 (t, 2H, $J = 7.4$ Hz, FH3), 7.72 (d, 2H, $J = 7.5$ Hz, FH2), 8.03 (d, 2H, $J = 8.1$ Hz, H2); δ_C (75 MHz, $CDCl_3$) 25.67 (CH δ), 26.33 (CH ϵ), 30.47 (CH γ), 36.50 (CH β), 47.24 (CH–CH $_2$), 55.89 (CH α), 67.04 (CH $_2$ –CH), 119.92 (ArC–FH2), 124.79 (ArC–H3), 126.84 (ArC–FH3), 126.92 (ArC–COOH), 126.99 (ArC–FH5), 127.65 (ArC–FH4), 131.01 (ArC–H2), 141.40 (ArC–F6), 143.71 (ArC–F1), 147.08 (ArC–N), 155.21 (N–COO), 171.23 (COOH); ν_{max}/cm^{-1} (solid state) = 3426 (NH), ~3015 (COOH), 1737 (CO), 1365 (C–N), 1216 (C–O); ESI-HRMS found m/z 478.2007 $[M+Na]^+$ $C_{29}H_{29}NaNO_4$ requires 478.1989.

6.1.2 Solid phase synthesis experimental and *N*-alkylated oligobenzamides characterisation (Chapters 2 and 3)

127 mg of Fmoc-Gly-Wang resin (0.79 mmol g^{-1} , 100-200 mesh; carrier: polystyrene, crosslinked with 1% DVB) from NovaSyn was used throughout for the p53-targeted library. The sub-library of oligobenzamides targeting the Bcl-2 family made use of: Fmoc-Leu-Wang resin (0.64 mmol g^{-1}), Fmoc-Ile-Wang resin (0.59 mmol g^{-1}), Fmoc-Val-Wang resin (0.61 mmol g^{-1}) and Fmoc-Asp(OtBu)-Wang resin (0.29 mmol g^{-1}). All solvents used were HPLC grade, anhydrous chloroform on molecular sieves was purchased from Acros Organics. 1-Chloro-*N,N*,2-trimethyl-1-propenylamine (Ghosez's reagent) was purchased from Sigma-Aldrich. The reactions were all carried out on a CEM Liberty® automated microwave assisted peptide synthesiser. For each monomer the concentration of the preactivation mixture was about 1 mmol mL^{-1} . The volume of the reaction mixture in the reaction vessel was 2.5 mL. The resin was swelled in Corning®

tubes in DMF for at least 30 minutes prior to coupling. Before coupling each amino acid, standard washing and deprotection cycles are carried out on the synthesiser. A filtered drain takes place in between every wash as follows: wash the reaction vessel from the top ('DMF top', 5 mL), then from the bottom ('DMF bottom', 7 mL), then 'DMF top' (5 mL), then add the deprotection mixture (6 mL), microwave method for the deprotection (cf. Fmoc deprotection paragraph); 'DMF top' (5 mL), 'DMF bottom' (7 mL) and finally 'DMF top' (5 mL) wash.

Coupling

Prior to the reaction, each fully protected monomer was dissolved in anhydrous chloroform (2.5 mL per coupling, *i.e.* 5 mL for a double coupling) in a dry 50 mL Corning® tube (stored in an oven at 60 °C for at least 24 hours), and preactivated with 0.9 eq. of Ghosez's reagent at room temperature for 1-3 hours under a nitrogen atmosphere. For each monomer, a double coupling of 20 minutes was carried out under microwave heating at 60 °C. When required, sodium bicarbonate (50 mg, 0.59 mmol, excess) was added to the resin tube prior to swelling.

Fmoc deprotection

Before coupling of each monomer and after the last coupling reaction, two deprotection cycles were carried out on the CEM synthesiser using 6 mL of a 25% piperidine solution in DMF, under microwave heating at 75 °C. The initial deprotection lasts 30 seconds and is followed by a 'DMF top' wash and filtered drain. After a second addition of deprotection mixture, the deprotection is maintained under microwave heating for 3 minutes, and is again followed by DMF washes.

Cleavage

The cleavage step was carried out manually, in 1.5 mL 'Extract-Clean' polypropylene reservoirs fitted with 20 µm polyethylene frits, both available from Alltech. Triisopropylsilane (TIPS) was first investigated as a scavenger for this cleavage step, but proved to introduce a large amount of impurities in the isolated compound (observable on the ¹H-NMR spectrum). It was also shown not

to be required, as cleavage without TIPS provided clean LC-MS and ¹H-NMR spectra. As a result, no scavenger was used during this step. The resin was transferred to a reservoir then washed with CH₂Cl₂, then 1 mL of a 1-1 mixture of TFA in CH₂Cl₂ was added and the mixture was allowed to stir at room temperature for 30 minutes then the content of the reservoir was collected and the procedure was repeated. The resulting solution was then concentrated under reduced pressure to afford the target compound.

***N*-(*N*-(*N*-(Benzyl-4-aminobenzoyl)-*N*-cyclopropylmethyl-4-aminobenzoyl)-*N*-isobutyl-4-aminobenzoyl)-glycine 26**

> 90% pure by NMR, isolated crude yield: 60 mg; δ_{H} (300 MHz, MeOD) 0.01 (m, 2H, 2-H γ/γ'), 0.35 (m, 2H, 2-H γ'/γ), 0.92-1.00 (m, 1H, 2-H β), 0.96 (d, 6H, $J = 6.7$ Hz, 3-H γ), 1.86 (m, 1H, 3-H β), 3.70 (d, 2H, $J = 7.1$ Hz, 3-H α), 3.84 (d, 2H, $J = 7.4$ Hz, 2-H α), 4.05 (s, 2H, 1-H α), 4.37 (s, 2H, 4-H α), 6.52 (d, 2H, $J = 8.7$ Hz, 2-H3), 6.99 (d, 2H, $J = 8.3$ Hz, 3-H2), 7.02 (d, 2H, $J = 8.5$ Hz, 2-H2), 7.17 (d, 2H, $J = 8.4$ Hz, 3-H3), 7.20 (d, 2H, $J = 8.4$ Hz, 1-H3), 7.27-7.34 (m, 5H, HAr2-4), 7.72 (d, 2H, $J = 8.5$ Hz, 1-H2); ESI-HRMS found m/z 631.2910 [M-H]⁻ C₃₈H₃₉N₄O₅ requires 631.2926.

***N*-(*N*-(*N*-(Benzyl-4-aminobenzoyl)-*N*-benzyl-4-aminobenzoyl)-*N*-isobutyl-4-aminobenzoyl)-glycine 27**

> 80% pure by NMR, isolated crude yield: 66 mg; δ_{H} (300 MHz, CDCl₃) 0.85 (d, 6H, $J = 6.6$ Hz, 3-H γ), 1.81 (m, 1H, 3-H β), 3.71 (d, 2H, $J = 7.3$ Hz, 3-H α), 3.87 (d, 2H, $J = 5.2$ Hz, 1-H α), 4.34 (s, 2H, 2-H α), 4.99 (s, 2H, 4-H α), 6.65 (d, 2H, $J = 8.4$ Hz, 2-H3), 6.88 (d, 2H, $J = 8.2$ Hz, 3-H2), 7.01 (d, 2H, $J = 8.4$ Hz, 2-H2), 7.08 (d, 2H, $J = 8.4$ Hz, 3-H3), 7.13 (d, 2H, $J = 7.7$ Hz, 1-H3), 7.16-7.22 (m, 6H, 1-HAr3-5 and 2-HAr3-5), 7.24-7.29 (m, 4H, 1-HAr2,6 and 2-HAr2,6), 7.52 (d, 2H, $J = 8.2$ Hz, 1-H2), 7.80 (t, 1H, $J = 5.2$ Hz, NH); ESI-HRMS found m/z 667.2912 [M-H]⁻ C₄₁H₃₉N₄O₅ requires 667.2926.

***N*-(*N*-(*N*-(Benzyl-4-aminobenzoyl)-*N*-phenethyl-4-aminobenzoyl)-*N*-isobutyl-4-aminobenzoyl)-glycine 28**

> 90% pure by NMR, isolated crude yield: 58 mg; δ_{H} (300 MHz, MeOD) 0.98 (d, 6H, $J = 6.7$ Hz, 3-H γ), 1.89 (m, 1H, 3-H β), 2.88 (m, 2H, 2-H β), 3.85 (d, 2H, $J = 7.5$ Hz,

3-H α), 4.01 (m, 2H, 2-H α), 4.34 (s, 2H, 1-H α), 4.90 (s, 2H, 4-H α), 6.37 (d, 2H, J = 8.9 Hz, 2-H3), 6.78 (d, 2H, J = 8.7 Hz, 3-H2), 6.93 (d, 2H, J = 8.7 Hz, 2-H2), 7.14-7.35 (m, 14H, ArCH), 7.77 (d, 2H, J = 8.5 Hz, 1-H2); ESI-MS m/z 681.2 [M-H]⁻; ESI-HRMS found m/z 681.3072 [M-H]⁻ C₄₂H₄₁N₄O₅ requires 681.3082.

***N*-(*N*-(*N*-(Benzyl-4-aminobenzoyl)-*N*-(3-trifluoromethyl)benzyl-4-aminobenzoyl)-*N*-isobutyl-4-aminobenzoyl)-glycine 30**

> 90% pure by NMR, isolated crude yield: 72 mg; δ_{H} (300 MHz, MeOD) 0.95 (d, 6H, J = 6.7 Hz, 3-H γ), 1.84 (m, 1H, 3-H β), 3.82 (d, 2H, J = 7.6 Hz, 3-H α), 4.07 (s, 2H, 1-H α), 4.35 (s, 2H, 2-H α), 5.14 (s, 2H, 4-H α), 6.50 (d, 2H, J = 8.8 Hz, 2-H3), 6.89 (d, 2H, J = 8.5 Hz, 3-H2), 7.07 (d, 2H, J = 8.8 Hz, 2-H2), 7.15 (d, 2H, J = 8.5 Hz, 3-H3), 7.16 (d, 2H, J = 8.7 Hz, 1-H3), 7.27-7.39 (m, 6H, 1-HAr2-6 and 2-HAr6), 7.44 (t, 1H, J = 7.7 Hz, 2-HAr5), 7.54 (d, 1H, J = 7.7 Hz, 2-HAr4), 7.60 (s, 1H, 2-HAr2), 7.73 (d, 2H, J = 8.7 Hz, 1-H2); ESI-HRMS found m/z 735.2791 [M-H]⁻ C₄₂H₃₈FN₄O₅ requires 735.2800.

***N*-(*N*-(*N*-(Benzyl-4-aminobenzoyl)-*N*-4-chlorobenzyl-4-aminobenzoyl)-*N*-isobutyl-4-aminobenzoyl)-glycine 31**

Purified by Flash chromatography, > 95% pure by NMR, isolated yield: 4 mg; δ_{H} (300 MHz, MeOD) 0.83 (d, 6H, J = 6.7 Hz, 3-H γ), 1.73 (m, 1H, 3-H β), 3.71 (d, 2H, J = 7.3 Hz, 3-H α), 3.89 (s, 2H, 1-H α), 4.21 (s, 2H, 2-H α), 4.91 (s, 2H, 4-H α), 6.24 (d, 2H, J = 8.8 Hz, 2-H3), 6.74 (d, 2H, J = 8.5 Hz, 3-H2), 6.88 (d, 2H, J = 8.8 Hz, 2-H2), 7.01-7.20 (m, 13H, ArCH), 7.64 (d, 2H, J = 8.3 Hz, 1-H2); ESI-MS m/z 701.3 [M-H]⁻; ESI-HRMS found m/z 701.2525 [M-H]⁻ C₄₁H₃₈ClN₄O₅ requires 701.2536.

***N*-(*N*-(*N*-(Benzyl-4-aminobenzoyl)-*N*-4-methylthiobenzyl-4-aminobenzoyl)-*N*-isobutyl-4-aminobenzoyl)-glycine 32**

> 70% pure by NMR, isolated crude yield: 60 mg; δ_{H} (300 MHz, MeOD) 0.96 (d, 6H, J = 6.6 Hz, 3-H γ), 1.86 (m, 1H, 3-H β), 2.45 (s, 3H, SMe), 3.83 (d, 2H, J = 7.3 Hz, 3-H α), 4.10 (s, 2H, 1-H α), 4.41 (s, 2H, 2-H α), 5.02 (s, 2H, 4-H α), 6.59 (d, 2H, J = 8.7 Hz, 2-H3), 6.86 (d, 2H, J = 7.9 Hz, 3-H2), 7.08-7.18 (m, 10H, ArCH), 7.27-7.30 (m, 1H, ArCH), 7.33-7.37 (m, 4H, ArCH), 7.74 (d, 2H, J = 8.2 Hz, 1-H2); ESI-MS m/z 715.5 [M+H]⁺; ESI-HRMS found m/z 713.2830 [M-H]⁻ C₄₂H₄₁N₄O₅S requires 713.2803.

***N*-(*N*-(*N*-(Benzyl-4-aminobenzoyl)-*N*-4-hydroxybenzyl-4-aminobenzoyl)-*N*-isobutyl-4-aminobenzoyl)-glycine 33**

Purified by MS-directed prep HPLC, > 95% pure by NMR, isolated crude yield: 68 mg; δ_{H} (300 MHz, MeOD) 0.96 (d, 6H, $J = 6.8$ Hz, 3-H γ), 1.87 (m, 1H, 3-H β), 3.83 (d, 2H, $J = 7.7$ Hz, 3-H α), 4.10 (s, 2H, 1-H α), 4.37 (s, 2H, 2-H α), 4.96 (s, 2H, 4-H α), 6.50 (d, 2H, $J = 8.3$ Hz, 2-H3), 6.65 (d, 2H, $J = 8.7$ Hz, 3-H2), 6.83 (d, 2H, $J = 8.3$ Hz, 2-H2), 6.98 (d, 2H, $J = 8.5$ Hz, 3-H3), 7.05 (d, 2H, $J = 8.5$ Hz, ArCH), 7.10-7.13 (m, 2H, ArCH), 7.16 (d, 2H, $J = 8.1$ Hz, ArCH), 7.25 (d, 2H, $J = 8.5$ Hz, ArCH), 7.30-7.35 (m, 4H, ArCH), 7.74 (d, 2H, $J = 8.3$ Hz, 1-H2); ESI-MS m/z 685.5 [M+H]⁺; ESI-HRMS found m/z 683.2885 [M-H]⁻ C₄₁H₃₉N₄O₆ requires 683.2875.

***N*-(*N*-(*N*-(Benzyl-4-aminobenzoyl)-*N*-2-carboxymethyl-4-aminobenzoyl)-*N*-isobutyl-4-aminobenzoyl)-glycine 36**

> 90% pure by NMR, isolated crude yield: 63 mg; δ_{H} (300 MHz, MeOD) 0.97 (d, 6H, $J = 6.7$ Hz, 3-H γ), 1.87 (m, 1H, 3-H β), 3.85 (d, 2H, $J = 7.3$ Hz, 3-H α), 4.05 (s, 2H, 1-H α), 4.37 (s, 2H, 2-H α), 4.48 (s, 2H, 4-H α), 6.45 (d, 2H, $J = 8.8$ Hz, 2-H3), 6.99 (d, 2H, $J = 8.7$ Hz, 3-H2), 7.03 (d, 2H, $J = 8.4$ Hz, 2-H2), 7.20 (d, 2H, $J = 8.1$ Hz, 3-H3), 7.1 (d, 2H, $J = 8.1$ Hz, 1-H3), 7.25-7.36 (m, 5H, 1-HAr2-6), 7.75 (d, 2H, $J = 8.4$ Hz, 1-H2); ESI-MS m/z 635.6 [M-H]⁻; ESI-HRMS found m/z 635.2517 [M-H]⁻ C₃₆H₃₅N₄O₇ requires 635.2511.

***N*-(*N*-(*N*-(4-Chlorobenzyl-4-aminobenzoyl)-*N*-(3-trifluoromethyl)benzyl-4-aminobenzoyl)-*N*-(2-methyl)butyl-4-aminobenzoyl)-glycine 37**

> 95% pure by NMR, isolated crude yield: 76 mg; δ_{H} (300 MHz, MeOD) 0.88 (t, 3H, $J = 7.5$ Hz, 3-H δ), 0.92 (d, 3H, $J = 6.7$ Hz, 3-H ϵ), 1.18 (m, 1H, 3-H γ), 1.44 (m, 1H, 3-H γ'), 1.61 (m, 1H, 3-H β), 3.87 (d, 2H, $J = 7.3$ Hz, 3-H α), 4.08 (s, 2H, 1-H α), 4.35 (s, 2H, 2-H α), 5.14 (s, 2H, 4-H α), 6.42 (d, 2H, $J = 8.8$ Hz, 2-H3), 6.88 (d, 2H, $J = 8.4$ Hz, 3-H2), 7.03 (d, 2H, $J = 8.8$ Hz, 2-H2), 7.14 (d, 2H, $J = 8.5$ Hz, 3-H3), 7.16 (d, 2H, $J = 8.5$ Hz, 1-H3), 7.29-7.34 (m, 5H, 1-HAr2-6), 7.36 (d, 1H, $J = 8.0$ Hz, 2-HAr6), 7.43 (t, 1H, $J = 7.0$ Hz, 2-HAr5), 7.53 (d, 1H, $J = 8.0$ Hz, 2-HAr4), 7.59 (s, 1H, 2-HAr2), 7.71 (d, 2H, $J = 8.5$ Hz, 1-H2); ESI-HRMS found m/z 783.2505 [M-H]⁻ C₄₃H₃₉ClF₃N₄O₅ requires 783.2567.

***N*-(*N*-(*N*-(Isobutyl-4-aminobenzoyl)-*N*-(4-trifluoromethyl)benzyl-4-aminobenzoyl)-*N*-isobutyl-4-aminobenzoyl)-glycine 41**

Crude: 70% pure; isolated crude yield: 44 mg then purified by Flash chromatography (6 mg), > 90% pure by NMR; δ_{H} (300 MHz, MeOD) 0.94 (d, 6H, $J = 6.7$ Hz, 1-H γ), 0.98 (d, 6H, $J = 6.6$ Hz, 3-H γ), 1.78-1.92 (m, 2H, 1-H β , 3-H β), 2.89 (d, 2H, $J = 6.8$ Hz, 1-H α), 3.82 (d, 2H, $J = 6.8$ Hz, 3-H α), 4.02 (s, 2H, 2-H α), 5.13 (s, 2H, 4-H α), 6.34 (d, 2H, $J = 8.7$ Hz, 2-H3), 6.91 (d, 2H, $J = 8.4$ Hz, 3-H2), 7.02 (d, 2H, $J = 8.9$ Hz, 2-H2), 7.17 (d, 2H, $J = 8.7$ Hz, 3-H3), 7.21 (d, 2H, $J = 8.9$ Hz, 1-H3), 7.41 (d, 2H, $J = 8.0$ Hz, 2-HAr3), 7.57 (d, 2H, $J = 8.9$ Hz, 2-HAr2), 7.79 (d, 2H, $J = 8.7$ Hz, 1-H2); ESI-MS found m/z 701.2 [M-H]⁻; ESI-HRMS found m/z 701.2926 [M-H]⁻ C₃₉H₄₀F₃N₄O₅ requires 701.2956.

***N*-(*N*-(*N*-(Benzyl-4-aminobenzoyl)-*N*-(2-methyl)naphth-1-yl-4-aminobenzoyl)-*N*-isobutyl-4-aminobenzoyl)-glycine 42**

> 95% pure by NMR, isolated crude yield: 70 mg; δ_{H} (300 MHz, MeOD) 0.90 (d, 6H, $J = 6.9$ Hz, 3-H γ), 1.79 (m, 1H, 3-H β), 3.76 (d, 2H, $J = 6.9$ Hz, 3-H α), 4.14 (s, 2H, 2-H α), 4.32 (s, 2H, 1-H α), 5.53 (s, 2H, 4-H α), 6.40-6.45 (m, 4H, ArCH), 6.90 (d, 2H, $J = 8.2$ Hz, 3-H2), 6.99 (d, 2H, $J = 8.2$ Hz, 2-H2), 7.05 (d, 2H, $J = 8.5$ Hz, 3-H3), 7.15 (d, 1H, $J = 8.7$ Hz, 1-H3), 7.25 (m, 1H, ArCH), 7.29-7.31 (m, 4H, ArCH), 7.40-7.51 (m, 2H, ArCH), 7.69 (d, 1H, $J = 8.9$ Hz, ArCH), 7.72 (d, 2H, $J = 8.3$ Hz, ArCH), 7.82 (d, 1H, $J = 8.0$ Hz, 1-H2), 8.12 (d, 1H, $J = 8.5$ Hz, ArCH); ESI-HRMS found m/z 731.3222 [M-H]⁻ C₄₆H₄₃N₄O₅ requires 731.3239.

***N*-(*N*-(*N*-(Phenethyl-4-aminobenzoyl)-*N*-4-chlorobenzyl-4-aminobenzoyl)-*N*-isobutyl-4-aminobenzoyl)-glycine 43**

> 90% pure by NMR, isolated crude yield: 58 mg, purified by precipitation: 12 mg; δ_{H} (300 MHz, MeOD) 0.94 (d, 6H, $J = 6.7$ Hz, 3-H γ), 1.84 (m, 1H, 3-H β), 2.91 (t, 2H, $J = 7.6$ Hz, 1-H β), 3.45 (t, 2H, $J = 7.6$ Hz, 1-H α), 3.82 (d, 2H, $J = 7.4$ Hz, 3-H α), 4.12 (s, 2H, 2-H α), 5.04 (s, 2H, 4-H α), 6.53 (d, 2H, $J = 8.7$ Hz, 2-H3), 6.88 (d, 2H, $J = 8.6$ Hz, 3-H2), 7.10 (d, 2H, $J = 8.8$ Hz, 2-H2), 7.15 (d, 2H, $J = 8.6$ Hz, 3-H3), 7.16-7.21 (m, 4H, ArCH), 7.22-7.31 (m, 7H, ArCH), 7.74 (d, 2H, $J = 8.7$ Hz, ArCH); ESI-MS found m/z 717.3 [M+H]⁺.

***N*-(*N*-(*N*-(Isobutyl-4-aminobenzoyl)-*N*-3-fluorobenzyl-4-aminobenzoyl)-*N*-isobutyl-4-aminobenzoyl)-glycine 44**

> 80% pure by NMR, isolated crude yield: 71 mg; δ_{H} (300 MHz, MeOD) 0.95 (d, 6H, $J = 6.8$ Hz, 3-H γ), 1.02 (d, 6H, $J = 6.4$ Hz, 1-H γ), 1.86 (m, 1H, 3-H β), 1.95 (m, 1H, 1-H β), 2.99 (t, 2H, $J = 7.2$ Hz, 3-H α), 3.83 (t, 2H, $J = 7.2$ Hz, 1-H α), 4.13 (s, 2H, 2-H α), 5.08 (s, 2H, 4-H α), 6.60 (d, 2H, $J = 8.3$ Hz, 2-H3), 6.90 (d, 2H, $J = 8.3$ Hz, 3-H2), 6.96-6.99 (m, 2H, ArCH), 7.02 (d, 1H, $J = 8.9$ Hz, ArCH), 7.13-7.16 (m, 4H, 2-H2, 3-H3), 7.18 (d, 2H, $J = 8.7$ Hz, 1-H3), 7.26 (m, 1H, ArCH), 7.75 (d, 2H, $J = 8.3$ Hz, 1-H2); ESI-HRMS found m/z 651.2960 [M-H]⁻ C₃₈H₄₀FN₄O₅ requires 651.2988.

***N*-(*N*-(*N*-(Benzyl-4-aminobenzoyl)-*N*-4-fluorobenzyl-4-aminobenzoyl)-*N*-isobutyl-4-aminobenzoyl)-glycine 45**

> 80% pure by NMR, isolated crude yield: 62 mg; δ_{H} (300 MHz, MeOD) 0.90 (d, 6H, $J = 6.6$ Hz, 3-H γ), 1.80 (m, 1H, 3-H β), 3.76 (d, 2H, $J = 7.2$ Hz, 3-H α), 4.03 (s, 2H, 2-H α), 4.33 (s, 2H, 1-H α), 4.98 (s, 2H, 4-H α), 6.49 (d, 2H, $J = 8.7$ Hz, 2-H3), 6.79 (d, 2H, $J = 8.3$ Hz, 3-H2), 6.90 (d, 2H, $J = 8.5$ Hz, 2-H2), 6.92 (d, 2H, $J = 8.7$ Hz, ArCH), 7.02 (d, 2H, $J = 8.5$ Hz, ArCH), 7.07 (d, 2H, $J = 8.3$ Hz, ArCH), 7.09 (d, 2H, $J = 8.3$ Hz, ArCH), 7.13 (d, 2H, $J = 8.2$ Hz, ArCH), 7.15 (d, 2H, $J = 8.3$ Hz, ArCH), 7.22 (m, 1H, 1-HAr4), 7.26-7.30 (m, 4H, 1-HAr2,3), 7.67 (d, 2H, $J = 8.3$ Hz, 1-H2); ESI-HRMS found m/z 685.2804 [M-H]⁻ C₄₁H₃₈FN₄O₅ requires 685.2832.

***N*-(*N*-(*N*-(Benzyl-4-aminobenzoyl)-*N*-3-fluorobenzyl-4-aminobenzoyl)-*N*-isobutyl-4-aminobenzoyl)-glycine 46**

> 95% pure by NMR, isolated crude yield: 68 mg; δ_{H} (300 MHz, MeOD) 0.95 (d, 6H, $J = 6.7$ Hz, 3-H γ), 1.84 (m, 1H, 3-H β), 3.82 (d, 2H, $J = 7.4$ Hz, 3-H α), 4.07 (s, 2H, 2-H α), 4.36 (s, 2H, 1-H α), 5.06 (s, 2H, 4-H α), 6.47 (d, 2H, $J = 8.8$ Hz, 2-H3), 6.88 (d, 2H, $J = 8.5$ Hz, 3-H2), 6.92-7.00 (m, 3H, 2-HAr4,5,6), 7.05 (d, 2H, $J = 8.6$ Hz, 2-H2), 7.14 (d, 2H, $J = 8.5$ Hz, 3-H3), 7.16 (d, 2H, $J = 8.6$ Hz, 1-H3), 7.21-7.27 (m, 2H, 1-HAr2), 7.29-7.36 (m, 3H, 1-HAr3,4), 7.34 (s, 1H, 2-HAr2), 7.75 (d, 2H, $J = 8.5$ Hz, 1-H2); ESI-HRMS found m/z 685.2849 [M-H]⁻ C₄₁H₃₈FN₄O₅ requires 685.2832.

***N*-(*N*-(*N*-(Benzyl-4-aminobenzoyl)-*N*-naphth-1-yl-4-aminobenzoyl)-*N*-isobutyl-4-aminobenzoyl)-glycine 47**

> 90% pure by NMR, isolated crude yield: 71 mg; Crude: 85% pure; δ_{H} (300 MHz, MeOD) 0.89 (d, 6H, $J = 6.6$ Hz, 3-H γ), 1.77 (m, 1H, 3-H β), 3.75 (d, 2H, $J = 7.6$ Hz, 3-H α), 4.10 (m, 2H, 1-H α), 4.40 (s, 2H, 2-H α), 5.55 (s, 2H, 4-H α), 6.66 (d, 2H, $J = 8.8$ Hz, 2-H3), 6.67 (d, 2H, $J = 8.5$ Hz, 3-H2), 6.97 (d, 2H, $J = 8.5$ Hz, ArCH), 7.05 (d, 2H, $J = 8.6$ Hz, ArCH), 7.11 (d, 2H, $J = 8.6$ Hz, ArCH), 7.16 (d, 1H, $J = 7.0$ Hz, ArCH), 7.25-7.31 (m, 2H, ArCH), 7.33-7.35 (m, 4H, ArCH), 7.45-7.55 (m, 2H, ArCH), 7.67 (d, 2H, $J = 8.5$ Hz, 1-H2), 7.75 (d, 1H, $J = 8.2$ Hz, ArCH), 7.85 (dd, 1H, $J_1 = 7.2$ Hz and $J_2 = 1.9$ Hz, ArCH), 8.17 (d, 1H, $J = 7.7$ Hz, ArCH); ESI-HRMS found m/z 717.3080 [M-H] $^-$ C₄₅H₄₁N₄O₅ requires 717.3082.

***N*-(*N*-(*N*-(Isobutyl-4-aminobenzoyl)-*N*-3-aminopropyl-4-aminobenzoyl)-*N*-isobutyl-4-aminobenzoyl)-glycine 48**

Purified by column chromatography, > 85% pure by NMR, isolated yield: 6%; δ_{H} (300 MHz, MeOD) 0.91-0.99 (m, 12H, 1-H γ and 3-H γ), 1.73 (m, 1H, 1-H β), 1.82 (m, 2H, 2-H β), 1.88 (m, 1H, 3-H β), 2.95 (m, 2H, 2-H γ), 3.17 (t, 2H, $J = 6.0$ Hz, 2-H α), 3.86 (d, 2H, $J = 8.0$ Hz, 1-H α), 4.09 (m, 2H, 3-H α), 4.88 (s, 2H, 4-H α , under solvent peak), 6.33 (d, 2H, $J = 9.1$ Hz, 2-H3), 6.99 (d, 2H, $J = 8.7$ Hz, 3-H2), 7.03 (d, 2H, $J = 8.7$ Hz, 2-H2), 7.20-7.26 (m, 4H, 3-H3, 1-H3), 7.78 (d, 2H, $J = 8.7$ Hz, 1-H2); ESI-MS m/z 602.4 [M+H] $^+$; ESI-HRMS found m/z 600.3182 [M-H] $^-$ C₃₄H₄₂N₅O₅ requires 600.3191.

***N*-(*N*-(*N*-(Benzyl-4-aminobenzoyl)-*N*-4-fluorobenzyl-4-aminobenzoyl)-*N*-propyl-4-aminobenzoyl)-glycine 49**

> 85% pure by NMR, isolated crude yield: 64 mg; δ_{H} (500 MHz, MeOD) 1.95 (t, 3H, $J = 7.6$ Hz, 3-H γ), 1.63 (m, 2H, 3-H β), 3.91 (t, 2H, $J = 7.6$ Hz, 3-H α), 4.10 (s, 2H, 1-H α), 4.41 (s, 2H, 2-H α), 5.05 (s, 2H, 4-H α), 6.67 (d, 2H, $J = 7.8$ Hz, 2-H3), 6.86 (d, 2H, $J = 8.5$ Hz, 3-H2), 6.98 (t, 2H, $J = 8.8$ Hz, 1-HAr4), 7.12-7.15 (m, 6H, ArCH), 7.21 (dd, 2H, $J_1 = 8.8$ Hz and $J_2 = 5.4$ Hz, ArCH), 7.31 (m, 1H, ArCH), 7.34-7.38 (m, 4H, ArCH), 7.73 (d, 2H, $J = 8.5$ Hz, 1-H2); ESI-HRMS found m/z 671.2653 [M-H] $^-$ C₄₀H₃₆FN₄O₅ requires 671.2675.

***N*-(*N*-(*N*-(3-Fluorobenzyl-4-aminobenzoyl)-*N*-(3-trifluoromethyl)benzyl-4-aminobenzoyl)-*N*-isobutyl-4-aminobenzoyl)-glycine 50**

> 85% pure by NMR, isolated crude yield: 71 mg; δ_{H} (300 MHz, MeOD) 0.95 (d, 6H, $J = 6.6$ Hz, 3-H γ), 1.83 (m, 1H, 3-H β), 3.82 (d, 2H, $J = 7.4$ Hz, 3-H α), 4.14 (s, 2H, 1-H α), 4.37 (s, 2H, 2-H α), 5.17 (s, 2H, 4-H α), 6.37 (d, 2H, $J = 8.8$ Hz, 2-H3), 6.90 (d, 2H, $J = 8.2$ Hz, 3-H2), 6.91 (d, 1H, $J = 8.2$ Hz, 1-HAr6), 7.02 (d, 2H, $J = 8.8$ Hz, 2-H2), 7.15 (d, 2H, $J = 8.5$ Hz, 3-H3), 7.16 (d, 2H, $J = 8.4$ Hz, 1-H3), 7.23 (d, 1H, $J = 8.5$ Hz, ArCH), 7.29 (m, 1H, ArCH), 7.37 (m, 1H, HAr), 7.44 (t, 1H, $J = 8.0$ Hz, 2-HAr5), 7.53 (d, 1H, $J = 8.5$ Hz, 2-HAr4), 7.60 (s, 1H, 2-HAr2), 7.72 (d, 1H, $J = 8.5$ Hz, ArCH), 7.73 (d, 2H, $J = 8.8$ Hz, 1-H2); ESI-HRMS found m/z 755.2832 $[\text{M}+\text{H}]^+$ C₄₂H₃₉F₄N₄O₅ requires 755.2851.

***N*-(*N*-(*N*-(4-Chlorobenzyl-4-aminobenzoyl)-*N*-(3-trifluoromethyl)benzyl-4-aminobenzoyl)-*N*-isobutyl-4-aminobenzoyl)-glycine 51**

> 85% pure by NMR, isolated crude yield: 67 mg; δ_{H} (300 MHz, MeOD) 0.95 (d, 6H, $J = 6.9$ Hz, 3-H γ), 1.84 (m, 1H, 3-H β), 3.83 (d, 2H, $J = 7.1$ Hz, 3-H α), 4.14 (s, 2H, 1-H α), 4.34 (s, 2H, 2-H α), 5.18 (s, 2H, 4-H α), 6.39 (d, 2H, $J = 8.8$ Hz, 2-H3), 6.90 (d, 2H, $J = 8.0$ Hz, 3-H2), 7.02 (d, 2H, $J = 8.8$ Hz, 2-H2), 7.13 (d, 2H, $J = 8.5$ Hz, 3-H3), 7.16 (d, 2H, $J = 8.5$ Hz, 1-H3), 7.28-7.32 (m, 4H, 1-HAr2,3,5,6), 7.37 (d, 1H, $J = 8.2$ Hz, 2-HAr6), 7.44 (t, 1H, $J = 7.9$ Hz, 2-HAr5), 7.53 (d, 1H, $J = 8.2$ Hz, 2-HAr4), 7.60 (s, 1H, 2-HAr2), 7.70 (d, 2H, $J = 8.8$ Hz, 1-H2); ESI-MS found m/z 772.2 $[\text{M}+\text{H}]^+$.

***N*-(*N*-(*N*-(4-Fluorobenzyl-4-aminobenzoyl)-*N*-(3-trifluoromethyl)benzyl-4-aminobenzoyl)-*N*-isobutyl-4-aminobenzoyl)-glycine 52**

> 85% pure by NMR, isolated crude yield: 74 mg; δ_{H} (300 MHz, MeOD) 0.94 (d, 6H, $J = 6.6$ Hz, 3-H γ), 1.84 (m, 1H, 3-H β), 3.82 (d, 2H, $J = 7.3$ Hz, 3-H α), 4.14 (s, 2H, 1-H α), 4.33 (s, 2H, 2-H α), 5.17 (s, 2H, 4-H α), 6.41 (d, 2H, $J = 8.8$ Hz, 2-H3), 6.87-6.92 (m, 2H, ArCH), 6.98-7.07 (m, 2H, ArCH), 7.13-7.17 (m, 4H, ArCH), 7.28 (d, 2H, $J = 8.7$ Hz, ArCH), 7.36 (dd, 1H, $J_1 = 8.8$ Hz and $J_2 = 5.8$ Hz, ArCH), 7.45 (d, 2H, $J = 8.2$ Hz, ArCH), 7.52-7.57 (m, 2H, ArCH), 7.60 (s, 1H, 2-HAr2), 7.70-7.74 (m, 2H, ArCH); ESI-HRMS found m/z 753.2734 $[\text{M}-\text{H}]^-$ C₄₂H₃₇F₄N₄O₅ requires 753.2706.

***N*-(*N*-(*N*-(Benzyl-4-aminobenzoyl)-*N*-5-bromoindol-3-yl-4-aminobenzoyl)-*N*-isobutyl-4-aminobenzoyl)-glycine 53**

> 85% pure by NMR, isolated crude yield: 73 mg; δ_{H} (300 MHz, MeOD) 0.93 (d, 6H, $J = 6.7$ Hz, 3-H γ), 1.86 (m, 1H, 3-H β), 3.81 (d, 2H, $J = 7.4$ Hz, 3-H α), 4.07 (s, 2H, 1-H α), 4.33 (s, 2H, 2-H α), 5.19 (s, 2H, 4-H α), 6.48 (d, 2H, $J = 8.6$ Hz, 2-H3), 6.72 (d, 2H, $J = 8.4$ Hz, 3-H2), 7.00-7.07 (m, 3H, ArCH), 7.10-7.18 (m, 4H, ArCH), 7.23 (d, 2H, $J = 8.9$ Hz, ArCH), 7.28-7.34 (m, 4H, ArCH), 7.71 (d, 2H, $J = 8.5$ Hz, 1-H2), 7.78 (d, 2H, $J = 8.8$ Hz, ArCH); ESI-HRMS found m/z 784.2137 [M-H]⁻ C₄₃H₃₉BrN₅O₅ requires 784.2140.

***N*-(*N*-(*N*-(Benzyl-4-aminobenzoyl)-*N*-cyclohexylmethyl-4-aminobenzoyl)-*N*-isobutyl-4-aminobenzoyl)-glycine 54**

> 80% pure by NMR, isolated crude yield: 69 mg; δ_{H} (300 MHz, MeOD) 0.91 (d, 6H, $J = 6.8$ Hz, 3-H γ), 0.91-0.95 (m, 2H, 2-H ϵ), 1.06-1.11 (m, 4H, 2-H δ,δ'), 1.56-1.66 (m, 5H, 2-H γ,γ',β), 1.82 (m, 1H, 3-H β), 3.68 (d, 2H, $J = 7.2$ Hz, 3-H α), 3.79 (d, 2H, $J = 7.6$ Hz, 2-H α), 4.01 (s, 2H, 1-H α), 4.34 (s, 2H, 4-H α), 6.50 (d, 2H, $J = 8.5$ Hz, 2-H3), 6.91 (d, 2H, $J = 8.3$ Hz, 3-H2), 6.85 (d, 2H, $J = 8.5$ Hz, 2-H2), 7.13 (d, 2H, $J = 8.3$ Hz, 3-H3), 7.14 (d, 2H, $J = 8.3$ Hz, 1-H3), 7.22 (m, 1H, 1-HAr4), 7.26-7.31 (m, 4H, 1-HAr2,3), 7.68 (d, 2H, $J = 8.5$ Hz, 1-H2); ESI-HRMS found m/z 673.3419 [M-H]⁻ C₄₁H₄₅N₄O₅ requires 673.3395.

***N*-(*N*-(*N*-(3-Fluorobenzyl-4-aminobenzoyl)-*N*-phenethyl-4-aminobenzoyl)-*N*-propyl-4-aminobenzoyl)-glycine 55**

> 75% pure by NMR, isolated crude yield: 57 mg; δ_{H} (300 MHz, MeOD) 0.94 (t, 3H, $J = 7.4$ Hz, 3-H γ), 1.62 (m, 2H, 3-H β), 2.86 (t, 2H, $J = 7.4$ Hz, 3-H α), 3.90 (t, 2H, $J = 7.5$ Hz, 2-H β), 3.99 (t, 2H, $J = 7.5$ Hz, 2-H α), 4.04 (s, 2H, 1-H α), 4.34 (s, 2H, 4-H α), 6.43 (d, 2H, $J = 8.7$ Hz, 2-H3), 6.75 (d, 2H, $J = 8.5$ Hz, 3-H2), 6.93 (d, 2H, $J = 8.7$ Hz, 2-H2), 7.12-7.16 (m, 6H, ArCH), 7.22-7.26 (m, 4H, ArCH), 7.29-7.33 (m, 4H, ArCH), 7.74 (d, 2H, $J = 8.7$ Hz, 1-H2); ESI-HRMS found m/z 667.2893 [M-H]⁻ C₄₁H₃₉N₄O₅ requires 667.2926.

***N*-(*N*-(*N*-(Benzyl-4-aminobenzoyl)-*N*-(3-trifluoromethyl)benzyl-4-aminobenzoyl)-*N*-cyclohexylmethyl-4-aminobenzoyl)-glycine 56**

> 90% pure by NMR, isolated crude yield: 72 mg; δ_{H} (300 MHz, MeOD) 1.04 (m, 2H, 3-H ϵ), 1.13-1.23 (m, 4H, 3-H δ , δ'), 1.55 (m, 1H, 3-H β), 1.65-1.74 (m, 4H, 3-H γ , γ'), 3.83 (d, 2H, $J = 7.0$ Hz, 3-H α), 4.07 (s, 2H, 1-H α), 4.37 (s, 2H, 2-H α), 5.14 (s, 2H, 4-H α), 6.51 (d, 2H, $J = 8.8$ Hz, 2-H3), 6.88 (d, 2H, $J = 8.4$ Hz, 3-H2), 7.07 (d, 2H, $J = 8.8$ Hz, 2-H2), 7.12-7.16 (m, 4H, ArCH), 7.30-7.36 (m, 4H, ArCH), 7.41-7.46 (m, 2H, ArCH), 7.53 (d, 1H, $J = 8.6$ Hz, 2-HAr4), 7.59 (s, 1H, 2-HAr2), 7.72 (d, 2H, $J = 8.5$ Hz, 1-H2), 7.99 (s, 1H, NH); ESI-HRMS found m/z 775.3127 [M-H]⁻ C₄₅H₄₂F₃N₄O₅ requires 775.3113.

***N*-(*N*-(*N*-(Cyclopropylmethyl-4-aminobenzoyl)-*N*-phenethyl-4-aminobenzoyl)-*N*-3-fluorobenzyl-4-aminobenzoyl)-glycine 57**

> 95% pure by NMR, isolated crude yield: 68 mg; δ_{H} (300 MHz, CDCl₃) 0.39 (m, 2H, 1-H γ), 0.71 (m, 2H, 1-H γ'), 1.12 (m, 1H, 1-H β), 2.94 (t, 2H, $J = 7.4$ Hz, 2-H β), 3.20 (d, 2H, $J = 7.4$ Hz, 1-H α), 4.11-4.16 (m, 4H, 2-H α and 3-H α), 5.13 (s, 2H, 4-H α), 6.66 (d, 2H, $J = 8.4$ Hz, 2-H3), 6.92 (d, 2H, $J = 8.5$ Hz, 3-H2), 6.96-7.02 (m, 4H, ArCH), 7.15-7.18 (m, 4H, ArCH), 7.22-7.25 (m, 4H, ArCH), 7.27-7.29 (m, 2H, ArCH), 7.32 (d, 2H, $J = 8.5$ Hz, 1-H3), 7.56 (d, 2H, $J = 8.5$ Hz, 1-H2), 8.82 (t, 1H, $J = 5.8$ Hz, Ar-NH); ESI-HRMS found m/z 697.2855 [M-H]⁻ C₄₂H₃₈FN₄O₅ requires 697.2832.

***N*-(*N*-(*N*-(3-Fluorobenzyl-4-aminobenzoyl)-*N*-phenethyl-4-aminobenzoyl)-*N*-cyclopropylmethyl-4-aminobenzoyl)-glycine 58**

> 90% pure by NMR, isolated crude yield: 69 mg; δ_{H} (300 MHz, CDCl₃) 0.19 (m, 2H, 3-H γ), 0.48 (m, 2H, 3-H γ'), 1.06 (m, 1H, 3-H β), 2.92 (t, 2H, $J = 7.5$ Hz, 2-H β), 3.84 (d, 2H, $J = 7.0$ Hz, 3-H α), 4.00 (m, 2H, 1-H α), 4.11 (t, 2H, $J = 7.5$ Hz, 2-H α), 4.42 (s, 2H, 4-H α), 6.64 (d, 2H, $J = 8.5$ Hz, 2-H3), 7.06 (d, 2H, $J = 8.4$ Hz, 3-H2), 7.11-7.19 (m, 10H, ArCH), 7.24-7.28 (m, 4H, ArCH), 7.31-7.35 (m, 1H, ArCH), 7.62 (d, 2H, $J = 8.4$ Hz, 1-H2), 8.78 (t, 1H, $J = 4.8$ Hz, Ar-NH); ESI-HRMS found m/z 697.2859 [M-H]⁻ C₄₂H₃₈FN₄O₅ requires 697.2832.

***N*-(*N*-(*N*-(Phenethyl-4-aminobenzoyl)-*N*-(4-trifluoromethyl)benzyl-4-aminobenzoyl)-*N*-isobutyl-4-aminobenzoyl)-glycine 59**

> 85% pure by NMR, isolated crude yield: 67 mg; δ_{H} (300 MHz, MeOD) 0.94 (d, 6H, $J = 6.7$ Hz, 3-H γ), 1.84 (m, 1H, 3-H β), 2.95 (t, 2H, $J = 7.5$ Hz, 1-H β), 3.45 (t, 2H, $J = 7.5$ Hz, 1-H α), 3.82 (d, 2H, $J = 7.5$ Hz, 3-H α), 4.12 (s, 2H, 2-H α), 5.15 (s, 2H, 4-H α), 6.69 (d, 2H, $J = 8.6$ Hz, 2-H3), 6.92 (d, 2H, $J = 8.5$ Hz, 3-H2), 7.14-7.19 (m, 6H, ArCH), 7.23-7.32 (m, 5H, ArCH), 7.42 (d, 2H, $J = 8.0$ Hz, ArCH), 7.58 (d, 2H, $J = 8.6$ Hz, ArCH), 7.73 (d, 2H, $J = 8.6$ Hz, 1-H2); ESI-HRMS found m/z 749.2967 [M-H]⁻ C₄₃H₄₀F₃N₄O₅ requires 749.2956.

***N*-(*N*-(*N*-(4-Fluorobenzyl-4-aminobenzoyl)-*N*-cyclohexylmethyl-4-aminobenzoyl)-*N*-propyl-4-aminobenzoyl)-glycine 60**

> 85% pure by NMR, isolated crude yield: 60 mg; δ_{H} (300 MHz, MeOD) 0.96 (t, 3H, $J = 7.2$ Hz, 3-H γ), 0.96-1.04 (m, 2H, 2-H ϵ), 1.10-1.19 (m, 2H, 2-H δ), 1.47 (m, 2H, 2-H δ'), 1.60-1.73 (m, 7H, 3H β , 2-H γ,γ',β), 3.73 (d, 2H, $J = 7.1$ Hz, 2-H α), 3.93 (t, 2H, $J = 7.6$ Hz, 3-H α), 4.06 (s, 2H, 1-H α), 4.33 (s, 2H, 4-H α), 6.40 (d, 2H, $J = 8.8$ Hz, 2-H3), 6.93 (d, 2H, $J = 8.5$ Hz, 3-H2), 6.96 (d, 2H, $J = 8.3$ Hz, 1-HAr2), 7.02 (d, 2H, $J = 8.8$ Hz, 2-H2), 7.18 (d, 2H, $J = 8.2$ Hz, 1-HAr3), 7.21 (d, 2H, $J = 8.5$ Hz, 3-H3), 7.35 (d, 2H, $J = 8.5$ Hz, 1-H3), 7.76 (d, 2H, $J = 8.5$ Hz, 1-H2); ESI-HRMS found m/z 677.3129 [M-H]⁻ C₄₀H₄₂FN₄O₅ requires 677.3145.

***N*-(*N*-(*N*-(Benzyl-4-aminobenzoyl)-*N*-isobutyl-4-aminobenzoyl)-*N*-benzyl-4-aminobenzoyl)-glycine 61**

> 75% pure by NMR, isolated crude yield: 58 mg; δ_{H} (500 MHz, CDCl₃) 0.89 (d, 6H, $J = 6.7$ Hz, 2-H γ), 1.81 (m, 1H, 2-H β), 3.78 (d, 2H, $J = 7.6$ Hz, 3-H α), 3.97 (d, 2H, $J = 5.7$ Hz, 1-H α), 4.41 (s, 2H, 2-H α), 5.13 (s, 2H, 4-H α), 6.85 (d, 2H, $J = 8.6$ Hz, 2-H3), 6.88 (d, 2H, $J = 8.5$ Hz, 3-H2), 7.11 (d, 2H, $J = 8.6$ Hz, 2-H2), 7.16 (d, 2H, $J = 8.5$ Hz, 3-H3), 7.20 (d, 2H, $J = 8.4$ Hz, 1-H3), 7.24-7.32 (m, 10H, ArCH), 7.52 (d, 2H, $J = 8.4$ Hz, 1-H2), 7.78 (t, 1H, $J = 6.0$ Hz, Ar-NH); ESI-HRMS found m/z 667.2926 [M-H]⁻ C₄₁H₃₉N₄O₅ requires 667.2926.

***N*-(*N*-(*N*-(Benzyl-4-aminobenzoyl)-*N*-naphth-2-yl-4-aminobenzoyl)-*N*-cyclopropylmethyl-4-aminobenzoyl)-glycine 62**

> 80% pure by NMR, isolated crude yield: 66 mg; δ_{H} (300 MHz, CDCl₃) 0.15 (m, 2H, 3-H γ), 0.43 (m, 2H, 3-H γ'), 0.86 (m, 1H, 3-H β), 3.78 (d, 2H, $J = 7.0$ Hz, 3-H α), 3.96 (d, 2H, $J = 4.9$ Hz, 1-H α), 4.40 (s, 2H, 2-H α), 5.22 (s, 2H, 4-H α), 6.75 (d, 2H, $J = 8.4$ Hz, 2-H β), 6.99 (d, 2H, $J = 8.2$ Hz, 3-H β), 7.06-7.11 (m, 4H, ArCH), 7.24 (s, 1H, 2-HAr₂), 7.34-7.37 (m, 5H, ArCH), 7.44-7.47 (m, 3H, ArCH), 7.59-7.65 (m, 3H, ArCH), 7.77 (d, 2H, $J = 8.8$ Hz, 1-H β), 7.74-7.81 (m, 2H, ArCH); ESI-HRMS found m/z 715.2929 [M-H]⁻ C₄₅H₃₉N₄O₅ requires 715.2926.

***N*-(*N*-(*N*-(4-Chlorobenzyl-4-aminobenzoyl)-*N*-naphth-2-yl-4-aminobenzoyl)-*N*-cyclopropylmethyl-4-aminobenzoyl)-glycine 63**

> 90% pure by NMR, isolated crude yield: 71 mg; δ_{H} (500 MHz, CDCl₃) 0.42 (m, 2H, 3-H γ), 0.72 (m, 2H, 3-H γ'), 0.86 (m, 1H, 3-H β), 3.19 (d, 2H, $J = 7.4$ Hz, 3-H α), 4.09 (d, 2H, $J = 5.2$ Hz, 1-H α), 5.07 (s, 2H, 2-H α), 5.27 (s, 2H, 4-H α), 6.81 (d, 2H, $J = 8.2$ Hz, 2-H β), 6.88 (d, 2H, $J = 8.2$ Hz, 3-H β), 7.13-7.19 (m, 4H, ArCH), 7.25 (d, 2H, $J = 8.4$ Hz, ArCH), 7.33-7.39 (m, 5H, ArCH), 7.45-7.48 (m, 2H, ArCH), 7.59 (d, 2H, $J = 8.2$ Hz, ArCH), 7.66 (s, 1H, 2-HAr₂), 7.78 (d, 2H, $J = 8.4$ Hz, 1-H β), 7.78-7.82 (m, 1H, ArCH), 7.95 (t, 1H, $J = 5.2$ Hz, Ar-NH); ESI-HRMS found m/z 749.2560 [M-H]⁻ C₄₅H₃₈ClN₄O₅ requires 749.2536.

***N*-(*N*-(*N*-((3-Trifluoromethyl)benzyl-4-aminobenzoyl)-*N*-(3-trifluoromethyl)benzyl-4-aminobenzoyl)-*N*-benzyl-4-aminobenzoyl)-glycine 64**

> 90% pure by NMR, isolated crude yield: 83 mg; δ_{H} (300 MHz, MeOD) 4.05 (s, 2H, 3-H α), 4.43 (s, 2H, 1-H α), 5.14 (s, 2H, 2-H α), 5.16 (s, 2H, 4-H α), 6.36 (d, 2H, $J = 8.8$ Hz, 2-H β), 6.89 (d, 2H, $J = 8.5$ Hz, 3-H β), 7.00 (d, 2H, $J = 8.5$ Hz, 3-H β), 7.01 (d, 2H, $J = 8.6$ Hz, 2-H β), 7.21 (d, 2H, $J = 8.5$ Hz, 1-H β), 7.24-7.28 (m, 6H, ArCH), 7.37 (d, 1H, $J = 7.8$ Hz, ArCH), 7.42 (d, 1H, $J = 7.7$ Hz, ArCH), 7.46-7.51 (m, 2H, ArCH), 7.57-7.59 (m, 3H, ArCH), 7.63 (d, 2H, $J = 8.6$ Hz, 1-H β); ESI-HRMS found m/z 837.2558 [M-H]⁻ C₄₆H₃₅F₆N₄O₅ requires 837.2517.

***N*-(*N*-(*N*-(4-Chlorobenzyl-4-aminobenzoyl)-*N*-naphth-2-yl-4-aminobenzoyl)-*N*-cyclopropylmethyl-4-aminobenzoyl)-glycine 65**

> 95% pure by NMR, isolated crude yield: 73 mg; δ_{H} (300 MHz, MeOD) 0.14 (m, 2H, 3-H γ), 0.45 (m, 2H, 3-H γ'), 1.06 (m, 1H, 3-H β), 3.81 (d, 2H, $J = 7.1$ Hz, 3-H α), 4.09 (s, 2H, 1-H α), 4.36 (s, 2H, 2-H α), 5.14 (s, 2H, 4-H α), 6.45 (d, 2H, $J = 8.8$ Hz, 2-H3), 6.88 (d, 2H, $J = 8.4$ Hz, 3-H2), 7.05 (d, 2H, $J = 8.8$ Hz, 2-H2), 7.17 (d, 2H, $J = 8.4$ Hz, 3-H3), 7.19 (d, 2H, $J = 8.5$ Hz, 1-H3), 7.30-7.33 (m, 4H, 1-HAr2,3), 7.37 (d, 1H, $J = 7.6$ Hz, 2-HAr6), 7.43 (t, 1H, $J = 7.6$ Hz, 2-HAr5), 7.53 (d, 1H, $J = 7.5$ Hz, 2-HAr4), 7.59 (s, 1H, 2-HAr2), 7.73 (d, 2H, $J = 8.5$ Hz, 1-H2); ESI-HRMS found m/z 767.2263 [M-H]⁻ C₄₂H₃₅ClF₃N₄O₅ requires 767.2254.

***N*-(*N*-(*N*-(4-Fluorobenzyl-4-aminobenzoyl)-*N*-naphth-2-yl-4-aminobenzoyl)-*N*-propyl-4-aminobenzoyl)-glycine 66**

> 90% pure by NMR, isolated crude yield: 69 mg; δ_{H} (300 MHz, MeOD) 0.91 (t, 3H, $J = 7.4$ Hz, 3-H γ), 1.59 (m, 2H, 3-H β), 3.87 (t, 2H, $J = 7.5$ Hz, 3-H α), 4.09 (s, 2H, 1-H α), 4.33 (s, 2H, 2-H α), 5.23 (s, 2H, 4-H α), 6.41 (d, 2H, $J = 8.8$ Hz, 2-H3), 6.88 (d, 2H, $J = 8.5$ Hz, 3-H2), 6.89 (d, 2H, $J = 8.5$ Hz, ArCH), 7.11 (d, 2H, $J = 8.5$ Hz, ArCH), 7.12 (d, 2H, $J = 8.8$ Hz, ArCH), 7.28 (d, 1H, $J = 8.8$ Hz, ArCH), 7.33-7.38 (m, 2H, ArCH), 7.42-7.47 (m, 4H, ArCH), 7.63 (d, 2H, $J = 8.2$ Hz, 1-H3), 7.70 (d, 1H, $J = 8.5$ Hz, ArCH), 7.72 (d, 1H, $J = 8.5$ Hz, ArCH), 7.79 (d, 2H, $J = 8.2$ Hz, 1-H2); ESI-HRMS found m/z 721.2843 [M-H]⁻ C₄₄H₃₈FN₄O₅ requires 721.2832.

***N*-(*N*-(*N*-(Naphth-2-yl-4-aminobenzoyl)-*N*-isobutyl-4-aminobenzoyl)-*N*-benzyl-4-aminobenzoyl)-glycine 67**

~ 70% pure by NMR, isolated crude yield: 61 mg; δ_{H} (300 MHz, CDCl₃) 0.89 (d, 6H, $J = 6.6$ Hz, 2-H γ), 1.82 (m, 1H, 2-H β), 3.67 (d, 2H, $J = 7.6$ Hz, 2-H α), 4.22 (s, 2H, 1-H α), 4.58 (s, 2H, 3-H α), 5.14 (s, 2H, 4-H α), 6.76 (d, 2H, $J = 8.8$ Hz, 2-H3), 6.83-6.91 (m, 4H, ArCH), 7.08-7.22 (m, 5H, ArCH), 7.27-7.32 (m, 2H, ArCH), 7.46 (d, 2H, $J = 8.5$ Hz, ArCH), 7.48-7.54 (m, 4H, ArCH), 7.62 (s, 1H, ArCH), 7.72 (m, 1H, ArCH), 7.77-7.85 (m, 3H, ArCH); ESI-MS found m/z 717.2 [M-H]⁻.

***N*-(*N*-(*N*-(4-Fluorobenzyl-4-aminobenzoyl)-*N*-(4-fluorobenzyl)-4-aminobenzoyl)-*N*-isobutyl-4-aminobenzoyl)-glycine 68**

~70% pure by NMR, no identifiable impurity on LC-MS; isolated crude yield: 62 mg; δ_{H} (300 MHz, MeOD) 0.95 (d, 6H, $J = 6.6$ Hz, 3-H γ), 1.85 (m, 1H, 3-H β), 3.82 (d, 2H, $J = 7.4$ Hz, 3-H α), 4.09 (s, 2H, 2-H α), 4.36 (s, 2H, 1-H α), 5.03 (s, 2H, 4-H α), 6.37 (d, 2H, $J = 9.0$ Hz, 2-H3), 6.84 (d, 2H, $J = 8.5$ Hz, 3-H2), 6.95 (d, 2H, $J = 8.8$ Hz, ArCH), 7.01 (d, 2H, $J = 8.8$ Hz, ArCH), 7.01-7.06 (m, 2H, ArCH), 7.13 (d, 2H, $J = 8.5$ Hz, ArCH), 7.14-7.20 (m, 6H, ArCH), 7.75 (d, 2H, $J = 8.5$ Hz, 1-H2); ESI-MS found m/z 703.1 [M-H]⁻; ESI-HRMS found m/z 705.2893 [M+H]⁺ C₄₁H₃₉F₂N₄O₅ requires 705.2883.

***N*-(*N*-(*N*-(4-Fluorobenzyl-4-aminobenzoyl)-*N*-(3-fluorobenzyl)-4-aminobenzoyl)-*N*-isobutyl-4-aminobenzoyl)-glycine 69**

> 85% pure by NMR, no identifiable impurity on LC-MS; isolated crude yield: 63 mg; δ_{H} (300 MHz, MeOD) 0.95 (d, 6H, $J = 6.6$ Hz, 3-H γ), 1.84 (m, 1H, 3-H β), 3.83 (d, 2H, $J = 7.4$ Hz, 3-H α), 4.08 (s, 2H, 2-H α), 4.32 (s, 2H, 1-H α), 5.06 (s, 2H, 4-H α), 6.38 (d, 2H, $J = 8.8$ Hz, 2-H3), 6.87 (d, 2H, $J = 8.5$ Hz, 3-H2), 6.92-6.98 (m, 3H, ArCH), 7.01-7.03 (m, 4H, ArCH), 7.14 (d, 2H, $J = 8.2$ Hz, ArCH), 7.16 (d, 2H, $J = 8.2$ Hz, ArCH), 7.23 (m, 1H, ArCH), 7.33-7.37 (m, 2H, ArCH), 7.73 (d, 2H, $J = 8.8$ Hz, 1-H2); ESI-MS found m/z 703.1 [M-H]⁻; ESI-HRMS found m/z 727.2716 [M+Na]⁺ C₄₁H₃₈F₂N₄NaO₅ requires 727.2702.

***N*-(*N*-(*N*-(Benzyl-4-aminobenzoyl)-*N*-(3-trifluoromethyl)benzyl-4-aminobenzoyl)-*N*-2-methylbutyl-4-aminobenzoyl)-glycine 70**

> 85% pure by NMR, isolated crude yield: 71 mg; δ_{H} (300 MHz, MeOD) 0.88 (t, 3H, $J = 7.4$ Hz, 3-H δ), 0.93 (d, 3H, $J = 6.6$ Hz, 3-H ϵ), 1.18 (m, 1H, 3-H β), 1.46 (m, 1H, 3-H γ), 1.60 (m, 1H, 3-H γ'), 3.87 (d, 2H, $J = 7.4$ Hz, 3-H α), 4.07 (s, 2H, 1-H α), 4.36 (s, 2H, 2-H α), 5.14 (s, 2H, 4-H α), 6.47 (d, 2H, $J = 8.6$ Hz, 2-H3), 6.89 (d, 2H, $J = 8.5$ Hz, 3-H2), 7.06 (d, 2H, $J = 8.6$ Hz, 2-H2), 7.14 (d, 2H, $J = 8.5$ Hz, 3-H3), 7.15 (d, 2H, $J = 8.5$ Hz, 1-H3), 7.25 (m, 1H, 1-HAr4), 7.29-7.35 (m, 4H, 1-HAr2,3), 7.37 (d, 1H, $J = 8.2$ Hz, 2-HAr6), 7.44 (t, 1H, $J = 7.5$ Hz, 2-HAr5), 7.53 (d, 1H, $J = 7.4$ Hz, 2-HAr4), 7.60 (s, 1H, 2-HAr2), 7.72 (d, 2H, $J = 8.5$ Hz, 1-H2); ESI-MS found m/z 749.2 [M-H]⁻; ESI-HRMS found m/z 773.2936 [M+Na]⁺ C₄₃H₄₁F₃NaN₄O₅ requires 773.2921.

***N*-(*N*-(*N*-(Benzyl-4-aminobenzoyl)-*N*-(4-trifluoromethyl)benzyl-4-aminobenzoyl)-*N*-2-methylbutyl-4-aminobenzoyl)-glycine 71**

> 95% pure by NMR, isolated crude yield: 68 mg; δ_{H} (300 MHz, MeOD) 0.88 (t, 3H, $J = 7.3$ Hz, 3-H δ), 0.93 (d, 3H, $J = 6.9$ Hz, 3-H ϵ), 1.19 (m, 1H, 3-H β), 1.45 (m, 1H, 3-H γ), 1.61 (m, 1H, 3-H γ'), 3.87 (d, 2H, $J = 7.4$ Hz, 3-H α), 4.07 (s, 2H, 1-H α), 4.37 (s, 2H, 2-H α), 5.13 (s, 2H, 4-H α), 6.47 (d, 2H, $J = 8.8$ Hz, 2-H3), 6.91 (d, 2H, $J = 8.4$ Hz, 3-H2), 7.05 (d, 2H, $J = 8.8$ Hz, 2-H2), 7.14 (d, 2H, $J = 8.4$ Hz, 3-H3), 7.16 (d, 2H, $J = 8.5$ Hz, 1-H3), 7.25 (m, 1H, 1-HAr4), 7.29-7.36 (m, 4H, 1-HAr2,3), 7.41 (d, 2H, $J = 8.2$ Hz, 2-HAr2), 7.57 (d, 2H, $J = 8.2$ Hz, 2-HAr4), 7.73 (d, 2H, $J = 8.5$ Hz, 1-H2); ESI-HRMS found m/z 751.3081 [M+H]⁺ C₄₃H₄₂F₃N₄O₅ requires 751.3102.

***N*-(*N*-(*N*-(4-Fluorobenzyl-4-aminobenzoyl)-*N*-(3-trifluoromethyl)benzyl-4-aminobenzoyl)-*N*-2-methylbutyl-4-aminobenzoyl)-glycine 72**

> 95% pure by NMR, isolated crude yield: 73 mg; δ_{H} (300 MHz, MeOD) 0.88 (t, 3H, $J = 7.4$ Hz, 3-H δ), 0.93 (d, 3H, $J = 6.9$ Hz, 3-H ϵ), 1.18 (m, 1H, 3-H β), 1.46 (m, 1H, 3-H γ), 1.59 (m, 1H, 3-H γ'), 3.87 (d, 2H, $J = 7.4$ Hz, 3-H α), 4.08 (s, 2H, 1-H α), 4.35 (s, 2H, 2-H α), 5.14 (s, 2H, 4-H α), 6.45 (d, 2H, $J = 8.6$ Hz, 2-H3), 6.88 (d, 2H, $J = 8.2$ Hz, 3-H2), 7.03 (d, 2H, $J = 8.6$ Hz, 2-H2), 7.06 (d, 2H, $J = 8.2$ Hz, 3-H3), 7.15 (d, 2H, $J = 8.5$ Hz, ArCH), 7.16 (d, 2H, $J = 8.5$ Hz, ArCH), 7.36 (d, 1H, $J = 8.2$ Hz, 2-HAr6), 7.37 (d, 2H, $J = 8.2$ Hz, 1-HAr3), 7.44 (t, 1H, $J = 7.7$ Hz, 2-HAr5), 7.53 (d, 1H, $J = 7.7$ Hz, 2-HAr4), 7.60 (s, 1H, 2-HAr2), 7.72 (d, 2H, $J = 8.5$ Hz, 1-H2); ESI-MS found m/z 767.3 [M-H]⁻; ESI-HRMS found m/z 767.2872 [M-H]⁻ C₄₃H₃₉F₄N₄O₅ requires 767.2862.

***N*-(*N*-(*N*-(Phenethyl-4-aminobenzoyl)-*N*-(3-trifluoromethyl)benzyl-4-aminobenzoyl)-*N*-2-methylbutyl-4-aminobenzoyl)-glycine 73**

> 95% pure by NMR, isolated crude yield: 67 mg; δ_{H} (300 MHz, MeOD) 0.87 (t, 3H, $J = 7.4$ Hz, 3-H δ), 0.92 (d, 3H, $J = 6.6$ Hz, 3-H ϵ), 1.18 (m, 1H, 3-H β), 1.45 (m, 1H, 3-H γ), 1.60 (m, 1H, 3-H γ'), 2.92 (t, 2H, $J = 7.45$ Hz, 1-H β), 3.41 (t, 2H, $J = 7.45$ Hz, 1-H α), 3.86 (d, 2H, $J = 7.2$ Hz, 3-H α), 4.11 (s, 2H, 2-H α), 5.15 (s, 2H, 4-H α), 6.55 (d, 2H, $J = 8.5$ Hz, 2-H3), 6.89 (d, 2H, $J = 8.2$ Hz, 3-H2), 7.12 (d, 2H, $J = 8.5$ Hz, 2-H2), 7.15 (d, 2H, $J = 8.2$ Hz, 3-H3), 7.17 (d, 2H, $J = 8.5$ Hz, 1-H3), 7.23 (m, 1H, 1-HAr4), 7.27-7.30 (m, 4H, 1-HAr2-3), 7.38 (d, 1H, $J = 8.0$ Hz, 2-HAr6), 7.45 (t, 1H, $J = 7.7$ Hz, 2-HAr5), 7.55 (d, 1H, $J = 7.7$ Hz, 2-HAr4), 7.61 (s, 1H, 2-HAr2), 7.73 (d, 2H, $J =$

8.5 Hz, 1-H₂); ESI-MS found m/z 766.0 [M+H]⁺; ESI-HRMS found m/z 763.3126 [M-H]⁻ C₄₄H₄₂F₃N₄O₅ requires 763.3113.

***N*-(*N*-(*N*-(4-Chlorobenzyl-4-aminobenzoyl)-*N*-(4-trifluoromethyl)benzyl-4-aminobenzoyl)-*N*-(2-methyl)butyl-4-aminobenzoyl)-glycine 74**

> 95% pure by NMR, isolated crude yield: 76 mg; δ_{H} (300 MHz, MeOD) 0.88 (t, 3H, $J = 7.4$ Hz, 3-H δ), 0.93 (d, 3H, $J = 6.7$ Hz, 3-H ϵ), 1.19 (m, 1H, 3-H β), 1.46 (m, 1H, 3-H γ), 1.60 (m, 1H, 3-H γ'), 3.87 (d, 2H, $J = 7.4$ Hz, 3-H α), 4.08 (s, 2H, 1-H α), 4.35 (s, 2H, 2-H α), 5.13 (s, 2H, 4-H α), 6.41 (d, 2H, $J = 8.7$ Hz, 2-H₃), 6.90 (d, 2H, $J = 8.2$ Hz, 3-H₂), 7.03 (d, 2H, $J = 8.7$ Hz, 2-H₂), 7.15 (d, 2H, $J = 8.2$ Hz, 3-H₃), 7.17 (d, 2H, $J = 8.5$ Hz, 1-H₃), 7.29-7.33 (m, 4H, 1-HAr_{2,3}), 7.40 (d, 2H, $J = 8.0$ Hz, 2-HAr₂), 7.57 (d, 2H, $J = 8.2$ Hz, 2-HAr₃), 7.70 (d, 2H, $J = 8.5$ Hz, 1-H₂); ESI-HRMS found m/z 783.2554 [M-H]⁻ C₄₃H₃₉ClF₃N₄O₅ requires 783.2567.

***N*-(*N*-(*N*-(Phenethyl-4-aminobenzoyl)-*N*-(4-trifluoromethyl)benzyl-4-aminobenzoyl)-*N*-(2-methyl)butyl-4-aminobenzoyl)-glycine 75**

> 95% pure by NMR, isolated crude yield: 70 mg; δ_{H} (300 MHz, MeOD) 0.87 (t, 3H, $J = 7.4$ Hz, 3-H δ), 0.92 (d, 3H, $J = 6.6$ Hz, 3-H ϵ), 1.18 (m, 1H, 3-H β), 1.45 (m, 1H, 3-H γ), 1.59 (m, 1H, 3-H γ'), 2.92 (t, 2H, $J = 7.5$ Hz, 1-H β), 3.39 (t, 2H, $J = 7.5$ Hz, 1-H α), 3.86 (d, 2H, $J = 7.4$ Hz, 3-H α), 4.11 (s, 2H, 2-H α), 5.14 (s, 2H, 4-H α), 6.52 (d, 2H, $J = 8.8$ Hz, 2-H₃), 6.92 (d, 2H, $J = 8.5$ Hz, 3-H₂), 7.11 (d, 2H, $J = 8.5$ Hz, 2-H₂), 7.16 (d, 2H, $J = 8.5$ Hz, 3-H₃), 7.18 (d, 2H, $J = 8.5$ Hz, 1-H₃), 7.22 (m, 1H, 1-HAr₄), 7.25-7.30 (m, 4H, 1-HAr_{2,3}), 7.42 (d, 2H, $J = 8.1$ Hz, 2-HAr₂), 7.58 (d, 2H, $J = 8.1$ Hz, 2-HAr₃), 7.75 (d, 2H, $J = 8.2$ Hz, 1-H₂); δ_{C} (75 MHz, MeOD) 11.52, 17.35, 28.01, 34.61, 36.31, 42.39, 45.75, 54.17, 56.27, 112.07, 122.48, 126.39, 127.29, 128.31, 129.10, 129.50, 129.86, 129.90, 130.24, 130.73, 132.33, 135.69, 140.92, 143.25, 146.42, 147.33, 152.15, 169.34, 171.98, 172.47, 173.17; $\nu_{\text{max}}/\text{cm}^{-1}$ (solid state) = ~3016 (COOH), 1738 (CO), 1365 (C-N), 1217 (C-O); ESI-HRMS found m/z 763.3108 [M-H]⁻ C₄₄H₄₂F₃N₄O₅ requires 763.3113.

***N*-(*N*-(*N*-(4-Chlorobenzyl-4-aminobenzoyl)-*N*-(3-fluorobenzyl-4-aminobenzoyl)-*N*-2-methylbutyl-4-aminobenzoyl)-glycine 76**

> 90% pure by NMR, isolated crude yield: 66 mg; δ_{H} (300 MHz, MeOD) 0.91 (t, 3H, $J = 7.8$ Hz, 3-H δ), 0.93 (d, 3H, $J = 6.9$ Hz, 3-H ϵ), 1.19 (m, 1H, 3-H β), 1.45 (m, 1H, 3-

H γ), 1.61 (m, 1H, 3-H γ'), 3.87 (d, 2H, J = 7.4 Hz, 3-H α), 4.08 (s, 2H, 1-H α), 4.33 (s, 2H, 2-H α), 5.06 (s, 2H, 4-H α), 6.38 (d, 2H, J = 8.5 Hz, 2-H3), 6.87 (d, 2H, J = 8.2 Hz, 3-H2), 6.93 (d, 2H, J = 7.6 Hz, ArCH), 6.97 (d, 2H, J = 8.2 Hz, ArCH), 7.02 (d, 2H, J = 8.5 Hz, ArCH), 7.14 (d, 2H, J = 8.2 Hz, ArCH), 7.15 (d, 2H, J = 8.2 Hz, ArCH), 7.25 (t, 1H, J = 7.8 Hz, 2-HAr5), 7.29 (d, 1H, J = 7.8 Hz, 2-HAr6), 7.31 (s, 1H, 2-HAr2), 7.41 (d, 1H, J = 7.7 Hz, 2-HAr4), 7.72 (d, 2H, J = 8.5 Hz, 1-H2); ESI-MS found m/z 733.4 [M-H]⁻; ESI-HRMS found m/z 733.2605 [M-H]⁻. C₄₂H₃₉ClFN₄O₅ requires 733.2598.

***N*-(*N*-(*N*-(4-Chlorobenzyl-4-aminobenzoyl)-*N*-4-chlorobenzyl-4-aminobenzoyl)-*N*-(2-methyl)butyl-4-aminobenzoyl)-glycine 77**

> 75% pure by NMR, isolated crude yield: 71 mg; δ_H (300 MHz, MeOD) 0.87-0.94 (m, 6H, 3-H δ,ϵ), 1.19 (m, 1H, 3-H β), 1.44 (m, 1H, 3-H γ), 1.60 (m, 1H, 3-H γ'), 3.85 (d, 2H, J = 7.5 Hz, 3-H α), 4.14 (s, 2H, 1-H α), 4.33 (s, 2H, 2-H α), 5.06 (s, 2H, 4-H α), 6.37 (d, 2H, J = 8.8 Hz, 2-H3), 6.88 (d, 2H, J = 8.0 Hz, 3-H2), 7.12-7.18 (m, 6H, ArCH), 7.21-7.28 (m, 6H, ArCH), 7.29 (d, 2H, J = 8.8 Hz, ArCH), 7.72 (d, 2H, J = 8.2 Hz, 1-H2); ESI-MS found m/z 749.7 [M-H]⁻; ESI-HRMS found m/z 749.2283 [M-H]⁻. C₄₂H₃₉Cl₂N₄O₅ requires 749.2303.

***N*-(*N*-(*N*-(4-Fluorobenzyl-4-aminobenzoyl)-*N*-(4-trifluoromethyl)benzyl-4-aminobenzoyl)-*N*-isobutyl-4-aminobenzoyl)-glycine 78**

> 90% pure by NMR, isolated crude yield: 71 mg; δ_H (300 MHz, MeOD) 0.94 (d, 6H, J = 6.6 Hz, 3-H γ), 1.84 (m, 1H, 3-H β), 3.82 (d, 2H, J = 7.3 Hz, 3-H α), 4.08 (s, 2H, 1-H α), 4.36 (s, 2H, 2-H α), 5.13 (s, 2H, 4-H α), 6.48 (d, 2H, J = 8.8 Hz, 2-H3), 6.90 (d, 2H, J = 8.4 Hz, 3-H2), 7.02-7.08 (m, 4H, ArCH), 7.13-7.18 (m, 4H, ArCH), 7.34-7.37 (m, 2H, ArCH), 7.40 (d, 2H, J = 7.7 Hz, ArCH), 7.56 (d, 2H, J = 8.2 Hz, ArCH), 7.73 (d, 2H, J = 8.5 Hz, 1-H2); ESI-HRMS found m/z 753.2729 [M-H]⁻. C₄₂H₃₇F₄N₄O₅ requires 753.2706.

***N*-(*N*-(*N*-(4-Fluorobenzyl-4-aminobenzoyl)-*N*-(4-trifluoromethyl)benzyl-4-aminobenzoyl)-*N*-cyclopropylmethyl-4-aminobenzoyl)-glycine 79**

> 90% pure by NMR, isolated crude yield: 65 mg; δ_H (300 MHz, MeOD) 0.14 (m, 2H, 3-H γ), 0.45 (m, 2H, 3-H γ'), 1.06 (m, 1H, 3-H β), 3.82 (d, 2H, J = 7.0 Hz, 3-H α), 4.08 (s, 2H, 1-H α), 4.35 (s, 2H, 2-H α), 5.13 (s, 2H, 4-H α), 6.45 (d, 2H, J = 8.8 Hz, 2-H3), 6.89 (d, 2H, J = 8.4 Hz, 3-H2), 7.02-7.10 (m, 4H, ArCH), 7.16-7.21 (m, 4H, 2-

H2 and 3-H3), 7.34 (m, 2H, ArCH), 7.40 (d, 2H, $J = 7.7$ Hz, ArCH), 7.56 (d, 2H, $J = 8.0$ Hz, 2-HAr3), 7.75 (d, 2H, $J = 8.5$ Hz, 1-H2); ESI-HRMS found m/z 751.2535 [M-H]⁻ C₄₂H₃₇F₄N₄O₅ requires 751.2549.

***N*-(*N*-(*N*-(Benzyl-4-aminobenzoyl)-*N*-(3-trifluoromethyl)benzyl-4-aminobenzoyl)-*N*-propyl-4-aminobenzoyl)-glycine 80**

> 90% pure by NMR, isolated crude yield: 69 mg; δ_{H} (300 MHz, MeOD) 0.94 (t, 3H, $J = 7.4$ Hz, 3-H γ), 1.61 (m, 2H, 3-H β), 3.89 (t, 2H, $J = 7.5$ Hz, 3-H α), 4.07 (s, 2H, 1-H α), 4.37 (s, 2H, 2-H α), 5.14 (s, 2H, 4-H α), 6.51 (d, 2H, $J = 8.8$ Hz, 2-H3), 6.87 (d, 2H, $J = 8.4$ Hz, 3-H2), 7.06 (d, 2H, $J = 8.8$ Hz, 2-H2), 7.12-7.17 (m, 6H, ArCH), 7.32-7.35 (m, 4H, ArCH), 7.43 (t, 1H, $J = 7.8$ Hz, 2-HAr4), 7.53 (d, 1H, $J = 8.1$ Hz, ArCH), 7.59 (s, 1H, 2-HAr2), 7.73 (d, 2H, $J = 8.5$ Hz, 1-H2); ESI-HRMS found m/z 721.2651 [M-H]⁻ C₄₁H₃₆F₃N₄O₅ requires 721.2643.

***N*-(*N*-(*N*-(Cyclohexylmethyl-4-aminobenzoyl)-*N*-naphth-2-yl-4-aminobenzoyl)-*N*-phenethyl-4-aminobenzoyl)-glycine 81**

> 85% pure by NMR, isolated crude yield: 75 mg; δ_{H} (300 MHz, CDCl₃) 1.04 (m, 2H, 1-H ϵ), 1.23-1.36 (m, 4H, 1-H δ, δ'), 1.65-1.89 (m, 5H, 1-H γ, γ', β), 2.93 (t, 2H, $J = 8.2$ Hz, 3-H β), 2.99 (d, 2H, $J = 6.9$ Hz, 1-H α), 4.10 (t, 2H, $J = 8.2$ Hz, 3-H α), 4.13 (s, 2H, 2-H α), 5.25 (s, 2H, 4-H α), 6.56 (d, 2H, $J = 8.2$ Hz, 2-H3), 6.91 (d, 2H, $J = 8.3$ Hz, 3-H2), 6.93 (d, 2H, $J = 8.2$ Hz, 2-H2), 7.07 (d, 2H, $J = 8.3$ Hz, 3-H3), 7.13 (d, 2H, $J = 8.7$ Hz, 1-H3), 7.16-7.20 (m, 2H, 3-HAr2), 7.21-7.28 (m, 3H, 3-HAr3,4), 7.36 (d, 1H, $J = 8.2$ Hz, ArCH), 7.44-7.48 (m, 2H, ArCH), 7.64 (s, 1H, 2-HAr1), 7.66 (d, 2H, $J = 8.7$ Hz, 1-H2), 7.73-7.83 (m, 3H, ArCH); ESI-MS found m/z 773.4 [M+H]⁺; ESI-HRMS found m/z 771.3543 [M-H]⁻ C₄₉H₄₇N₄O₅ requires 771.3552.

***N*-(*N*-(*N*-(Benzyl-4-aminobenzoyl)-*N*-(3-trifluoromethyl)benzyl-4-aminobenzoyl)-*N*-cyclopropylmethyl-4-aminobenzoyl)-glycine 82**

> 75% pure by NMR, isolated crude yield: 70 mg; δ_{H} (500 MHz, CDCl₃) 0.17 (m, 2H, 3-H γ), 0.46 (m, 2H, 3-H γ'), 1.05 (m, 1H, 3-H β), 3.81 (d, 2H, $J = 7.1$ Hz, 3-H α), 3.99 (d, 2H, $J = 4.2$ Hz, 1-H α), 4.44 (s, 2H, 2-H α), 5.12 (s, 2H, 4-H α), 6.74 (d, 2H, $J = 8.2$ Hz, 2-H3), 7.03 (d, 2H, $J = 8.0$ Hz, 3-H2), 7.12 (d, 2H, $J = 8.0$ Hz, ArCH), 7.14 (d, 2H, $J = 8.0$ Hz, ArCH), 7.25 (d, 2H, $J = 8.5$ Hz, ArCH), 7.34-7.37 (m, 5H, 1-HAr2-4), 7.39 (d, 2H, $J = 8.0$ Hz, 1-H3), 7.52 (m, 2H, ArCH), 7.60 (d, 2H, $J = 8.0$ Hz, 1-H2),

7.75 (m, 1H, Ar-NH); ESI-HRMS found m/z 733.2672 [M-H]⁻ C₄₂H₃₆F₃N₄O₅ requires 733.2643.

***N*-(*N*-(*N*-(Phenethyl-4-aminobenzoyl)-*N*-3-fluorobenzyl-4-aminobenzoyl)-*N*-2-isobutyl-4-aminobenzoyl)-glycine 83**

> 80% pure by NMR, isolated crude yield: 49 mg; δ_{H} (300 MHz, MeOD) 0.93 (d, 6H, $J = 6.6$ Hz, 3-H γ), 1.78 (m, 1H, 3-H β), 2.83 (t, 2H, $J = 7.7$ Hz, 1-H β), 3.83 (d, 2H, $J = 7.7$ Hz, 3-H α), 4.06 (t, 2H, $J = 7.7$ Hz, 1-H α), 4.18 (s, 2H, 2-H α), 5.07 (s, 2H, 4-H α), 6.39 (d, 2H, $J = 8.8$ Hz, 2-H₃), 6.88 (d, 2H, $J = 8.2$ Hz, 3-H₂), 7.12 (d, 2H, $J = 8.5$ Hz, ArCH), 7.15 (d, 2H, $J = 8.2$ Hz, ArCH), 7.19 (d, 2H, $J = 8.5$ Hz, ArCH), 7.23-7.30 (m, 7H, ArCH), 7.71 (d, 2H, $J = 8.2$ Hz, 1-H₂), 7.75-7.80 (m, 2H, ArCH); ESI-HRMS found m/z 699.2986 [M-H]⁻ C₄₂H₄₀FN₄O₅ requires 699.2988.

***N*-(*N*-(*N*-(4-Chlorobenzyl-4-aminobenzoyl)-*N*-3-fluorobenzyl-4-aminobenzoyl)-*N*-isobutyl-4-aminobenzoyl)-glycine 84**

> 85% pure by NMR, isolated crude yield: 61 mg; δ_{H} (300 MHz, MeOD) 0.95 (d, 6H, $J = 5.9$ Hz, 3-H γ), 1.84 (m, 1H, 3-H β), 3.83 (d, 2H, $J = 6.9$ Hz, 3-H α), 4.08 (s, 2H, 1-H α), 4.33 (s, 2H, 2-H α), 5.06 (s, 2H, 4-H α), 6.36 (d, 2H, $J = 8.7$ Hz, 2-H₃), 6.87 (d, 2H, $J = 8.7$ Hz, 3-H₂), 6.95 (d, 2H, $J = 8.2$ Hz, ArCH), 7.01 (d, 2H, $J = 7.7$ Hz, ArCH), 7.11-7.17 (m, 5H, ArCH), 7.23 (t, 1H, $J = 7.8$ Hz, 2-HAr₅), 7.28-7.31 (m, 4H, 1-HAr_{2,3}), 7.72 (d, 2H, $J = 8.2$ Hz, 1-H₂); ESI-HRMS found m/z 719.2463 [M-H]⁻ C₄₁H₃₇ClFN₄O₅ requires 719.2442.

***N*-(*N*-(*N*-(4-Chlorobenzyl-4-aminobenzoyl)-*N*-4-fluorobenzyl-4-aminobenzoyl)-*N*-isobutyl-4-aminobenzoyl)-glycine 85**

> 85% pure by NMR, isolated crude yield: 60 mg; δ_{H} (300 MHz, MeOD) 0.95 (d, 6H, $J = 6.1$ Hz, 3-H γ), 1.85 (m, 1H, 3-H β), 3.83 (d, 2H, $J = 7.1$ Hz, 3-H α), 4.08 (s, 2H, 1-H α), 4.32 (s, 2H, 2-H α), 5.03 (s, 2H, 4-H α), 6.35 (d, 2H, $J = 8.2$ Hz, 2-H₃), 6.83-6.88 (m, 4H, ArCH), 6.97 (d, 2H, $J = 7.1$ Hz, ArCH), 6.99 (d, 2H, $J = 7.7$ Hz, ArCH), 7.12-7.21 (m, 6H, ArCH), 7.30 (d, 2H, $J = 7.0$ Hz, ArCH), 7.72 (d, 2H, $J = 7.1$ Hz, 1-H₂); ESI-HRMS found m/z 719.2432 [M-H]⁻ C₄₁H₃₇ClFN₄O₅ requires 719.2442.

***N*-(*N*-(*N*-(Phenethyl-4-aminobenzoyl)-*N*-4-fluorobenzyl-4-aminobenzoyl)-*N*-isobutyl-4-aminobenzoyl)-glycine 86**

> 90% pure by NMR, isolated crude yield: 61 mg; δ_{H} (300 MHz, MeOD) 0.94 (d, 6H, $J = 6.6$ Hz, 3-H γ), 1.84 (m, 1H, 3-H β), 2.91 (t, 2H, $J = 7.4$ Hz, 1-H β), 3.39 (t, 2H, $J = 7.4$ Hz, 1-H α), 3.82 (d, 2H, $J = 7.4$ Hz, 3-H α), 4.11 (s, 2H, 1-H α), 5.04 (s, 2H, 4-H α), 6.51 (d, 2H, $J = 8.8$ Hz, 2-H3), 6.86 (d, 2H, $J = 8.5$ Hz, 3-H2), 6.98 (t, 2H, $J = 8.8$ Hz, ArCH), 7.08 (d, 2H, $J = 8.8$ Hz, 2-H2), 7.14 (d, 2H, $J = 8.5$ Hz, 3-H3), 7.16-7.23 (m, 5H, ArCH), 7.24-7.27 (m, 2H, ArCH), 7.29 (d, 2H, $J = 8.1$ Hz, 1-H3), 7.73 (d, 2H, $J = 8.5$ Hz, 1-H2); ESI-HRMS found m/z 699.2981 [M-H]⁻ C₄₂H₄₀N₄O₅ requires 699.2988.

***N*-(*N*-(*N*-(Phenethyl-4-aminobenzoyl)-*N*-(2-methyl)naphth-1-yl-4-aminobenzoyl)-*N*-isobutyl-4-aminobenzoyl)-glycine 87**

> 95% pure by NMR, isolated crude yield: 58 mg; δ_{H} (300 MHz, MeOD) 0.90 (d, 6H, $J = 6.6$ Hz, 3-H γ), 1.79 (m, 1H, 3-H β), 2.89 (t, 2H, $J = 7.4$ Hz, 1-H β), 3.36 (t, 2H, $J = 7.4$ Hz, 1-H α), 3.75 (d, 2H, $J = 7.4$ Hz, 3-H α), 4.15 (s, 2H, 1-H α), 4.90 (s, 3H, 2-Me), 5.54 (s, 2H, 4-H α), 6.43 (d, 2H, $J = 8.2$ Hz, 2-H3), 6.53 (d, 2H, $J = 8.5$ Hz, ArCH), 6.90 (d, 2H, $J = 8.2$ Hz, ArCH), 7.02 (d, 2H, $J = 8.8$ Hz, ArCH), 7.06 (d, 2H, $J = 8.8$ Hz, ArCH), 7.14 (d, 1H, $J = 8.5$ Hz, ArCH), 7.19-7.29 (m, 5H, ArCH), 7.48 (m, 1H, ArCH), 7.69 (d, 2H, $J = 8.2$ Hz, ArCH), 7.73 (d, 2H, $J = 8.5$ Hz, ArCH), 7.82 (d, 1H, $J = 8.2$ Hz, ArCH), 8.13 (d, 1H, $J = 8.5$ Hz, ArCH); ESI-HRMS found m/z 745.3383 [M-H]⁻ C₄₇H₄₅N₄O₅ requires 745.3395.

***N*-(*N*-(*N*-(4-Chlorobenzyl-4-aminobenzoyl)-*N*-naphth-2-yl-4-aminobenzoyl)-*N*-isobutyl-4-aminobenzoyl)-glycine 88**

> 80% pure by NMR, isolated crude yield: 71 mg; δ_{H} (500 MHz, MeOD) 0.94 (d, 6H, $J = 6.4$ Hz, 3-H γ), 1.83 (m, 1H, 1-H β), 3.81 (d, 2H, $J = 7.3$ Hz, 3-H α), 4.10 (s, 2H, 1-H α), 4.35 (s, 2H, 2-H α), 5.24 (s, 2H, 4-H α), 6.41 (d, 2H, $J = 8.7$ Hz, 2-H3), 6.90 (d, 2H, $J = 8.2$ Hz, 3-H2), 7.06 (d, 2H, $J = 8.7$ Hz, 2-H2), 7.11 (d, 2H, $J = 8.2$ Hz, ArCH), 7.14 (d, 2H, $J = 7.8$ Hz, ArCH), 7.30-7.36 (m, 4H, ArCH), 7.39 (m, 1H, ArCH), 7.45 (d, 2H, $J = 7.8$ Hz, ArCH), 7.64 (s, 1H, 2-HAr2), 7.70 (d, 2H, $J = 8.2$ Hz, ArCH), 7.77 (d, 2H, $J = 8.7$ Hz, ArCH), 7.81 (d, 1H, $J = 8.2$ Hz, ArCH); ESI-HRMS found m/z 751.2664 [M-H]⁻ C₄₅H₄₀ClN₄O₅ requires 751.2693.

***N*-(*N*-(*N*-(Phenethyl-4-aminobenzoyl)-*N*-(5-bromoindol-3-yl)-4-aminobenzoyl)-*N*-isobutyl-4-aminobenzoyl)-glycine 89**

> 80% pure by NMR, isolated crude yield: 53 mg; δ_{H} (300 MHz, MeOD) 0.93 (d, 6H, $J = 6.6$ Hz, 3-H γ), 1.65 (s, 9H, *t*Bu), 1.92 (m, 1H, 3-H β), 2.90 (t, 2H, $J = 7.2$ Hz, 1-H β), 3.81 (d, 2H, $J = 7.1$ Hz, 3-H α), 4.03 (t, 2H, $J = 7.2$ Hz, 1-H α), 4.10 (s, 2H, 2-H α), 5.20 (s, 2H, 4-H α), 6.42 (d, 2H, $J = 8.6$ Hz, 2-H3), 6.59 (d, 2H, $J = 8.8$ Hz, 3-H2), 6.85 (d, 2H, $J = 8.6$ Hz, 2-H2), 7.03 (d, 2H, $J = 8.8$ Hz, 3-H3), 7.13 (d, 1H, $J = 8.9$ Hz, 2-HAr6), 7.20 (d, 2H, $J = 8.2$ Hz, 1-H3), 7.24-7.29 (m, 5H, 1-HAr2-4), 7.41 (s, 1H, 2-HAr4), 7.72 (d, 1H, $J = 8.8$ Hz, 2-HAr7), 7.77 (d, 2H, $J = 8.5$ Hz, 1-H2), 7.82 (s, 1H, 2-HAr2); ESI-MS found m/z 900.7 [M+H]⁺; ESI-HRMS found m/z 898.2781 [M-H]⁻ C₄₉H₄₉BrN₅O₇ requires 898.2781.

***N*-(*N*-(*N*-(Phenethyl-4-aminobenzoyl)-*N*-4-amidobenzoyl)-*N*-isobutyl-4-aminobenzoyl)-glycine 90**

> 95% pure by NMR, isolated crude yield: 18 mg; δ_{H} (300 MHz, MeOD) 0.98 (d, 6H, $J = 6.6$ Hz, 3-H γ), 1.92 (m, 1H, 3-H β), 2.92 (t, 2H, $J = 7.4$ Hz, 1-H β), 3.43 (t, 2H, $J = 7.4$ Hz, 1-H α), 3.89 (d, 2H, $J = 7.4$ Hz, 3-H α), 4.06 (s, 2H, 4-H α), 6.69 (d, 2H, $J = 8.8$ Hz, 2-H3), 7.28 (d, 2H, $J = 8.0$ Hz, 3-H2), 7.28-7.31 (m, 7H, 1-HAr2-4, 2-H2), 7.57 (d, 2H, $J = 8.5$ Hz, 3-H3), 7.75 (d, 2H, $J = 8.8$ Hz, 1-H3), 7.78 (d, 2H, $J = 8.5$ Hz, 1-H2); ESI-MS found m/z 593.3 [M+H]⁺; ESI-HRMS found m/z 591.2598 [M-H]⁻ C₃₅H₃₅N₄O₅ requires 591.2613.

***N*-(*N*-(*N*-(Benzyl-4-aminobenzoyl)-*N*-(4-trifluoromethyl)benzyl-4-aminobenzoyl)-*N*-isobutyl-4-aminobenzoyl)-glycine 91**

> 80% pure by NMR, isolated crude yield: 69 mg; δ_{H} (300 MHz, MeOD) 0.94 (d, 6H, $J = 6.9$ Hz, 3-H γ), 1.84 (m, 1H, 3-H β), 3.82 (d, 2H, $J = 7.4$ Hz, 3-H α), 4.07 (s, 2H, 2-H α), 4.36 (s, 2H, 1-H α), 5.13 (s, 2H, 4-H α), 6.44 (d, 2H, $J = 8.8$ Hz, 2-H3), 6.89-6.94 (m, 2H, ArCH), 6.99-7.06 (m, 2H, ArCH), 7.12-7.18 (m, 4H, ArCH), 7.30 (dd, 2H, $J_1 = 8.5$ Hz, $J_2 = 2.5$ Hz, 1-HAr2), 7.33-7.39 (m, 3H, ArCH), 7.43 (d, 2H, $J = 8.8$ Hz, ArCH), 7.56 (d, 2H, $J = 7.8$ Hz, ArCH), 7.70-7.75 (m, 2H, ArCH); ESI-HRMS found m/z 735.2776 [M-H]⁻ C₄₂H₃₈F₃N₄O₅ requires 735.2800.

***N*-(*N*-(*N*-(Propyl-4-aminobenzoyl)-*N*-phenethyl-4-aminobenzoyl)-*N*-cyclohexylmethyl-4-aminobenzoyl)-valine 92**

> 85% pure by NMR, isolated crude yield: 70 mg; δ_{H} (300 MHz, CDCl_3) 0.97-1.17 (m, 5H, 3-H δ , δ' , ϵ), 1.02 (d, 6H, $J = 7.4$ Hz, 4-H γ), 1.11 (t, 3H, $J = 7.2$ Hz, 1-H γ), 1.61-1.77 (m, 7H, 1-H β , 3-H γ , γ' , β), 1.86 (m, 1H, 4-H β), 2.95 (m, 2H, 2-H β), 3.29 (t, 2H, $J = 8.2$ Hz, 1-H α), 3.70 (dd, 1H, $J_1 = 13.8$ Hz, $J_2 = 6.6$ Hz, 3-H α), 4.00 (m, 2H, 2-H α), 4.26 (m, 1H, 3-H α'), 4.34 (d, 1H, $J = 6.6$ Hz, 4-H α), 6.81 (d, 2H, $J = 7.2$ Hz, 2-H3), 7.03 (d, 2H, $J = 8.4$ Hz, 3-H2), 7.19 (d, 2H, $J = 8.4$ Hz, 3-H3), 7.25 (d, 2H, $J = 7.2$ Hz, 2-H2), 7.28-7.32 (m, 5H, 2-HAr2-4), 7.37 (d, 2H, $J = 8.5$ Hz, 1-H3), 7.59 (d, 2H, $J = 8.5$ Hz, 1-H2); ESI-MS found m/z 715.3 [M-H]⁻; ESI-HRMS found m/z 715.3853 [M-H]⁻ C₄₄H₅₁N₄O₅ requires 715.3865.

***N*-(*N*-(*N*-(Propyl-4-aminobenzoyl)-*N*-cyclohexylmethyl-4-aminobenzoyl)-*N*-propyl-4-aminobenzoyl)-isoleucine 93**

> 90% pure by NMR, isolated crude yield: 61 mg; δ_{H} (300 MHz, CDCl_3) 0.93-1.05 (m, 15H, 1-H γ , 2-H δ , δ' , ϵ , 3-H γ , 4-H γ), 1.08 (d, 3H, $J = 6.9$ Hz, 4-H ϵ), 1.11-1.16 (m, 2H, 4-H γ), 1.30 (m, 1H, 3-H β), 1.60-1.70 (m, 7H, 1-H β , 2-H β , γ , γ'), 1.83 (m, 1H, 2-H β), 2.07 (m, 1H, 4-H β), 3.29 (t, 2H, $J = 7.9$ Hz, 3-H α), 3.59 (dd, 1H, $J_1 = 13.4$ Hz, $J_2 = 6.6$ Hz, 2-H α), 3.63 (m, 1H, 2-H α'), 4.03 (m, 2H, 1-H α), 4.47 (d, 1H, $J = 6.6$ Hz, 4-H α), 6.96 (d, 2H, $J = 7.2$ Hz, 2-H3), 7.06 (d, 2H, $J = 8.2$ Hz, 3-H2), 7.07 (d, 2H, $J = 7.2$ Hz, 2-H2), 7.27 (d, 2H, $J = 8.5$ Hz, 3-H3), 7.32 (d, 2H, $J = 8.3$ Hz, 1-H3), 7.59 (d, 2H, $J = 8.3$ Hz, 1-H2); ESI-MS found m/z 667.3 [M-H]⁻; ESI-HRMS found m/z 667.3867 [M-H]⁻ C₄₀H₅₁N₄O₅ requires 667.3865.

***N*-(*N*-(*N*-(3-Fluorobenzyl-4-aminobenzoyl)-*N*-phenethyl-4-aminobenzoyl)-*N*-propyl-4-aminobenzoyl)-leucine 94**

> 90% pure by NMR, isolated crude yield: 70 mg; δ_{H} (300 MHz, CDCl_3) 0.93 (t, 3H, $J = 7.4$ Hz, 3-H γ), 0.94 (d, 6H, $J = 7.4$ Hz, 4-H δ), 1.55-1.72 (m, 5H, 3-H β , 4-H β , γ), 2.91 (t, 2H, $J = 7.2$ Hz, 2-H β), 3.82 (m, 1H, 3-H α), 3.98 (t, 2H, $J = 7.4$ Hz, 2-H α), 4.20 (m, 1H, 3-H α'), 4.34 (s, 2H, 1-H α), 4.44 (m, 1H, 4-H α), 6.63 (d, 2H, $J = 7.9$ Hz, 2-H3), 6.98 (d, 2H, $J = 8.2$ Hz, 3-H2), 7.10 (d, 2H, $J = 7.9$ Hz, 2-H2), 7.11 (d, 2H, $J = 8.2$ Hz, 3-H3), 7.13-7.19 (m, 7H, ArCH), 7.23 (d, 1H, $J = 6.9$ Hz, 1-HAr4), 7.27 (d, 2H, $J = 8.1$ Hz, 1-H3), 7.30 (m, 1H, 1-HAr5), 7.59 (d, 2H, $J = 8.1$ Hz, 1-H2); ESI-MS found

m/z 741.2 [M-H]⁻; ESI-HRMS found m/z 741.3456 [M-H]⁻ C₄₅H₄₆FN₄O₅ requires 741.3458.

***N*-(*N*-(*N*-(2-Methylbutyl-4-aminobenzoyl)-*N*-(2-methyl)butyl-4-aminobenzoyl)-*N*-2-methylbutyl-4-aminobenzoyl)-isoleucine 95**

> 95% pure by NMR, isolated crude yield: 63 mg; δ_{H} (300 MHz, MeOD) 0.71-0.81 (m, 9H, 1-H δ , 2-H δ , 4-H δ), 0.83-0.89 (m, 9H, 1-H ϵ , 3-H γ), 0.91-0.95 (m, 6H, 2-H ϵ , 4-H ϵ), 1.03-1.15 (m, 3H, 1-H γ , 1-H β), 1.22-1.33 (m, 2H, 2-H γ), 1.37-1.45 (m, 4H, 4-H γ , 2-H β , 3-H β), 1.56-1.69 (m, 1H, 4-H β), 2.89 (dd, 1H, $J_1 = 12.6$ Hz and $J_2 = 7.4$ Hz, 1-H α), 3.02 (dd, 1H, $J_1 = 12.6$ Hz and $J_2 = 7.4$ Hz, 1-H α'), 3.68 (d, 2H, $J = 7.1$ Hz, 3-H α), 3.79 (d, 2H, $J = 7.4$ Hz, 2-H α), 4.45 (d, 1H, $J = 6.4$ Hz, 4-H α), 6.55 (d, 2H, $J = 8.0$ Hz, 2-H3), 6.91 (d, 2H, $J = 8.5$ Hz, 3-H2), 6.97 (d, 2H, $J = 8.5$ Hz, 2-H2), 7.10 (d, 2H, $J = 8.5$ Hz, 3-H3), 7.11 (d, 2H, $J = 8.5$ Hz, 1-H3), 7.63 (d, 2H, $J = 8.5$ Hz, 1-H2); ESI-HRMS found m/z 697.4356 [M-H]⁻ C₄₂H₅₇N₄O₅ requires 697.4334.

***Valine-N*-(*N*-(*N*-(isobutyl-4-aminobenzoyl)-*N*-(isobutyl-4-aminobenzoyl)-*N*-isobutyl-4-aminobenzoyl)-glycine 96**

> 90% pure by NMR, isolated crude yield: 62 mg; δ_{H} (300 MHz, MeOD) 0.80 (d, 6H, $J = 7.1$ Hz, 2-H γ), 0.87 (d, 6H, $J = 7.1$ Hz, 3-H γ), 0.92 (d, 6H, $J = 6.6$ Hz, 4-H γ), 0.96 (d, 6H, $J = 6.6$ Hz, 1-H γ), 1.66-1.80 (m, 2H, 2-H β , 3-H β), 1.84-1.98 (m, 2H, 1-H β , 4-H β), 3.71-3.80 (m, 4H, 3-H α , 4-H α), 3.83-3.86 (m, 2H, 2-H α), 4.07-4.11 (m, 1H, 1-H α), 4.09 (s, 2H, 5-H α), 7.04 (d, 2H, $J = 8.5$ Hz, 2-H3), 7.18 (d, 2H, $J = 7.9$ Hz, 3-H2), 7.21 (d, 2H, $J = 7.9$ Hz, 3-H3), 7.25 (d, 2H, $J = 8.5$ Hz, 2-H2), 7.34 (d, 2H, $J = 8.3$ Hz, 1-H3), 7.77 (d, 2H, $J = 8.3$ Hz, 1-H2); ESI-MS found m/z 700.5 [M+H]⁺; ESI-HRMS found m/z 698.3916 [M-H]⁻ C₄₀H₅₂N₅O₆ requires 698.3923.

***N*-(*N*-(*N*-(Isobutyl-4-aminobenzoyl)-*N*-(2-methylbutyl-4-aminobenzoyl)-*N*-2-methylbutyl-4-aminobenzoyl)-isoleucine 97**

> 95% pure by NMR, isolated crude yield: 63 mg; δ_{H} (300 MHz, MeOD) 0.83 (t, 3H, $J = 7.4$ Hz, 3-H δ), 0.87 (d, 3H, $J = 6.6$ Hz, 3-H ϵ), 0.89 (t, 3H, $J = 7.4$ Hz, 2-H δ), 0.94 (d, 3H, $J = 6.9$ Hz, 2-H ϵ), 0.97 (d, 3H, $J = 7.7$ Hz, 4-H ϵ), 1.02 (d, 6H, $J = 6.6$ Hz, 1-H γ), 1.03 (t, 3H, $J = 6.6$ Hz, 4-H δ), 1.09-1.26 (m, 2H, 3-H γ), 1.29-1.41 (m, 2H, 2-H γ), 1.43-1.54 (m, 2H, 4-H γ), 1.56-1.68 (m, 2H, 3-H β , 1-H β), 1.95 (m, 1H, 2-H β), 2.04 (m, 1H, 4-H β), 3.00 (d, 2H, $J = 6.9$ Hz, 1-H α), 3.78 (d, 2H, $J = 7.1$ Hz, 2-H α), 3.89 (d,

2H, $J = 7.4$ Hz, 3-H α), 4.55 (d, 1H, $J = 6.3$ Hz, 4-H α), 6.60 (d, 2H, $J = 8.7$ Hz, 2-H3), 7.01 (d, 2H, $J = 8.2$ Hz, 3-H2), 7.05 (d, 2H, $J = 8.7$ Hz, 2-H2), 7.20 (d, 2H, $J = 8.2$ Hz, 3-H3), 7.21 (d, 2H, $J = 8.5$ Hz, 1-H3), 7.74 (d, 2H, $J = 8.5$ Hz, 1-H2); ESI-MS found m/z 683.5 [M-H]⁻; ESI-HRMS found m/z 683.4182 [M-H]⁻ C₄₁H₅₅N₄O₅ requires 683.4178.

***N*-(*N*-(*N*-(*Isobutyl*-4-aminobenzoyl)-*N*-naphth-2-yl-4-aminobenzoyl)-*N*-2-methylbutyl-4-aminobenzoyl)-isoleucine 98**

> 95% pure by NMR, isolated crude yield: 70 mg; δ_{H} (300 MHz, MeOD) 0.85 (t, 3H, $J = 7.4$ Hz, 3-H δ), 0.89 (d, 3H, $J = 6.9$ Hz, 3-H ϵ), 0.98 (t, 3H, $J = 7.4$ Hz, 4-H δ), 1.02 (d, 6H, $J = 7.2$ Hz, 1-H γ), 1.04 (d, 3H, $J = 7.4$ Hz, 4-H ϵ), 1.15 (m, 1H, 3-H γ), 1.30-1.47 (m, 2H, 3-H γ' , 4-H γ), 1.54-1.68 (m, 2H, 4-H γ' , 1-H β), 1.94 (m, 1H, 3-H β), 2.03 (m, 1H, 4-H β), 2.99 (d, 2H, $J = 6.9$ Hz, 1-H α), 3.84 (d, 2H, $J = 7.1$ Hz, 3-H α), 4.58 (d, 1H, $J = 6.3$ Hz, 4-H α), 5.24 (s, 2H, 2-H α), 6.59 (d, 2H, $J = 8.7$ Hz, 2-H3), 6.90 (d, 2H, $J = 8.4$ Hz, 3-H2), 7.11 (d, 2H, $J = 8.7$ Hz, 2-H2), 7.14 (d, 2H, $J = 8.4$ Hz, 3-H3), 7.15 (d, 2H, $J = 8.5$ Hz, 1-H3), 7.36 (m, 1H, ArCH), 7.43-7.46 (m, 2H, ArCH), 7.64 (s, 1H, 3-HAr2), 7.70 (d, 2H, $J = 8.5$ Hz, 1-H2), 7.74-7.78 (m, 2H, ArCH), 7.81 (m, 1H, 2-ArCH); ESI-MS found m/z 755.5 [M+H]⁺; ESI-HRMS found m/z 753.4007 [M-H]⁻ C₄₇H₅₃N₄O₅ requires 753.4021.

***N*-(*N*-(*N*-(*Isobutyl*-4-aminobenzoyl)-*N*-2-methylbutyl-4-aminobenzoyl)-*N*-naphth-2-yl-4-aminobenzoyl)-valine 99**

> 95% pure by NMR, isolated crude yield: 73 mg; δ_{H} (300 MHz, MeOD) 0.83 (t, 3H, $J = 7.4$ Hz, 2-H δ), 0.86 (d, 3H, $J = 6.6$ Hz, 2-H ϵ), 0.99 (d, 6H, $J = 6.7$ Hz, 1-H γ), 1.01 (d, 6H, $J = 6.8$ Hz, 4-H γ), 1.14 (m, 1H, 2-H γ), 1.37 (m, 1H, 2-H γ'), 1.53 (m, 1H, 1-H β), 1.91 (m, 1H, 2-H β), 2.23 (m, 1H, 4-H β), 2.96 (d, 2H, $J = 6.9$ Hz, 1-H α), 3.76 (d, 2H, $J = 7.2$ Hz, 2-H α), 4.43 (d, 1H, $J = 6.3$ Hz, 4-H α), 5.36 (s, 2H, 3-H α), 6.56 (d, 2H, $J = 8.5$ Hz, 2-H3), 7.01 (d, 2H, $J = 8.5$ Hz, 3-H2), 7.04 (d, 2H, $J = 8.5$ Hz, 2-H2), 7.09 (d, 2H, $J = 8.5$ Hz, 3-H3), 7.32 (d, 2H, $J = 8.5$ Hz, 1-H3), 7.43-7.51 (m, 3H, ArCH), 7.63 (d, 2H, $J = 8.5$ Hz, 1-H2), 7.69 (s, 1H, ArCH), 7.76 (m, 1H, ArCH), 7.81-7.83 (m, 2H, ArCH); ESI-MS found m/z 740.1 [M-H]⁻; ESI-HRMS found m/z 739.3878 [M-H]⁻ C₄₆H₅₁N₄O₅ requires 739.3865.

***N*-(*N*-(*N*-(Isobutyl-4-aminobenzoyl)-*N*-2-methylbutyl-4-aminobenzoyl)-*N*-4-chlorobenzyl-4-aminobenzoyl)-valine 100**

> 95% pure by NMR, isolated crude yield: 69 mg; δ_{H} (300 MHz, MeOD) 0.83 (t, 3H, $J = 7.2$ Hz, 2-H δ), 0.86 (d, 3H, $J = 7.2$ Hz, 2-H ϵ), 1.01 (d, 6H, $J = 6.9$ Hz, 1-H γ), 1.04 (d, 6H, $J = 7.4$ Hz, 4-H γ), 1.13 (m, 1H, 2-H γ), 1.39 (m, 1H, 2-H γ'), 1.52 (m, 1H, 1-H β), 1.94 (m, 1H, 2-H β), 2.28 (m, 1H, 4-H β), 2.98 (d, 2H, $J = 6.9$ Hz, 1-H α), 3.78 (d, 2H, $J = 6.9$ Hz, 2-H α), 4.46 (d, 1H, $J = 6.3$ Hz, 4-H α), 5.17 (s, 2H, 3-H α), 6.59 (d, 2H, $J = 8.5$ Hz, 2-H3), 7.01 (d, 2H, $J = 8.2$ Hz, 3-H2), 7.03 (d, 2H, $J = 8.5$ Hz, 2-H2), 7.05 (d, 2H, $J = 8.2$ Hz, 3-H3), 7.28 (d, 2H, $J = 8.2$ Hz, 1-H3), 7.28-7.30 (m, 4H, 3-HAr2,3), 7.67 (d, 2H, $J = 8.5$ Hz, 1-H2); ESI-MS found m/z 724.8 [M+H]⁺; ESI-HRMS found m/z 723.3346 [M-H]⁻ C₄₂H₄₈ClN₄O₅ requires 723.3319.

***N*-(*N*-(*N*-(Isobutyl-4-aminobenzoyl)-*N*-4-chlorobenzyl-4-aminobenzoyl)-*N*-isobutyl-4-aminobenzoyl)-isoleucine 101**

> 95% pure by NMR, isolated crude yield: 61 mg; δ_{H} (300 MHz, MeOD) 0.92 (d, 6H, $J = 6.6$ Hz, 1-H γ), 0.98 (t, 3H, $J = 7.8$ Hz, 4-H δ), 1.01 (d, 6H, $J = 6.9$ Hz, 3-H γ), 1.04 (d, 3H, $J = 6.9$ Hz, 4-H ϵ), 1.35 (m, 1H, 1-H β), 1.63 (m, 1H, 3-H β), 1.85 (m, 1H, 4-H γ), 1.94 (m, 1H, 4-H γ'), 2.05 (m, 1H, 4-H β), 2.98 (d, 2H, $J = 6.9$ Hz, 1-H α), 3.82 (d, 2H, $J = 7.4$ Hz, 3-H α), 4.57 (d, 1H, $J = 6.1$ Hz, 4-H α), 5.03 (s, 2H, 2-H α), 6.55 (d, 2H, $J = 8.5$ Hz, 2-H3), 6.88 (d, 2H, $J = 8.2$ Hz, 3-H2), 7.11 (d, 2H, $J = 8.5$ Hz, 2-H2), 7.15 (d, 2H, $J = 8.2$ Hz, 3-H3), 7.17-7.20 (m, 4H, 2-HAr2,3), 7.26 (d, 2H, $J = 8.5$ Hz, 1-H3), 7.74 (d, 2H, $J = 8.5$ Hz, 1-H2); ESI-MS found m/z 723.8 [M-H]⁻; ESI-HRMS found m/z 723.3324 [M-H]⁻ C₄₂H₄₈ClN₄O₅ requires 723.3319.

***N*-(*N*-(*N*-(Carboxymethyl-4-aminobenzoyl)-*N*-2-methylbutyl-4-aminobenzoyl)-*N*-isobutyl-4-aminobenzoyl)-valine 102**

> 80% pure by NMR, isolated crude yield: 56 mg; δ_{H} (300 MHz, MeOD) 0.82 (t, 3H, $J = 7.4$ Hz, 2-H δ), 0.85 (d, 3H, $J = 5.9$ Hz, 2-H ϵ), 0.96 (d, 6H, $J = 6.6$ Hz, 3-H γ), 1.05 (d, 6H, $J = 6.6$ Hz, 4-H γ), 1.03-1.08 (m, 2H, 2-H γ), 1.51 (m, 1H, 2-H β), 1.87 (m, 1H, 3-H β), 2.30 (m, 1H, 4-H β), 3.76 (m, 2H, 2-H α), 3.85 (d, 2H, $J = 7.4$ Hz, 3-H α), 3.91 (s, 2H, 1-H α), 4.52 (m, 1H, 4-H α), 6.37 (d, 2H, $J = 8.5$ Hz, 2-H3), 6.98 (d, 4H, $J = 8.2$ Hz, 3-H2, 2-H2), 7.20 (d, 4H, $J = 8.0$ Hz, 3-H3, 1-H3), 7.77 (d, 2H, $J = 8.5$ Hz, 1-H2); ESI-HRMS found m/z 657.3280 [M-H]⁻ C₃₇H₄₅N₄O₇ requires 657.3294.

***N*-(*N*-(*N*-(Carboxymethyl-4-aminobenzoyl)-*N*-2-methylbutyl-4-aminobenzoyl)-*N*-2-methylbutyl-4-aminobenzoyl)-valine 103**

> 80% pure by NMR, isolated crude yield: 52 mg; δ_{H} (300 MHz, MeOD) 0.86 (t, 3H, $J = 7.1$ Hz, 2-H δ), 0.88 (t, 3H, $J = 7.1$ Hz, 3-H δ), 0.86-0.90 (m, 2H, 3-H γ), 0.94 (d, 6H, $J = 6.9$ Hz, 3-H ϵ , 2-H ϵ), 1.05 (d, 6H, $J = 6.3$ Hz, 4-H γ), 1.03-1.08 (m, 2H, 2-H γ), 1.49 (m, 1H, 3-H β), 1.61 (m, 1H, 2-H β), 2.29 (m, 1H, 4-H β), 3.77 (m, 2H, 2-H α), 3.82 (s, 2H, 1-H α), 3.90 (d, 2H, $J = 7.2$ Hz, 3-H α), 4.52 (m, 1H, 4-H α), 6.35 (d, 2H, $J = 8.5$ Hz, 2-H3), 6.98 (d, 2H, $J = 8.3$ Hz, 3-H2), 7.04 (d, 2H, $J = 8.5$ Hz, 2-H2), 7.20 (d, 2H, $J = 8.3$ Hz, 3-H3), 7.21 (d, 2H, $J = 8.3$ Hz, 1-H3), 7.78 (d, 2H, $J = 8.3$ Hz, 1-H2); ESI-HRMS found m/z 671.3423 [M-H]⁻ C₃₈H₄₇N₄O₇ requires 671.3450.

***N*-(*N*-(*N*-(Isobutyl-4-aminobenzoyl)-*N*-(2-methyl)butyl-4-aminobenzoyl)-*N*-isobutyl-4-aminobenzoyl)-aspartic acid 104**

> 90% pure by NMR, isolated crude yield: 52 mg; δ_{H} (300 MHz, MeOD) 0.84 (t, 3H, $J = 7.4$ Hz, 2-H δ), 0.88 (d, 3H, $J = 6.6$ Hz, 2-H ϵ), 0.96 (d, 6H, $J = 6.6$ Hz, 1-H γ), 1.04 (d, 6H, $J = 6.6$ Hz, 3-H γ), 1.14 (m, 2H, 2-H γ), 1.40 (m, 1H, 2-H β), 1.87 (m, 1H, 3-H β), 1.97 (m, 1H, 1-H β), 2.90 (m, 2H, 4-H β), 3.02 (d, 2H, $J = 6.9$ Hz, 2-H α), 3.77 (d, 2H, $J = 7.4$ Hz, 3-H α), 3.84 (d, 2H, $J = 7.4$ Hz, 1-H α), 4.98 (m, 1H, 4-H α), 6.65 (d, 2H, $J = 8.5$ Hz, 2-H3), 7.01 (d, 2H, $J = 8.2$ Hz, 3-H2), 7.07 (d, 2H, $J = 8.5$ Hz, 2-H2), 7.21 (d, 2H, $J = 8.2$ Hz, 3-H3), 7.22 (d, 2H, $J = 8.5$ Hz, 1-H3), 7.73 (d, 2H, $J = 8.2$ Hz, 1-H2); ESI-HRMS found m/z 671.3444 [M-H]⁻ C₃₈H₄₇N₄O₇ requires 671.3450.

***N*-(*N*-(*N*-(Isobutyl-4-aminobenzoyl)-*N*-naphth-2-yl-4-aminobenzoyl)-*N*-isobutyl-4-aminobenzoyl)-isoleucine 105**

> 95% pure by NMR, isolated crude yield: 71 mg; δ_{H} (300 MHz, MeOD) 0.91 (d, 6H, $J = 6.9$ Hz, 1-H γ), 0.98 (t, 3H, $J = 7.4$ Hz, 4-H δ), 1.02 (d, 6H, $J = 6.9$ Hz, 3-H γ), 1.03 (d, 3H, $J = 6.9$ Hz, 4-H ϵ), 1.35 (m, 1H, 1-H β), 1.62 (m, 1H, 3-H β), 1.82 (m, 1H, 4-H γ), 1.95 (m, 1H, 4-H γ'), 2.04 (m, 1H, 4-H β), 2.99 (d, 2H, $J = 6.9$ Hz, 1-H α), 3.79 (d, 2H, $J = 7.4$ Hz, 3-H α), 4.58 (d, 1H, $J = 6.3$ Hz, 4-H α), 5.24 (s, 2H, 2-H α), 6.58 (d, 2H, $J = 8.8$ Hz, 2-H3), 6.90 (d, 2H, $J = 8.5$ Hz, 3-H2), 7.11 (d, 2H, $J = 8.8$ Hz, 2-H2), 7.15 (d, 2H, $J = 8.5$ Hz, 3-H3), 7.16 (d, 2H, $J = 8.5$ Hz, 1-H3), 7.36 (m, 1H, ArCH), 7.43-7.46 (m, 2H, ArCH), 7.63 (s, 1H, ArCH), 7.71 (d, 2H, $J = 8.5$ Hz, 1-H2), 7.73-7.78 (m, 2H, ArCH), 7.81 (m, 1H, ArCH); ESI-HRMS found m/z 739.3831 [M-H]⁻ C₄₆H₅₁N₄O₅ requires 739.3865.

***N*-(*N*-(*N*-(Isobutyl-4-aminobenzoyl)-*N*-isobutyl-4-aminobenzoyl)-*N*-isobutyl-4-aminobenzoyl)-glycine 106**

> 95% pure by NMR, isolated crude yield: 53 mg; δ_{H} (300 MHz, MeOD) 0.90 (d, 6H, $J = 6.6$ Hz, 3-H γ), 0.96 (d, 6H, $J = 6.9$ Hz, 1-H γ), 1.03 (d, 6H, $J = 6.6$ Hz, 2-H γ), 1.79 (m, 1H, 3-H β), 1.87 (m, 1H, 1-H β), 1.96 (m, 1H, 2-H β), 3.01 (d, 2H, $J = 6.9$ Hz, 3-H α), 3.73 (d, 2H, $J = 7.6$ Hz, 1-H α), 3.85 (d, 2H, $J = 7.7$ Hz, 2-H α), 4.11 (s, 2H, 4-H α), 6.66 (d, 2H, $J = 8.8$ Hz, 2-H3), 7.01 (d, 2H, $J = 8.5$ Hz, 3-H2), 7.07 (d, 2H, $J = 8.8$ Hz, 2-H2), 7.20 (d, 4H, $J = 8.5$ Hz, 3-H3, 1-H3), 7.74 (d, 2H, $J = 8.5$ Hz, 1-H2); ESI-HRMS found m/z 599.3240 [M-H] $^-$ C₃₅H₄₃N₄O₅ requires 599.3239.

***N*-(*N*-(*N*-(Isobutyl-4-aminobenzoyl)-*N*-isobutyl-4-aminobenzoyl)-*N*-naphth-2-yl-4-aminobenzoyl)-leucine 107**

> 90% pure by NMR, isolated crude yield: 70 mg; δ_{H} (300 MHz, MeOD) 0.89 (d, 6H, $J = 6.6$ Hz, 2-H γ), 0.95 (d, 6H, $J = 6.9$ Hz, 4-H δ), 0.97 (m, 1H, 4-H γ), 0.99 (d, 6H, $J = 6.6$ Hz, 1-H γ), 1.72 (m, 2H, 4-H β), 1.79 (m, 1H, 2-H β), 1.92 (m, 1H, 1-H β), 2.96 (d, 2H, $J = 6.9$ Hz, 1-H α), 3.73 (d, 2H, $J = 7.4$ Hz, 2-H α), 4.59 (d, 1H, $J = 6.9$ Hz, 4-H α), 5.35 (s, 2H, 3-H α), 6.56 (d, 2H, $J = 8.5$ Hz, 2-H3), 7.02 (d, 2H, $J = 8.5$ Hz, 3-H2), 7.03 (d, 2H, $J = 8.5$ Hz, 2-H2), 7.09 (d, 2H, $J = 8.8$ Hz, 3-H3), 7.31 (d, 2H, $J = 8.8$ Hz, 1-H3), 7.43-7.51 (m, 3H, ArCH), 7.62 (d, 2H, $J = 8.8$ Hz, 1-H2), 7.69 (s, 1H, ArCH), 7.76 (m, 1H, ArCH), 7.83 (d, 2H, $J = 8.8$ Hz, ArCH); ESI-MS found m/z 741.4 [M+H] $^+$; ESI-HRMS found m/z 739.3875 [M-H] $^-$ C₄₆H₅₁N₄O₅ requires 739.3865.

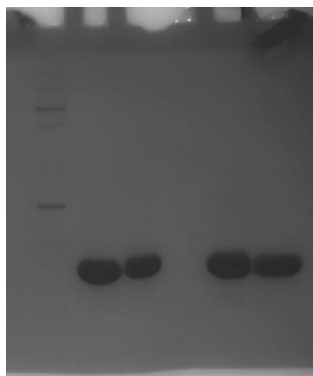
6.2 Biophysical assessment of the proteomimetics (Chapters 3 and 4)

6.2.1 Molecular cloning and protein expression

Expression and purification of *hDM2*₁₇₋₁₂₆ L33E.

The *hDM2*₁₇₋₁₂₆ construct was initially provided by John Robinson at the University of Zürich. The pET14b plasmid (Novagen) containing cDNA encoding *hDM2* residues Ser17 to Asn126, with a single mutation L33E (for increased protein stability *in vivo* [Vassilev *et al.*, *Science*, 2004, 303, 844-848]; mutagenesis by T. Burnley, Edwards lab), was transformed into *E. coli* BL21 (DE3) GOLD.

Protein production in 2xYT medium with ampicillin (100 mg mL⁻¹) was induced with IPTG (0.5 mM) when the optical density of the cell suspension reached OD₆₀₀ = 0.6. Induced cells were grown at 18 °C for 12 h and harvested by centrifugation at 6000 rpm for 10 min. Cells were resuspended in buffer A (20 mM Tris, 500 mM NaCl, pH 7.9) with 0.1% Triton X-100, disrupted by 20 kPsi on a Cell Disruptor (Constant System Ltd.) and sonicated in the presence of DNaseI, 1 U mL⁻¹ (EPICENTRE biotechnologies) and 5 mM MgCl₂. Cell lysate was centrifuged at 17 000 rpm for 30 min. Supernatant was loaded onto a Ni²⁺-nitriloacetic acid (NTA) column equilibrated with buffer A. His₆-tagged *hDM2* recombinant fragment was washed with 50 mL buffer A and buffer A with 60 mM imidazole added. The protein was eluted with 120 mM and 300 mM imidazole and the column was washed with 1 M imidazole in buffer A. Fractions containing protein were detected by 16% SDS-PAGE and concentrated to 5 mL then loaded onto a SuperdexTM 75 column and washer with buffer B (25 mM Tris, 150 mM NaCl, 5% glycerol, 1 mM EDTA, 1 mM DTT, pH 7.3). The purified protein was concentrated to a final concentration of 191 μM and stored at -80 °C until use.



SDS-PAGE gel of *hDM2* 17-126 L33E after Superdex purification.

From the left: broad range markers (2-212 kDa), 191 μM *hDM2*, 240.6 μM *hDM2*

Molecular cloning of recombinant *hDMX*

The cDNA coding for *hDMX* was used as a template in PCR using the primers listed in Table E1 to introduce a *Bam*HI restriction site 5' and *Xho*I restriction site 3' to the *hDMX* (26-110) sequence. The PCR product was purified and digested with *Bam*HI-HF and *Xho*I (New England Biolabs) following the manufacturers recommended protocol. *hDMX* (26-110) was then ligated into both pET-SUMO-28a and pET28b-GFP-P that had been cut with *Bam*HI-HF and *Xho*I using T4 DNA ligase (Invitrogen). Ligation products were transformed into DH5α cells. Colony

PCR was subsequently used to check for the presence of the insert and the identity of the insert confirmed by DNA sequencing (Beckman Coulter Genomics).

Table E1. Primers used during PCR on the *hDMX* cDNA

Primer Name	Sequence (5'-3')
<i>hDMX-BamHI</i> -HF	AAAGGATCCCAGGTACGACCAAAACTG
<i>hDMX-EcoRI</i>	TTTGAATTCCTAGGCTAAAGTGACAAGATTC

Expression and purification of GFP-P-*hDMX*₂₆₋₁₁₀

The sequenced recombinant *hDMX* construct was transformed into *E. coli* BL21 (DE3) STAR cells. Protein production in 2xYT medium with kanamycin (100 mg mL⁻¹) was induced with IPTG (0.5 mM) when the optical density of the cell suspension reached OD₆₀₀ = 0.6. Induced cells were grown at 18 °C for 14 h and harvested by centrifugation at 7000 rpm for 12 min. Cells were resuspended in buffer A (20 mM Tris, 500 mM NaCl, pH 7.9) with 0.1% Triton X-100, disrupted by 20 kPsi on a Cell Disruptor (Constant System Ltd.) and sonicated in the presence of DNaseI, 1 U mL⁻¹ (EPICENTRE biotechnologies) and 5 mM MgCl₂. Cell lysate was centrifuged at 4 000 rpm for 10 min. Supernatant was loaded onto a Ni²⁺-nitriloacetic acid (NTA) column equilibrated with buffer A. His₆-tagged GFP-P-*hDMX* recombinant fragment was washed with 15 mL buffer A and buffer A with 60 mM imidazole added. The protein was eluted with 120 mM and 300 mM imidazole and the column was washed with 1 M imidazole in buffer A. Fractions containing protein were detected by 15% SDS-PAGE and the purified His-Tev-GFP-P-*hDMX* protein was then incubated overnight with PreScission protease in order to cleave the GFP-tag. Examination of the 15% SDS-PAGE after Sephadex column purification showed the cleavage did not work. This construct can however be used to express GFP-tagged *hDMX* for future FRET assays.

Molecular cloning of SUMO-*hDMX*₂₆₋₁₁₀

The sequenced recombinant GFP-tagged *hDMX* plasmid was digested with *Bam*HI-HF and *Xho*I (New England Biolabs) following the manufacturers recommended protocol. *hDMX* (26-110) was then ligated into pET-SUMO-28a that had been cut with *Bam*HI-HF and *Xho*I using T4 DNA ligase (Invitrogen). Ligation products were transformed into DH5 α cells. Colony PCR was subsequently carried out and no insert was detected. It was reasoned that the PCR might not be working properly, so the whole procedure was repeated, but skipping the initial PCR step. After the ligation, the presence of the insert was checked using 2 diagnostic digests, one with *Hind*III-*Xba*I and the second with *Bgl*III. Both digests confirmed the presence of the insert in 7 colonies, which was further validated on two colonies by DNA sequencing (Beckman Coulter Genomics).

Table E2. Primers used during PCR on the *hDMX* cDNA

Primer Name	Sequence (5'-3')
<i>hDMX</i> - <i>Bam</i> HI-HF	AAAGGATCCCAGGTACGACCAAACTG
<i>hDMX</i> - <i>Xho</i> I	TTTCTCGAGCTAGGCTAAAGTGACAAGATTC

Expression and purification of SUMO-*hDMX*₂₆₋₁₁₀

The sequenced recombinant SUMO-*hDMX* construct was transformed into *E. coli* BL21 (DE3) Rosetta cells. Protein production in 2xYT medium with kanamycin (100 mg mL⁻¹) was induced with IPTG (0.5 mM) when the optical density of the cell suspension reached OD₆₀₀ = 0.6. Induced cells were grown at 18 °C for 14 h and harvested by centrifugation at 7000 rpm for 15 min. Cells were resuspended in buffer A (20 mM Tris, 500 mM NaCl, pH 7.9) with 0.1% Triton X-100, disrupted by 20 kPsi on a Cell Disruptor (Constant System Ltd.) and sonicated in the presence of DNaseI, 1 U mL⁻¹ (EPICENTRE biotechnologies) and 5 mM MgCl₂. Cell lysate was centrifuged at 4 000 rpm for 25 min. Supernatant was loaded onto a

Chapter 6: Experimental Section

Ni²⁺-nitriloacetic acid (NTA) column equilibrated with buffer A. His₆-tagged GFP-P-*hDMX* recombinant fragment was washed with 15 mL buffer A and buffer A with 60 mM imidazole added. The protein was eluted with 120 mM and 300 mM imidazole and the column was washed with 1 M imidazole in buffer A. Fractions containing protein were detected by 15% SDS-PAGE. Fractions were then concentrated to 5 mL then purified on a Sephadex gel filtration column. Examination of the fractions by 15% SDS-PAGE revealed that the SUMO-tag was mostly cleaved off, which might be due to intrinsic instability of the fusion protein. It was then decided to combine all the *hDMX* containing fractions and complete the cleavage by incubating overnight with SUMO protease. Purification by Ni²⁺-nitriloacetic acid (NTA) column (this time collecting the flow through, as the His-tag was cleaved off along with SUMO) provided pure, untagged *hDMX* protein, as confirmed by 15% SDS-PAGE. All the fractions were combined and concentrated to 2 mL. The resulting protein was then tested for binding in a preliminary fluorescence anisotropy assay, but unfortunately no binding to p53 was detected. This protein was thus not suitable for use in the library screening.

Expression and purification of Mcl-1₁₇₂₋₃₂₇

The molecular cloning on recombinant SUMO-Mcl-1, along with the Sumo cleavage, protein expression and purification were carried out by Dr. A. Bartlett to yield untagged Mcl-1₁₇₂₋₃₂₇. (Two batches were made, with final concentrations of 143.3 μM and 240.7 μM).

6.2.2 Fluorescence anisotropy competition assay

p53₁₅₋₃₁ transactivation domain peptide (Ac-SQETFSDLWKLLPENNV(NH₂)) (p53) and its fluorescein-labelled analogue (Ac-SQETFSDLWKLLPENNV(Flu)-NH₂) (p53₁₅₋₃₁Flu) were purchased from Peptide Protein Research Ltd. Fluorescence anisotropy assays were performed in 96- or 384-well plates (Greiner Bio-one). Each experiment was run in triplicate and the fluorescence anisotropy measured using a Perkin Elmer EnVision™ 2103 MultiLabel plate reader, with excitation at 480 nm and emission at 535 nm (5 nm bandwidth).

All experiments were performed in assay buffer: 40 mM phosphate buffer at pH 7.49, containing 200 mM NaCl and 0.02 mg mL⁻¹ bovine serum albumin (BSA). Stocks of ligand (typically at 450 μM in 90:10 (v/v) assay buffer:DMSO) were used to prepare a 24-point serial dilution of ligand across the plate, tracer peptide (p53₁₅₋₃₁-Flu) and hDM2₁₇₋₁₂₆ L33E were then added to each well to give a final concentration of 54.5 nM and 154.2 nM, respectively. For control wells the tracer peptide was replaced with an identical volume of assay buffer. The total volume in each well was 150 μL. In all experiments the G factor, or ratio between the efficiency of the S(ame) and P(erpendicular) channels, was set to 1.

Determination of the association constant between the p53 tracer and hDM2:

The procedure followed was described in our previous paper on *O*-alkylated aromatic oligoamides [J. P. Plante *et al.*, *Chem. Commun.*, 2009, 5091-5093]. Briefly: hDM2 was serially diluted (10 μM – 0.89 nM) into a solution of p53-Flu (54.5 nM in assay buffer) - the total volume of each well was 150 μL. Each experiment was run in triplicate and the data for both the perpendicular (P) and same (S) channel were corrected by subtracting the corresponding control wells. These corrected values were used to calculate the total intensity and anisotropy for each point (Equations 1 and 2). The average anisotropy from 3 replicates was plotted against the ligand concentration and fitted to a logistic model using Origin 8.6 to determine the minimum and maximum anisotropies (r_{\min} and r_{\max}). Using equation 3, the data for the anisotropy was converted to fraction bound and

Chapter 6: Experimental Section

multiplied by the p53₁₅₋₃₁-Flu concentration then fitted in origin 8.6 (equation 4, cf. binding curve below) to give the dissociation constant $K_d = 164.4 \pm 10.8$ nM.

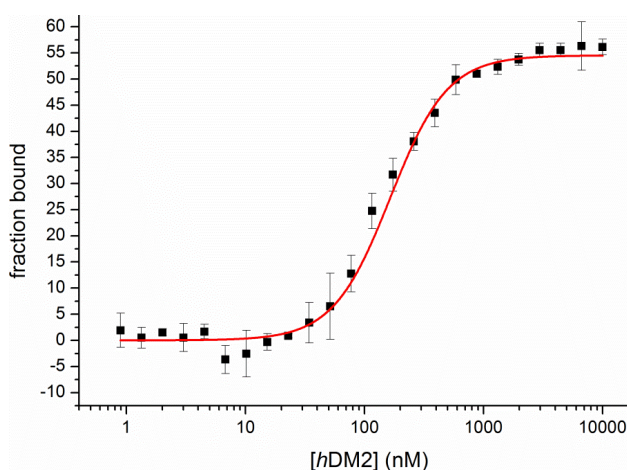
$$I = 2PG + S \quad \text{Equation 1}$$

$$r = \frac{S - PG}{I} \quad \text{Equation 2}$$

$$L_b = \frac{(r - r_{\min})}{\lambda(r_{\max} - r) + r - r_{\min}} \quad \text{Equation 3}$$

$$y = \frac{\{(k_1 + [hDM2] + [FL]) - \sqrt{\{(k_1 + [hDM2] + [FL])^2 - 4[hDM2][FL]\}}\}}{2} \quad \text{Equation 4}$$

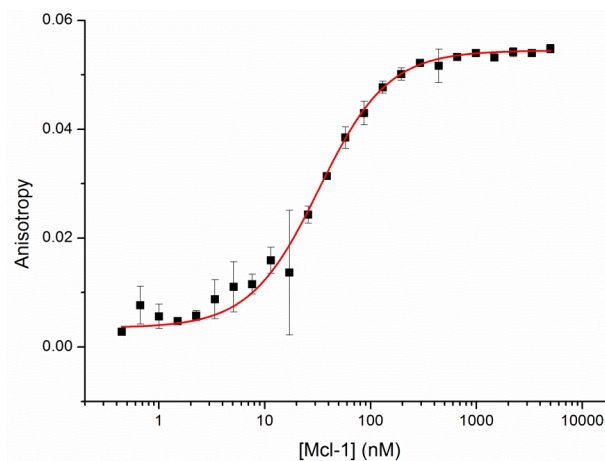
r = anisotropy, I = total intensity, P = perpendicular intensity, S = parallel intensity, L_b = fraction ligand bound, $\lambda = I_{\text{bound}}/I_{\text{unbound}} = 1$ (intensity variation), $[FL]$ = concentration of fluorescent ligand (*i.e.* p53₁₅₋₃₁Flu), $k_1 = K_d$, $y = L_b * p53_{15-31}\text{-Flu}$ and $x = [\text{added titrant}]$, G is an instrument factor set to 1.



Direct titration of p53₁₅₋₃₅-Flu with increasing concentrations of hDM2, plotted in Origin 8.6.

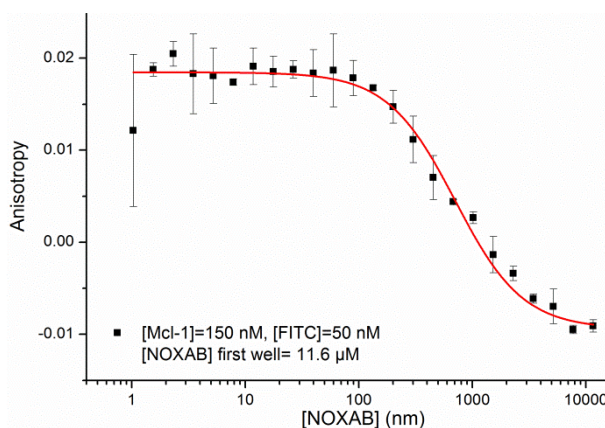
Determination of the association constant between the Noxa B tracer and Mcl-1

Using the same protocol and mathematical treatment as for the p53/hDM2 interaction, a K_d of 32.5 ± 1.14 nM was determined (this titration was carried out by D. J. Yeo).



Direct titration of FITC-Noxa B with increasing concentrations of Mcl-1, plotted in Origin 8.

Displacement of the tracer by an unlabelled Noxa B peptide (150 nM protein - 50 nM tracer)



Displacement of the FITC-Noxa B tracer (50 nM) by an unlabelled Noxa B peptide (carried out myself).

Single point fluorescence anisotropy screening for inhibition of the p53/hDM2 interaction

A one point assay was carried out at a fixed concentration of inhibitor (10 μ M), p53₁₅₋₃₅-Flu (54.5 nM) and hDM2 (154.5 nM) in phosphate buffer. Each compound was assessed in triplicate and left to equilibrate for 1.5 hour in the dark. No protein denaturation was observed over time, as evidenced by the control/blank experiment lacking ligand in which the p53 tracer remains fully bound to the protein. A positive control was present on each test plate (Nutlin-3a in this case) at the same concentration as the test compounds. A set of controls was present at two diagonally opposed corner of the plate. A typical plate layout is represented in Figure E2. The anisotropy values were then determined and a percentage of efficiency was calculated for each compound relative to Nutlin-3a's efficiency.

	1	2	3	4	5	6	7	8	9	10	11	12
A					< Compound 1 >	< Compound 2 >	< Compound 3 >	< Compound 4 >	< Compound 5 >	< Compound 6 >	< Compound 7 >	< Compound 8 >
B	hDM2 (102 μ L) + Buffer (58 μ L)	p53* (50 μ L) + Buffer (110 μ L)	hDM2 (102 μ L) p53* (50 μ L) + Buffer (8 μ L)	hDM2 (94 μ L) p53* (50 μ L) + Nutlin (16 μ L)								
C												
D	/	/	/	/	Blank Cpd 1	Blank Cpd 2	Blank Cpd 3	Blank Cpd 4	Blank Cpd 5	Blank Cpd 6	Blank Cpd 7	Blank Cpd 8
E	< Compound 9 >	< Compound 10 >	< Compound 11 >	< Compound 12 >	< Compound 13 >	< Compound 14 >	< Compound 15 >	< Compound 16 >				
F									hDM2 (102 μ L) + Buffer (58 μ L)	p53* (50 μ L) + Buffer (110 μ L)	hDM2 (102 μ L) p53* (50 μ L) + Buffer (8 μ L)	hDM2 (94 μ L) p53* (50 μ L) + Nutlin (16 μ L)
G												
H	Blank Cpd 9	Blank Cpd 10	Blank Cpd 11	Blank Cpd 12	Blank Cpd 13	Blank Cpd 14	Blank Cpd 15	Blank Cpd 16	/	/	/	/

Figure E2. 96-well plate layout for single point screening

Automated single point fluorescence anisotropy screening for inhibition of the p53/hDM2 and Noxa B/Mcl-1 interactions

The same protocol and robot method was used for testing against both targeted interactions. Single point assays using the automated method on the Hamilton Microlab Star robot were carried out in 384-well plates (Perkin Elmer). Stock solutions of compounds to be tested were plated in a V-bottomed 96-well plate (source plate). The robot was programmed to prepare 3 test wells for each compound and one blank. The method initially transferred 10 μM of assay buffer to each well of the test plate. Subsequently 30 μL of protein was added to each well, followed by 15 μL tracer (or buffer for control wells). Protein and tracer were added in first in order to minimize the use of pipette tips. The stock compounds (typically at 100 μM in 99:1 (v/v) assay buffer: DMSO; 5 μL per well) were then transferred from the source plate. The first and last rows of each plate were not used in order to minimize error on the measurements due to uneven evaporation of the solution. Blanks and controls were present at either side of the plate, and the values were averaged in the intensity/anisotropy calculations. The final concentrations of tracer and protein were identical to those in the manual single point assay (100 nM protein and 50 nM tracer). The total volume in each well was 60 μL .

Fluorescence anisotropy competition assay titrations

Titrations carried out manually generally made use of 96-well plates. Initially, 50 μL of assay buffer were transferred into each well of the test plate. The compound was then serially diluted (100 μM - 9 nM, typically from 450 μM in 90:10 (v/v) assay buffer: DMSO) across both plates. A solution of p53-Flu in assay buffer was then added (50 μL , 54.5 nM final concentration), followed by hDM2 (50 μL , 154 nM final concentration) - the total volume of each well was 150 μL . The plates were then left to incubate for 1.5 hour in the dark and at room temperature prior to fluorescence polarization measurement. The results were analysed as described for the determination of the binding between the p53 tracer and hDM2, except the anisotropy values were plotted to a logistic model in Origin 8.6 (equation 5) and the IC_{50} was extracted directly from this curve.

$$y = r_{\min} + \frac{r_{\max} - r_{\min}}{1 + 10^{(x - \log x_0)^p}} \quad \text{Equation 5}$$

Where r_{\min} and r_{\max} are the minimum and maximum anisotropies determined from the protein titration, x_0 is the midpoint or IC_{50} and p is the power.

Automated method for competition assay titrations (Chapter 4)

Competition assay titrations prepared using the automated method were carried out in 384-well plates (Perkin Elmer). The Hamilton Microlab Star robot was programmed to prepare serial dilutions of each compound in triplicate. The method initially transferred 20 μ M of assay buffer to each well of the test plate. The stock compound (typically at 450 μ M in 90:10 (v/v) assay buffer: DMSO) was then transferred from the source plate and used to prepare a serial dilution across the test plate. Subsequently 20 μ L of tracer (or buffer for control wells) was added to each well, followed by 20 μ L protein. The final concentrations of tracer and protein were identical to those in the manual competition assay. The total volume in each well was 60 μ L.

High content imaging

The high content imaging experiment were carried out by Dr. H. Martin (Leeds Institute for Molecular Medicine) and in collaboration with Dr. D. Tomlinson (Astbury Centre for Molecular Biology, University of Leeds).

6.3 Solid phase synthesis of a library of oligoureas

General conditions

Unless otherwise noted, materials were obtained from commercial suppliers and used without further purification. NovaPEG Rink amide resin was purchased from Novabiochem. All organic solvents for solid phase synthesis were of analytical grade. Anhydrous THF was obtained from Sigma Aldrich and anhydrous dichloromethane was distilled over CaH_2 . RP-HPLC-quality

acetonitrile (CH₃CN) and MilliQ water were used for RP-HPLC analyses and purification. Thin layer chromatography (TLC) was performed on silica gel 60 F254 (Merck) with detection by UV light and charring with 1% ninhydrin in ethanol followed by heating. Flash column chromatography was carried out on silica gel (40-63 μm, Merck). ¹H NMR and ¹³C NMR spectra were recorded on an Avance II NMR spectrometer (Bruker Biospin) with a vertical 7.05T narrow-bore/ultrashield magnet operating at 300 MHz for ¹H observation and 75 MHz for ¹³C observation by means of a 5-mm direct BBO 1H/19F_XBB_H probe with Z gradient capabilities. Chemical shifts are reported in parts per million (ppm) relative to the ¹H residual signal of the deuterated solvent used. ¹H NMR splitting patterns with observed first-order coupling are designated as singlet (s), doublet (d), triplet (t), or quartet (q). Coupling constants (J) are reported in hertz (Hz). Analytical RP-HPLC analyses were performed on a Dionex U3000SD using a Macherey-Nagel Nucleodur column (4.6 × 100 mm, 3 μm) at a flow rate of 1 mL·min⁻¹. The mobile phase was composed of 0.1% (v/v) TFA-H₂O (Solvent A) and 0.1% TFA-CH₃CN (Solvent B). Semi-preparative purifications were performed on a Dionex U3000SD using a Macherey-Nagel Nucleodur column (10 × 250 mm, 5 μm). A gradient elution of 30 to 100% of B in 20 min at a flow rate of 4 mL min⁻¹ was applied. Column effluent was monitored by UV detection at 200 nm and 254 nm. ESI-MS analyses were carried out on a ThermoElectron LCQ Advantage spectrometer equipped with an ion trap mass analyzer and coupled with a ThermoElectron Surveyor HPLC system. Solid phase syntheses of oligoureas and hybrids with microwave irradiation were conducted on the Discover[®] System from CEM (CEM μWaves S.A.S., Orsay, France).

6.3.1 Monomer building blocks

(R)-benzyl (1-(tert-butoxy)-3-hydroxypropan-2-yl)carbamate 120a

The *N*-protected α-amino acid **119a** (5.00 g, 16.9 mmol) was dissolved in THF (50 mL) under nitrogen and cooled to 0 °C. After addition of isobutyl chloroformate (2.4 mL, 17.8 mmol) and *N*-methyldmorpholine (2.1 mL, 18.6 mmol), the mixture was stirred at 0 °C for 30 min. The resulting white suspension

was then filtered off and the filtrate was added at 0 °C to a solution of NaBH₄ (1.28 g, 33.9 mmol) in water (30 mL). The reaction mixture was left to react overnight and then a 1M solution of KHSO₄ (50 mL) was added. The resulting aqueous solution was extracted twice with EtOAc (50 mL). The combined organic layers were washed twice with 1M KHSO₄ (50 mL), twice with a saturated solution of NaHCO₃ (50 mL), once with brine (50 mL), dried over sodium sulfate and concentrated under reduced pressure then dried under high vacuum. The resulting colourless oil (4.80 g, quant.) did not require further purification. δ_{H} (CDCl₃, 300 MHz) 1.20 (s, 9H), 3.63 (d, 2H, $J = 3.0$ Hz), 3.75 (dd, 1H, $J = 10.6$ and 4.1 Hz), 3.83 (m, 1H), 3.89 (d, 1H, $J = 10.6$ Hz), 5.15 (s, 2H), 5.55 (d, 1H, $J = 7.2$ Hz), 7.34 – 7.41 (m, 5H).

(R)-2-amino-3-(tert-butoxy)propan-1-ol 121a

To a round bottom flask containing *N-Z* protected alcohol **120a** (4.80 g, 16.9 mmol) and 10% Pd/C was gently added MeOH (140 mL). The reaction was stirred overnight under 1 bar H₂ atmosphere (balloon). After filtration over Millipore filter paper, the filtrate was concentrated under reduced pressure to quantitatively furnish the target material as a pale yellow oil (2.49 g, 16.9 mmol, quant.). The amino derivative was not isolated and was directly engaged in the next step.

(R)-2-azido-3-(tert-butoxy)propan-1-ol 122a

To a solution of amine **121a** (2.49 g, 16.9 mmol) in MeOH (80 mL) were successively added K₂CO₃ (2.91 g, n + 0.5 mmol), CuSO₄·5H₂O (0.043 g, 0.1 mmol), and imidazole-1-sulfonyl azide hydrochloride (4.30 g, 20.5 mmol). The reaction mixture was stirred at room temperature for 2 hours and then filtered to remove the remaining K₂CO₃, concentrated under reduced pressure and dissolved in CH₂Cl₂ (80 mL). The resulting solution was washed twice with 1M KHSO₄ (50 mL), then with brine (50 mL), dried over sodium sulfate and concentrated under reduced pressure to furnish after silica gel purification (EtOAc – cyclohexane 3-7) the desired azide as a colourless oil (1.84 g, 10.62 mmol, 62%); δ_{H} (CDCl₃, 300 MHz) 1.25 (s, 9H), 3.60-3.64 (m, 3H), 3.69-3.75 (m, 1H), 3.77-3.83 (m, 1H); δ_{C} (CDCl₃, 75 MHz) 27.31, 62.26, 62.90, 63.46, 74.00.

(R)-2-(2-azido-3-(tert-butoxy)propyl)isoindoline-1,3-dione 123a

To a solution of triphenylphosphine (2.78 g, 10.6 mmol) in anhydrous THF (20 mL) at 0 °C and under positive N₂ atmosphere pressure were successively added DIAD (2.1 mL, 10.6 mmol) and phthalimide (1.56 g, 10.6 mmol). Azido alcohol **122a** (1.84 g, 10.6 mmol) was dissolved in anhydrous THF (10 mL) then added dropwise and the reaction mixture was stirred and allowed to reach room temperature. After 4 hours the reaction was complete. THF was evaporated under reduced pressure and the resulting material was purified by column chromatography (EtOAc – cyclohexane 2-8) to yield the desired azide (2.71 g, 9.0 mmol, 84%) as a pale yellow oil; δ_{H} (CDCl₃, 300 MHz) 1.24 (s, 9H), 3.56-3.61 (m, 1H), 3.64-3.68 (m, 1H), 3.73-3.80 (m, 1H), 3.85-3.96 (m, 2H), 7.76-7.78 (m, 2H), 7.89-7.92 (m, 2H).

(R)-2-azido-3-(tert-butoxy)propan-1-amine 124a

To a solution of azido phthalimide **123a** (2.71 g, 9.0 mmol) in MeOH (45 mL) was added hydrazine hydrate (1.3 mL, 26.9 mmol). The reaction mixture was refluxed for 4 hours then left to stir at room temperature overnight, with apparition of a white precipitate. The reaction mixture was filtered off, washed with MeOH and the filtrate was concentrated under reduced pressure. The crude material was dissolved in EtOAc (80 mL). The organic layer was washed twice with 1M KHSO₄ (2 × 25 mL). The combined aqueous phases were washed with EtOAc (2 × 25 mL) then neutralized by addition of solid NaHCO₃ until pH 8. The aqueous phase was finally extracted with CH₂Cl₂ (5 × 25 mL) and the combined organic layers were washed with brine (20 mL), dried over Na₂SO₄ and concentrated under reduced pressure to give the desired amine **124a** as a yellow oil (1.04 g, 6.0 mmol, 67%). The crude material was directly engaged in the activation step without further purification.

(R)-2,5-dioxopyrrolidin-1-yl (2-azido-3-(tert-butoxy)propyl)carbamate 116

To a stirred suspension of disuccinimidyl carbonate (1.81 g, 7.1 mmol) in anhydrous CH₂Cl₂ (50 mL) was added dropwise a solution of azido amine **124a** (1.02 g, 5.9 mmol) in anhydrous CH₂Cl₂ (40 mL). The resulting mixture was stirred at room temperature for 3 hours, then the solvent was evaporated under reduced pressure and the crude material dissolved in EtOAc (70 mL). The organic

phase was washed with 1M KHSO₄ (2 × 30 mL) then with brine (30 mL), dried over Na₂SO₄, filtered and concentrated under reduced pressure to give activated carbamate **116** (1.84 g, 5.8 mmol, 99%) as a pale yellow oil; δ_H (CDCl₃, 300 MHz) 1.24 (s, 9H), 2.85 (s, 4H), 3.35 (ddd, 1H, *J* = 5.3, 6.4 and 13.8 Hz), 3.49 (ddd, 1H, *J* = 5.3, 6.4 and 13.8 Hz), 3.58-3.60 (m, 2H), 3.73 (m, 1H), 5.75 (t, 1H, *J* = 5.3 Hz); δ_C (CDCl₃, 75 MHz) 25.49, 27.28, 43.05, 60.18, 62.82, 74.10, 151.52, 169.63.

(S)-tert-butyl(1-cyclohexyl-3-hydroxypropan-2-yl)carbamate 120b

The *N*-protected α-amino acid **119b** (3.00 g, 11.1 mmol) was dissolved in THF (35 mL) under nitrogen and cooled to 0 °C. After addition of isobutyl chloroformate (1.5 mL, 11.6 mmol) and *N*-methylemorpholine (1.3 mL, 12.2 mmol), the mixture was stirred at 0 °C for 30 min. The resulting white suspension was then filtered off and the filtrate was added at 0 °C to a solution of NaBH₄ (0.84 g, 22.1 mmol) in water (20 mL). The reaction mixture was left to react overnight and then a 1M solution of KHSO₄ (35 mL) was added. The resulting aqueous solution was extracted twice with EtOAc (35 mL). The combined organic layers were washed twice with 1M KHSO₄ (35 mL), twice with a saturated solution of NaHCO₃ (35 mL), once with brine (35 mL), dried over sodium sulfate and concentrated under reduced pressure then dried under high vacuum. The resulting colourless oil (2.48 g, 88%) did not require further purification. δ_H (CDCl₃, 300 MHz) 0.94 (m, 2H), 1.21 (m, 2H), 1.34 (m, 2H), 1.48 (s, 9H), 1.65-1.76 (m, 5H), 1.84 (m, 2H), 3.53 (dd, 1H, *J* = 6.4 and 11.3 Hz), 3.70 (m, 1H), 3.78 (br s, 1H), 4.58 (br d, 1H, *J* = 5.4 Hz).

(S)-2-amino-3-cyclohexylpropan-1-ol 121b

N-Boc protected amino alcohol **120b** (2.48 g, 9.72 mmol) was dissolved in pure TFA (7.0 mL) and left to react without stirring for 30 min. The TFA was then removed under reduced pressure and the TFA salt was dried under high vacuum overnight. The resulting crude material was not isolated and directly engaged in the next step.

(S)-2-azido-3-cyclohexylpropan-1-ol 122b

To a solution of amine **121b** (9.72 mmol) in MeOH (50 mL) were successively added K₂CO₃ (3.03 g, n + 0.5 mmol), CuSO₄·5H₂O (24 mg, 0.1 mmol), and imidazole-1-sulfonyl azide hydrochloride (2.45 g, 11.7 mmol). The reaction

mixture was stirred at room temperature for 2 hours and then filtered to remove the remaining K_2CO_3 , concentrated under reduced pressure and dissolved in CH_2Cl_2 (50 mL). The resulting solution was washed twice with 1M $KHSO_4$ (2×30 mL), then with brine (30 mL), dried over sodium sulfate and concentrated under reduced pressure to furnish after silica gel purification (EtOAc – cyclohexane 3-7) the desired azide as a colourless oil (0.78 g, 4.26 mmol, 44%); δ_H ($CDCl_3$, 300 MHz) 0.96 (m, 2H), 1.23 (m, 2H), 1.35 (m, 2H), 1.47 (m, 2H), 1.68-1.82 (m, 5H), 3.54-3.63 (m, 2H), 3.73 (m, 1H); δ_C ($CDCl_3$, 75 MHz) 26.08, 26.22, 26.44, 32.83, 33.76, 34.33, 38.00, 61.89, 65.76.

(S)-2-(2-azido-3-cyclohexylpropyl)isoindoline-1,3-dione 123b

To a solution of triphenylphosphine (1.12 g, 4.3 mmol) in anhydrous THF (15 mL) at 0 °C and under positive N_2 atmosphere pressure were successively added DIAD (0.9 mL, 4.3 mmol) and phthalimide (0.63 g, 4.3 mmol). Azido alcohol **122b** (0.78 g, 4.3 mmol) was dissolved in anhydrous THF (10 mL) then added dropwise and the reaction mixture was stirred and allowed to reach room temperature. After 4 hours the reaction was complete. THF was evaporated under reduced pressure and the resulting material was purified by column chromatography (EtOAc – cyclohexane 2-8) to yield the desired azide (1.01 g, 3.1 mmol, 71%) as a yellow oil; δ_H ($CDCl_3$, 300 MHz) 0.98 (m, 2H), 1.27 (m, 2H), 1.47 (m, 2H), 1.55 (m, 2H), 1.68-1.85 (m, 5H), 3.72 (m, 1H), 3.81-3.88 (m, 2H), 7.76-7.79 (m, 2H), 7.90-7.93 (m, 2H); δ_C ($CDCl_3$, 75 MHz) 26.04, 26.23, 26.42, 32.67, 33.68, 34.39, 39.59, 41.71, 58.01, 123.52, 131.88, 134.21, 168.21.

(S)-2-azido-3-cyclohexylpropan-1-amine 124b

To a solution of azido phthalimide **123b** (1.01 g, 3.1 mmol) in MeOH (20 mL) was added hydrazine hydrate (0.44 mL, 9.1 mmol). The reaction mixture was refluxed for 4 hours then left to stir at room temperature overnight, with apparition of a white precipitate. The reaction mixture was filtered off, washed with MeOH and the filtrate was concentrated under reduced pressure. The crude material was dissolved in EtOAc (40 mL). The organic layer was washed twice with 1M $KHSO_4$ (2×15 mL). The combined aqueous phases were washed with EtOAc (2×10 mL) then neutralized by addition of solid $NaHCO_3$ until pH 8. The aqueous phase was finally extracted with CH_2Cl_2 (5×15 mL) and the combined organic layers were

washed with brine (10 mL), dried over Na₂SO₄ and concentrated under reduced pressure to give the desired amine **124b** as a colourless oil (0.32 g, 1.78 mmol, 58%). The crude material was directly engaged in the activation step without further purification.

(S)-2,5-dioxopyrrolidin-1-yl (2-azido-3-cyclohexylpropyl)carbamate 117

To a stirred suspension of disuccinimidyl carbonate (0.55 g, 2.1 mmol) in anhydrous CH₂Cl₂ (20 mL) was added dropwise a solution of azido amine **124b** (0.32 g, 1.8 mmol) in anhydrous CH₂Cl₂ (15 mL). The resulting mixture was stirred at room temperature for 3 hours, then the solvent was evaporated under reduced pressure and the crude material dissolved in EtOAc (30 mL). The organic phase was washed with 1M KHSO₄ (2 × 10 mL) then with brine (10 mL), dried over Na₂SO₄, filtered and concentrated under reduced pressure to give activated carbamate **117** (0.42 g, 1.3 mmol, 73%) as a pale pink solid; δ_H (CDCl₃, 300 MHz) 0.93 (m, 2H), 1.22 (m, 2H), 1.41 (m, 2H), 1.51 (m, 2H), 1.64-1.82 (m, 5H), 2.87 (s, 4H), 3.15 (m, 1H), 3.51 (m, 1H), 3.69 (m, 1H); δ_C (CDCl₃, 75 MHz) 25.49, 26.02, 26.14, 26.36, 32.89, 33.52, 34.26, 39.33, 45.69, 59.37, 151.59, 169.63.

(S)-tert-butyl (1-(3,4-dichlorophenyl)-3-hydroxypropan-2-yl)carbamate 120c

The *N*-protected α-amino acid **119c** (0.70 g, 2.1 mmol) was dissolved in THF (10 mL) under nitrogen and cooled to 0 °C. After addition of isobutyl chloroformate (0.29 mL, 2.2 mmol) and *N*-methylmorpholine (0.25 mL, 2.3 mmol), the mixture was stirred at 0 °C for 30 min. The resulting white suspension was then filtered off and the filtrate was added at 0 °C to a solution of NaBH₄ (0.16 g, 4.2 mmol) in water (3 mL). The reaction mixture was left to react overnight and then a 1M solution of KHSO₄ (6 mL) was added. The resulting aqueous solution was extracted twice with EtOAc (10 mL). The combined organic layers were washed twice with 1M KHSO₄ (2 × 7 mL), twice with a saturated solution of NaHCO₃ (2 × 7 mL), once with brine (7 mL), dried over sodium sulfate and concentrated under reduced pressure then dried under high vacuum. The resulting white solid (0.61 g, 1.9 mmol, 90%) did not require further purification. δ_H (CDCl₃, 300 MHz) 1.45 (s, 9H), 2.85 (d, 2H, *J* = 7.2 Hz), 3.59 (dd, 1H, *J* = 4.3 and 10.9 Hz), 3.71 (dd, 1H, *J* =

4.3 and 10.9 Hz), 3.85 (m, 1H), 4.81 (br d, 1H, $J = 8.3$ Hz), 7.10 (dd, 1H, $J = 1.9$ and 8.3 Hz), 7.35 (d, 1H, $J = 1.9$ Hz), 7.40 (d, 1H, $J = 8.3$ Hz).

(S)-2-amino-3-(3,4-dichlorophenyl)propan-1-ol 121c

N-Boc protected amino alcohol **120c** (0.61 g, 1.89 mmol) was dissolved in pure TFA (2.0 mL) and left to react without stirring for 1 hour. The TFA was then removed under reduced pressure and the TFA salt was dried under high vacuum overnight. The resulting crude oil was not isolated and directly engaged in the next step.

(S)-2-azido-3-(3,4-dichlorophenyl)propan-1-ol 122c

To a solution of amine **121c** (1.89 mmol) in MeOH (10 mL) were successively added K_2CO_3 (0.64 g, $n + 0.5$ mmol where n is the total number of moles of acid present in the reaction mixture), $CuSO_4 \cdot 5H_2O$ (4.6 mg, 0.019 mmol), and imidazole-1-sulfonyl azide hydrochloride (0.47 g, 2.22 mmol). The reaction mixture was stirred at room temperature overnight and then filtered to remove the remaining K_2CO_3 , concentrated under reduced pressure and dissolved in EtOAc (20 mL). The resulting solution was washed twice with 1M $KHSO_4$ (2×10 mL), then with brine (10 mL), dried over sodium sulfate and concentrated under reduced pressure to furnish after silica gel purification (EtOAc – cyclohexane 3-7) the desired azide as a colourless oil (0.30 g, 1.23 mmol, 67%); δ_H ($CDCl_3$, 300 MHz) 2.80 (dd, 1H, $J = 7.7$ and 14.0 Hz), 2.90 (dd, 1H, $J = 5.5$ and 13.8 Hz), 3.62 (m, 1H), 3.68-3.80 (m, 2H), 7.13 (dd, 1H, $J = 1.7$ and 8.3 Hz), 7.38 (m, 1H), 7.43 (d, 1H, $J = 8.2$ Hz).

(S)-2-(2-azido-3-(3,4-dichlorophenyl)propyl)isoindoline-1,3-dione 123c

To a solution of triphenylphosphine (0.32 g, 1.2 mmol) in anhydrous THF (5 mL) at 0 °C and under positive N_2 atmosphere pressure were successively added DIAD (0.24 mL, 1.2 mmol) and phthalimide (0.18 g, 1.2 mmol). Azido alcohol **122c** (0.30 g, 1.2 mmol) was dissolved in anhydrous THF (1 mL) then added dropwise and the reaction mixture was stirred and allowed to reach room temperature. After 4 hours the reaction was complete. THF was evaporated under reduced pressure and the resulting material was purified by column chromatography (EtOAc – cyclohexane 2-8) to yield the desired azide (0.27 g, 0.74 mmol, 60%) as a yellow oil; δ_H ($CDCl_3$, 300 MHz) 2.83 (dd, 1H, $J = 8.7$ and 14.2 Hz), 2.94 (dd, 1H, J

= 5.3 and 14.2 Hz), 3.80 (dd, 1H, J = 5.3 and 13.6 Hz), 3.91 (dd, 1H, J = 8.3 and 14.0 Hz), 4.06 (m, 1H), 7.14 (dd, 1H, J = 1.9 and 8.3 Hz), 7.39-7.42 (m, 2H), 7.78 (dd, 2H, J = 3.0 and 5.3 Hz), 5.90 (dd, 2H, J = 3.0 and 5.3 Hz).

(S)-2-azido-3-(3,4-dichlorophenyl)propan-1-amine 124c

To a solution of azido phthalimide **123c** (0.27 g, 0.74 mmol) in MeOH (5 mL) was added hydrazine hydrate (0.11 mL, 2.3 mmol). The reaction mixture was refluxed for 4 hours then left to stir at room temperature overnight, with apparition of a white precipitate. The reaction mixture was filtered off, washed with MeOH and the filtrate was concentrated under reduced pressure. The crude material was dissolved in EtOAc (10 mL). The organic layer was washed twice with 1M KHSO₄ (2 × 5 mL). The combined aqueous phases were washed with EtOAc (2 × 50 mL) then neutralized by addition of solid NaHCO₃ until pH 8. The aqueous phase was finally extracted with CH₂Cl₂ (5 × 5 mL) and the combined organic layers were washed with brine (5 mL), dried over Na₂SO₄ and concentrated under reduced pressure to give the desired amine **6c** as a colourless oil (0.15 g, 0.53 mmol, 73%). The crude material was directly engaged in the activation step without further purification.

(S)-2,5-dioxopyrrolidin-1-yl (2-azido-3-(3,4-dichlorophenyl)propyl) carbamate 118

To a stirred suspension of disuccinimidyl carbonate (0.16 g, 0.63 mmol) in anhydrous CH₂Cl₂ (5 mL) was added dropwise a solution of azido amine **124c** (0.15 g, 0.53 mmol) in anhydrous CH₂Cl₂ (3 mL). The resulting mixture was stirred at room temperature for 3 hours, then the solvent was evaporated under reduced pressure and the crude material dissolved in EtOAc (20 mL). The organic phase was washed with 1M KHSO₄ (2 × 10 mL) then with brine (10 mL), dried over Na₂SO₄, filtered and concentrated under reduced pressure to give activated carbamate **118** (0.15 g, 0.38 mmol, 72%) as a pale yellow solid; δ_{H} (CDCl₃, 300 MHz) 2.82 (s, 4H), 2.89 (d, 2H, J = 7.2 Hz), 3.17 (m, 1H), 3.46 (m, 1H), 3.84 (m, 1H), 7.19 (d, 2H, J = 7.8 Hz), 7.26 (d, 2H, J = 7.8 Hz), 7.37 (s, 1H); δ_{C} (CDCl₃, 75 MHz) 25.48, 38.41, 44.93, 62.94, 76.64, 77.07, 77.49, 127.23, 128.86, 129.32, 136.20, 139.24, 142.26, 151.63, 169.82.

6.3.2 Microwave assisted solid phase synthesis of oligoureas

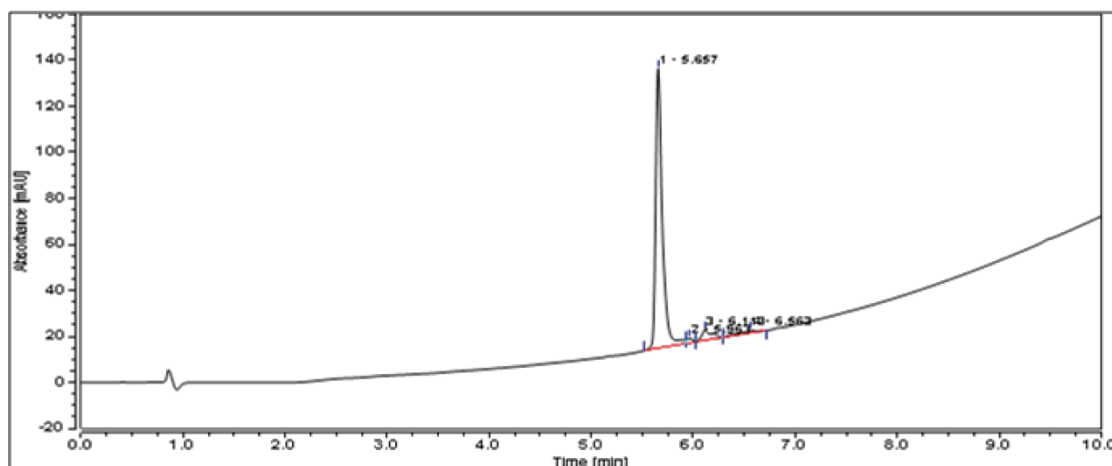
The NovaPEG Rink amide resin (0.10 g, 0.049 mmol) was placed in a polypropylene SPE tube (CEM), suspended in DMF (2 mL) and the first activated monomer (0.074 mmol, 1.5 equiv relative to resin loading) and DIEA (26 μ L, 0.148 mmol) were successively added. The tube was then placed inside the microwave reactor (CEM Discover) and irradiated (25 W maximum power, 70 °C, ramp 5 min, hold 15 min). All microwave experiments were conducted at atmospheric pressure. The temperature was maintained by modulation of power and controlled with a fiber optic sensor. Coupling with the activated monomer was repeated once. The tube was then removed from the microwave reactor and the resin was filtered off, washed four times with DMF (3 mL) and two times with DCM (3 mL). The coupling efficiency was monitored using chloranil test. Reduction of the azide group was next done with microwave assistance by swelling the resin in a mixture of dioxane/water (70:30, v/v, 2 mL) and adding 1M PMe₃ solution in THF (0.490 mL, 10 equiv relative to the resin loading), irradiating with 25 W power, heating at 70 °C for 30 min. The reaction was repeated once. The resin was then filtered off, washed with the dioxane/water mixture (2 \times 3 mL) and DMF (3 \times 3 mL). The preceding acylation steps and reduction of azides were repeated. End-capping was carried out once in presence of isopropylisocyanate (3 equiv) and DIEA (3 equiv) and under microwave assistance (25 W, 70 °C, 15 min). Resin was filtered off, washed with DMF (2 \times 2 mL) and DCM (2 \times 2 mL) and dried. The resin was finally swelled in pure TFA and left to react for 120 min. After that time, the resin was filtered off, washed with DCM and the filtrate was evaporated under reduced pressure.

Purification

All oligoureas were purified by preparative HPLC, the gradient elution is specified for each compound and a typical flow rate of 4 mL \cdot min⁻¹ was applied. Column effluent was monitored by UV detection at 200 nm and 254 nm. Oligoureas **129** – **135** were purified and characterized by Dr. C. Casassus (Guichard group). A representative analytical HPLC trace was included for compound **125**.

Oligourea 125 (*i*Pr-^UPhe-^UPhe-^UAla-^UTrp-^UOrn-^ULeu)

Oligourea **125** was prepared following the standard procedure using the following amount of each reagents: ^UPhe 4 × 23.3 mg, ^UAla 2 × 17.6 mg, ^UTrp 2 × 33.4 mg, ^UOrn 2 × 28.1 mg, ^ULeu 2 × 20.8 mg, DIEA 26 μL per coupling, isopropyl isocyanate 2 × 14 μL. HPLC purity of crude product 80%. Yield after cleavage/purification 3.8%; white powder; RP-HPLC t_R 5.66 min (gradient, 30-100% of B in 10 min); ESI-HRMS found m/z 1055.4 [M+H]⁺, C₄₉H₈₃N₁₇O₇ requires 1055.66.



Oligourea 126 (*i*Pr-^UPhe-^UOrn-^UAla-^UTrp-^UOrn-^ULeu)

Oligourea **126** was prepared following the standard procedure using the following amount of each reagents: ^UPhe 2 × 23.3 mg, ^UOrn 4 × 28.1 mg, ^UAla 2 × 17.6 mg, ^UTrp 2 × 33.4 mg, ^ULeu 2 × 20.8 mg, DIEA 26 μL per coupling, isopropyl isocyanate 2 × 14 μL. HPLC purity of crude product 50%. Yield after cleavage/purification 2.6%; white powder; RP-HPLC t_R 4.06 min (gradient, 30-100% of B in 10 min); ESI-MS found m/z 512.3 [M+2H]²⁺; ESI-HRMS found m/z 1022.6781 [M+H]⁺, C₅₃H₈₃N₁₆O₇ requires 1022.67.

Oligourea 127 (^UPhe-^UOrn-^UAla-^UTrp-^UOrn-^ULeu)

Oligourea **127** was prepared following the standard procedure using the following amount of each reagents: ^UPhe 2 × 23.3 mg, ^UOrn 4 × 28.1 mg, ^UAla 2 × 17.6 mg, ^UTrp 2 × 33.4 mg, ^ULeu 2 × 20.8 mg, DIEA 26 μL per coupling. HPLC purity of crude product 40%. Yield after cleavage/purification 3%; white powder; RP-HPLC t_R 2.68 min (gradient, 30-100% of B in 10 min).

Oligourea 128 (^UPhe-^UOrn-^UTrp-^UAla-^UOrn-^ULeu)

Oligourea **128** was prepared following the standard procedure using the following amount of each reagents: ^UPhe 2 × 23.3 mg, ^UOrn 4 × 28.1 mg, ^UTrp 2 × 33.4 mg, ^UAla 2 × 17.6 mg, ^ULeu 2 × 20.8 mg, DIEA 26 μL per coupling. HPLC purity of crude product 60%. Yield after cleavage/purification 4%; white powder; RP-HPLC *t_R* 1.08 min (gradient, 30-100% of B in 10 min).

Oligourea 129 (αPhe-^UOrn-^UAla-^UTrp-^UOrn-^ULeu)

Oligourea **129** was prepared following the standard procedure using the following amount of each reagents: αPhe 2 × 95 mg, ^UOrn 4 × 28.1 mg, ^UAla 2 × 17.6 mg, ^UTrp 2 × 33.4 mg, ^ULeu 2 × 20.8 mg, DIEA 26 μL per coupling. For α-amino acids, a single coupling of 30 min was carried out using 5 equiv of amino acid per coupling, 5 equiv of BOP *i.e.* 108 mg and 7 equiv of DIEA *i.e.* 60 μL. HPLC purity of crude product 80%. Yield after cleavage/purification 7.4%; white powder; RP-HPLC *t_R* 1.20 min (gradient, 30-100% of B in 10 min).

Oligourea 130 (αPhe-^UOrn-^UAla-^UTrp-^UOrn-αLeu-αSer)

Oligourea **130** was prepared following the standard procedure using the following amount of each reagents: αPhe 95 mg, ^UOrn 4 × 28.1 mg, ^UAla 2 × 17.6 mg, ^UTrp 2 × 33.4 mg, αLeu 87 mg, αSer(OtBu) 94 mg, DIEA 26 μL per coupling. For α-amino acids, a single coupling of 30 min was carried out using 5 equiv of amino acid per coupling, 5 equiv of BOP *i.e.* 108 mg and 7 equiv of DIEA *i.e.* 60 μL. HPLC purity of crude product 80%. Yield after cleavage/purification 0.65%; white powder; RP-HPLC *t_R* 1.08 min (gradient, 30-100% of B in 10 min).

Oligourea 131 (*i*Pr-^UPhe-^USer-^UAla-^UTrp-^UOrn-^ULeu)

Oligourea **131** was prepared following the standard procedure using the following amount of each reagents: ^UPhe 2 × 23.3 mg, ^USer 2 × 22.7 mg, ^UAla 2 × 17.6 mg, ^UTrp 2 × 33.4 mg, ^UOrn 2 × 28.1 mg, ^ULeu 2 × 20.8 mg, DIEA 26 μL per coupling, isopropyl isocyanate 2 × 14 μL. HPLC purity of crude product 75%. Yield after cleavage/purification 6.7%; white powder; RP-HPLC *t_R* 4.57 min (gradient, 30-100% of B in 10 min); ESI-HRMS found *m/z* 995.4 [M+H]⁺, C₄₇H₇₉N₁₆O₈ requires 995.63.

Oligourea 132 (^UPhe-^USer-^UAla-^UTrp-^UOrn-^ULeu)

Oligourea **132** was prepared following the standard procedure. HPLC purity of crude product 75%. Yield after cleavage/purification 1.1%; white powder; RP-HPLC t_R 1.11 min (gradient, 30-100% of B in 10 min).

Oligourea 133 (*i*Pr-^UPhe-^UOrn-^UAla-^UTrp-^USer-^ULeu)

Oligourea **133** was prepared following the standard procedure using the following amount of each reagents: ^UPhe 2 × 23.3 mg, ^UOrn 2 × 28.1 mg, ^UAla 2 × 17.6 mg, ^UTrp 2 × 33.4 mg, ^USer 2 × 22.7 mg, ^ULeu 2 × 20.8 mg, DIEA 26 μL per coupling, isopropyl isocyanate 2 × 14 μL. HPLC purity of crude product 80%. Yield after cleavage/purification 8.1%; white powder; RP-HPLC t_R 4.41 min (gradient, 30-100% of B in 10 min); ESI-MS found m/z 498.6 [M+2H]⁺, ESI-HRMS found m/z 995.6 [M+H]⁺, C₄₇H₇₉N₁₆O₈ requires 995.63.

Oligourea 134 (^UPhe-^UOrn-^UAla-^UTrp-^USer-^ULeu)

Oligourea **134** was prepared following the standard procedure using the following amount of each reagents: ^UPhe 2 × 23.3 mg, ^UOrn 2 × 28.1 mg, ^UAla 2 × 17.6 mg, ^UTrp 2 × 33.4 mg, ^USer 2 × 22.7 mg, ^ULeu 2 × 20.8 mg, DIEA 26 μL per coupling. HPLC purity of crude product 60%. Yield after cleavage/purification 4.7%; white powder; RP-HPLC t_R 2.08 min (gradient, 30-100% of B in 10 min).

Oligourea 135 (*i*Pr-^UPhe-^USer-^ULeu-^UTrp-^UOrn-^ULeu)

Oligourea **135** was prepared following the standard procedure using the following amount of each reagents: ^UPhe 2 × 23.3 mg, ^USer 2 × 22.7 mg, ^ULeu 4 × 20.8 mg, ^UTrp 2 × 33.4 mg, ^UOrn 2 × 28.1 mg, DIEA 26 μL per coupling, isopropyl isocyanate 2 × 14 μL. HPLC purity of crude product 60%. Yield after cleavage/purification 5.5%; white powder; RP-HPLC t_R 2.08 min (gradient, 30-100% of B in 10 min); ESI-MS found m/z 520.2 [M+2H]⁺; ESI-HRMS found m/z 1037.3 [M+H]⁺, C₅₀H₈₅N₁₆O₈ requires 1037.68.

References

1. V. Azzarito, K. Long, N. S. Murphy and A. J. Wilson, *Nat. Chem.*, 2013, **5**, 161-173.
2. A. J. Wilson, *Chem. Soc. Rev.*, 2009, **38**, 3289 - 3300.
3. G. C. Kresheck, L. B. Vitello and J. E. Erman, *Biochemistry*, 1995, **34**, 8398-8405.
4. J. A. Wells and C. L. McClendon, *Nature*, 2007, **450**, 1001-1009.
5. D. R. Burton, *Acc. Chem. Res.*, 1993, **26**, 405-411.
6. B. Li, J. Y. K. Tom, D. Oare, R. Yen, W. J. Fairbrother, J. A. Wells and B. C. Cunningham, *Science*, 1995, **270**, 1657-1660.
7. L. T. Vassilev, B. T. Vu, B. Graves, D. Carvajal, F. Podlaski, Z. Filipovic, N. Kong, U. Kammlott, C. Lukacs, C. Klein, N. Fotouhi and E. A. Liu, *Science*, 2004, **303**, 844-848.
8. S. P. Brown and P. J. Hajduk, *ChemMedChem*, 2006, **1**, 70-72.
9. D. M. Rosenbaum, S. G. F. Rasmussen and B. K. Kobilka, *Nature*, 2009, **459**, 356-363.
10. K. Lundstrom, *Bioorg. Med. Chem. Lett.*, 2005, **15**, 3654-3657.
11. J. M. Davis, L. K. Tsou and A. D. Hamilton, *Chem. Soc. Rev.*, 2007, **36**, 326-334.
12. B. N. Bullock, A. L. Jochim and P. S. Arora, *J. Am. Chem. Soc.*, 2011, **133**, 14220-14223.
13. W. T. Astbury and H. J. Woods, *Nature*, 1930, **126**, 913-914.
14. L. Pauling, R. B. Corey and H. R. Branson, *Proc. Natl. Acad. Sci. USA*, 1951, **37**, 205-211.
15. T. Clackson and J. A. Wells, *Science*, 1995, **267**, 383-386.
16. W. E. Stites, *Chem. Rev.*, 1997, **97**, 1233-1250.
17. L. Pauling and R. B. Corey, *Fortschr. Chem. Org. Natur.*, 1954, **11**, 180-239.
18. D. C. Chan, C. T. Chutkowski and P. S. Kim, *Proc. Natl. Acad. Sci. USA*, 1998, **95**, 15613-15617.
19. P. Chene, *Nat. Rev. Cancer*, 2003, **3**, 102-109.
20. J. K. Murray and S. H. Gellman, *Peptide Science*, 2007, **88**, 657-686.
21. S. Patel and M. R. Player, *Expert Opin. Investig. Drugs*, 2008, **17**, 1865-1882.
22. P. H. Kussie, S. Gorina, V. Marechal, B. Elenbaas, J. Moreau, A. J. Levine and N. P. Pavletich, *Science*, 1996, **274**, 948-953.
23. S. Cory and J. M. Adams, *Nat. Rev. Cancer*, 2002, **2**, 647-656.
24. M. Sattler, H. Liang, D. Nettlesheim, R. P. Meadows, J. E. Harlan, M. Eberstadt, H. S. Yoon, S. B. Shuker, B. S. Chang, A. J. Minn, C. B. Thompson and S. W. Fesik, *Science*, 1997, **275**, 983-986.
25. G. Lessene, P. E. Czabotar and P. M. Colman, *Nat. Rev. Drug Discov.*, 2008, **7**, 989-1000.
26. B. P. Orner, J. T. Ernst and A. D. Hamilton, *J. Am. Chem. Soc.*, 2001, **123**, 5382-5383.
27. B. Vogelstein, D. Lane and A. J. Levine, *Nature*, 2000, **408**, 307-310.
28. M. A. Ziemer, A. Mason and D. M. Carlson, *J. Biol. Chem.*, 1982, **257**, 1176-1180.
29. L. Romer, C. Klein, A. Dehner, H. Kessler and J. Buchner, *Angew. Chem. Int. Ed.*, 2006, **45**, 6440-6460.

30. A. Satyanarayana, M. B. Hilton and P. Kaldis, *Mol. Biol. Cell*, 2008, **19**, 65-77.
31. M. Hollstein, D. Sidransky, B. Vogelstein and C. Harris, *Science*, 1991, **253**, 49-53.
32. E.-S. Han, F. L. Muller, V. I. Perez, W. Qi, H. Liang, L. Xi, C. Fu, E. Doyle, M. Hickey, J. Cornell, C. J. Epstein, L. J. Roberts, H. Van Remmen and A. Richardson, *Physiol. Genomics*, 2008, **34**, 112-126.
33. A. J. Levine, W. Hu and Z. Feng, *Cell Death Differ.*, 2006, **13**, 1027-1036.
34. Z. N. Oltvai, C. L. Milliman and S. J. Korsmeyer, *Cell*, 1993, **74**, 609-619.
35. M. Y. Li, C. L. Brooks, F. Wu-Baer, D. L. Chen, R. Baer and W. Gu, *Science*, 2003, **302**, 1972-1975.
36. R. Honda, H. Tanaka and H. Yasuda, *FEBS Lett.*, 1997, **420**, 25-27.
37. S. N. Jones, A. E. Roe, L. A. Donehower and A. Bradley, *Nature*, 1995, **378**, 206-208.
38. R. M. D. Luna, D. S. Wagner and G. Lozano, *Nature*, 1995, **378**, 203-206.
39. J. Parant, A. Chavez-Reyes, N. A. Little, W. Yan, V. Reinke, A. G. Jochemsen and G. Lozano, *Nat. Genet.*, 2001, **29**, 92-95.
40. J. Phan, Z. Y. Li, A. Kasprzak, B. Z. Li, S. Sebt, W. Guida, E. Schonbrunn and J. D. Chen, *J. Biol. Chem.*, 2010, **285**, 2174-2183.
41. J. M. Cummins, C. Rago, M. Kohli, K. W. Kinzler, C. Lengauer and B. Vogelstein, *Nature*, 2004, **428**.
42. J. J. Gu, H. Kawai, L. G. Nie, H. Kitao, D. Wiederschain, A. G. Jochemsen, J. Parant, G. Lozano and Z. M. Yuan, *J. Biol. Chem.*, 2002, **277**, 19251-19254.
43. J. C. Marine and A. G. Jochemsen, *Biochem. Biophys. Res. Commun.*, 2005, **331**, 750-760.
44. Y. Haupt, R. Maya, A. Kazaz and M. Oren, *Nature*, 1997, **387**, 296-299.
45. J. D. Oliner, J. A. Pietenpol, S. Thiagalingam, J. Gvuris, K. W. Kinzler and B. Vogelstein, *Nature*, 1993, **362**, 857-860.
46. P. Chene, J. Fuchs, I. Carena, P. Furet and C. G. Echeverria, *FEBS Lett.*, 2002, **529**, 293-297.
47. H. Wang, L. Nan, D. Yu, S. Agrawal and R. W. Zhang, *Clin. Cancer Res.*, 2001, **7**, 3613-3624.
48. G. M. Popowicz, A. Czarna and T. A. Holak, *Cell Cycle*, 2008, **7**, 2441-2443.
49. X. M. Yin, Z. N. Oltvai and S. J. Korsmeyer, *Nature*, 1994, **369**, 321-323.
50. T. Chittenden, C. Flemington, A. B. Houghton, R. G. Ebb, G. J. Gallo, B. Elangovan, G. Chinnadurai and R. J. Lutz, *EMBO J.*, 1995, **14**, 5589-5596.
51. M. Hirotsu, Y. K. Zhang, N. Fujita, M. Naito and T. Tsuruo, *J. Biol. Chem.*, 1999, **274**, 20415-20420.
52. R. J. Youle and A. Strasser, *Nat. Rev. Molec. Cell Biol.*, 2008, **9**, 47-59.
53. T. Kuwana, M. R. Mackey, G. Perkins, M. H. Ellisman, M. Latterich, R. Schneider, D. R. Green and D. D. Newmeyer, *Cell*, 2002, **111**, 331-342.
54. T. Lindsten, A. J. Ross, A. King, W. X. Zong, J. C. Rathmell, H. A. Shiels, E. Ulrich, K. G. Waymire, P. Mahar, K. Frauwirth, Y. F. Chen, M. Wei, V. M. Eng, D. M. Adelman, M. C. Simon, A. Ma, J. A. Golden, G. Evan, S. J. Korsmeyer, G. R. MacGregor and C. B. Thompson, *Mol. Cell*, 2000, **6**, 1389-1399.
55. M. C. Wei, W. X. Zong, E. H. Y. Cheng, T. Lindsten, V. Panoutsakopoulou, A. J. Ross, K. A. Roth, G. R. MacGregor, C. B. Thompson and S. J. Korsmeyer, *Science*, 2001, **292**, 727-730.
56. C. Ploner, R. Kofler and A. Villunger, *Oncogene*, 2008, **27**, S84-S92.

57. E. Oda, R. Ohki, H. Murasawa, J. Nemoto, T. Shibue, T. Yamashita, T. Tokino, T. Taniguchi and N. Tanaka, *Science*, 2000, **288**, 1053-1058.
58. L. Chen, S. N. Willis, A. Wei, B. J. Smith, J. I. Fletcher, M. G. Hinds, P. M. Colman, C. L. Day, J. M. Adams and D. C. S. Huang, *Mol. Cell*, 2005, **17**, 393-403.
59. A. Strasser, D. C. S. Huang and D. L. Vaux, *Biochim. Biophys. Acta*, 1997, **1333**, F151-F178.
60. X. Lin, S. Morgan-Lappe, X. Huang, L. Li, D. M. Zakula, L. A. Verneti, S. W. Fesik and Y. Shen, *Oncogene*, 2007, **26**, 3972-3979.
61. A. Degtarev, A. Lugovskoy, M. Cardone, B. Mulley, G. Wagner, T. Mitchison and J. Y. Yuan, *Nat. Cell Biol.*, 2001, **3**, 173-182.
62. M. Nguyen, R. C. Marcellus, A. Roulston, M. Watson, L. Serfass, S. R. Murthy-Madiraju, D. Goulet, J. Viallet, L. Belec, X. Billot, S. Acoca, E. Purisima, A. Wiegmanns, L. Cluse, R. W. Johnstone, P. Beauparlant and G. C. Shore, *Proc. Natl. Acad. Sci. USA*, 2007, **104**, 19512-19517.
63. S. Shangary, D. Qin, D. McEachern, M. Liu, R. S. Miller, S. Qiu, Z. Nikolovska-Coleska, K. Ding, G. Wang, J. Chen, D. Bernard, J. Zhang, Y. Lu, Q. Gu, R. B. Shah, K. J. Pienta, X. Ling, S. Kang, M. Guo, Y. Sun, D. Yang and S. Wang, *Proc. Natl. Acad. Sci. USA*, 2008, **105**, 3933-3938.
64. J. L. Wang, D. X. Liu, Z. J. Zhang, S. M. Shan, X. B. Han, S. M. Srinivasula, C. M. Croce, E. S. Alnemri and Z. W. Huang, *Proc. Natl. Acad. Sci. USA*, 2000, **97**, 7124-7129.
65. T. Oltersdorf, S. W. Elmore, A. R. Shoemaker, R. C. Armstrong, D. J. Augeri, B. A. Belli, M. Bruncko, T. L. Deckwerth, J. Dinges, P. J. Hajduk, M. K. Joseph, S. Kitada, S. J. Korsmeyer, A. R. Kunzer, A. Letai, C. Li, M. J. Mitten, D. G. Nettesheim, S.-C. Ng, P. M. Nimmer, J. M. O'Connor, A. Oleksijew, A. M. Petros, J. C. Reed, W. Shen, S. K. Tahir, C. B. Thompson, K. J. Tomaselli, B. Wang, M. D. Wendt, H. Zhang, S. W. Fesik and S. H. Rosenberg, *Nature*, 2005, **435**, 677-681.
66. M. X. Xia, D. Knezevic, C. Tovar, B. Y. Huang, D. C. Heimbrook and L. T. Vassilev, *Cell Cycle*, 2008, **7**, 1604-1612.
67. Clinicaltrials.gov, NCT01143519, Study of the Effect of SNPs in p53 and p53 Response Elements on the Inflammatory Response to DNA Damage (using Nutlin or Doxorubicin as chemotherapeutic agents).
68. B. L. Grasberger, T. Lu, C. Schubert, D. J. Parks, T. E. Carver, H. K. Koblish, M. D. Cummings, L. V. LaFrance, K. L. Milkiewicz, R. R. Calvo, D. Maguire, J. Lattanze, C. F. Franks, S. Zhao, K. Ramachandren, G. R. Bylebyl, M. Zhang, C. L. Manthey, E. C. Petrella, M. W. Pantoliano, I. C. Deckman, J. C. Spurlino, A. C. Maroney, B. E. Tomczuk, C. J. Molloy and R. F. Bone, *J. Med. Chem.*, 2005, **48**, 909-912.
69. H. K. Koblish, S. Y. Zhao, C. F. Franks, R. R. Donatelli, R. M. Tominovich, L. V. LaFrance, K. A. Leonard, J. M. Gushue, D. J. Parks, R. R. Calvo, K. L. Milkiewicz, J. J. Marugan, P. Raboisson, M. D. Cummings, B. L. Grasberger, D. L. Johnson, T. B. Lu, C. J. Molloy and A. C. Maroney, *Mol. Cancer Ther.*, 2006, **5**, 160-169.
70. J. Li, J. Viallet and E. B. Haura, *Cancer Chemother. Pharmacol.*, 2008, **61**, 525-534.
71. G. Z. Tang, Z. Nikolovska-Coleska, S. Qiu, C. Y. Yang, J. Guo and S. M. Wang, *J. Med. Chem.*, 2008, **51**, 717-720.

72. L. Zhang, H. X. Jiang, X. X. Cao, H. Y. Zhao, F. Wang, Y. X. Cui and B. Jiang, *Eur. J. Med. Chem.*, 2009, **44**, 3961-3972.
73. K. Ding, Y. Lu, Z. Nikolovska-Coleska, S. Qiu, Y. S. Ding, W. Gao, J. Stuckey, K. Krajewski, P. P. Roller, Y. Tomita, D. A. Parrish, J. R. Deschamps and S. M. Wang, *J. Am. Chem. Soc.*, 2005, **127**, 10130-10131.
74. J. A. Canner, M. Sobo, S. Ball, B. Hutzen, S. DeAngelis, W. Willis, A. W. Studebaker, K. Ding, S. Wang, D. Yang and J. Lin, *Br. J. Cancer*, 2009, **101**, 774-781.
75. A. M. Petros, J. Dinges, D. J. Augeri, S. A. Baumeister, D. A. Betebenner, M. G. Bures, S. W. Elmore, P. J. Hajduk, M. K. Joseph, S. K. Landis, D. G. Nettesheim, S. H. Rosenberg, W. Shen, S. Thomas, X. L. Wang, I. Zanze, H. C. Zhang and S. W. Fesik, *J. Med. Chem.*, 2006, **49**, 656-663.
76. P. J. Hajduk, *Mol. Interv.*, 2006, **6**, 266-272.
77. E. F. Lee, P. E. Czabotar, B. J. Smith, K. Deshayes, K. Zobel, P. M. Colman and W. D. Fairlie, *Cell Death Differ.*, 2007, **14**, 1711-1713.
78. Clinicaltrials.gov, 2011-present.
79. S. J. Duncan, S. Gruschow, D. H. Williams, C. McNicholas, R. Purewal, M. Hajek, M. Gerlitz, S. Martin, S. K. Wrigley and M. Moore, *J. Am. Chem. Soc.*, 2001, **123**, 554-560.
80. S. J. Duncan, M. A. Cooper and D. H. Williams, *Chem. Commun.*, 2003, 316-317.
81. A. M. Petros, D. G. Nettesheim, Y. Wang, E. T. Olejniczak, R. P. Meadows, J. Mack, K. Swift, E. D. Matayoshi, H. C. Zhang, C. B. Thompson and S. W. Fesik, *Protein Sci.*, 2000, **9**, 2528-2534.
82. O. M. Stephens, S. Kim, B. D. Welch, M. E. Hodsdon, M. S. Kay and A. Schepartz, *J. Am. Chem. Soc.*, 2005, **127**, 13126-12127.
83. J. A. Kritzer, O. M. Stephens, D. A. Guarracino, S. K. Reznik and A. Schepartz, *Bioorg. Med. Chem.*, 2005, **13**, 11-16.
84. E. A. Harker, D. S. Daniels, D. A. Guarracino and A. Schepartz, *Bioorg. Med. Chem.*, 2009, **17**, 2038-2046.
85. J. A. Kritzer, J. D. Lear, M. E. Hodsdon and A. Schepartz, *J. Am. Chem. Soc.*, 2004, **126**, 9468-9469.
86. D. S. Daniels, E. J. Petersson, J. X. Qiu and A. Schepartz, *J. Am. Chem. Soc.*, 2007, **129**, 1532-1533.
87. J. D. Sadowsky, W. D. Fairlie, E. B. Hadley, H.-S. Lee, N. Umezawa, Z. Nikolovska-Coleska, S. Wang, D. C. S. Huang, Y. Tomita and S. H. Gellman, *J. Am. Chem. Soc.*, 2007, **129**, 139-154.
88. W. S. Horne, L. M. Johnson, T. J. Ketas, P. J. Klasse, M. Lu, J. P. Moore and S. H. Gellman, *Proc. Natl. Acad. Sci. USA*, 2009, **106**, 14751-14756.
89. W. S. Horne, M. D. Boersma, M. A. Windsor and S. H. Gellman, *Angew. Chem. Int. Ed.*, 2008, **47**, 2853-2856.
90. E. F. Lee, J. D. Sadowsky, B. J. Smith, P. E. Czabotar, K. J. Peterson-Kaufman, P. M. Colman, S. H. Gellman and W. D. Fairlie, *Angew. Chem. Int. Ed.*, 2009, **48**, 4318-4322.
91. E. R. Blout, P. Doty and J. T. Yang, *J. Am. Chem. Soc.*, 1957, **79**, 749-750.
92. A. J. Doig and R. L. Baldwin, *Protein Sci.*, 1995, **4**, 1325-1336.
93. M. E. Houston, C. L. Gannon, C. M. Kay and R. S. Hodges, *J Pept Sci*, 1995, **1**, 274-282.

94. D. Y. Jackson, D. S. King, J. Chmielewski, S. Singh and P. G. Schultz, *J. Am. Chem. Soc.*, 1991, **113**, 9391-9392.
95. A. K. Galande, K. S. Bramlett, J. O. Trent, T. P. Burris, J. L. Wittliff and A. F. Spatola, *ChemBioChem*, 2005, **6**, 1991-1998.
96. A. M. Leduc, J. O. Trent, J. L. Wittliff, K. S. Bramlett, S. L. Briggs, N. Y. Chirgadze, Y. Wang, T. P. Burris and A. F. Spatola, *Proc. Natl. Acad. Sci. USA*, 2003, **100**, 11273-11278.
97. M. Chorev, E. Roubini, R. L. McKee, S. W. Gibbons, M. E. Goldman, M. P. Caulfield and M. Rosenblatt, *Biochemistry*, 1991, **30**, 5968-5974.
98. H. E. Blackwell and R. H. Grubbs, *Angew. Chem. Int. Ed.*, 1998, **37**, 3281-3284.
99. S. Baek, P. S. Kutchukian, G. L. Verdine, R. Huber, T. A. Holak, K. W. Lee and G. M. Popowicz, *J. Am. Chem. Soc.*, 2012, **134**, 103-106.
100. L. D. Walensky, A. L. Kung, I. Escher, T. J. Malia, S. Barbuto, R. D. Wright, G. Wagner, G. L. Verdine and S. J. Korsmeyer, *Science*, 2004, **305**, 1466-1470.
101. M. L. Stewart, E. Fire, A. E. Keating and L. D. Walensky, *Nat. Chem. Biol.*, 2010, **6**, 595-601.
102. L. D. Walensky, K. Pitter, J. Morash, K. J. Oh, S. Barbuto, J. Fisher, E. Smith, G. L. Verdine and S. J. Korsmeyer, *Mol. Cell*, 2006, **24**, 199-210.
103. R. E. Moellering, M. Cornejo, T. N. Davis, C. D. Bianco, J. C. Aster, S. C. Blacklow, A. L. Kung, D. G. Gilliland, G. L. Verdine and J. E. Bradner, *Nature*, 2009, **462**, 182-188.
104. G. H. Bird, N. Madani, A. F. Perry, A. M. Princiotta, J. G. Supko, X. He, E. Gavathiotis, J. G. Sodroski and L. D. Walensky, *Proc. Natl. Acad. Sci. USA*, 2010, **107**, 14093-14098.
105. E. Cabezas and A. C. Satterthwait, *J. Am. Chem. Soc.*, 1999, **121**, 3862-3875.
106. D. Y. Wang, W. Liao and P. S. Arora, *Angew. Chem. Int. Ed.*, 2005, **44**, 6525-6529.
107. D. Wang, M. Lu and P. S. Arora, *Angew. Chem. Int. Ed.*, 2008, **47**, 1879-1882.
108. R. Fasan, R. L. A. Dias, K. Moehle, O. Zerbe, J. W. Vrijbloed, D. Obrecht and J. A. Robinson, *Angew. Chem. Int. Ed.*, 2004, **43**, 2109-2112.
109. R. Fasan, R. L. A. Dias, K. Moehle, O. Zerbe, D. Obrecht, P. R. E. Mittl, M. G. Grüttner and J. A. Robinson, *ChemBioChem*, 2006, **7**, 515-526.
110. D. Seebach, S. Abele, J. V. Schreiber, B. Martinoni, A. K. Nussbaum, H. Schild, H. Schulz, H. Hennecke, R. Woessner and F. Bitsch, *Chimia*, 1998, **52**, 734-739.
111. J. D. Glickson and Applequi, J., *J. Am. Chem. Soc.*, 1971, **93**, 3276-3281.
112. S. H. Gellman, *Acc. Chem. Res.*, 1998, **31**, 173-180.
113. R. P. Cheng, S. H. Gellman and W. F. DeGrado, *Chem. Rev.*, 2001, **101**, 3219-3232.
114. E. P. English, R. S. Chumanov, S. H. Gellman and T. Compton, *J. Biol. Chem.*, 2006, **281**, 2661-2667.
115. J. A. Kritzer, J. D. Lear, M. E. Hodsdon and A. Schepartz, *J. Am. Chem. Soc.*, 2004, **126**, 9468-9469.
116. E. A. Harker, D. S. Daniels, D. A. Guarracino and A. Schepartz, *Bioorg. Med. Chem.*, 2009, **17**, 2038-2046.
117. M. Hintersteiner, T. Kimmerlin, G. Garavel, T. Schindler, R. Bauer, N.-C. Meisner, J.-M. Seifert, V. Uhl and M. Auer, *ChemBioChem*, 2009, **10**, 994-998.

118. S. Acton, A. Rigotti, K. T. Landschulz, S. Xu, H. H. Hobbs and M. Krieger, *Science*, 1996, **271**, 518-520.
119. M. Werder, H. Hauser, S. Abele and D. Seebach, *Helv. Chim. Acta*, 1999, **82**, 1774-1783.
120. E. F. Lee, B. J. Smith, W. S. Horne, K. N. Mayer, M. Evangelista, P. M. Colman, S. H. Gellman and W. D. Fairlie, *ChemBioChem*, 2011, **12**, 2025-2032.
121. T. Hara, S. R. Durell, M. C. Myers and D. H. Appella, *J. Am. Chem. Soc.*, 2006, **128**, 1995-2004.
122. R. Hayashi, D. Wang, T. Hara, J. A. Iera, S. R. Durell and D. H. Appella, *Bioorg. Med. Chem.*, 2009, **17**, 7884-7893.
123. A. Tavassoli, Q. Lu, J. Gam, H. Pan, S. J. Benkovic and S. N. Cohen, *ACS Chem. Biol.*, 2008, **3**, 757-764.
124. A. Tavassoli and S. J. Benkovic, *Nat. Protocols*, 2007, **2**, 1126-1133.
125. H. Yin, G. I. Lee, H. S. Park, G. A. Payne, J. M. Rodriguez, S. M. Sebti and A. D. Hamilton, *Angew. Chem. Int. Ed.*, 2005, **44**, 2704-2707.
126. J. T. Ernst, O. Kutzki, A. K. Debnath, S. Jiang, H. Lu and A. D. Hamilton, *Angew. Chem. Int. Ed.*, 2002, **41**, 278-282.
127. A. Kazi, J. Sun, K. Doi, S.-S. Sung, Y. Takahashi, H. Yin, J. M. Rodriguez, J. Becerril, N. Berndt, A. D. Hamilton, H.-G. Wang and S. M. Sebti, *J. Biol. Chem.*, 2011, **286**, 9382-9392.
128. J. T. Ernst, J. Becerril, H. S. Park, H. Yin and A. D. Hamilton, *Angew. Chem. Int. Ed.*, 2003, **42**, 535-539.
129. J.-M. Ahn and S.-Y. Han, *Tetrahedron Lett.*, 2007, **48**, 3543-3547.
130. J. Plante, F. Campbell, B. Malkova, C. Kilner, S. L. Warriner and A. J. Wilson, *Org. Biomol. Chem.*, 2008, **6**, 138-146.
131. J. P. Plante, T. Burnley, B. Malkova, M. E. Webb, S. L. Warriner, T. A. Edwards and A. J. Wilson, *Chem. Commun.*, 2009, 5091-5093.
132. J. M. Davis, A. Truong and A. D. Hamilton, *Org. Lett.*, 2005, **7**, 5405.
133. H. Yin and A. D. Hamilton, *Bioorg. Med. Chem. Lett.*, 2004, **14**, 1375-1379.
134. H. Yin, G. I. Lee, K. A. Sedey, J. M. Rodriguez, H. G. Wang, S. M. Sebti and A. D. Hamilton, *J. Am. Chem. Soc.*, 2005, **127**, 5463-5468.
135. S. M. Biros, L. Moisan, E. Mann, A. Carella, D. Zhai, J. C. Reed and J. Rebek, *Bioorg. Med. Chem. Lett.*, 2007, **17**, 4641-4645.
136. J. M. Rodriguez, L. Nevola, N. T. Ross, G.-i. Lee and A. D. Hamilton, *ChemBioChem*, 2009, **10**, 829-833.
137. J. M. Rodriguez, N. T. Ross, W. P. Katt, D. Dhar, G.-i. Lee and A. D. Hamilton, *ChemMedChem*, 2009, **4**, 649-656.
138. M. J. Adler and A. D. Hamilton, *J. Org. Chem.*, 2011, **76**, 7040-7047.
139. M. J. Adler, R. T. W. Scott and A. D. Hamilton, *Chem. Eur. J.*, 2012, **18**, 12974-12977.
140. F. Lu, S.-W. Chi, D.-H. Kim, K.-H. Han, I. D. Kuntz and R. K. Guy, *J. Combi. Chem.*, 2006, **8**, 315-325.
141. A. Shaginian, L. R. Whitby, S. Hong, I. Hwang, B. Farooqi, M. Searcey, J. Chen, P. K. Vogt and D. L. Boger, *J. Am. Chem. Soc.*, 2009, **131**, 5564-5572.
142. H. M. König, R. Abbel, D. Schollmeyer and A. F. M. Kilbinger, *Org. Lett.*, 2006, **8**, 1819-1822.
143. F. Campbell, J. P. Plante, T. A. Edwards, S. L. Warriner and A. J. Wilson, *Org. Biomol. Chem.*, 2010, **8**, 2344-2351.

144. K. Long, T. A. Edwards and A. J. Wilson, *Bioorg. Med. Chem.*, 2013, dx.doi.org/10.1016/j.bmc.2012.1009.1053.
145. D. Seebach, A. K. Beck and D. J. Bierbaum, *Chem. Biodivers.*, 2004, **1**, 1111-1239.
146. C. M. Goodman, S. Choi, S. Shandler and W. F. DeGrado, *Nat. Chem. Biol.*, 2007, **3**, 252-262.
147. J. M. Davis, L. K. Tsou and A. D. Hamilton, *Chem. Soc. Rev.*, 2007, **36**, 326-334.
148. C. M. Goodman, S. Choi, S. Shandler and W. F. DeGrado, *Nat Chem Biol*, 2007, **3**, 252-262.
149. T. Edwards and A. Wilson, *Amino Acids*, 2011, **41**, 743-754.
150. H. Zhou, J. Chen, J. L. Meagher, C.-Y. Yang, A. Aguilar, L. Liu, L. Bai, X. Cong, Q. Cai, X. Fang, J. A. Stuckey and S. Wang, *J. Med.Chem.*, 2012, **55**, 4664-4682.
151. A. Patgiri, K. K. Yadav, P. S. Arora and D. Bar-Sagi, *Nat Chem Biol*, 2011, **7**, 585-587.
152. L. M. Johnson, D. E. Mortenson, H. G. Yun, W. S. Horne, T. J. Ketas, M. Lu, J. P. Moore and S. H. Gellman, *J. Am. Chem. Soc.*, 2012, **134**, 7317-7320.
153. E. F. Lee, B. J. Smith, W. S. Horne, K. N. Mayer, M. Evangelista, P. M. Colman, S. H. Gellman and W. D. Fairlie, *Chem. Bio. Chem.*, 2011, **12**, 2025-2032.
154. A. D. Bautista, J. S. Appelbaum, C. J. Craig, J. Michel and A. Schepartz, *J. Am. Chem. Soc.*, 2010, **132**, 2904-2906.
155. I. Ehlers, P. Maity, J. Aubé and B. König, *Eur. J. Org. Chem.*, 2011, **2011**, 2474-2490.
156. J. H. Lee, Q. Zhang, S. Jo, S. C. Chai, M. Oh, W. Im, H. Lu and H. S. Lim, *J. Am. Chem. Soc.*, 2011, **133**, 676-679.
157. I. Huc, *Eur. J. Org. Chem.*, 2004, 17-29.
158. V. Azzarito, P. Prabhakaran, A. I. Bartlett, N. S. Murphy, M. J. Hardie, C. A. Kilner, T. A. Edwards, S. L. Warriner and A. J. Wilson, *Org. Biomol. Chem.*, 2012, **10**, 6469-6472.
159. J. L. Yap, X. Cao, K. Vanommeslaeghe, K.-Y. Jung, C. Peddaboina, P. T. Wilder, A. Nan, A. D. MacKerell, W. R. Smythe and S. Fletcher, *Org. Biomol. Chem.*, 2012, **10**, 2928-2933.
160. S. Saito, Y. Toriumi, N. Tomioka and A. Itai, *J. Org. Chem.*, 1995, **60**, 4715-4720.
161. F. Campbell, J. Plante, C. Carruthers, M. J. Hardie, T. J. Prior and A. J. Wilson, *Chem. Commun.*, 2007, 2240 - 2242.
162. B. Blankemeyer-Menge, M. Nimtz and R. Frank, *Tetrahedron Lett.*, 1990, **31**, 1701-1704.
163. A. J. Mancuso, D. S. Brownfain and D. Swern, *J. Org. Chem.*, 1979, **44**, 4148-4151.
164. C. A. Hood, G. Fuentes, H. Patel, K. Page, M. Menakuru and J. H. Park, *J. Pept. Sci.*, 2008, **14**, 97-101.
165. J. Coste, D. Lenguyen and B. Castro, *Tetrahedron Lett.*, 1990, **31**, 205-208.
166. A. El-Faham and S. N. Khattab, *Synlett*, 2009, 886-904.
167. L. A. Carpino and A. El-Faham, *Tetrahedron*, 1999, **55**, 6813-6830.
168. S. A. Kates, N. A. Sole, C. R. Johnson, D. Hudson, G. Barany and F. Albericio, *Tetrahedron Lett.*, 1993, **34**, 1549-1552.

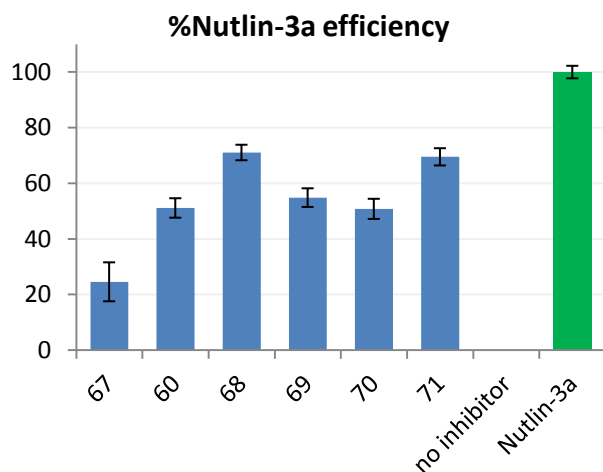
169. I. Azumaya, T. Okamoto, F. Imabeppu and H. Takayanai, *Tetrahedron*, 2003, **59**, 2325-2331.
170. A. Devos, J. Remion, A. M. Frisque-Hesbain, A. Colens and L. Ghosez, *J. Chem. Soc., Chem. Commun.*, 1979, 1180-1181.
171. V. H. Rawal and M. P. Cava, *Tetrahedron Lett.*, 1985, **26**, 6141-6142.
172. J. H. Lee, Q. Zhang, S. Jo, S. C. Chai, M. Oh, W. Im, H. Lu and H.-S. Lim, *J. Am. Chem. Soc.*, 2011, **133**, 676-679.
173. R. B. Kapust, J. Tozser, T. D. Copeland and D. S. Waugh, *Biochem. Biophys. Res. Comm.*, 2002, **294**, 949-955.
174. J. A. Kritzer, R. Zutshi, M. Cheah, F. A. Ran, R. Webman, T. M. Wongjirad and A. Schepartz, *ChemBioChem*, 2006, **7**, 29-31.
175. L. H. Chen, H. Yin, B. Farooqi, S. Sebti, A. D. Hamilton and J. D. Chen, *Mol. Cancer Ther.*, 2005, **4**, 1019-1025.
176. H. Yin, G.-I. Lee, K. A. Sedey, O. Kutzki, H. S. Park, B. P. Orner, J. T. Ernst, H.-G. Wang, S. M. Sebti and A. D. Hamilton, *J. Am. Chem. Soc.*, 2005, **127**, 10191-10196.
177. L. Chen, S. N. Willis, A. Wei, B. J. Smith, J. I. Fletcher, M. G. Hinds, P. M. Colman, C. L. Day, J. M. Adams and D. C. S. Huang, *Mol. Cell*, 2005, **17**, 393-403.
178. U. M. Moll and A. Zaika, *Drug Resist. Update*, 2000, **3**, 217-221.
179. D. M. Moran and C. G. Maki, *Mol. Cancer Ther.*, 2010, **9**, 895-905.
180. J. Pan, C. Cheng, S. Verstovsek, Q. Chen, Y. Jin and Q. Cao, *Cancer Lett.*, 2010, **293**, 167-174.
181. S. A. Malik, I. Orhon, E. Morselli, A. Criollo, S. Shen, G. Marino, A. BenYounes, P. Benit, P. Rustin, M. C. Maiuri and G. Kroemer, *Oncogene*, 2011, **30**, 3918-3929.
182. T. Hintermann and D. Seebach, *Chimia*, 1997, **51**, 244-247.
183. J. Frackenhohl, P. I. Arvidsson, J. V. Schreiber and D. Seebach, *ChemBioChem*, 2001, **2**, 445-455.
184. D. Wang, W. Liao and P. S. Arora, *Angew. Chem. Int. Ed.*, 2005, **44**, 6525-6529.
185. N. Tamilarasu, I. Huq and T. M. Rana, *J. Am. Chem. Soc.*, 1999, **121**, 1597-1598.
186. K. Burgess, D. S. Linthicum and H. W. Shin, *Angew. Chem. Int. Ed.*, 1995, **34**, 907-909.
187. K. Burgess, J. Ibarzo, D. S. Linthicum, D. H. Russell, H. Shin, A. Shitangkoon, R. Totani and A. J. Zhang, *J. Am. Chem. Soc.*, 1997, **119**, 1556-1564.
188. J. M. Kim, Y. Z. Bi, S. J. Paikoff and P. G. Schultz, *Tetrahedron Lett.*, 1996, **37**, 5305-5308.
189. A. Boeijen, J. van Ameijde and R. M. J. Liskamp, *J. Org. Chem.*, 2001, **66**, 8454-8462.
190. G. Guichard, V. Semetey, M. Rodriguez and J. P. Briand, *Tetrahedron Lett.*, 2000, **41**, 1553-1557.
191. L. Fischer, V. Semetey, J.-M. Lozano, A.-P. Schaffner, J.-P. Briand, C. Didierjean and G. Guichard, *Eur. J. Org. Chem.*, 2007, 2511-2525.
192. C. Douat-Casassus, K. Pulka, P. Claudon and G. Guichard, *Org. Lett.*, 2012, **14**, 3130-3133.
193. V. Semetey, D. Rognan, C. Hemmerlin, R. Graff, J. P. Briand, M. Marraud and G. Guichard, *Angew. Chem. Int. Ed.*, 2002, **41**, 1893-1895.

194. A. Violette, M. C. Averlant-Petit, V. Semetey, C. Hemmerlin, R. Casimir, R. Graff, M. Marraud, J. P. Briand, D. Rognan and G. Guichard, *J. Am. Chem. Soc.*, 2005, **127**, 2156-2164.
195. L. Fischer, P. Claudon, N. Pendem, E. Miclet, C. Didierjean, E. Ennifar and G. Guichard, *Angew. Chem. Int. Ed.*, 2010, **49**, 1067-1070.
196. C. Hemmerlin, M. Marraud, D. Rognan, R. Graff, V. Semetey, J. P. Briand and G. Guichard, *Helv. Chim. Acta*, 2002, **85**, 3692-3711.
197. A. Violette, N. Lancelot, A. Poschalko, M. Piotto, J.-P. Briand, J. Raya, K. Elbayed, A. Bianco and G. Guichard, *Chem. Eur. J.*, 2008, **14**, 3874-3882.
198. P. Claudon, A. Violette, K. Lamour, M. Decossas, S. Fournel, B. Heurtault, J. Godet, Y. Mely, B. Jamart-Gregoire, M.-C. Averlant-Petit, J.-P. Briand, G. Duportail, H. Monteil and G. Guichard, *Angew. Chem. Int. Ed.*, 2010, **49**, 333-336.
199. C. Aisenbrey, N. Pendem, G. Guichard and B. Bechinger, *Org. Biomol. Chem.*, 2012, **10**, 1440-1447.
200. V. Semetey, C. Didierjean, J. P. Briand, A. Aubry and G. Guichard, *Angew. Chem. Int. Ed.*, 2002, **41**, 1895-1898.
201. A. Hennig, L. Fischer, G. Guichard and S. Matile, *J. Am. Chem. Soc.*, 2009, **131**, 16889-16895.
202. N. Pendem, Y. R. Nelli, C. Douat, L. Fischer, M. Laguerre, E. Ennifar, B. Kauffmann and G. Guichard, *Angew. Chem. Int. Ed.*, 2013, **52**, 4147-4151.
203. D. H. Appella, L. A. Christianson, D. A. Klein, D. R. Powell, X. L. Huang, J. J. Barchi and S. H. Gellman, *Nature*, 1997, **387**, 381-384.
204. E. D. Goddard-Borger and R. V. Stick, *Org. Lett.*, 2007, **9**, 3797-3800.
205. J. Y. Lin, J. D. Chen, B. Elenbaas and A. J. Levine, *Genes Dev.*, 1994, **8**, 1235-1246.
206. I. Massova and P. A. Kollman, *J. Am. Chem. Soc.*, 1999, **121**, 8133-8143.
207. P. E. Czabotar, E. F. Lee, M. F. van Delft, C. L. Day, B. J. Smith, D. C. S. Huang, W. D. Fairlie, M. G. Hinds and P. M. Colman, *Proc. Natl. Acad. Sci. USA*, 2007, **104**, 6217-6222.

Appendix I

Repeat of the single point screen against compounds 60, 67-71

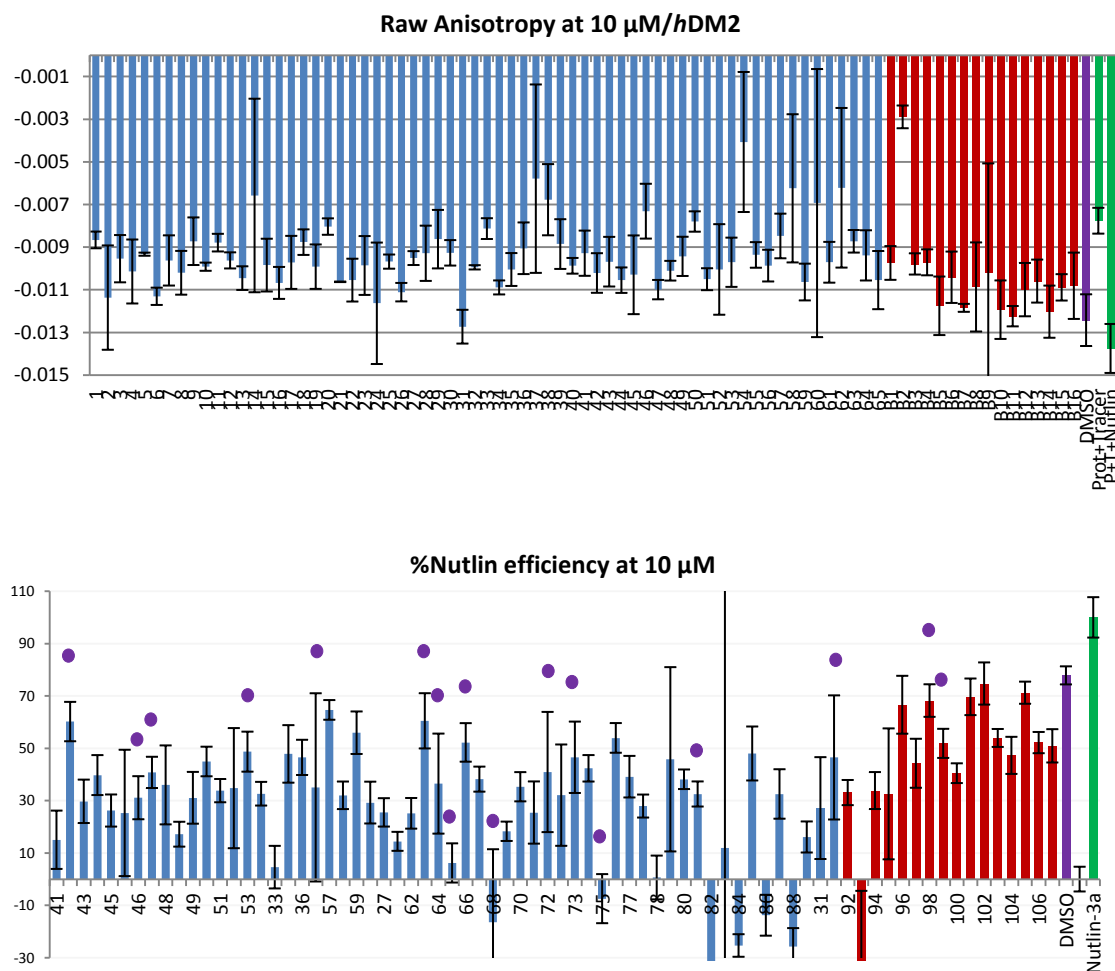
Repeat of the single point assay on selected compounds from the third set of compounds (60 – 77, Fig. 3.9, Chapter 3). This subset was re-tested to confirm the hit identification. Compounds 68-69 and 70-71 were two pairs of trimers with side chains matching those of the p53 helix which displayed very different relative efficiencies in the single point assay, but this gap in efficiencies only translated to a small difference in IC₅₀s in the dose-response assay.



These compounds were tested in the single point assay conditions described in the Experimental Section. Initially, the relative efficiencies for 68/69 and 70/71 were: 86%/37% and 34%/81% respectively, and 25% for 67. The repeat provided: 71%/56% and 51%/69% respectively and 25% for 67.

Appendix II

Automated single point assay against p53/hDM2

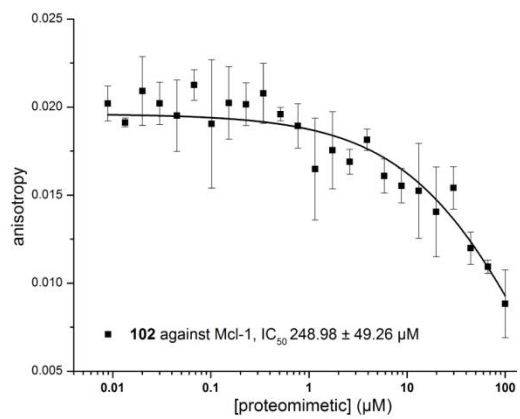
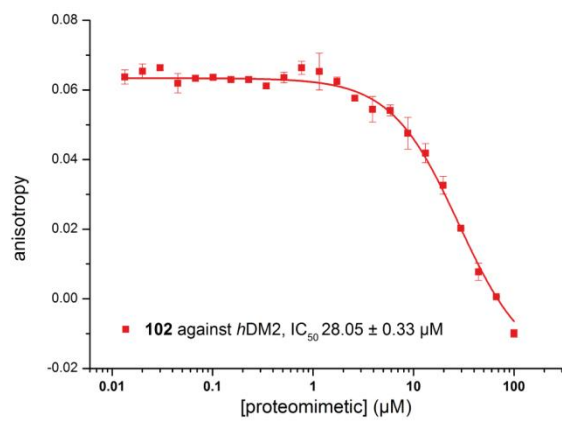


Results from the single point screening at 10 μ M against hDM2 presented as a %Nutlin-3a efficiency. Bars in blue correspond to compounds initially designed to target the p53/hDM2 PPI (bearing 3 side chains). Red bars correspond to compounds initially designed to target the Bcl-2 family (bearing 4 side chains, mostly aliphatic). Most potent from initial screens are indicated by purple dots.

The broad range of relative efficiencies that correspond to these hits indicated that results from this automated screening failed to reproduce results from the initial screens carried out manually in 96-well plates. Some compounds and in particular **93** gave an even higher anisotropy than the protein + tracer; these compounds might be inducing aggregation.

Appendix III

Selectivity study for compound 102

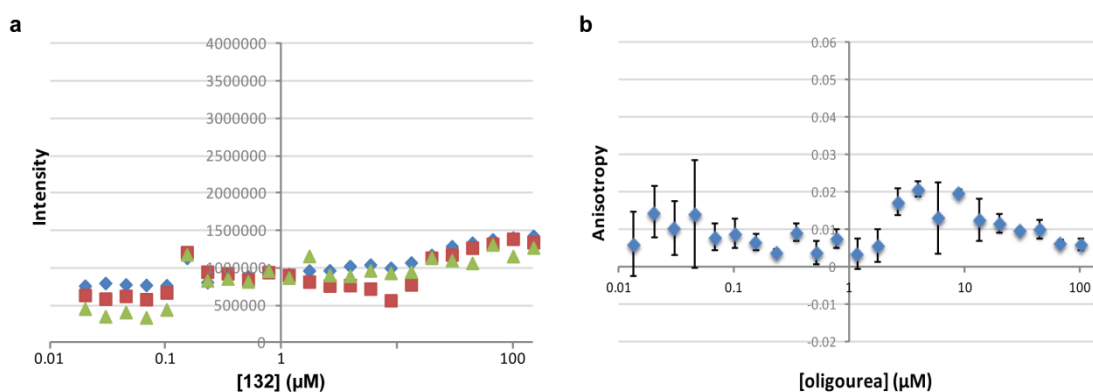


Dose-response curves for compound 102 against both PPIs (red: p53/hDM2, black: Noxa B/Mcl-1).

Appendix IV

Investigating a potential interaction between an oligourea and the p53-Flu tracer

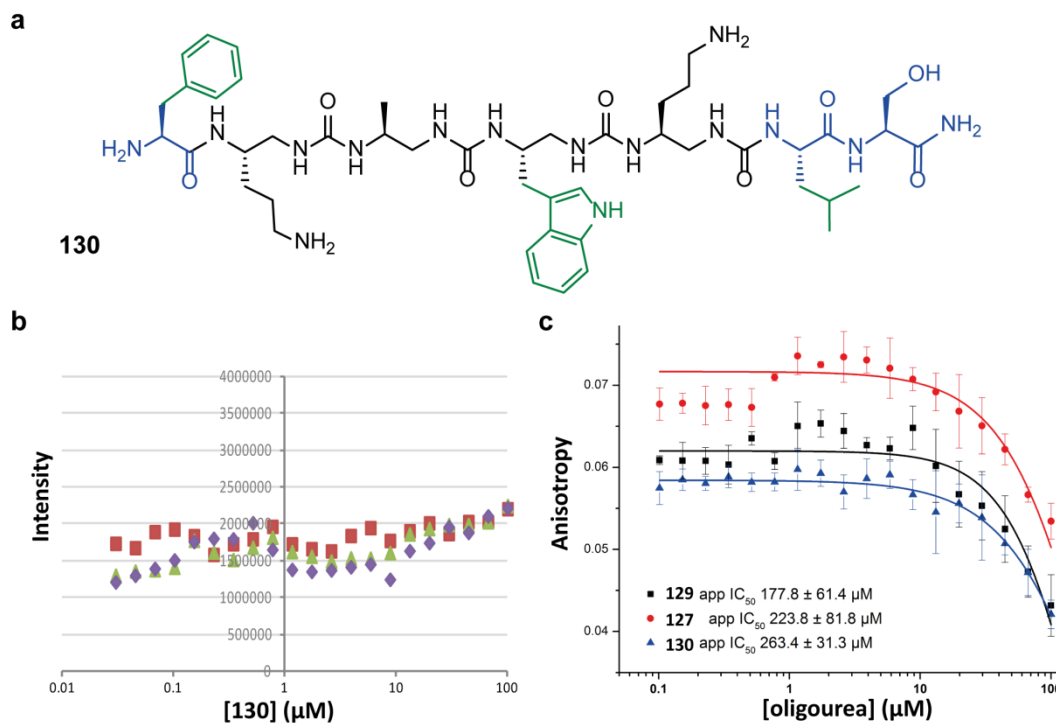
In this experiment, an oligourea (**132**) was serially diluted from 150 μM down to 13 nM, then the tracer was added at a constant concentration of 81.7 nM. In the case where there is no interaction between the oligourea and the tracer, the anisotropy should remain constant over the range of concentration tested; otherwise, a dose-dependent variation of the anisotropy should be observed.



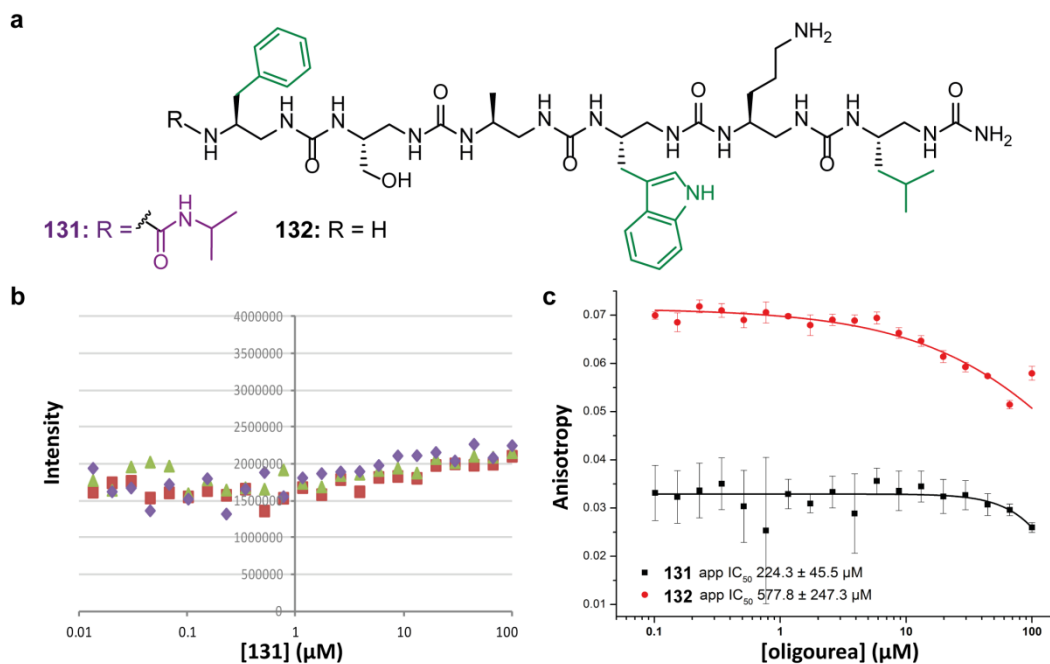
Investigating potential interaction between oligourea compounds and the p53 tracer. a. Intensity for the 3 repeats. **b.** Plot of the average anisotropy against the concentration in oligourea.

Appendix V

Dose-response curves for oligoureas 129, 130, 131, 132



Overlay of dose-response curves for oligoureas 127, 129 and 130.



Overlay of dose-response curves for oligoureas 131 and 132.

Appendix VI

Attempt to obtain the complete binding curve for oligourea 135, using 50 nM *hDM2* and 54 nM p53-Flu (concentration in the wells).

